



KTH Electrical Engineering

Control of Single and Multiple Thrust Propelled Systems with Applications to Attitude Synchronization

PEDRO MIGUEL ÓTÃO PEREIRA

Licentiate Thesis
Stockholm, Sweden 2016

TRITA-EE 2016:115
ISSN 1653-5146
ISBN 978-91-7729-066-7

KTH School of Electrical Engineering
Automatic Control Lab
SE-100 44 Stockholm
SWEDEN

Akademisk avhandling som med tillstånd av Kungliga Tekniska högskolan framläggas till offentlig granskning för avläggande av teknologie licenciatexamen i reglerteknik fredagen den 25 november 2016 klockan 14.00 i sal V3 Kungliga Tekniska högskolan, Teknikringen 72, KTH, Stockholm.

© Pedro Miguel Ótão Pereira, November 2016. All rights reserved.

Tryck: Universitetsservice US AB

Abstract

Control of aerial vehicles is an active topic of research, with many practical applications, such as the inspection and maintenance of aging infrastructures. Control of multi-agent systems is another active topic of research, where agents are required to accomplish some common goal. This thesis contributions lie in the scope of the previous topics, and they were particularly inspired and influenced by the application scenarios addressed by the AEROWORKS european research project, whose main goal is to deploy multiple heterogeneous unmanned aerial vehicles in environments where human intervention is restricted.

In the first part of the thesis, we consider a so-called thrust-propelled system, for which we develop a stabilizing controller by means of nonlinear control techniques. By transforming real physical systems into the form of the thrust-propelled system, we are able to leverage the previous controller to solve multiple position tracking problems. The list of those physical systems, studied in this thesis, includes a quadrotor system; a slung-load system, composed of a load and either one or two aerial vehicles, attached to the load by a cable; and a system composed of an aerial vehicle and a rigid manipulator. Experiments and simulations illustrate the performance of the proposed control strategies.

In the second part of the thesis, we consider a multi-agent system composed of either unit vectors or rotation matrices, and we design controllers that guarantee asymptotic synchronization. We refer to synchronization of unit vectors as incomplete synchronization, and to synchronization of rotation matrices as complete synchronization, where neither problem is a subcase of the other. We develop decentralized output feedback controllers for the agents, firstly for their angular velocity, and, in a second stage, for their torque. For the case of incomplete synchronization, and when the unit vectors to be synchronized are principal axes, we are able to propose torque control laws that do not require torque input in all bodies directions, but rather only in the body directions orthogonal to the respective principal axis. Several simulations are presented which illustrate the performance of the proposed control strategies.

Acknowledgements

I would like to thank my family and friends, and hope they forgive me for my negligent companionship in the last years.

Pedro Pereira
Stockholm, November 2016.

Contents

1	Introduction	1
1.1	Motivation	1
1.2	Outline and Contributions	2
1.3	Notation	5
2	Thrust propelled systems	13
2.1	Background	14
2.2	Control of the thrust-propelled system	16
2.3	Controller for a quadrotor	28
2.4	Controller for load lifting by a quadrotor	32
2.5	Load lifting stability under attitude control delay	38
2.6	Decoupled design of controllers for aerial manipulation	48
2.7	Controller for load lifting by two quadrotors	57
3	Attitude Synchronization	69
3.1	Background	70
3.2	Preliminaries	72
3.3	A common framework for attitude synchronization	76
3.4	Controllers for attitude synchronization on the sphere	97
4	Summary and future research directions	119
	Bibliography	123

Chapter 1

Introduction

1.1 Motivation

This thesis contributions lie in the scope of control of aerial vehicles and of multi-agent systems. In particular, the work developed was inspired by the application scenarios proposed and addressed by the AEROWORKS european research project [1]. The project's main goal is to deploy multiple heterogeneous unmanned aerial vehicles in environments where human intervention is restricted, forbidden, costly or dangerous, and as illustrated in Fig. 1.1. The application scenarios range from the inspection to maintenance of aging infrastructures in developing-and-developed countries. With an automated fleet of aerial vehicles, it is possible to inspect difficult-to-access infrastructures and to detect anomalies that such structures incur during their life span. One of the core ideas of the project is to deploy such a fleet in a decentralized manner, where each vehicle interacts and plans its future actions in cooperation with a subset of the whole fleet. The deployment of such a team of vehicles is expected to reduce the costs of inspection and repair tasks, and, more importantly, to remove humans from intervening in dangerous environments.



- (a) Removing humans from dangerous environments by performing aerial automated inspection.
(b) An automated fleet of aerial vehicles performing inspection and repair tasks on a wind mill.
(c) Cooperation between aerial vehicles when transporting a corona ring from an electrical pole.

Figure 1.1: AEROWORKS application scenarios that inspired some of the thesis contributions.

Drones, and in particular quadrotor drones, have been used for performing several different tasks, owing to their high maneuverability, low maintenance costs, low mechanical complexity and, most importantly of all, their ability to hover and to take-off and land vertically. For example, unmanned aerial vehicles (UAVs) have been used to detect methane, a greenhouse gas that is colorless, odorless, and explosive when its percentage on air exceeds 15%. By combining a laser-based methane detector on the UAV moving on a circular trajectory around a methane leak, it is possible to deduce the leak rate and narrow down the leak location [2]. Drones have also been used to inspect equipment integrity and to assess damaged components on steam boilers, where the manual inspection takes usually between three to four days and is done by technicians hanging from ropes, while the UAV inspection takes only one day [3]. Another popular application is to use UAVs to monitor and manage large landscapes. In particular, UAVs have been used to assess the immediate damage after wildfires and to keep track of vegetation regrowth afterwards [4]. In contrast, a crew of biologists would take weeks to complete the data collection of damaged areas [4]; together with monitoring the biodiversity restoration, such tasks amount to considerable monetary costs. Quadrotor UAVs have also been tested for the purposes of delivery of essential medical samples after natural disasters [5]. In these scenarios, roads may suffer from service disruptions, due to, for example, floods or traffic congestion; and aerial transportation of medical samples or other immediate necessities, such as potable water, consists of a fast means of assisting people in need. UAVs have been used in many other application scenarios, and the previous list is a small but representative subset of the practical applications of which UAVs are an essential component. Despite these several contributions, many problems, of practical and theoretical importance, remain unsolved, and this thesis contributions, specified in the next subsection, aim at adding and solidifying the contributions in this field of aerial vehicles.

1.2 Outline and Contributions

The thesis is divided in two main parts, corresponding to Chapters 2 and 3. In the first, we develop controllers for thrust-propelled systems, while in the second, we study synchronization of unit vectors and of rotation matrices. Pictorial illustrations of these two problems are presented in Fig. 1.2. In this section, we explain the outline of the thesis and list the contributions of each chapter and sections therein.

Chapter 2

In this chapter, the vector field of a thrust-propelled system is presented and described, and a control law is constructed, which steers the system's position to the origin. In addition, several examples of systems whose open-loop vector field is equivalent to that of the thrust-propelled system are provided, for which the previous control may be used. We start with a literature review on control of aerial vehicles in Section 2.1. The following sections are described next, in more detail.

Section 2.2

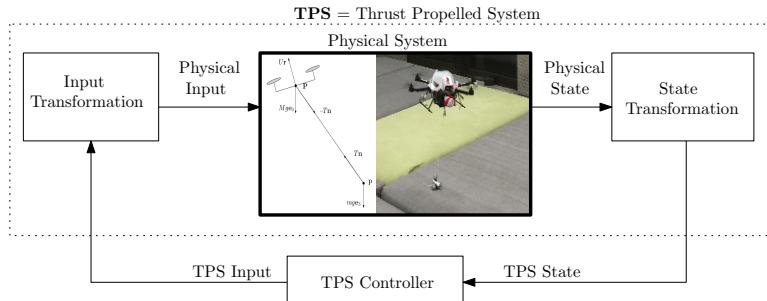
In this section, we describe the abstract notion of a thrust-propelled system, and propose a control law, which is constructed by means of a backstepping procedure, that steers the position of the thrust-propelled system to the origin. These results are based on

- Pereira, P. and Dimarogonas, D.V. *Lyapunov-based Generic Controller Design for Thrust-Propelled Underactuated Systems*. IEEE European Control Conference, pp. 594–599, 2016.

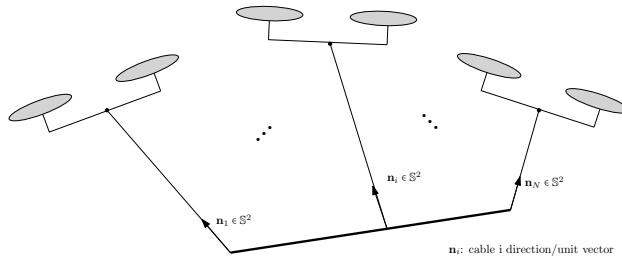
In the subsequent sections, we consider different physical systems, and we show that the thrust-propelled vector field is equivalent to that of each physical system, completely or partially. As such, via proper state and input transformations, the proposed control law, referred to before, may be used to control those physical systems.

Section 2.3

In this section, we consider, as a first example, the quadrotor dynamics, which we transform into the thrust-propelled dynamics. This first example also provides some intuition on the physical interpretation of the state of a thrust-propelled system.



(a) In Chapter 2, we develop controllers for thrust-propelled systems.



(b) In Chapter 3, we study synchronization of unit vectors and of rotation matrices.

Figure 1.2: This thesis is divided in two main parts.

Section 2.4

In this section, we consider a load and a quadrotor attached to each other by a cable of fixed length. After modeling the system, we transform it into the thrust-propelled form, and apply the previously mentioned controller. We also design a disturbance estimator that asymptotically removes a constant thrust input disturbance acting on the quadrotor. The results presented in this section are based on

- Pereira, P. and Herzog, M. and Dimarogonas, D. V. *Slung Load Transportation with Single Aerial Vehicle and Disturbance Removal*. IEEE Mediterranean Conference on Control and Automation, pp. 671–676, 2016.

Section 2.5

In this section, we consider again the system composed of a load and a quadrotor attached to each other by a cable of fixed length. We propose a controller that is easier to tune in an experimental setup and that provides an initial guess for other controllers gains. We also study the effect of the attitude inner-loop on the stability of the equilibrium, and find a tight upper bound on that delay for which asymptotic stability of the equilibrium is preserved. These section results are based on

- Pereira, P. and Dimarogonas, D. V. *Stability of Load Lifting by a Quadrotor under Attitude Control Delay*. IEEE International Conference on Robotics and Automation, 2017 (submitted).

Section 2.6

In this section, we consider a system composed of a rigid manipulator and a quadrotor attached to each other by a ball joint. We transform the system into the thrust-propelled form by considering the dynamics of the center of mass of the whole system. The results presented in this section are based on

- Pereira, P. and Zanella, R. and Dimarogonas, D.V. *Decoupled Design of Controllers for Aerial Manipulation with Quadrotors*. IEEE/RSJ International Conference on Intelligent Robots and Systems, pp. 4849–4855, 2016.

Section 2.7

In this section, we consider a system composed of a load and two quadrotors, with the load and each quadrotor attached to each other by a cable of fixed length. After transforming the system into the thrust-propelled form, we are left with two degrees of freedom, namely, the angle between the cables and the rotation of the plane that contains both cables around a chosen axis. These section results are based on

- Pereira, P. and Dimarogonas, D.V. *Control Framework for Slung Load Transportation with Two Aerial Vehicles*. American Control Conference, 2017 (submitted).

Chapter 3

In this chapter, we consider the problem of attitude synchronization among a group of agents in the group of unit vectors, or a group of agents in the group of rotation matrices. We start with a literature review on attitude synchronization in Section 3.1, and layout some preliminary concepts in Section 3.2. The following sections are described next, in more detail.

Section 3.3

In this section, we consider agents controlled at the angular velocity level (similar to first-order integrators) and where the network graph is allowed to change in time. By transforming the problems of synchronization on the group of unit vectors and of synchronization on the group of rotation matrices into a common form, we are able to study synchronization under a common framework. Moreover, asymptotic synchronization is guaranteed for a large set of initial conditions. The results presented in this section are based on

- Pereira, P. and Dimitris, B. and Dimarogonas, D.V. *A Common Framework for Attitude Synchronization of Unit Vectors in Networks with Switching Topology*. 55th IEEE Conference on Decision and Control, 2016 (to appear).

Section 3.4

In contrast with Section 3.3, in this section, we consider agents in the group of unit vectors controlled at the torque level (similar to second-order integrators), under a static network graph. We propose constrained torque control laws, which do not require torque on the space orthogonal to the unit vector each agent is supposed to synchronize. The results presented in this section are based on

- Pereira, P. and Dimarogonas, D.V. *Family of controllers for attitude synchronization in \mathbb{S}^2* . 54th IEEE Conference on Decision and Control, pp. 6761–6766, 2015; and,
- Pereira, P. and Dimarogonas, D.V. *Family of controllers for attitude synchronization on the sphere*. Automatica (accepted for publication).

1.3 Notation

In this section, we present the notation that is used in both chapters and sections therein. Notation specific to a section is presented at the begining of the respective section.

Definition 1.3.1. *Let Ω_1 and Ω_2 be manifolds of any dimension. Given $k \in \mathbb{N}_0$ and a function $\mathbf{f} : \Omega_1 \mapsto \Omega_2$, we say \mathbf{f} is of class \mathcal{C}^k , or equivalently $\mathbf{f} \in \mathcal{C}^k(\Omega_1, \Omega_2)$, if all its partial derivatives, up to order k inclusive, are continuous in Ω_1 .*

Definition 1.3.2. Let $n, p, m \in \mathbb{N}$. Let also $\mathbf{x} := (x_1, \dots, x_n) \in \mathbb{R}^n$, and denote, for $i \in \{1, \dots, n\}$, $\mathbf{x}_{|i} := (x_1, \dots, x_{i-1}, x_{i+1}, \dots, x_n) \in \mathbb{R}^{n-1}$. Then, given $\mathbf{f} := (f_1, \dots, f_p) \in \mathcal{C}^1(\mathbb{R}^n, \mathbb{R}^p)$, we define, for all $i \in \{1, \dots, n\}$ and $j \in \{1, \dots, p\}$,

$$g_{\mathbf{x}_{|i}, j} : \mathbb{R} \ni \tilde{x}_i \mapsto g_{\mathbf{x}_{|i}, j}(\tilde{x}_i) := f_j(x_1, \dots, \tilde{x}_i, \dots, x_n) \in \mathbb{R}$$

and denote

$$d\mathbf{f} : \mathbb{R}^n \ni (x_1, \dots, x_n) =: \mathbf{x} \mapsto d\mathbf{f}(\mathbf{x}) := \begin{bmatrix} g'_{\mathbf{x}_{|1}, 1}(x_1) & \cdots & g'_{\mathbf{x}_{|n}, 1}(x_n) \\ \vdots & \ddots & \vdots \\ g'_{\mathbf{x}_{|1}, p}(x_1) & \cdots & g'_{\mathbf{x}_{|n}, p}(x_n) \end{bmatrix} \in \mathbb{R}^{p \times n}.$$

Also, given $n_1, n_2, n_3 \in \mathbb{N}$ such that $n_1 + n_2 + n_3 = n \wedge n_2 \neq 0$, we denote, given $(\mathbf{x}_1, \mathbf{x}_2, \mathbf{x}_3) \in \mathbb{R}^{n_1} \times \mathbb{R}^{n_2} \times \mathbb{R}^{n_3}$,

$$\begin{aligned} \partial_z \mathbf{f}(\mathbf{x}_1, \mathbf{z}, \mathbf{x}_3)|_{\mathbf{z}=\mathbf{x}_2} &:= d\mathbf{g}_{(\mathbf{x}_1, \mathbf{x}_3)}(\mathbf{x}_2) \in \mathbb{R}^{p \times n}, \text{ with} \\ \mathbf{g}_{(\mathbf{x}_1, \mathbf{x}_3)} : \mathbb{R}^{n_2} \ni \tilde{\mathbf{x}}_2 &\mapsto \mathbf{g}_{(\mathbf{x}_1, \mathbf{x}_3)}(\tilde{\mathbf{x}}_2) := \mathbf{f}(\mathbf{x}_1, \tilde{\mathbf{x}}_2, \mathbf{x}_3) \in \mathbb{R}^p, \end{aligned}$$

where we emphasize that \mathbf{z} is just a dummy variable, that serves only the purpose of indicating the position of the argument w.r.t. which the differentiation is taken.

Let $I \subseteq \mathbb{R}$ be nonempty and open, and Ω_x and \mathcal{U}_x be manifolds. Consider then a trajectory $\mathbf{x} \in \mathcal{C}^1(I, \Omega_x)$ and a control input $\mathbf{u}_x \in \mathcal{C}(I, \mathcal{U}_x)$. If $\dot{\mathbf{x}}(t) = \mathbf{f}_x(t, \mathbf{x}(t), \mathbf{u}_x(t))$ for all $t \in I$ and for some $\mathbf{f}_x : I \times \Omega_x \times \mathcal{U}_x \ni (t, \mathbf{x}, \mathbf{u}_x) \mapsto \mathbf{f}_x(t, \mathbf{x}, \mathbf{u}_x) \in T_{\mathbf{x}}\Omega_x$, we call \mathbf{f}_x the open-loop vector field. If $\mathbf{u}(t) = \mathbf{u}_x^{cl}(t, \mathbf{x}(t))$ for all $t \in I$ and for some $\mathbf{u}_x^{cl} \in \mathcal{C}(I \times \Omega_x, \mathcal{U}_x)$, we call \mathbf{u}_x^{cl} the control law and $\mathbf{f}_x^{cl} : I \times \Omega_x \ni (t, \mathbf{x}) \mapsto \mathbf{f}_x^{cl}(t, \mathbf{x}) := \mathbf{f}_x(t, \mathbf{x}, \mathbf{u}_x^{cl}(t, \mathbf{x})) \in T_{\mathbf{x}}\Omega_x$ the closed-loop vector field. We say (the open-loop vector field) $\mathbf{f}_y : I \times \Omega_y \times \mathcal{U}_y \ni (t, \mathbf{y}, \mathbf{u}_y) \mapsto \mathbf{f}_y(t, \mathbf{y}, \mathbf{u}_y) \in T_{\mathbf{y}}\Omega_y$ is equivalent to (the open-loop vector field) $\mathbf{f}_x : I \times \Omega_x \times \mathcal{U}_x \ni (t, \mathbf{x}, \mathbf{u}_x) \mapsto \mathbf{f}_x(t, \mathbf{x}, \mathbf{u}_x) \in T_{\mathbf{x}}\Omega_x$ if, for every $t \in I$, there exists a diffeomorphism $\mathbf{g}_x^y(t, \cdot) : \Omega_x \mapsto \Omega_y$ (denote $\mathbf{g}_y^x(t, \cdot) := (\mathbf{g}_x^y(t, \cdot))^{-1}$) and a function $\mathbf{u}_x^{cl} : I \times \Omega_y \times \mathcal{U}_y \mapsto \mathcal{U}_x$ such that, for all $(t, \mathbf{y}, \mathbf{u}_y) \in I \times \Omega_y \times \mathcal{U}_y$,

$$\mathbf{f}_y(t, \mathbf{y}, \mathbf{u}_y) := (\partial_t \mathbf{g}_x^y(t, \mathbf{x})|_{\bar{t}=t} + \partial_{\mathbf{x}} \mathbf{g}_x^y(t, \bar{\mathbf{x}})|_{\bar{\mathbf{x}}=\mathbf{x}} \mathbf{f}_x(t, \mathbf{x}, \mathbf{u}_x))|_{\mathbf{x}=\mathbf{g}_y^x(t, \mathbf{y}), \mathbf{u}_x=\mathbf{u}_x^{cl}(t, \mathbf{y}, \mathbf{u}_y)}. \quad (1.3.1)$$

Example 1.3.1. Consider the manifolds $\Omega_n := \mathbb{S}^2 \setminus \{\mathbf{n} \in \mathbb{S}^2 : \mathbf{e}_1^T \mathbf{n} > 0\}$ and $\Omega_\theta := (-\frac{\pi}{2}, \frac{\pi}{2})^2$, $\mathcal{U}_n = \mathbb{R}^3$ and $\mathcal{U}_\theta = \mathbb{R}^2$, and the vector fields

$$\begin{aligned} \mathbb{R} \times \Omega_n \times \mathcal{U}_n \ni (t, \mathbf{n}, \boldsymbol{\omega}) &\mapsto \mathbf{f}_n(t, \mathbf{n}, \boldsymbol{\omega}) := \mathcal{S}(\boldsymbol{\omega}) \mathbf{n} \in T_{\mathbf{n}}\Omega_n := \{\delta \mathbf{n} \in \mathbb{R}^3 : \delta \mathbf{n}^T \mathbf{n} = 0\}, \\ \mathbb{R} \times \Omega_\theta \times \mathcal{U}_\theta \ni (t, \boldsymbol{\theta}, \boldsymbol{\omega}_\theta) &\mapsto \mathbf{f}_\theta(t, \boldsymbol{\theta}, \boldsymbol{\omega}_\theta) := \boldsymbol{\omega}_\theta \in T_{\boldsymbol{\theta}}\Omega_\theta := \mathbb{R}^2. \end{aligned}$$

Consider also (let $\boldsymbol{\theta} = (\psi, \theta)$)

$$\mathbb{R} \times \Omega_\theta \times \mathcal{U}_\theta \ni (t, \boldsymbol{\theta}, \boldsymbol{\omega}_\theta) \mapsto \boldsymbol{\omega}_n^{cl}(t, \boldsymbol{\theta}, \boldsymbol{\omega}_\theta) := \begin{bmatrix} \cos(\theta) \sin(\theta) \cos(\psi) & -\sin(\psi) \\ \cos(\theta) \sin(\theta) \sin(\psi) & \cos(\psi) \\ \cos^2(\theta) & 0 \end{bmatrix} \boldsymbol{\omega}_\theta,$$

and

$$\begin{aligned}\mathbb{R} \times \Omega_n &\ni (t, \mathbf{n}) \mapsto \mathbf{g}_n^\theta(t, \mathbf{n}) := \left(\arctan\left(\frac{\mathbf{e}_2^T \mathbf{n}}{\mathbf{e}_1^T \mathbf{n}}\right), \arcsin(-\mathbf{e}_3^T \mathbf{n}) \right) \in \Omega_\theta, \\ \mathbb{R} \times \Omega_\theta &\ni (t, \boldsymbol{\theta}) \mapsto \mathbf{g}_\theta^n(t, \boldsymbol{\theta}) := (c(\theta)c(\psi), c(\theta)s(\psi), -s(\theta)) \in \Omega_n.\end{aligned}$$

It thus follows that \mathbf{f}_θ is equivalent to \mathbf{f}_n , since (1.3.1) holds (with $(x, y) = (n, \theta)$).

The formalism introduced in (1.3.1) may seem unnecessary in Example 1.3.1, but it proves itself useful in the sections to come.

Definition 1.3.3. Let $n \in \mathbb{N}$, $\alpha \in [0, \pi]$ and $\boldsymbol{\nu} \in \mathcal{S}^n$. We define $\mathcal{C}(\alpha, \boldsymbol{\nu}) := \{\mathbf{n} \in \mathbb{S}^n : \mathbf{n}^T \boldsymbol{\nu} > \cos(\alpha)\}$ as the open α cone around $\boldsymbol{\nu}$. Similarly, we define $\bar{\mathcal{C}}(\alpha, \boldsymbol{\nu}) := \{\mathbf{n} \in \mathbb{S}^n : \mathbf{n}^T \boldsymbol{\nu} \geq \cos(\alpha)\}$ as the closed α -cone around $\boldsymbol{\nu}$.

In Fig. 1.3, we illustrate an open cone for $n = 3$, $\alpha = 30^\circ$ and some $\bar{\boldsymbol{\nu}} \in \mathbb{S}^2$: in particular, three unit vectors $\boldsymbol{\nu}_1$, $\boldsymbol{\nu}_2$ and $\boldsymbol{\nu}_3$ are shown which belong to $\bar{\mathcal{C}}(30^\circ, \bar{\boldsymbol{\nu}})$, i.e., the closed 30° -cone formed by the unit vector $\bar{\boldsymbol{\nu}}$.

Proposition 1.3.4 (Triangle Inequality). Let $n \in \mathbb{N}$, and $\boldsymbol{\nu}_1, \boldsymbol{\nu}_2, \boldsymbol{\nu} \in \mathcal{S}^n$. For $\theta_{1,2} = \arccos(\boldsymbol{\nu}_1^T \boldsymbol{\nu}_2) \in [0, \pi]$, $\theta_1 = \arccos(\boldsymbol{\nu}_1^T \boldsymbol{\nu}) \in [0, \pi]$ and $\theta_2 = \arccos(\boldsymbol{\nu}_2^T \boldsymbol{\nu}) \in [0, \pi]$, it follows that $\theta_{1,2} \leq \theta_1 + \theta_2$.

Proof. The equality $\theta_{1,2} = \theta_1 + \theta_2$ follows immediately when $\theta_1 = 0$ or $\theta_2 = 0$, since $\boldsymbol{\nu}_1 = \boldsymbol{\nu}$ or $\boldsymbol{\nu}_2 = \boldsymbol{\nu}$, respectively. Assume then that $\theta_1 \neq 0 \wedge \theta_2 \neq 0$. Notice that $\boldsymbol{\nu}_i = (\boldsymbol{\nu}_i^T \boldsymbol{\nu})\boldsymbol{\nu} + \Pi(\boldsymbol{\nu})\boldsymbol{\nu}_i = \cos(\theta_i)\boldsymbol{\nu} + \sin(\theta_i)\boldsymbol{\nu}^{\perp,i}$, for $i = \{1, 2\}$ and where $\boldsymbol{\nu}^{\perp,i} = \frac{\Pi(\boldsymbol{\nu})\boldsymbol{\nu}_i}{\|\Pi(\boldsymbol{\nu})\boldsymbol{\nu}_i\|}$ is a unit vector orthogonal to $\boldsymbol{\nu}$ (well defined since $\theta_i \neq 0$). It then follows that $\cos(\theta_{1,2}) = \boldsymbol{\nu}_1^T \boldsymbol{\nu}_2 = \cos(\theta_1)\cos(\theta_2) + \sin(\theta_1)\sin(\theta_2)(\boldsymbol{\nu}^{\perp,1})^T \boldsymbol{\nu}^{\perp,2} = \cos(\theta_1 + \theta_2) + \sin(\theta_1)\sin(\theta_2)(1 + (\boldsymbol{\nu}^{\perp,1})^T \boldsymbol{\nu}^{\perp,2}) \geq \cos(\theta_1 + \theta_2)$, and thus the Proposition's conclusion follows. \square

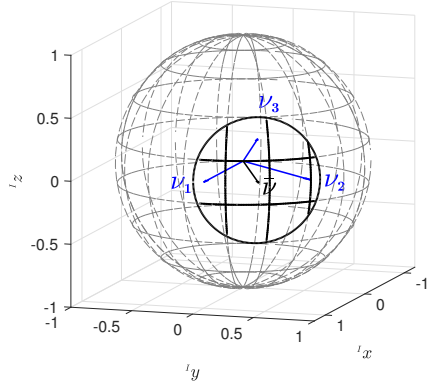


Figure 1.3: Three unit vectors, $\boldsymbol{\nu}_1$, $\boldsymbol{\nu}_2$ and $\boldsymbol{\nu}_3$, in \mathbb{R}^3 contained in closed 30° -cone formed by unit vector $\bar{\boldsymbol{\nu}}$.

In the lists below, let $n \in \mathbb{N}$, $\epsilon > 0$ and Ω be some set.

Variables

$\mathbf{0}_n = (0, \dots, 0) \in \mathbb{R}^n$	Zero vector in \mathbb{R}^n
$\mathbf{1}_n = (1, \dots, 1) \in \mathbb{R}^n$	Vector of ones in \mathbb{R}^n
$\mathbf{I}_n \in \mathbb{R}^{n \times n}$	Identity matrix
$ \Omega \in \mathbb{N}$	Cardinality of a finite set Ω
$A \otimes B \in \mathbb{R}^{m \times n \times t}$	Kronecker product between $A \in \mathbb{R}^{m \times n}$ and $B \in \mathbb{R}^{s \times t}$, for $n, m, s, t \in \mathbb{N}$
$A_1 \oplus \dots \oplus A_n$	Block diagonal matrix with block diagonal entries A_1 to A_n (square matrices of any dimensions)
$\mathbf{e}_1, \dots, \mathbf{e}_n \in \mathbb{R}^n$	Canonical basis vectors of \mathbb{R}^n

Sets

$M_{3,3} \subset \mathbb{R}^{3 \times 3}, \bar{M}_{3,3} \subset \mathbb{R}^{3 \times 3}$	Set of symmetric and antisymmetric matrices, respectively
$\mathbb{S}^n := \{\mathbf{x} \in \mathbb{R}^{n+1} : \mathbf{x}^T \mathbf{x} = 1\}$	Set of unit vectors in \mathbb{R}^{n+1}
$\mathbb{SO}(3) \subset \mathbb{R}^{3 \times 3}$	Set of three dimensional rotation matrices
$\Omega^\epsilon := \{\mathbf{x} \in \mathbb{R}^n : \exists \mathbf{z} \in \Omega : \ \mathbf{x} - \mathbf{z}\ < \epsilon\}$	Open set of all points which are ϵ -close to the set $\Omega \subseteq \mathbb{R}^n$
$\mathcal{B}(\epsilon)[\bar{\mathcal{B}}(\epsilon)] := \{\mathbf{x} \in \mathbb{R}^n : \ \mathbf{x}\ < [\leq] \epsilon\}$	Open [Closed] ball of radius ϵ and centered around $\mathbf{0}$

Functions

$\mathcal{S} : \mathbb{R}^3 \mapsto \bar{M}_{3,3}$	$\mathcal{S}(\mathbf{a})\mathbf{b} := \mathbf{a} \times \mathbf{b}$, for all $\mathbf{a}, \mathbf{b} \in \mathbb{R}^3$ (see (1.3.2))
$\mathcal{S}^{-1} : \bar{M}_{3,3} \rightarrow \mathbb{R}^3$	$\mathbf{X} = \mathcal{S}(\mathcal{S}^{-1}(\mathbf{X}))$ and $\mathbf{x} = \mathcal{S}^{-1}(\mathcal{S}(\mathbf{x}))$ for all $\mathbf{X} \in \bar{M}_{3,3}, \mathbf{x} \in \mathbb{R}^3$ (see (1.3.3))
$\Pi : \mathbb{S}^n \mapsto \mathbb{R}^{(n+1) \times (n+1)}$	$\Pi(\mathbf{x}) := \mathbf{I} - \mathbf{x}\mathbf{x}^T$, orthogonal projection operator onto the subspace perpendicular to $\mathbf{x} \in \mathbb{S}^n$
$\text{dist} : \mathbb{R}^n \times 2^{\mathbb{R}^n} \mapsto \mathbb{R}_{\geq 0}$	Distance of point $\mathbf{x} \in \mathbb{R}^n$ to set $\Omega \subseteq \mathbb{R}^n$, $\text{dist}(\mathbf{x}, \Omega) := \inf_{\mathbf{y} \in \Omega} \ \mathbf{x} - \mathbf{y}\ $

The functions, introduced in the previous page, are defined as

$$\mathcal{S} : \mathbb{R}^3 \ni (x, y, z) \mapsto \begin{bmatrix} 0 & -z & y \\ z & 0 & -x \\ -y & x & 0 \end{bmatrix} \in \bar{M}_{3,3}, \quad (1.3.2)$$

$$\mathcal{S}^{-1} : \bar{M}_{3,3} \ni \begin{bmatrix} 0 & -z & y \\ z & 0 & -x \\ -y & x & 0 \end{bmatrix} \mapsto (x, y, z) \in \mathbb{R}^3, \quad (1.3.3)$$

and satisfy the following properties,

$$(P1) \quad \mathcal{R}\mathcal{S}(\mathbf{x}) = \mathcal{S}(\mathcal{R}\mathbf{x})\mathcal{R}, \forall \mathbf{x} \in \mathbb{R}^3, \mathcal{R} \in \mathbb{SO}(3); \quad (1.3.4)$$

$$(P2) \quad \Pi(\mathbf{n}) = (\mathcal{S}(\mathbf{n}))^T \mathcal{S}(\mathbf{n}) = -\mathcal{S}(\mathbf{n})\mathcal{S}(\mathbf{n}), \forall \mathbf{n} \in \mathbb{S}^2; \quad (1.3.5)$$

$$(P3) \quad \|\mathcal{S}(\mathbf{n})\mathbf{m}\|^2 = \|\Pi(\mathbf{n})\mathbf{m}\|^2 = 1 - (\mathbf{n}^T \mathbf{m})^2, \forall \mathbf{n}, \mathbf{m} \in \mathbb{S}^2; \quad (1.3.6)$$

$$(P4) \quad \mathcal{R}\mathcal{S}^{-1}(A - A^T) = \mathcal{S}^{-1}(\mathcal{R}A\mathcal{R}^T - \mathcal{R}A^T\mathcal{R}^T) \forall \mathcal{R} \in \mathbb{SO}(3), A \in \mathbb{R}^{3 \times 3}; \quad (1.3.7)$$

which we use repeatedly in this thesis.

Definition 1.3.5. (*Equilibrium*) Let \mathbf{f}_x be a vector field on a manifold Ω_x , i.e., $\mathbf{f}_x : \mathbb{R} \times \Omega_x \ni (t, \mathbf{x}) \mapsto \mathbf{f}_x(t, \mathbf{x}) \in T_{\mathbf{x}}\Omega_x$. We say $\mathbf{x}^* \in \Omega_x$ is an equilibrium point of \mathbf{f}_x , if $\mathbf{f}_x(t, \mathbf{x}^*) = \mathbf{0}$ for all $t \in \mathbb{R}$.

Definition 1.3.6. (*Stability of an equilibrium*) Let \mathbf{f}_x be a vector field on a manifold Ω_x . An equilibrium point $\mathbf{x}^* \in \Omega_x$ is

- stable if for every (arbitrarily small) neighborhood $\Omega_1 \subseteq \Omega_x$ of \mathbf{x}^* there exists a neighborhood $\Omega_2 \subseteq \Omega_1$ of \mathbf{x}^* such that $\mathbb{R} \ni t \mapsto \mathbf{x}(t) = \mathbf{x}_0 + \int_0^t \mathbf{f}_x(\tau, \mathbf{x}(\tau))d\tau \in \Omega_1$ for any $\mathbf{x}_0 \in \Omega_2$.
- attractive if there exists a neighborhood $\Omega_2 \subseteq \Omega_x$ of \mathbf{x}^* such that, for $\mathbb{R} \ni t \mapsto \mathbf{x}(t) = \mathbf{x}_0 + \int_0^t \mathbf{f}_x(\tau, \mathbf{x}(\tau))d\tau \in \Omega_x$ with any $\mathbf{x}_0 \in \Omega_2$, it holds that $\lim_{t \rightarrow \infty} \mathbf{x}(t) = \mathbf{x}^*$.
- (locally) asymptotically stable if it is stable and attractive.
- globally asymptotically stable if it is stable and attractive and $\Omega_2 = \Omega_x$.
- unstable (unattractive) if it is not stable (not attractive).

Example 1.3.2. Let $\mathbf{k} \in \mathbb{R}^3$, and consider the manifold \mathbb{S}^2 and the vector field

$$\mathbf{f}_n : \mathbb{S}^2 \ni \mathbf{n} \mapsto \mathbf{f}_n(\mathbf{n}) := \mathcal{S}(\mathbf{n})(\mathbf{k} - \mathcal{S}(\mathbf{n})\mathbf{e}_1) \in T_{\mathbf{n}}\mathbb{S}^2 := \{\delta\mathbf{n} \in \mathbb{R}^3 : \mathbf{n}^T \delta\mathbf{n} = 0\}. \quad (1.3.8)$$

It follows that

- for $\mathbf{k} = \mathbf{e}_3 \in \mathbb{R}^3$, $\mathbf{n}^* = -\mathbf{e}_2 \in \mathbb{S}^2$ is attractive and unstable (see Fig. 1.4b);
- for $\mathbf{k} = k\mathbf{e}_3 \in \mathbb{R}^3$ with $k > 1$, $\mathbf{n}^* = \left(0, -\frac{1}{k}, \pm\frac{\sqrt{k^2-1}}{k}\right) \in \mathbb{S}^2$ is stable but not attractive (see Fig. 1.4a);
- for $\mathbf{k} = \mathbf{0} \in \mathbb{R}^3$, $\mathbf{n}^* = \mathbf{e}_1 \in \mathbb{S}^2$ is asymptotically stable (see Fig. 1.4c);
- for $\mathbf{k} = \mathbf{0} \in \mathbb{R}^3$, $\mathbf{n}^* = -\mathbf{e}_1 \in \mathbb{S}^2$ is unstable and unattractive (see Fig. 1.4c).

Let us focus only on the last two cases. For this case $\mathbf{f}_n(\mathbf{n}) := \Pi(\mathbf{n})\mathbf{e}_1 \Rightarrow \mathbf{e}_1^T \mathbf{f}_n(\mathbf{n}) = \|\mathcal{S}(\mathbf{n})\mathbf{e}_1\|^2 = 1 - (\mathbf{n}^T \mathbf{e}_1)^2$; and therefore, for $V : \mathbb{S}^2 \ni \mathbf{n} \mapsto V(\mathbf{n}) := 1 - \mathbf{n}^T \mathbf{e}_1 \in [0, 2]$, it follows that $dV(\mathbf{n})\mathbf{f}_n(\mathbf{n}) = -V(\mathbf{n})(2 - V(\mathbf{n})) \leq 0$ for all $\mathbf{n} \in \mathbb{S}^2$. As such, for $\mathbb{R}_{\geq 0} \ni t \mapsto \mathbf{n}(t) = \mathbf{n}_0 + \int_0^t \mathbf{f}_n(\mathbf{x}(\tau))d\tau \in \mathbb{S}^2$ with any $\mathbf{n}_0 \in \mathbb{S}^2$, it follows that $\mathbb{R}_{\geq 0} \ni t \mapsto V(\mathbf{n}(t)) = \frac{2V(\mathbf{n}(0))}{e^{2t(V(\mathbf{n}(0))-2)+V(\mathbf{n}(0))}} \in [0, 2]$. This suffices to infer that $\mathbf{n}^* = \mathbf{e}_1 \in \mathbb{S}^2$ is asymptotically stable and that $\mathbf{n}^* = -\mathbf{e}_1 \in \mathbb{S}^2$ is unstable and unattractive. With respect to neighborhoods around the equilibria, the concept of cone as in Definition 1.3.3 may be used, in which case, it follows from the previous discussion that, in fact, $\mathbb{R}_{\geq 0} \ni t \mapsto \mathbf{n}(t) \in \bar{\mathcal{C}}(\arccos(1 - \mathbf{e}_1^T \mathbf{n}_0), \mathbf{e}_1)$.

Remark 1.3.7. *Asymptotic stability of an equilibrium point may be inferred from several different approaches. Consider the Example 1.3.2 for the case $\mathbf{k} = \mathbf{0}_3$, and the asymptotically stable equilibrium $\mathbf{n}^* = \mathbf{e}_1 \in \mathbb{S}^2$.*

- A linearization procedure around the equilibrium yields $d\mathbf{f}_n(\mathbf{n}^*) = -\Pi(\mathbf{e}_1) (= -\mathbf{I} + \mathbf{e}_1 \mathbf{e}_1^T)$, and therefore stability cannot be inferred from this linearization procedure (one zero eigenvalue).
- Consider (let $\Omega_n := \mathbb{S}^2 \setminus \{\mathbf{n} \in \mathbb{S}^2 : \mathbf{e}_1^T \mathbf{n} > 0\}$ and $\Omega_\theta := (-\frac{\pi}{2}, \frac{\pi}{2})^2$)
$$\mathbf{g}_n^\theta : \Omega_n \ni \mathbf{n} \mapsto \mathbf{g}_n^\theta(\mathbf{n}) = \left(\arctan\left(\frac{\mathbf{e}_2^T \mathbf{n}}{\mathbf{e}_1^T \mathbf{n}}\right), \arcsin(-\mathbf{e}_3^T \mathbf{n}) \right) \in \Omega_\theta,$$

$$\mathbf{g}_\theta^n : \Omega_\theta \ni (\psi, \theta) =: \boldsymbol{\theta} \mapsto \mathbf{g}_\theta^n(\boldsymbol{\theta}) \equiv (\mathbf{g}_n^\theta)^{-1}(\boldsymbol{\theta}) := (c(\theta)c(\psi), c(\theta)s(\psi), -s(\theta)) \in \Omega_n.$$

It follows that, for $\mathbf{f}_\theta : \Omega_\theta \ni \boldsymbol{\theta} \mapsto \mathbf{f}_\theta(\boldsymbol{\theta}) := d\mathbf{g}_n^\theta(\mathbf{n})\mathbf{f}_n(\mathbf{n})|_{\mathbf{n}=\mathbf{g}_\theta^n(\boldsymbol{\theta})} \in \mathbb{R}^2$, $\boldsymbol{\theta}^* = \mathbf{0}_2$ is an equilibrium point and it holds that $d\mathbf{f}_\theta(\boldsymbol{\theta}^*) = -\mathbf{I}_2$; thus $\mathbf{n}^* = \mathbf{g}_\theta^n(\boldsymbol{\theta}^*)$ is asymptotically stable.

- Consider $\mathbf{f}_x : \mathbb{R}^3 \ni \mathbf{x} \mapsto \mathbf{f}_x(\mathbf{x}) := \mathbf{f}_n(\mathbf{x}) + \frac{1}{2}\mathbf{x}(1 - \mathbf{x}^T \mathbf{x}) \in \mathbb{R}^3$, where we emphasize that $\mathbf{f}_x(\mathbf{x}) = \mathbf{f}_n(\mathbf{x})$ for all $\mathbf{x} \in \mathbb{S}^2$. A linearization procedure around the equilibrium $\mathbf{x}^* = \mathbf{e}_1 \in \mathbb{S}^2$ yields $d\mathbf{f}_x(\mathbf{x}^*) = -\mathbf{I}_3$, and therefore stability is inferred from this linearization procedure (in particular, stability of \mathbf{x}^* w.r.t. \mathbf{f}_n is inferred).

Definition 1.3.8. (*Trajectory tracking*) Let \mathbf{f}_x be a vector field on a manifold Ω_x , i.e., $\mathbf{f}_x : \mathbb{R} \times \Omega_x \ni (t, \mathbf{x}) \mapsto \mathbf{f}_x(t, \mathbf{x}) \in T_{\mathbf{x}}\Omega_x$, and let $\mathbf{x} : \mathbb{R}_{\geq 0} \mapsto \Omega_x$ be a trajectory. Given a trajectory $\mathbf{x}^* \in \mathcal{C}^1(\mathbb{R}_{\geq 0}, \Omega_x)$ satisfying $\dot{\mathbf{x}}^*(t) = \mathbf{f}_x(t, \mathbf{x}^*(t))$ for all $t \in \mathbb{R}_{\geq 0}$, we say there is trajectory tracking if \mathbf{x} converges to \mathbf{x}^* as time evolves and for all $\mathbf{x}(0)$ in some neighborhood of $\mathbf{x}^*(0)$. We then call \mathbf{x}^* an equilibrium trajectory.

Remark 1.3.9. In Definition 1.3.8, when one says that \mathbf{x} converges to \mathbf{x}^* as time evolves, one can write $\lim_{t \rightarrow \infty} (\mathbf{x}(t) - \mathbf{x}^*(t)) = \mathbf{0}$ but with the caveat that the addition and the additive inverse are defined in Ω_x (if not, one must embed the manifold in some Euclidean space). On this issue, we also refer to the notion of contraction region as defined in [6].

Proposition 1.3.10. Denote (let $\tilde{\mathbb{R}}^3 := \mathbb{R}^3 \setminus \{\mathbf{0}_3\}$)

$$\tilde{\mathbb{R}}^3 \ni \mathbf{p} \mapsto \mathbf{n}(\mathbf{p}) := \frac{\mathbf{p}}{\|\mathbf{p}\|}, \quad (1.3.9)$$

$$\tilde{\mathbb{R}}^3 \times \tilde{\mathbb{R}}^3 \ni (\mathbf{p}, \mathbf{v}) \mapsto \boldsymbol{\omega}(\mathbf{p}, \mathbf{v}) := \mathcal{S}(\mathbf{n}(\mathbf{p})) \frac{\mathbf{v}}{\|\mathbf{p}\|}, \quad (1.3.10)$$

$$\tilde{\mathbb{R}}^3 \times \tilde{\mathbb{R}}^3 \times \tilde{\mathbb{R}}^3 \ni (\mathbf{p}, \mathbf{v}, \mathbf{a}) \mapsto \boldsymbol{\tau}(\mathbf{p}, \mathbf{v}, \mathbf{a}) := \mathcal{S}(\mathbf{n}(\mathbf{p})) \left(\frac{\mathbf{a}}{\|\mathbf{p}\|} - 2 \frac{\mathbf{v}}{\|\mathbf{p}\|} \frac{\mathbf{v}^T}{\|\mathbf{p}\|} \mathbf{n}(\mathbf{p}) \right). \quad (1.3.11)$$

Given $\mathbf{p}, \mathbf{v}, \mathbf{a} : \mathbb{R} \mapsto \mathbb{R}^3$ (with $\mathbf{p}(t) \neq \mathbf{0}$ for all $t \in \mathbb{R}$), satisfying $(\dot{\mathbf{p}}(t), \dot{\mathbf{v}}(t)) = (\mathbf{v}(t), \mathbf{a}(t))$ for all $t \in \mathbb{R}$, it follows that

$$\dot{\mathbf{n}}(\mathbf{p}(t)) = \mathcal{S}(\boldsymbol{\omega}(\mathbf{p}(t), \mathbf{v}(t))) \mathbf{n}(\mathbf{p}(t)), \quad (1.3.12)$$

$$\dot{\boldsymbol{\omega}}(\mathbf{p}(t), \mathbf{v}(t)) = \boldsymbol{\tau}(\mathbf{p}(t), \mathbf{v}(t), \mathbf{a}(t)). \quad (1.3.13)$$

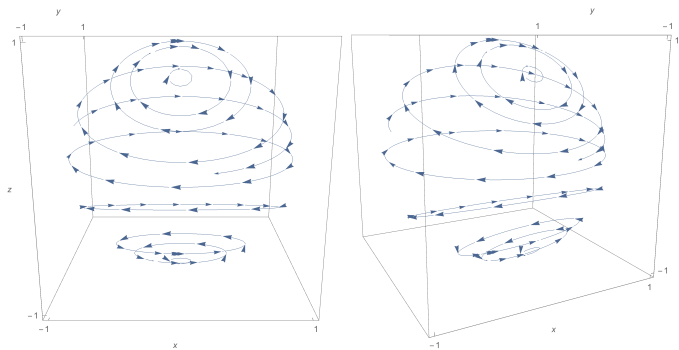
Proof. The proof follows from straightforward calculations. In what follows let $(\mathbf{p}, \mathbf{v}, \mathbf{a}) \in (\mathbb{R}^3)^3$. First, since

$$d\mathbf{n}(\mathbf{p})\mathbf{v} = \left(\mathbf{I} - \frac{\mathbf{p}}{\|\mathbf{p}\|} \frac{\mathbf{p}^T}{\|\mathbf{p}\|} \right) \frac{\mathbf{v}}{\|\mathbf{p}\|} = \Pi(\mathbf{n}(\mathbf{p})) \frac{\mathbf{v}}{\|\mathbf{p}\|} = \mathcal{S}(\boldsymbol{\omega}(\mathbf{p}, \mathbf{v})) \mathbf{n}(\mathbf{p}),$$

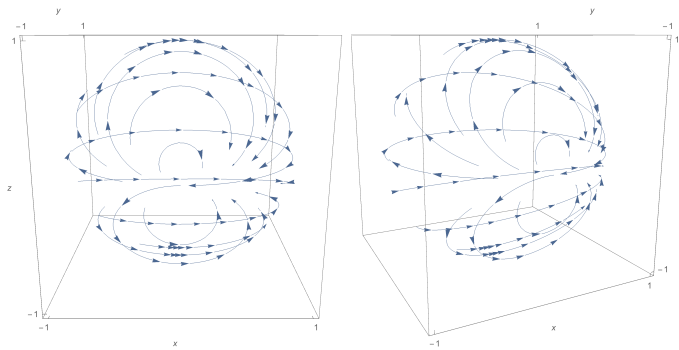
it follows that (1.3.12) holds. Secondly, since

$$\begin{aligned} & \partial_{\bar{\mathbf{p}}} \boldsymbol{\omega}(\bar{\mathbf{p}}, \mathbf{v})|_{\bar{\mathbf{p}}=\mathbf{p}} \mathbf{v} + \partial_{\bar{\mathbf{v}}} \boldsymbol{\omega}(\mathbf{p}, \bar{\mathbf{v}})|_{\bar{\mathbf{v}}=\mathbf{v}} \mathbf{a} = \\ &= \mathcal{S}(\mathbf{n}(\mathbf{p})) \frac{\mathbf{a}}{\|\mathbf{p}\|} - \mathcal{S}\left(\frac{\mathbf{v}}{\|\mathbf{p}\|}\right) \mathcal{S}(\boldsymbol{\omega}(\mathbf{p}, \mathbf{v})) \mathbf{n}(\mathbf{p}) - \mathcal{S}(\mathbf{n}(\mathbf{p})) \frac{\mathbf{v}}{\|\mathbf{p}\|} \frac{\mathbf{p}^T}{\|\mathbf{p}\|} \frac{\mathbf{v}}{\|\mathbf{p}\|} \\ &= \mathcal{S}(\mathbf{n}(\mathbf{p})) \frac{\mathbf{a}}{\|\mathbf{p}\|} + \mathbf{n}(\mathbf{p}) \frac{\mathbf{v}^T \boldsymbol{\omega}(\mathbf{p}, \mathbf{v})}{\|\mathbf{p}\|} - \boldsymbol{\omega}(\mathbf{p}, \mathbf{v}) \frac{\mathbf{v}^T \mathbf{n}(\mathbf{p})}{\|\mathbf{p}\|} - \mathcal{S}(\mathbf{n}(\mathbf{p})) \frac{\mathbf{v}}{\|\mathbf{p}\|} \frac{\mathbf{v}^T \mathbf{n}(\mathbf{p})}{\|\mathbf{p}\|} \\ &= \mathcal{S}(\mathbf{n}(\mathbf{p})) \left(\frac{\mathbf{a}}{\|\mathbf{p}\|} - 2 \frac{\mathbf{v}}{\|\mathbf{p}\|} \frac{\mathbf{v}^T}{\|\mathbf{p}\|} \mathbf{n}(\mathbf{p}) \right) = \boldsymbol{\tau}(\mathbf{p}, \mathbf{v}, \mathbf{a}), \end{aligned}$$

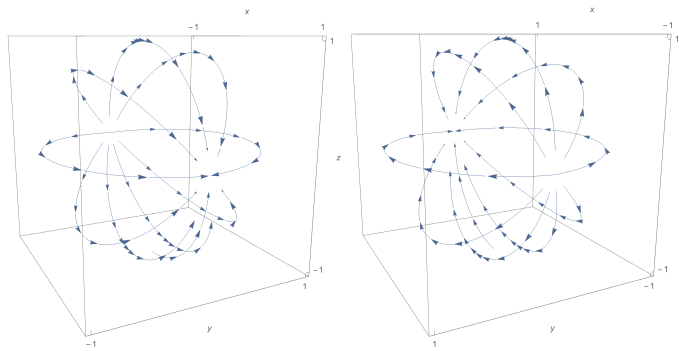
it follows that (1.3.13) holds. \square



(a) Two stable equilibria, but not attractive.



(b) One attractive equilibrium, but not stable.



(c) Two equilibria, one asymptotically stable (in focus in left) and one unattractive (in focus on the right).

Figure 1.4: Stability concepts illustrated for vector field in (1.3.8), for different values of $\mathbf{k} \in \mathbb{R}^3$. In the figures, the vector field is plotted on the sphere. (Each pair of figures above is computed for the same value of \mathbf{k} , but the same figure is presented from different perspectives.)

Chapter 2

Thrust propelled systems

In this chapter, the *abstract* notion of a thrust-propelled system is defined, and a controller is designed that steers the position of this system to the origin. The designed controller is a function of a subset of double integrator controllers and, as such, forms a family of controllers. One major benefit of this design process is the separation of the controller design steps: one may separately, and with no specific order, focus attention and design a bounded controller for a double integrator and a controller for a thrust-propelled system. Afterwards, different *physical* systems are, totally or partially, transformed into thrust-propelled systems, and the previous controller is immediately applicable. For those physical systems that are only partially transformed into thrust-propelled systems, one or more degrees of freedoms (DoFs) are left for which controllers must also be designed. The previous description is illustrated in Fig. 2.1, which pictorially describes the framework explored in this chapter.

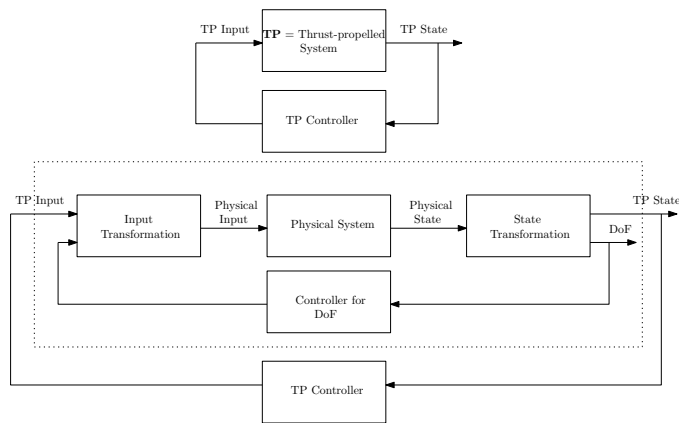


Figure 2.1: A physical system is, totally or partially, transformed into a thrust-propelled system, for which a controller is designed.

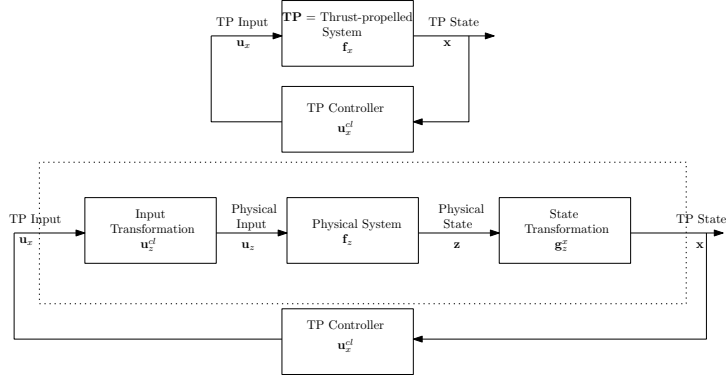


Figure 2.2: State, open-loop vector field, and input of the thrust-propelled system, and of a physical system. \mathbf{u}_x^{cl} is the control law for the thrust-propelled system, and \mathbf{g}_z^x is the mapping between the physical state (\mathbf{z}) and the thrust-propelled state (\mathbf{x}).

Let us provide some more details on the control design steps. Let \mathbf{x} , \mathbf{f}_x and \mathbf{u}_x represent, respectively, the state, the open-loop vector field, and the input to the thrust-propelled system. Similarly, let \mathbf{z} , \mathbf{f}_z and \mathbf{u}_z represent, respectively, the state, the open-loop vector field, and the input to a physical system. In the first section of this chapter, we design a control law \mathbf{u}_x^{cl} for the thrust-propelled system. In the following sections, we show that \mathbf{f}_x is in fact equivalent to \mathbf{f}_z , i.e., (see the notation in Section 1.3) we find a diffeomorphism \mathbf{g}_z^x and a function \mathbf{u}_z^{cl} such that, loosely speaking

$$\begin{aligned} \mathbf{x} = \mathbf{g}_z^x(t, \mathbf{z}) &\Rightarrow \dot{\mathbf{x}} = \partial_t \mathbf{g}_z^x(t, \mathbf{z}) + \partial_{\mathbf{z}} \mathbf{g}_z^x(t, \mathbf{z}) \dot{\mathbf{z}} \\ &\Rightarrow \mathbf{f}_x = (\partial_t \mathbf{g}_z^x(t, \mathbf{z}) + \partial_{\mathbf{z}} \mathbf{g}_z^x(t, \mathbf{z}) \mathbf{f}_z) |_{\mathbf{u}_z = \mathbf{u}_z^{cl}, \mathbf{z} = (\mathbf{g}_z^x(t, \cdot))^{-1}(\mathbf{x})}. \end{aligned} \quad (2.0.1)$$

As such, the control law \mathbf{u}_x^{cl} may be applied to control the physical system, owing to the equivalence above. Figure 2.2, illustrates the previous control design ideas.

2.1 Background

For the last decade, a great research effort has been put on executing tasks with aerial vehicles in complex, unstructured and dynamic environments. Compared to ground robots, aerial robots allow for manipulation tasks to be executed in difficult to access spaces, opening the doors to new applications, such as the inspection and maintenance of aging infrastructures [1]. Multi-rotor helicopters, and in particular quadrotors, are preferred to others types of UAVs owing to their capability to hover, to take off and land vertically, to the availability of inexpensive components and to their high maneuverability [7].

Multi-rotors have been used to perform complex automated tasks [8], including the construction of infrastructures useful in emergency scenarios [9], and manipulation tasks with grippers, robotic arms and cables [10–15]. Autonomy is usually

achieved with the help of vision [16–18], and stability of control laws may be guaranteed even when an extra load is attached to the aerial vehicle [19]. However, quadrotors and other multi-rotors form a class of under-actuated systems. The dynamics of an n -dimensional generalized coordinate of an under-actuated system cannot be reduced to those of n decoupled double integrator systems, which explains why control of aerial vehicles exhibits specific challenges.

Apart from research on stabilization and on trajectory tracking of quadrotors [8, 20, 21], there is also noteworthy research on using quadrotors to perform specific tasks [9, 11–13, 17, 19, 22–25], which include, among other examples, coverage, vision-based navigation, interaction with the environment by means of a mobile manipulator and construction of three-dimensional structures. In [22], a strategy for (almost) time-optimal coverage of simple 3D objects by a UAV that is moving with constant speed is proposed. In [17], quadrotors use onboard cameras in combination with inertial sensors for navigation, essential in GPS denied environments; it also describes how to create maps of previously unknown terrains. [12] describes a controller for a quadrotor with a moving a manipulator in contact with another object and along the surface of the object. In [19], grasping of objects from the ground is achieved with a small UAV helicopter that is controlled with a PID controller. In [11], an adaptive controller that compensates forces exerted between a manipulator and a quadrotor is proposed. Quadrotors with fixed manipulators moving a cart on rails is found in [23]. In [13], multiple UAVs, rigidly connected to different points of a single load, carry that load by means of a sliding mode controller in combination with a trajectory planner that uses the RRT* algorithm. Quadcopters building three-dimensional structures consisting of ropes is also demonstrated in [9].

In this chapter, the focus is on two particular systems, namely the slung load system and a system composed of a rigid manipulator attached to an aerial vehicle.

In a slung load system, an aerial vehicle and a load are attached to each other by a cable, and the control challenge lies in dampening the sway of the load with respect to the transporting vehicle. Slung load transportation by aerial vehicles is an under-actuated problem for which trajectory tracking control strategies are necessary [26]. A model of this system is found in [27], and controllers for position trajectory tracking of the load are found in the literature [14, 26, 26, 28–32]. Controllers for helicopters with experimental validation are found in [26, 28], where vision was used to estimate the state used in the feedback loop. For quadrotors, controllers are found in [14, 29–33], which explore differential flatness for planning trajectories for the transporting quadrotors and which minimize sway; or which explore the dynamics to design controllers based on Lyapunov methods, such as backstepping. Adaptive strategies that compensate for the presence of unmodeled or unknown parameters, such as the load’s mass or the cables lengths, are also found [28, 34]. Load lifting by multiple aerial vehicles has also been studied and is found in [10, 14, 35]. In particular, in [10], the relations in static equilibrium between three quadrotors and a load are analyzed. In [14] a controller is designed for three of more vehicles transporting a rigid body. In [35], a control architecture for deploying cooperative missions between multiple UAVs is described and experimentally validated, where

the interactions between UAVs are not only the physical couplings (associated to the joint transportation of a single load) but also the information exchanges.

A slung load system, despite mechanically simple (only a cable is necessary), is not adequate in scenarios of constrained manipulation, since the load's position relative to the transporting UAV depends on the trajectory the load is required to track. Different forms of manipulation with aerial vehicles are found in the literature, and most take advantage of trajectory tracking controllers for quadrotors such as those found in [20]. One approach to manipulation is by means of a gripper attached to an aerial vehicle. In [36, 37], a gripper is mounted under a UAV that grasps, holds and transports an object. Carrying an external load rigidly attached to the UAV body through a gripper changes the flight characteristics of the aerial vehicle, such as the inertia of the system, and [37] provides bounds on the controller gains that guarantee that stability is preserved when a load is gripped. In [38], the problem of high-speed grasping and transportation of loads is studied, and it draws inspiration from aerial hunting by birds of prey. In [39], a team of quadrotors are employed to collaboratively pick up an object using a similar gripper.

An alternative to a gripper is a robotic manipulator with actuated joints, which provide additional degrees of freedom [40]. Control strategies for UAVs with robotic manipulators are found that consider the UAV and manipulator as two independent subsystems, and their coupling is seen as an external disturbance to each other. In [41, 42], the controller considers the variation of the center of mass position and of the inertia matrix caused by the manipulator motion. A task-based control strategy is proposed in [43], where the manipulator tracks the aerial robot attitude dynamics during all the translational motion. In [24], the manipulator static effects on the UAV are estimated and compensated through the thrust and torques with a multilayer architecture control. In [44, 45], the problem of disturbance due to the manipulator's presence is handled by adaptation of the control law. In [44], the problem of disturbance due to the manipulator's presence is handled by adaptation of an outer (position) control loop that compensates the external moments introduced on the airframe, while the manipulator is controlled with an independent joint control method. In [45], an adaptive controller also considers the manipulator's motion in its adaptation, and it is compared with another controller that ignores the manipulator's presence.

The focus of this chapter is mainly on the slung load system and on the system composed of a rigid manipulator attached to an aerial vehicle. Both systems are transformed into the thrust-propelled system form, which is described in the next section, and for which a controller is also proposed in the same section.

2.2 Control of the thrust-propelled system

In this section, the vector field of the thrust-propelled system is described and a controller that steers the system's position towards the origin is presented. A thrust-propelled system is composed of a three dimensional position and velocity, and a

three dimensional body direction and angular velocity. The system is controlled via a thrust input along the body direction, and via a torque that acts on the angular velocity, and thus on the body direction along which thrust is provided. We propose a control law, which is constructed by means of a backstepping procedure, and that steers the position of the thrust-propelled system to the origin. The results here presented are based on those in [46].

2.2.1 Background

The thrust-propelled system here presented is similar to a quadrotor system, and thus the control design steps presented in this section share similarities with the control design steps found in trajectory tracking controllers for quadrotors. Many control strategies have been proposed for quadrotor position trajectory tracking [8, 20, 21, 47–51], which range from linearization techniques [47, 48] to global and robust techniques [50, 51].

2.2.2 Notation

TPS	Thrust-propelled system
$\mathbf{p} = (p_x, p_y, p_z) \in \mathbb{R}^3$	Position of TPS
$\mathbf{v} = (v_x, v_y, v_z) \in \mathbb{R}^3$	Velocity of TPS
$\mathbf{n} = (n_x, n_y, n_z) \in \mathbb{S}^2$	Thrust propelling direction of TPS
$\boldsymbol{\omega} = (\omega_x, \omega_y, \omega_z) \in \mathbb{R}^3$	Angular velocity of thrust propelling direction of TPS
$\mathbf{x} = (\mathbf{p}, \mathbf{v}, \mathbf{n}, \boldsymbol{\omega}) \in \mathbb{R}^{12}$	State of the TPS
$\xi = (\mathbf{p}, \mathbf{v}) \in (\mathbb{R}^3)^2$	Partial state of the TPS
$\bar{\mathbf{x}} = (\xi, \mathbf{n}) \in \mathbb{R}^6 \times \mathbb{S}^2$	Partial state of the TPS
$T \in \mathbb{R}_{\geq 0}$	Thrust input to the TPS
$\boldsymbol{\tau} \in \mathbb{R}^3$	Torque input input to the TPS
$\mathbf{u}_x = (T, \boldsymbol{\tau})$	Input to the TPS

In this Section, given $\mathbf{x} = (x_1, x_2, x_3) \in \mathbb{R}^3$ and $\mathbf{r} = (r_1, r_2, r_3) \in ((0, \infty))^3$ we denote $\bar{\mathcal{B}}(\mathbf{r}, \mathbf{x}) := \{(y_1, y_2, y_3) \in \mathbb{R}^3 : |y_i - x_i| \leq r_i, i \in \{1, 2, 3\}\}$ as the box centered around \mathbf{x} and with sides of length $2\mathbf{r}$.

2.2.3 System Model

Given the definitions in the notation above, let us describe next the thrust-propelled system, which is illustrated in Fig 2.3. Denote (see Remark 2.2.2, in page 19)

$$\mathbf{x} := (\bar{\mathbf{x}}, \boldsymbol{\omega}) := ((\xi, \mathbf{n}), \boldsymbol{\omega}) := (((\mathbf{p}, \mathbf{v}), \mathbf{n}), \boldsymbol{\omega}) \in \Omega_x, \quad (2.2.1)$$

$$\mathbf{u}_x := (T, \boldsymbol{\tau}) \in \mathbb{R}_{\geq 0} \times \mathbb{R}^3 =: \mathcal{U}_x, \quad (2.2.2)$$

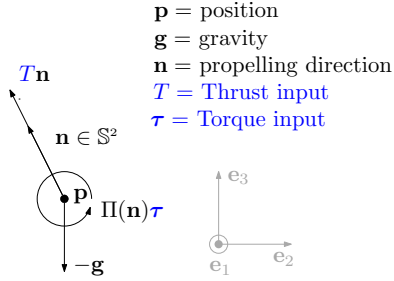


Figure 2.3: Thrust-propelled system: thrust T along body direction \mathbf{n} which can be rotated by means of the torque $\boldsymbol{\tau}$.

with \mathbf{x} and \mathbf{u}_x as the state of and input to the thrust-propelled system, and where

$$\Omega_{\bar{x}} = \{(\mathbf{p}, \mathbf{v}, \mathbf{n}) \in (\mathbb{R}^3)^3 : \mathbf{n}^T \mathbf{n} = 1\} = \mathbb{R}^6 \times \mathbb{S}^2, \quad (2.2.3)$$

$$\Omega_x = \{((\mathbf{p}, \mathbf{v}, \mathbf{n}), \boldsymbol{\omega}) \in \Omega_{\bar{x}} \times \mathbb{R}^3 : \mathbf{n}^T \boldsymbol{\omega} = 0\}, \quad (2.2.4)$$

$$T_x \Omega_x = \{(\delta\mathbf{p}, \delta\mathbf{v}, \delta\mathbf{n}, \delta\boldsymbol{\omega}) \in (\mathbb{R}^3)^4 : \mathbf{n}^T \delta\mathbf{n} = 0, \delta\mathbf{n}^T \boldsymbol{\omega} + \mathbf{n}^T \delta\boldsymbol{\omega} = 0\}, \quad (2.2.5)$$

denote, respectively, the state set and the tangent space of Ω_x at $\mathbf{x} \in \Omega_x$. Consider an appropriate $\mathbf{u}_x := (T, \boldsymbol{\tau}) : \mathbb{R}_{\geq 0} \mapsto \mathcal{U}_x$, and consider $\mathbf{x} := (\mathbf{p}, \mathbf{v}, \mathbf{n}, \boldsymbol{\omega}) : \mathbb{R}_{\geq 0} \ni t \mapsto \mathbf{x}(t) \in \Omega_x$ which evolves according to

$$\dot{\mathbf{x}}(t) = \mathbf{f}_x(t, \mathbf{x}(t), \mathbf{u}_x(t)), \mathbf{x}(0) \in \Omega_x, \quad (2.2.6)$$

where $\mathbf{f}_x : \mathbb{R}_{\geq 0} \times \Omega_x \times \mathcal{U}_x \ni (t, \mathbf{x}, \mathbf{u}_x) \mapsto \mathbf{f}_x(t, \mathbf{x}, \mathbf{u}_x) \in T_x \Omega_x$ is given by (consider \mathbf{x} as in (2.2.1) and \mathbf{u}_x as in (2.2.2))

$$\mathbf{f}_x(t, \mathbf{x}, \mathbf{u}_x) := (\mathbf{f}_{\bar{x}}(t, \bar{\mathbf{x}}, \boldsymbol{\omega}, T), \mathbf{f}_{\omega}(\mathbf{n}, \boldsymbol{\tau})) \quad (2.2.7)$$

$$:= ((\mathbf{f}_{\xi}(t, \bar{\mathbf{x}}, T), \mathbf{f}_n(\mathbf{n}, \boldsymbol{\omega})), \mathbf{f}_{\omega}(\mathbf{n}, \boldsymbol{\tau})) \quad (2.2.8)$$

$$:= (((\mathbf{v}, T\mathbf{n} - \mathbf{g}(t)), \mathcal{S}(\boldsymbol{\omega})\mathbf{n}), \Pi(\mathbf{n})\boldsymbol{\tau}) \quad (2.2.9)$$

$$= (\mathbf{v}, T\mathbf{n} - \mathbf{g}(t), \mathcal{S}(\boldsymbol{\omega})\mathbf{n}, \Pi(\mathbf{n})\boldsymbol{\tau}). \quad (2.2.10)$$

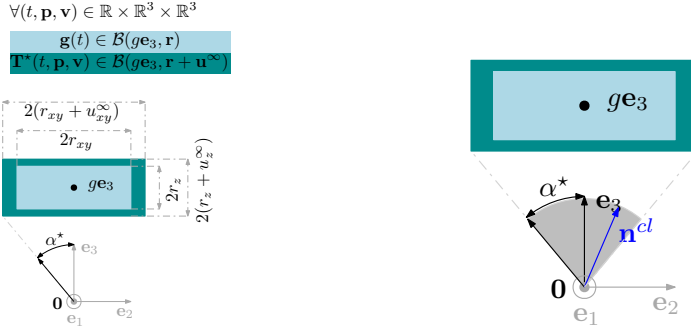
and where, given $\mathbf{r} = (r_{xy}, r_{xy}, r_z) \in ((0, \infty))^3$,

$$\mathbf{g} \in \mathcal{C}^2(\mathbb{R}, \bar{\mathcal{B}}(g\mathbf{e}_3, \mathbf{r})), \text{ with } \max_{i \in \{0, 1, 2\}} \sup_{t \in \mathbb{R}} \|\mathbf{g}^{(i)}(t)\| < \infty, \quad (2.2.11)$$

is a known time-varying gravity term (see the definition of box $\bar{\mathcal{B}}$ in the notation of this section). We thus assume that \mathbf{g} is sufficiently smooth with essentially bounded derivatives; and that the image of \mathbf{g} is contained in a box around a constant gravity term $g\mathbf{e}_3$, as illustrated in Fig 2.4a. For reasons that will be apparent later, we require $r_z < g$, which implies that $\mathbf{0} \notin \bar{\mathcal{B}}(g\mathbf{e}_3, \mathbf{r})$. Also notice that $\mathbf{f}_x(t, \mathbf{x}, \mathbf{u}_x) \in T_x \Omega_x$, for any $(t, \mathbf{x}, \mathbf{u}_x) \in \mathbb{R} \times \Omega_x \times \mathcal{U}_x$, implying that Ω_x is indeed positively invariant. In fact, if $(\delta\mathbf{p}, \delta\mathbf{v}, \delta\mathbf{n}, \delta\boldsymbol{\omega}) \stackrel{(2.2.10)}{=} \mathbf{f}_x(t, \mathbf{x}, \mathbf{u}_x)$ it follows that

$$\mathbf{n}^T \delta\mathbf{n} \stackrel{(2.2.10)}{=} \mathbf{n}^T \mathcal{S}(\boldsymbol{\omega})\mathbf{n} = 0, \quad (2.2.12)$$

$$\delta\mathbf{n}^T \boldsymbol{\omega} + \mathbf{n}^T \delta\boldsymbol{\omega} \stackrel{(2.2.10)}{=} -\mathbf{n}^T \mathcal{S}(\boldsymbol{\omega})\boldsymbol{\omega} + \mathbf{n}^T \Pi(\mathbf{n})\boldsymbol{\tau} = 0, \quad (2.2.13)$$

(a) Illustration of boxes around ge_3 and α^* . (b) Illustration of Proposition 2.2.6.**Figure 2.4:** Illustrations for boxes that contain the gravity \mathbf{g} and the control law \mathbf{T}^{cl} .

and thus, it follows from (2.2.5) that, indeed $(\delta\mathbf{p}, \delta\mathbf{v}, \delta\mathbf{n}, \delta\boldsymbol{\omega}) = \mathbf{f}_x(t, \mathbf{x}, \mathbf{u}_x) \in T_{\mathbf{x}}\Omega_x$.

Problem 2.2.1. Given the open loop vector field (2.2.10), design $\mathbf{u}_x = (T, \boldsymbol{\tau}) : \mathbb{R}_{\geq 0} \mapsto \mathbb{R}^3$ such that $\lim_{t \rightarrow \infty} \mathbf{p}(t) = \mathbf{0}$ along trajectories of (2.2.6).

Remark 2.2.2. The decomposition of the state in (2.2.1) and of the vector field in (2.2.10) in three parts (namely, ξ , $\bar{\mathbf{x}}$ and \mathbf{x} ; and \mathbf{f}_ξ , $\mathbf{f}_{\bar{\mathbf{x}}}$ and \mathbf{f}_x) will become clear next, and, in foresight, it is related with the fact that the controller design is done in three steps.

Remark 2.2.3. Many trajectory tracking problems can be converted into the form (2.2.10), and restated as in Problem 2.2.1, which is the topic of the next sections. Our approach is particularly motivated by quadrotor control applications.

2.2.4 Control Design

We design the controller in three steps. These three steps justify the definitions made in the state definition (2.2.1) and the open loop vector field definition (2.2.10). First, we construct a thrust $T^{cl} : \mathbb{R}_{\geq 0} \times \Omega_{\bar{\mathbf{x}}} \ni (t, \bar{\mathbf{x}}) \mapsto T^{cl}(t, \bar{\mathbf{x}}) \in \mathbb{R}$ such that the vector field

$$\mathbf{f}_\xi^{cl} : \mathbb{R}_{\geq 0} \times \Omega_{\bar{\mathbf{x}}} \ni (t, \bar{\mathbf{x}}) \mapsto \mathbf{f}_\xi^{cl}(t, \bar{\mathbf{x}}) := \mathbf{f}_\xi(t, \bar{\mathbf{x}}, T^{cl}(t, \bar{\mathbf{x}})) \quad (2.2.14)$$

approximates that of a double integrator, up to an error. In the second step, we construct an angular velocity that guarantees that the previous error is steered to $\mathbf{0}$; more precisely, we construct a $\boldsymbol{\omega}^{cl} : \mathbb{R}_{\geq 0} \times \Omega_{\bar{\mathbf{x}}} \ni (t, \bar{\mathbf{x}}) \mapsto \boldsymbol{\omega}^{cl}(t, \bar{\mathbf{x}}) \in \mathbb{R}^3$ such that $\lim_{t \rightarrow \infty} \dot{\mathbf{p}}(t) = \mathbf{0}$ along trajectories satisfying $\dot{\bar{\mathbf{x}}}(t) = \mathbf{f}_{\bar{\mathbf{x}}}^{cl}(t, \bar{\mathbf{x}}(t))$, where

$$\begin{aligned} \mathbf{f}_{\bar{\mathbf{x}}}^{cl} : \mathbb{R}_{\geq 0} \times \Omega_{\bar{\mathbf{x}}} \ni (t, \bar{\mathbf{x}}) &\mapsto \mathbf{f}_{\bar{\mathbf{x}}}^{cl}(t, \bar{\mathbf{x}}) := \mathbf{f}_{\bar{\mathbf{x}}}(t, \bar{\mathbf{x}}, \boldsymbol{\omega}^{cl}(t, \bar{\mathbf{x}}), T^{cl}(t, \bar{\mathbf{x}})) \\ &= (\mathbf{f}_\xi^{cl}(t, \bar{\mathbf{x}}), \mathbf{f}_n(\mathbf{n}, \boldsymbol{\omega}^{cl}(t, \bar{\mathbf{x}}))) \end{aligned} \quad (2.2.15)$$

and where \mathbf{f}_ξ^{cl} is given from the first step, in (2.2.14). In the final step, we design $\boldsymbol{\tau}^{cl} : \mathbb{R}_{\geq 0} \times \Omega_x \ni (t, \mathbf{x}) \mapsto \boldsymbol{\tau}^{cl}(t, \mathbf{x}) \in \mathbb{R}^3$ that steers the error $\mathbf{e} : \mathbb{R}_{\geq 0} \times \Omega_x \ni (t, \mathbf{x}) \mapsto$

$\mathbf{e}(t, \mathbf{x}) = \mathcal{S}(\mathbf{n})(\boldsymbol{\omega} - \boldsymbol{\omega}^{cl}(t, \bar{\mathbf{x}})) \in \mathbb{R}^3$ to zero. This design follows a backstepping procedure, and, in the end, Problem 2.2.1 is satisfied along trajectories satisfying $\dot{\mathbf{x}}(t) = \mathbf{f}_x^{cl}(t, \mathbf{x}(t))$, where

$$\begin{aligned}\mathbf{f}_x^{cl} : \mathbb{R}_{\geq 0} \times \Omega_x &\ni (t, \mathbf{x}) \mapsto \mathbf{f}_x^{cl}(t, \mathbf{x}) := \mathbf{f}_x(t, \mathbf{x}, \mathbf{u}_x^{cl}(t, \bar{\mathbf{x}})) \\ &:= \mathbf{f}_x(t, \mathbf{x}, (T^{cl}(t, \bar{\mathbf{x}}), \boldsymbol{\tau}^{cl}(t, \mathbf{x}))).\end{aligned}\quad (2.2.16)$$

First Step

Consider the double integrator system $\boldsymbol{\xi} = (\mathbf{p}, \mathbf{v}) : \mathbb{R}_{\geq 0} \ni t \mapsto \boldsymbol{\xi} \in (\mathbb{R}^3)^2$, which, given $\mathbf{u} : \mathbb{R}_{\geq 0} \ni t \mapsto \mathbf{u}(t) \in \mathbb{R}^3$, evolves according to $\dot{\boldsymbol{\xi}}(t) = \mathbf{f}_{di}(\boldsymbol{\xi}(t), \mathbf{u}(t))$ where

$$\mathbf{f}_{di} : \mathbb{R}^6 \times \mathbb{R}^3 \ni (\boldsymbol{\xi}, \mathbf{u}) \mapsto \mathbf{f}_{di}(\boldsymbol{\xi}, \mathbf{u}) := (\mathbf{v}, \mathbf{u}) \in \mathbb{R}^6.\quad (2.2.17)$$

Definition 2.2.4. Let $\mathbf{u}_{di}^{cl} : \mathbb{R}^6 \ni \boldsymbol{\xi} \mapsto \mathbf{u}_{di}^{cl}(\boldsymbol{\xi}) \in \mathbb{R}^3$ and denote $\mathbf{f}_{di}^{cl} : \mathbb{R}^6 \ni \boldsymbol{\xi} \mapsto \mathbf{f}_{di}^{cl}(\boldsymbol{\xi}) := \mathbf{f}_{di}(\boldsymbol{\xi}(t), \mathbf{u}_{di}^{cl}(\boldsymbol{\xi})) \in \mathbb{R}^6$. We say that $\mathbf{u}_{di}^{cl} \in \mathcal{C}^{di}$ if

1. $\mathbf{u}_{di}^{cl} \in \mathcal{C}^2(\mathbb{R}^6, \bar{\mathcal{B}}(\mathbf{0}, \mathbf{u}^\infty))$, where $\mathbf{u}^\infty := (u_{xy}^\infty, u_{xy}^\infty, u_z^\infty) \in ((0, \infty])^2 \times (0, g - r_z)$.

2. there exists a positive definite $V_{di} \in \mathcal{C}^2(\mathbb{R}^6, \mathbb{R}_{\geq 0})$ such that, for all $\boldsymbol{\xi} \in \mathbb{R}^6$,

a) $V_{di}(\boldsymbol{\xi}) \geq \alpha_{di}(\|\boldsymbol{\xi}\|)$ for some $\alpha_{di} \in \mathcal{K}^\infty$, and

b) $W_{di} \in \mathcal{C}^1(\mathbb{R}^6, \mathbb{R})$, given by $W_{di}(\boldsymbol{\xi}) := -dV_{di}(\boldsymbol{\xi})\mathbf{f}_{di}^{cl}(\boldsymbol{\xi})$, is positive definite.

It follows from Definition 2.2.4 that, given $\mathbf{u}_{di}^{cl} \in \mathcal{C}^{di}$, $\lim_{t \rightarrow \infty} \mathbf{p}(t) = 0$ along solutions of $\dot{\boldsymbol{\xi}}(t) = (\dot{\mathbf{p}}(t), \dot{\mathbf{v}}(t)) = \mathbf{f}_{di}(\boldsymbol{\xi}(t), \mathbf{u}_{di}^{cl}(\boldsymbol{\xi}(t)))$ for any $\boldsymbol{\xi}(0) \in \mathbb{R}^6$. This is the case, since $\sup_{t \geq 0} \|\boldsymbol{\xi}(t)\| < \infty$ and therefore, from positive definiteness of W_{di} , it follows that

$$\lim_{t \rightarrow \infty} W_{di}(\boldsymbol{\xi}(t)) = 0 \Rightarrow \lim_{t \rightarrow \infty} \boldsymbol{\xi}(t) = 0.\quad (2.2.18)$$

Hereafter, let $\mathbf{u}_{di}^{cl} \in \mathcal{C}^{di}$ be a chosen controller for the double integrator system. In Subsection 2.2.5, one can find an example of such a control law. Consider then $\mathbf{T}^{cl} \in \mathcal{C}^2(\mathbb{R}_{\geq 0} \times \mathbb{R}^6, \bar{\mathcal{B}}(g\mathbf{e}_3, \mathbf{r} + \mathbf{u}^\infty))$, given by

$$\mathbf{T}^{cl} : \mathbb{R}_{\geq 0} \times \mathbb{R}^6 \ni (t, \boldsymbol{\xi}) \mapsto \mathbf{T}^{cl}(t, \boldsymbol{\xi}) := \mathbf{g}(t) + \mathbf{u}_{di}^{cl}(\boldsymbol{\xi}) \in \bar{\mathcal{B}}(g\mathbf{e}_3, \mathbf{r} + \mathbf{u}^\infty),\quad (2.2.19)$$

which corresponds to the three dimensional force that one would choose if $T\mathbf{n}$ in (2.2.10) were a control input.

Remark 2.2.5. The spirit of the proposed controller is that it is a function of an externally provided controller for a double integrator satisfying the conditions of Definition 2.2.4. In this spirit, the notation

$$\mathbf{T}^{cl} : \mathbb{R}_{\geq 0} \times \mathcal{C}^{di} \ni (t, \mathbf{u}_{di}^{cl}) \mapsto \mathbf{T}^{cl}(t, \mathbf{u}_{di}^{cl}) := \mathbf{g}(t) + \mathbf{u}_{di}^{cl} \in \mathcal{C}^2(\mathbb{R}^6, \bar{\mathcal{B}}(g\mathbf{e}_3, \mathbf{r} + \mathbf{u}^\infty)),\quad (2.2.20)$$

is more appropriate since, given $(t, \mathbf{u}_{di}^{cl}) \in \mathbb{R}_{\geq 0} \times \mathcal{C}^{di}$, $\mathbf{T}^{cl}(t, \mathbf{u}_{di}^{cl})$ is a function rather than a three dimensional force. On the other hand, pointwise, i.e., given an $\xi \in \mathbb{R}^6$,

$$\mathbf{T}^{cl}(t, \mathbf{u}_{di}^{cl})(\xi) = \mathbf{g}(t) + \mathbf{u}_{di}^{cl}(\xi) \in \bar{\mathcal{B}}(g\mathbf{e}_3, \mathbf{r} + \mathbf{u}^\infty),$$

which is then the three dimensional force contained in $\bar{\mathcal{B}}(g\mathbf{e}_3, \mathbf{r} + \mathbf{u}^\infty)$. Another possible notation is one where

$$\mathbf{T}^{cl} : \mathbb{R}_{\geq 0} \times \mathcal{C}^{di} \times \mathbb{R}^6 \ni (t, \mathbf{u}_{di}^{cl}, \xi) \mapsto \mathbf{T}^{cl}(t, \mathbf{u}_{di}^{cl}, \xi) := \mathbf{g}(t) + \mathbf{u}_{di}^{cl}(\xi) \in \bar{\mathcal{B}}(g\mathbf{e}_3, \mathbf{r} + \mathbf{u}^\infty). \quad (2.2.21)$$

Both notations (2.2.20) and (2.2.21) make explicit the dependency of the control law on a controller for a double integrator satisfying the conditions of Definition 2.2.4. However, both notations are dismissed due to their more involved notation.

Notice the codomain and smoothness properties of (2.2.19) follows from (2.2.11) and the conditions in Definition 2.2.4. Since, $g - r_z - u_z^\infty > 0$, it follows that $\|\mathbf{T}^{cl}(\cdot, \cdot)\| \geq g - r_z - u_z^\infty > 0$. We can then define the unit vector associated to (2.2.19), $\mathbf{n}^{cl} \in \mathcal{C}^2(\mathbb{R}_{\geq 0} \times \mathbb{R}^6, \mathbb{S}^2)$, given by

$$\mathbf{n}^{cl} : \mathbb{R}_{\geq 0} \times \mathbb{R}^6 \ni (t, \xi) \mapsto \mathbf{n}^{cl}(t, \xi) := \frac{\mathbf{T}^{cl}(t, \mathbf{u}_{di}^{cl}(\xi))}{\|\mathbf{T}^{cl}(t, \mathbf{u}_{di}^{cl}(\xi))\|} \in \mathbb{S}^2, \quad (2.2.22)$$

whose smoothness properties follow from (2.2.19). Denote also $\mathbf{n}^* \in \mathcal{C}^2(\mathbb{R}_{\geq 0}, \mathbb{S}^2)$, defined as

$$\mathbf{n}^* : \mathbb{R}_{\geq 0} \ni t \mapsto \mathbf{n}^*(t) := \mathbf{n}^{cl}(t, \mathbf{u}_{di}^{cl}(\mathbf{0})) = \mathbf{n}^{cl}(t, \mathbf{0}) = \frac{\mathbf{g}(t)}{\|\mathbf{g}(t)\|} \in \mathbb{S}^2, \quad (2.2.23)$$

as the equilibrium thrust propelling direction. It then follows that

$$\lim_{\xi \rightarrow 0} \|\mathcal{S}(\mathbf{n}) \mathbf{n}^{cl}(t, \mathbf{u}_{di}^{cl}(\xi))\| = 0 \Rightarrow \mathbf{n} = \pm \mathbf{n}^*(t), \forall (t, \mathbf{n}) \in \mathbb{R}_{\geq 0} \times \mathbb{S}^2. \quad (2.2.24)$$

Proposition 2.2.6. Consider (2.2.22) and recall Definition 1.3.3. It follows that, in fact, $\mathbf{n}^{cl} : \mathbb{R}_{\geq 0} \times \mathbb{R}^6 \mapsto \mathcal{C}\left(\frac{\pi}{2}, \mathbf{e}_3\right)$. Moreover, if $u_{xy}^\infty < \infty$ in Definition 2.2.4, then $\mathbf{n}^{cl} : \mathbb{R}_{\geq 0} \times \mathbb{R}^6 \mapsto \mathcal{C}(\alpha^*, \mathbf{e}_3)$ with α^* as defined in (2.2.25).

Proof. Let $(t, \xi) \in \mathbb{R}_{\geq 0} \times \mathbb{R}^6$. Given (2.2.22), it follows from (2.2.11) and Definition 2.2.4 that

$$\begin{aligned} \mathbf{e}_3^T \mathbf{n}^{cl}(t, \xi) &= \frac{\mathbf{e}_3^T(\mathbf{g}(t) + \mathbf{u}_{di}^{cl}(\xi))}{\|\mathbf{g}(t) + \mathbf{u}_{di}^{cl}(\xi)\|} = \frac{\mathbf{e}_3^T(\mathbf{g}(t) + \mathbf{u}_{di}^{cl}(\xi))}{\sqrt{\sum_{i=1}^{i=3} (\mathbf{e}_i^T(\mathbf{g}(t) + \mathbf{u}_{di}^{cl}(\xi)))^2}} \\ &\geq \frac{g - r_z - u_z^\infty}{\sqrt{(g - r_z - u_z^\infty)^2 + 2(r_{xy} + u_{xy}^\infty)^2}} =: \cos(\alpha^*) \geq \cos\left(\frac{\pi}{2}\right) = 0. \end{aligned} \quad (2.2.25)$$

Moreover, $\lim_{u_{xy}^\infty \rightarrow \infty} \alpha^* \stackrel{(2.2.25)}{=} \frac{\pi}{2}$. The Proposition's conclusion follows then immediately from Definition 1.3.3. \square

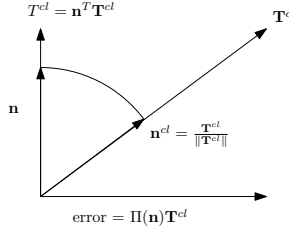


Figure 2.5: Illustration of reasoning for control law (2.2.26).

As shall be seen later, \mathbf{n}^{cl} corresponds to the desired thrust propelling direction. Thus, Proposition 2.2.6 guarantees that \mathbf{n}^{cl} points upwards for any time instant $t \in \mathbb{R}_{\geq 0}$ and any position and velocity $(\mathbf{p}, \mathbf{v}) \in \mathbb{R}^6$ (i.e., $\mathbf{e}_3^T \mathbf{n}^{cl}(t, \mathbf{p}, \mathbf{v}) > 0$, see Fig 2.4b). Notice that $\mathbf{e}_3^T \mathbf{n} < 0$ implies a pitch angle greater than 90° which may violate safety constraints, and thus \mathbf{n}^{cl} never requires the desired pitch to be greater than 90° .

Proposition 2.2.7. Consider (2.2.22), α^* as in Proposition 2.2.6 and recall Definition 1.3.3. Let $\boldsymbol{\nu} \in \mathcal{C}(\delta, \mathbf{e}_3)$ for some $\delta \in [0, \frac{\pi}{2}]$. If $u_{xy}^\infty < \infty$, it follows that $\boldsymbol{\nu} \in \mathcal{C}(\delta + \alpha^*, \mathbf{n}^{cl}(t, \xi)) \Leftrightarrow 1 - \boldsymbol{\nu}^T \mathbf{n}^{cl}(t, \xi) < 1 - \cos(\delta + \alpha^*)$ for all $(t, \xi) \in \mathbb{R}_{\geq 0} \times \mathbb{R}^6$. If $u_{xy}^\infty = \infty$, the same conclusion holds if α^* is replaced by $\frac{\pi}{2}$.

Proof. Let $(t, \xi) \in \mathbb{R}_{\geq 0} \times \mathbb{R}^6$, and, for brevity, denote $\theta_1 := \arccos(\mathbf{e}_3^T \mathbf{n}^{cl}(t, \xi))$, $\theta_2 := \arccos(\mathbf{e}_3^T \boldsymbol{\nu}) < \delta$ and $\theta := \arccos(\boldsymbol{\nu}^T \mathbf{n}^{cl}(t, \xi))$. Consider the case $u_{xy}^\infty < \infty$. From Proposition 2.2.6, $\theta_1 \leq \alpha^*$. Thus, $\theta_1 + \theta_2 < \alpha^* + \delta$. Then, since $\arccos(\boldsymbol{\nu}^T \mathbf{n}^{cl}(t, \xi)) = \theta \leq \theta_1 + \theta_2$, it follows that $1 - \boldsymbol{\nu}^T \mathbf{n}^{cl}(t, \xi) < 1 - \cos(\delta + \alpha^*) \stackrel{\text{Def. 1.3.3}}{\Leftrightarrow} \boldsymbol{\nu} \in \mathcal{C}(\delta + \alpha^*, \mathbf{n}^{cl}(t, \xi))$, for all $(t, \xi) \in \mathbb{R}_{\geq 0} \times \mathbb{R}^6$. For $u_{xy}^\infty = \infty$, it suffices to replace α^* by $\frac{\pi}{2}$, since $\theta_2 < \delta$. \square

For the thrust controller, we propose then the control law $T^{cl} \in \mathcal{C}^2(\mathbb{R}_{\geq 0} \times \Omega_{\bar{x}}, \mathbb{R})$, defined as

$$T^{cl} : \mathbb{R}_{\geq 0} \times \Omega_{\bar{x}} \ni (t, \bar{x}) \mapsto T^{cl}(t, \bar{x}) := \mathbf{n}^T \mathbf{T}^{cl}(t, \xi) \in \mathbb{R}, \quad (2.2.26)$$

which is the projection of the desired force in (2.2.19) onto the direction where thrust can be provided (see Fig 2.5), and whose smoothness properties follow from (2.2.19). Note that $T^{cl}(t, \bar{x}) = \arg \min_{T \in \mathbb{R}} \|T \mathbf{n} - \mathbf{T}^{cl}(t, \xi)\|$, i.e., (2.2.26) minimizes the error between the provided force and the desired force. Consider then (2.2.14). Taking T^{cl} in (2.2.26) and \mathbf{f}_ξ in (2.2.10), it follows that

$$\begin{aligned} \mathbf{f}_\xi^{cl} : \mathbb{R}_{\geq 0} \times \Omega_{\bar{x}} \ni (t, \bar{x}) &\mapsto \mathbf{f}_\xi^{cl}(t, \bar{x}) := \mathbf{f}_\xi(t, \bar{x}, T^{cl}(t, \bar{x})) \\ &\stackrel{(2.2.10)}{=} (\mathbf{v}, \mathbf{n} \mathbf{n}^T \mathbf{T}^{cl}(t, \xi) - \mathbf{g}(t)) \\ &\stackrel{(2.2.19)}{=} (\mathbf{v}, \mathbf{u}_{di}^{cl}(\xi) - \Pi(\mathbf{n}) \mathbf{T}^{cl}(t, \xi)) \\ &\stackrel{(2.2.22)}{=} (\mathbf{v}, \mathbf{u}_{di}^{cl}(\xi) - \Pi(\mathbf{n}) \mathbf{n}^{cl}(t, \xi) \|\mathbf{T}^{cl}(t, \xi)\|) \\ &\stackrel{(2.2.17)}{=} \mathbf{f}_{di}^{cl}(\xi) - (\mathbf{0}, \Pi(\mathbf{n}) \mathbf{n}^{cl}(t, \xi) \|\mathbf{T}^{cl}(t, \xi)\|), \end{aligned} \quad (2.2.27)$$

which means the vector field \mathbf{f}_ξ^{cl} approximates the double integrator vector field \mathbf{f}_{di}^{cl} in Definition 2.2.4, up to an error, namely $(\mathbf{0}, \Pi(\mathbf{n}) \mathbf{T}^{cl}(t, \xi))$ as illustrated in Fig 2.5. Finally, notice that for all $(t, \bar{\mathbf{x}}) \in \mathbb{R}_{\geq 0} \times \Omega_{\bar{x}}$ (let $\bar{\mathbf{x}}$ be as in (2.2.1))

$$\begin{aligned} & -dV_{di}(\xi)\mathbf{f}_\xi^{cl}(t, \bar{\mathbf{x}}) = \\ (2.2.27) \quad & = -dV_{di}(\xi)\mathbf{f}_{di}^{cl}(\xi) + \partial_{\bar{\mathbf{v}}} V_{di}(\mathbf{p}, \bar{\mathbf{v}})|_{\bar{\mathbf{v}}=\mathbf{v}} \Pi(\mathbf{n}) \mathbf{T}^{cl}(t, \xi) \\ \text{Definition 2.2.4} \quad & = -W_{di}(\xi) + \partial_{\bar{\mathbf{v}}} V_{di}(\mathbf{p}, \bar{\mathbf{v}})|_{\bar{\mathbf{v}}=\mathbf{v}} \Pi(\mathbf{n}) \mathbf{T}^{cl}(t, \xi). \end{aligned} \quad (2.2.28)$$

Second Step

We now construct a control law for the angular velocity $\boldsymbol{\omega}^{cl}$ such that $\lim_{t \rightarrow \infty} \mathbf{p}(t) = \mathbf{0}$ along the trajectory $\mathbb{R}_{\geq 0} \ni t \mapsto \bar{\mathbf{x}}(t) = \bar{\mathbf{x}}_0 + \int_0^t \mathbf{f}_{\bar{x}}^{cl}(\tau, \bar{\mathbf{x}}(\tau)) d\tau$, with the vector field $\mathbf{f}_{\bar{x}}^{cl}$ as in (2.2.15) (and $\bar{\mathbf{x}}_0 \in \tilde{\Omega}_{\bar{x}}(0)$). In order to construct such angular velocity, consider $\epsilon > 0$ and a positive definite function

$$V_\theta \in \mathcal{C}^2([0, \epsilon), \mathbb{R}_{\geq 0}), \text{ and, if } \epsilon \leq 2, \lim_{s \rightarrow \epsilon^-} V_\theta(s) = \infty, \quad (2.2.29)$$

satisfying $V_\theta(0) = 0$ and $V'_\theta(s) > 0, \forall s \in [0, \epsilon)$. It follows that V_θ is invertible, and for $\epsilon \leq 2$, the domain of V_θ^{-1} is $[0, \infty)$ (i.e., the image of V_θ is $[0, \infty)$). Examples of such functions, for $\epsilon \in (0, 2]$, are $V_\theta(s) = ks(\epsilon^\alpha - s^\alpha)^{-\frac{1}{\alpha}}$ with $k > 0$ and $\alpha \geq 1$; and for $\epsilon > 2$, examples are $V_\theta(s) = ks$ with $k > 0$. The idea behind the choice of ϵ is explained in Remark 2.2.9. For convenience, denote $\xi \in \mathcal{C}^2(\mathbb{R}_{\geq 0} \times \Omega_{\bar{x}}, [0, 2])$, defined as

$$\xi : \mathbb{R}_{\geq 0} \times \Omega_{\bar{x}} \ni (t, \bar{\mathbf{x}}) \mapsto \xi(t, \bar{\mathbf{x}}) := 1 - \mathbf{n}^T \mathbf{n}^{cl}(t, \xi) \in [0, 2], \quad (2.2.30)$$

whose smoothness properties follow from (2.2.22), and corresponding to the deviation between the thrust propelling direction and the desired thrust propelling direction. Consider also $\boldsymbol{\omega}^{n^{cl}} \in \mathcal{C}^1(\mathbb{R}_{\geq 0} \times \Omega_{\bar{x}}, \mathbb{R}^3)$ defined as $(\boldsymbol{\omega}^{n^{cl}} : \mathbb{R}_{\geq 0} \times \Omega_{\bar{x}} \ni (t, \bar{\mathbf{x}}) \mapsto \boldsymbol{\omega}^{n^{cl}}(t, \bar{\mathbf{x}}) \in \mathbb{R}^3)$

$$\begin{aligned} \boldsymbol{\omega}^{n^{cl}}(t, \bar{\mathbf{x}}) &:= \mathcal{S}(\mathbf{n}^{cl}(t, \xi)) \left(\partial_{\bar{t}} \mathbf{n}^{cl}(\bar{t}, \xi)|_{\bar{t}=t} + \partial_{\xi} \mathbf{n}^{cl}(t, \bar{\xi})|_{\bar{\xi}=\xi} \mathbf{f}_\xi^{cl}(t, \bar{\mathbf{x}}) \right) \\ (2.2.22) \quad &= \mathcal{S}(\mathbf{n}^{cl}(t, \xi)) \Pi(\mathbf{n}^{cl}(t, \xi)) \frac{\partial_{\bar{t}} \mathbf{T}^{cl}(\bar{t}, \xi)|_{\bar{t}=t} + \partial_{\xi} \mathbf{T}^{cl}(t, \bar{\xi})|_{\bar{\xi}=\xi} \mathbf{f}_\xi^{cl}(t, \bar{\mathbf{x}})}{\|\mathbf{T}^{cl}(t, \xi)\|} \\ (2.2.19) \quad &= \mathcal{S}(\mathbf{n}^{cl}(t, \xi)) \frac{\dot{\mathbf{g}}(t) + d\mathbf{u}_{di}^{cl}(\xi) \mathbf{f}_\xi^{cl}(t, \bar{\mathbf{x}})}{\|\mathbf{T}^{cl}(t, \xi)\|}, \end{aligned} \quad (2.2.31)$$

which corresponds to the angular velocity of \mathbf{n}^{cl} under the vector field \mathbf{f}_ξ^{cl} , and whose smoothness properties follow from (2.2.11) and (2.2.22). Similarly to (2.2.23), denote $\boldsymbol{\omega}^* \in \mathcal{C}^1(\mathbb{R}_{\geq 0}, \mathbb{R}^3)$, defined as

$$\boldsymbol{\omega}^* : \mathbb{R}_{\geq 0} \ni t \mapsto \boldsymbol{\omega}^*(t) = \boldsymbol{\omega}^{n^{cl}}(t, \mathbf{0}_6, \pm \mathbf{n}^*(t)) \stackrel{(2.2.31)}{=} \mathcal{S}\left(\frac{\mathbf{g}(t)}{\|\mathbf{g}(t)\|}\right) \frac{\dot{\mathbf{g}}(t)}{\|\mathbf{g}(t)\|} \in \mathbb{R}^3, \quad (2.2.32)$$

where $\pm \dot{\mathbf{n}}^*(t) = \pm \mathcal{S}(\boldsymbol{\omega}^*(t)) \mathbf{n}^*(t)$. In fact, $\boldsymbol{\omega}^*(\cdot)$ is the angular velocity $\boldsymbol{\omega}^{n^{cl}}(\cdot, \bar{\mathbf{x}}(\cdot))$ converges to when $\lim_{t \rightarrow \infty} \{\mathbf{p}(t), \mathbf{v}(t), (\mathbf{n}(t) \pm \mathbf{n}^{cl}(t))\} = 0$. We now proceed to the design of the control law $\boldsymbol{\omega}^{cl}$ for the angular velocity. For that purpose, denote

$$\begin{aligned}\tilde{\Omega}_{\bar{x}}(t) &= \{\bar{\mathbf{x}} \in \Omega_{\bar{x}} : \xi(t, \bar{\mathbf{x}}) < \epsilon\}, \forall t \in \mathbb{R}_{\geq 0} \\ \Delta_{\bar{x}} &= \{(t, \bar{\mathbf{x}}) \in \mathbb{R}_{\geq 0} \times \Omega_{\bar{x}} : \bar{\mathbf{x}} \in \tilde{\Omega}_{\bar{x}}(t)\},\end{aligned}$$

corresponding to the domain of some functions introduced next. Consider then the function $V_{\bar{x}} \in \mathcal{C}^2(\Delta_{\bar{x}}, \mathbb{R}_{\geq 0})$ defined as (take $\bar{\mathbf{x}}$ as in (2.2.1))

$$V_{\bar{x}} : \Delta_{\bar{x}} \ni (t, \bar{\mathbf{x}}) \mapsto V_{\bar{x}}(t, \bar{\mathbf{x}}) := V_{di}(\boldsymbol{\xi}) + V_\theta(\xi(t, \bar{\mathbf{x}})), \quad (2.2.33)$$

whose smoothness properties follow from Definition 2.2.4, (2.2.29) and (2.2.30). It follows from (2.2.15), (2.2.31), (2.2.28) and (2.2.33) that

$$\begin{aligned}\tilde{W}_{\bar{x}}(t, \bar{\mathbf{x}}, \boldsymbol{\omega}) &:= -\partial_{\bar{t}} V_{\bar{x}}(\bar{t}, \bar{\mathbf{x}})|_{\bar{t}=t} - \partial_{\bar{\mathbf{x}}} V_{\bar{x}}(t, \bar{\mathbf{x}})|_{\bar{\mathbf{x}}=\bar{\mathbf{x}}} \mathbf{f}_{\bar{x}}^{cl}(t, \bar{\mathbf{x}}, \boldsymbol{\omega}, T^{cl}(t, \bar{\mathbf{x}})) \\ &= W_{di}(\boldsymbol{\xi}) - V'_\theta(\xi(t, \bar{\mathbf{x}})) (\mathcal{S}(\mathbf{n}^{cl}(t, \boldsymbol{\xi})) \mathbf{n})^T \times \\ &\quad \times \left(\boldsymbol{\omega} - \boldsymbol{\omega}^{n^{cl}}(t, \bar{\mathbf{x}}) + \frac{\|\mathbf{T}^{cl}(t, \boldsymbol{\xi})\|}{V'_\theta(\xi(t, \bar{\mathbf{x}}))} \mathcal{S}(\mathbf{n}) \partial_{\bar{\mathbf{v}}} V_{di}(\mathbf{p}, \bar{\mathbf{v}})|_{\bar{\mathbf{v}}=\mathbf{v}} \right).\end{aligned} \quad (2.2.34)$$

Motivated by (2.2.34), we define $\boldsymbol{\omega}^{cl} \in \mathcal{C}^1(\Delta_{\bar{x}}, \mathbb{R}_{\geq 0})$ as

$$\boldsymbol{\omega}^{cl}(t, \bar{\mathbf{x}}) = \boldsymbol{\omega}^{n^{cl}}(t, \bar{\mathbf{x}}) - k_\theta \mathcal{S}(\mathbf{n}^{cl}(t, \boldsymbol{\xi})) \mathbf{n} - \frac{\|\mathbf{T}^{cl}(t, \boldsymbol{\xi})\|}{V'_\theta(\xi(t, \bar{\mathbf{x}}))} \mathcal{S}(\mathbf{n}) \partial_{\bar{\mathbf{v}}} V_{di}(\mathbf{p}, \bar{\mathbf{v}})|_{\bar{\mathbf{v}}=\mathbf{v}}, \quad (2.2.35)$$

whose smoothness properties follow from Definition 2.2.4, (2.2.19), (2.2.22), (2.2.31) and (2.2.29). It then follows that

$$W_{\bar{x}}(t, \bar{\mathbf{x}}) := \tilde{W}_{\bar{x}}(t, \bar{\mathbf{x}}, \boldsymbol{\omega}^{cl}(t, \bar{\mathbf{x}})) \quad (2.2.36)$$

$$\text{and } (2.2.34), (2.2.35) = W_{di}(\boldsymbol{\xi}) + k_\theta V'_\theta(\xi(t, \bar{\mathbf{x}})) \|\mathcal{S}(\mathbf{n}) \mathbf{n}^{cl}(t, \boldsymbol{\xi})\|^2 \quad (2.2.37)$$

is non-negative. Note that, if $\epsilon > 2$, then $\min_{s \in [0, 2]} V'_\theta(s) > 0$; and if $\epsilon \leq 2$, then $\min_{s \in [0, \epsilon]} V'_\theta(s) > 0$; therefore, in either case, (2.2.35) is well defined. Given (2.2.26) and (2.2.35) it follows that $\mathbf{f}_{\bar{x}}^{cl} \in \mathcal{C}^1(\Delta_{\bar{x}}, \mathbb{R}^9)$, with $\mathbf{f}_{\bar{x}}^{cl}$ as in (2.2.15), and whose smoothness properties follow from (2.2.31).

Third Step

We now perform the final step, where we construct a control law $\boldsymbol{\tau}^{cl}$ for the torque which guarantees $\lim_{t \rightarrow \infty} \mathbf{p}(t) = \mathbf{0}$ along the trajectory $\mathbb{R}_{\geq 0} \ni t \mapsto \mathbf{x}(t) = \mathbf{x}_0 + \int_0^t \mathbf{f}_{\bar{x}}^{cl}(\tau, \mathbf{x}(\tau)) d\tau$, with the vector field $\mathbf{f}_{\bar{x}}^{cl}$ as in (2.2.16) (and $\mathbf{x}_0 \in \tilde{\Omega}_{\bar{x}}(0)$). Similarly to the procedures in the second step (where we introduced $\boldsymbol{\omega}^{n^{cl}}$), denote $\boldsymbol{\tau}^{\boldsymbol{\omega}^{cl}} \in \mathcal{C}^0(\Delta_x, \mathbb{R}^3)$, defined as

$$\boldsymbol{\tau}^{\boldsymbol{\omega}^{cl}}(t, \mathbf{x}) := \partial_{\bar{t}} \boldsymbol{\omega}^{cl}(\bar{t}, \bar{\mathbf{x}})|_{\bar{t}=t} + \partial_{\bar{\mathbf{x}}} \boldsymbol{\omega}^{cl}(t, \bar{\mathbf{x}})|_{\bar{\mathbf{x}}=\mathbf{x}} \mathbf{f}_{\bar{x}}^{cl}(t, \bar{\mathbf{x}}, \boldsymbol{\omega}, T^{cl}(t, \bar{\mathbf{x}})), \quad (2.2.38)$$

which, physically, provides the time derivative of $\omega^{cl}(t, \bar{\mathbf{x}}(t))$, i.e., $\dot{\omega}^{cl}(t, \bar{\mathbf{x}}(t)) = \tau^{\omega^{cl}}(t, \mathbf{x}(t))$ along trajectories of $\dot{\bar{\mathbf{x}}}(t) = \mathbf{f}_{\bar{x}}(t, \bar{\mathbf{x}}(t), \boldsymbol{\omega}(t), T^{cl}(t, \bar{\mathbf{x}}(t)))$. Again, similarly to the previous step, denote

$$\tilde{\Omega}_x(t) = \Omega_{\bar{x}}(t) \times \mathbb{R}^3, \forall t \in \mathbb{R}_{\geq 0} \quad (2.2.39)$$

$$\Delta_x = \{(t, \mathbf{x}) \in \mathbb{R}_{\geq 0} \times \Omega_x : \mathbf{x} \in \tilde{\Omega}_x(t)\}, \quad (2.2.40)$$

corresponding to the domain of some functions introduced next.

Recall that we do not control the angular velocity $\boldsymbol{\omega}$, otherwise choosing $\boldsymbol{\omega}(t) = \omega^{cl}(t, \bar{\mathbf{x}}(t))$ at each time instant t would suffice to accomplish the goal of Problem 2.2.1. Denote then $\mathbf{e}_\omega \in \mathcal{C}^1(\Delta_x, \mathbb{R}^3)$, defined as

$$\Delta_x \ni (t, \mathbf{x}) \mapsto \mathbf{e}_\omega(t, \mathbf{x}) := \mathcal{S}(\mathbf{n})(\boldsymbol{\omega} - \omega^{cl}(t, \bar{\mathbf{x}})) \in \mathbb{R}^3, \quad (2.2.41)$$

corresponding to an error that we shall use in a backstepping procedure, and whose smoothness properties follow from (2.2.35). Moreover, notice that

$$\begin{aligned} \mathbf{f}_{\bar{x}}(t, \bar{\mathbf{x}}, \boldsymbol{\omega}, T^{cl}(t, \bar{\mathbf{x}})) &= \mathbf{f}_{\bar{x}}(t, \bar{\mathbf{x}}, \boldsymbol{\omega} - \omega^{cl}(t, \bar{\mathbf{x}}) + \omega^{cl}(t, \bar{\mathbf{x}}), T^{cl}(t, \bar{\mathbf{x}})) \\ (2.2.41) \quad &= (\mathbf{f}_{\bar{x}}^{cl}(t, \bar{\mathbf{x}}), \mathbf{0}_3) - (\mathbf{0}_6, \mathbf{e}_\omega(t, \mathbf{x})), \end{aligned} \quad (2.2.42)$$

which justifies why we wish to steer the error \mathbf{e}_ω to zero. Intuitively, the vector field in (2.2.42) approximates the vector field $\mathbf{f}_{\bar{x}}^{cl}$, designed in the previous step, and for which it follows that $\lim_{t \rightarrow \infty} \mathbf{p}(t) = \mathbf{0}$ along trajectories of $\dot{\bar{\mathbf{x}}}(t) = \mathbf{f}_{\bar{x}}^{cl}(t, \bar{\mathbf{x}}(t))$. Consider now the function $V_\omega : \mathbb{R}^3 \ni \mathbf{z} \mapsto V_\omega(\mathbf{z}) = \frac{1}{2} v_\omega \mathbf{z}^T \mathbf{z}$, with $v_\omega > 0$, and $V_x \in \mathcal{C}^1(\Delta_x, \mathbb{R}_{\geq 0})$, defined as

$$\Delta_x \ni (t, \mathbf{x}) \mapsto V_x(t, \mathbf{x}) = V_{\bar{x}}(t, \bar{\mathbf{x}}) + V_\omega(\mathbf{e}_\omega(t, \mathbf{x})) \in \mathbb{R}_{\geq 0}, \quad (2.2.43)$$

whose smoothness properties follow from (2.2.33), (2.2.41) and smoothness of V_ω . Then, it follows that (see details in [46])

$$\begin{aligned} \tilde{W}_x(t, \mathbf{x}, \boldsymbol{\tau}) &:= -\partial_{\bar{x}} V_x(\bar{x}, \bar{\mathbf{x}})|_{\bar{x}=x} \mathbf{f}_x(t, \mathbf{x}, (T^{cl}(t, \bar{\mathbf{x}}), \boldsymbol{\tau})) \\ &= W_x(t, \bar{\mathbf{x}}) + v_\omega \mathbf{e}_\omega^T(t, \mathbf{x}) \left(\boldsymbol{\tau} - \mathcal{S}(\mathbf{n}) \boldsymbol{\tau}^d(t, \mathbf{x}) - \Pi(\mathbf{n}) \boldsymbol{\omega}^{n^{cl}}(t, \bar{\mathbf{x}}) \mathbf{n}^T \boldsymbol{\omega}^{n^{cl}}(t, \bar{\mathbf{x}}) + \frac{V'_\theta(\xi(t, \bar{\mathbf{x}}))}{v_\omega} \Pi(\mathbf{n}) \mathbf{n}^{cl}(t, \xi) \right), \end{aligned} \quad (2.2.44)$$

and, motivated by (2.2.44), we design $\boldsymbol{\tau}^{cl} \in \mathcal{C}^0(\Delta_x, \mathbb{R}^3)$, defined as

$$\boldsymbol{\tau}^{cl}(t, \mathbf{x}) = \Pi(\mathbf{n}) \boldsymbol{\tau}^{\omega^{cl}}(t, \mathbf{x}) + \mathcal{S}(\mathbf{n}) \boldsymbol{\omega}^{cl}(t, \bar{\mathbf{x}}) \mathbf{n}^T \boldsymbol{\omega}^{cl}(t, \bar{\mathbf{x}}) + k_\omega \mathcal{S}(\mathbf{n}) \mathbf{e}_\omega(t, \mathbf{x}) + \frac{V'_\theta(\xi(t, \bar{\mathbf{x}}))}{v_\omega} \mathcal{S}(\mathbf{n}) \mathbf{n}^{cl}(t, \xi), \quad (2.2.45)$$

for some $k_\omega \geq 0$, and whose smoothness properties follow from (2.2.22), (2.2.29), (2.2.41) and (2.2.38). For this choice, it follows that

$$W_x(t, \mathbf{x}) := \tilde{W}_x(t, \mathbf{x}, \boldsymbol{\tau}^{cl}(t, \mathbf{x})) = W_{\bar{x}}(t, \bar{\mathbf{x}}) + 2k_\omega V_\omega(\mathbf{e}_\omega(t, \mathbf{x})) \geq 0, \quad (2.2.46)$$

where $W_x \in \mathcal{C}^1(\Delta_x, \mathbb{R}_{\geq 0})$ and whose smoothness properties follow from (2.2.37), (2.2.41) and smoothness of V_ω .

Let us now summarize the previous results. Given (2.2.26) and (2.2.45), we define the control law $\mathbf{u}_x^{cl} \in \mathcal{C}^0(\Delta_x, \mathbb{R}^4)$ as

$$\mathbf{u}_x^{cl}(t, \mathbf{x}) := (T^{cl}(t, \bar{\mathbf{x}}), \boldsymbol{\tau}^{cl}(t, \mathbf{x})), \quad (2.2.47)$$

and, for this choice, it follows that along a trajectory of $\dot{\mathbf{x}}(t) = \mathbf{f}_x^{cl}(t, \mathbf{x}(t))$,

$$\dot{V}_x(t, \mathbf{x}(t)) = -W_x(t, \mathbf{x}(t)) \leq 0, \quad (2.2.48)$$

where $\mathbf{f}_x^{cl} \in \mathcal{C}^0(\Delta_x, \mathbb{R}^{12})$, with $\mathbf{f}_x^{cl}(t, \mathbf{x}) = \mathbf{f}_x(t, \mathbf{x}, \mathbf{u}_x^{cl}(t, \mathbf{x}))$, owing to (2.2.11), (2.2.26) and (2.2.45). Finally, we can verify that along a trajectory of $\dot{\mathbf{x}}(t) = \mathbf{f}_x^{cl}(t, \mathbf{x}(t))$

$$\sup_{t \geq 0} |\dot{W}_x(t, \mathbf{x}(t))| < \infty, \quad (2.2.49)$$

which means that $\ddot{V}(t, \mathbf{x}(t)) = \dot{W}_x(t, \mathbf{x}(t))$ is uniformly bounded (as a function of $t \in \mathbb{R}_{\geq 0}$) [46].

Theorem 2.2.8. *Consider the open loop vector field (2.2.10), the control law (2.2.47) and the closed loop vector field (2.2.16). Then, it follows that $\lim_{t \rightarrow \infty} \mathbf{p}(t) = \mathbf{0}$, along any trajectory of $\dot{\mathbf{x}}(t) = \mathbf{f}_x^{cl}(t, \mathbf{x}(t))$ with $\mathbf{x}(0) \in \Omega_x(0)$. Moreover, when $\epsilon \leq 2$, $\lim_{t \rightarrow \infty} (\mathbf{n}(t) - \mathbf{n}^*(t)) = \mathbf{0}$, with \mathbf{n}^* in (2.2.23).*

Sketch of proof. Consider a solution $\mathbf{x} : \mathbb{R}_{\geq 0} \ni t \mapsto \mathbf{x}(t) = \mathbf{x}_0 + \int_0^t \mathbf{f}_x^{cl}(\tau, \mathbf{x}(\tau)) d\tau \in \Omega_x$ with $\mathbf{x}_0 \in \Omega_x(0)$ (and with \mathbf{x} decomposed as in (2.2.1)). By definition, V_x in (2.2.43) is lower bounded by 0. It then follows from (2.2.48) and (2.2.49), and by invoking Barbalat's lemma that $\lim_{t \rightarrow \infty} \dot{V}_x(t, \mathbf{x}(t)) = -\lim_{t \rightarrow \infty} W_x(t, \mathbf{x}(t)) = 0$. It then follows from (2.2.37) that $\lim_{t \rightarrow \infty} W_{di}(\xi(t)) = 0$, and therefore (2.2.18) holds, which implies that $\lim_{t \rightarrow \infty} \xi(t) = \mathbf{0} \Rightarrow \lim_{t \rightarrow \infty} \mathbf{p}(t) = \mathbf{0}$. It also follows from (2.2.37) that $\lim_{t \rightarrow \infty} \|\mathcal{S}(\mathbf{n}) \mathbf{n}^{cl}(t, \xi(t))\|^2 = \lim_{t \rightarrow \infty} \|\mathcal{S}(\mathbf{n}) \mathbf{n}^{cl}(t, \mathbf{0})\|^2 = \lim_{t \rightarrow \infty} (\mathbf{n}(t) \pm \mathbf{n}^*(t)) = \mathbf{0}$. Thus, when $\epsilon \leq 2$, $\lim_{t \rightarrow \infty} (\mathbf{n}(t) - \mathbf{n}^*(t)) = \mathbf{0}$, since $V_x(t, \mathbf{x}(t)) \leq V_x(0, \mathbf{x}(0)) < \infty$ for all $t \in \mathbb{R}_{\geq 0}$, and $\lim_{\mathbf{n} \rightarrow \mathbf{n}^*(t)} V_{\bar{x}}(t, \mathbf{0}_6, \mathbf{n}) = \infty$ for any $t \in \mathbb{R}_{\geq 0}$. \square

Remark 2.2.9. *The idea behind the choice of ϵ is the following: if $\epsilon > 2$, $\mathbf{n}(\cdot)$ may converge to either $\mathbf{n}^*(\cdot)$ or $-\mathbf{n}^*(\cdot)$; on the other hand, if $\epsilon \leq 2$, $\mathbf{n}(\cdot)$ converges to $\mathbf{n}^{cl}(\cdot)$ (assuming that $\mathbf{x}(0) \in \Omega_x(0)$). Moreover, if $0 < \epsilon \leq 1$, and along a trajectory $\mathbf{x}(\cdot)$ of (2.2.16) for $\mathbf{x}(0) \in \Omega_x(0)$, it follows from Theorem 2.2.8 that $\xi(t, \bar{\mathbf{x}}(t)) \in [0, \epsilon] \Rightarrow \mathbf{n}(t) \in \mathcal{C}(\arccos(1 - \epsilon), \mathbf{n}^{cl}(t, \mathbf{p}(t), \mathbf{v}(t)))$ for all $t \geq 0$, and therefore, from Proposition 2.2.7, $\mathbf{n}(t) \in \mathcal{C}(\arccos(1 - \epsilon) + \alpha^*, \mathbf{e}_3)$ for all $t \geq 0$. This means that ϵ , in conjunction with α^* , may be chosen such that, for example, $\mathbf{n}(\cdot)$ points upwards at all times (provided, obviously, that $\mathbf{n}(0)$ points upwards).*

2.2.5 Bounded Control of Double Integrator

The proposed control law for the double integrator is inspired by the strategy proposed in [52]. Also, the same control law depends on functions whose properties we describe in the next definition.

Definition 2.2.10. We say $\sigma \in \Sigma$, if $\sigma \in \mathcal{C}^3(\mathbb{R}, [-\bar{\sigma}, \bar{\sigma}])$ for some $\bar{\sigma} \in \mathbb{R}_{>0}$, $\sigma(s)s > 0$ for all $s \in \mathbb{R}$, $\sigma'(s) > 0$ for all $s \in \mathbb{R}$, and $\bar{\sigma}' := \sup_{s \in \mathbb{R}} |\sigma'(s)| < \infty$.

Let $n \in \mathbb{N}$ and let

$$\xi = (\mathbf{p}, \mathbf{v}) = ((p_1, \dots, p_n), (v_1, \dots, v_n)) \in \mathbb{R}^{2n}, \mathbf{u}_\xi \in \mathbb{R}^n \quad (2.2.50)$$

be the state of and input to an n -dimensional double integrator, with vector field $\mathbf{f}_\xi : \mathbb{R}^{2n} \times \mathbb{R}^n \mapsto \mathbb{R}^{2n}$, given by

$$\mathbf{f}_\xi : \mathbb{R}^{2n} \times \mathbb{R}^n \ni (\xi, \mathbf{u}_\xi) \mapsto \mathbf{f}_\xi(\xi, \mathbf{u}_\xi) := (\mathbf{v}, \mathbf{u}_\xi) \in \mathbb{R}^{2n}, \quad (2.2.51)$$

with ξ decomposed as in (2.2.50). A control law \mathbf{u}_ξ^{cl} can be found that satisfies the conditions of Definition 2.2.4, i.e. $\mathbf{u}_\xi^{cl} \in \mathcal{C}^{di}$. Indeed, consider $\mathbf{u}_\xi^{cl} : \mathbb{R}^{2n} \ni \xi \mapsto \mathbf{u}_\xi^{cl}(\xi) \in \mathbb{R}^n$ given by

$$\mathbf{u}_\xi^{cl}(\xi) := (u_\xi^{cl}(p_1, v_1), \dots, u_\xi^{cl}(p_n, v_n)) \in \mathbb{R}^n, \quad (2.2.52)$$

$$u_\xi^{cl}(p, v) := -\rho(\Omega(v) + \sigma(p)) - k \frac{v + \sigma(p)}{\Omega(v) + \sigma(p)} \frac{\sigma(p)}{\Omega'(v)} - \sigma'(p) \frac{v}{\Omega'(v)}, \quad (2.2.53)$$

with ξ as in (2.2.50), and where $\sigma, \rho \in \Sigma$, and $k > 0$, and $\Omega \in \mathcal{C}^3(\mathbb{R}, \mathbb{R})$ satisfies $\Omega(v) = v$, $\forall v \in \Omega_v$, $[-\bar{\sigma}, \bar{\sigma}] \subset \Omega_v \subset \mathbb{R}$ and $|\Omega(v)| > |v| \wedge \Omega'(v) \geq |v|$, $\forall v \notin \Omega_v$. It follows that $\sup_{v \in \mathbb{R}} \left| \frac{v}{\Omega'(v)} \right| =: M < \infty$, where $M > \bar{\sigma}$ necessarily. Therefore we have that, in fact, $|u_\xi^{cl}(\cdot, \cdot)| \leq B := \bar{\rho} + k\bar{\sigma} + \bar{\sigma}'M < \infty$ and consequently $\mathbf{u}_\xi^{cl} : \mathbb{R}^{2n} \mapsto \bar{\mathcal{B}}(B\mathbf{1}_n, \mathbf{0})$. The equilibrium $\mathbf{0}_{2n}$ of $\mathbf{f}_\xi^{cl}(\xi) = \mathbf{f}_\xi(\xi, \mathbf{u}_\xi^{cl}(\xi))$ is asymptotically stable, and for $V_\xi \in \mathcal{C}^2(\mathbb{R}^{2n}, \mathbb{R}_{\geq 0})$ defined as (ξ as in (2.2.50))

$$V_\xi(\xi) := \sum_{i=1}^{i=n} \left(k \int_0^{p_i} \sigma(s) ds + \frac{1}{2} (\Omega(v_i) + \sigma(p_i))^2 \right) \quad (2.2.54)$$

it follows that $W_\xi \in \mathcal{C}^1(\mathbb{R}^2, \mathbb{R})$, defined as (ξ as in (2.2.50))

$$W_\xi(\xi) := -dV_\xi(\xi)\mathbf{f}_\xi^{cl}(\xi) \quad (2.2.55)$$

$$= \sum_{i=1}^{i=n} k\sigma^2(p_i) + \Omega'(v_i)(\Omega(v_i) + \sigma(p_i))\rho(\Omega(v_i) + \sigma(p_i)), \quad (2.2.56)$$

is in fact definite positive.

Example 2.2.1. Consider the functions $\sigma(s) = 0.25 \frac{s}{\sqrt{1+s^2}}$, $\rho(s) = 0.70 \frac{s}{\sqrt{1+s^2}}$, $k = 1$ and Ω as an odd function and as the solution to the differential equation $\Omega'''(s) = 0$ for $s \in [0, 1]$, $\Omega'''(s) = s - 1$ for $s \in [1, 2]$ and $\Omega'''(s) = 1$ for $s > 2$ and initial conditions $\Omega(0) = 0$, $\Omega'(0) = 1$ and $\Omega''(0) = 0$. These three functions satisfy the conditions prescribed before.

2.3 Controller for a quadrotor

2.3.1 Background

Quadrotors are aerial vehicles, whose popularity stems from their ability to be used in relatively small spaces, their reduced mechanical complexity, and inexpensive components.

Many control strategies have been proposed for trajectory tracking of quadrotors [8, 20, 21, 47–51]. Controllers can be designed by linearizing the system around the hover condition, but these are only stable for small roll and pitch angles [47, 48]. Controllers have also been designed based on an inner attitude control loop and an outer position control loop [49]. Controllers that guarantee trajectory tracking for all initial conditions can also be found [50]. Since the quadrotor dynamics depend on the vehicle’s rotation matrix, most control strategies also provide a control law for the space corresponding to the yaw motion. Different parameterizations for the vehicle’s rotation matrix have also been used, such as euler angles [49], and unit quaternions [50, 51].

2.3.2 Notation

m, J	Quadrotor’s mass and moment of inertia
$\mathbf{p}, \mathbf{v} \in \mathbb{R}^3$	Quadrotor’s position and velocity
$\mathcal{R} \in \mathbb{SO}(3), \boldsymbol{\omega} \in \mathbb{R}^3$	Quadrotor’s rotation matrix and angular velocity
$\mathbf{r} := \mathcal{R}\mathbf{e}_3 \in \mathbb{S}^2$	Quadrotor’s direction along which input thrust is provided
$\mathbf{z} = (\mathbf{p}, \mathbf{v}, \mathcal{R}, \boldsymbol{\omega})$	State of the quadrotor
$T \in \mathbb{R}, \boldsymbol{\tau} \in \mathbb{R}^3$	Quadrotor’s input thrust propelling force and input torque
$\mathbf{u}_z = (T, \boldsymbol{\tau})$	Input to the quadrotor system

2.3.3 Modeling

A sketch of a simplified model of a quadrotor is presented in Fig. 2.6. Consider then

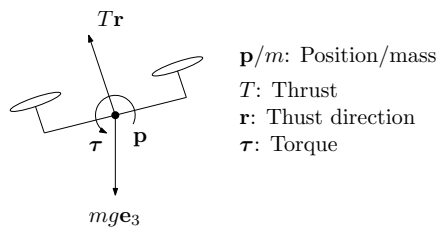


Figure 2.6: Modeling of a quadrotor system

the notation as above, and denote then

$$\mathbf{z} := (\mathbf{p}, \mathbf{v}, \mathcal{R}, \boldsymbol{\omega}) \in \Omega_x, \quad (2.3.1)$$

$$\mathbf{u}_z := (T, \boldsymbol{\tau}) \in \mathbb{R}_{\geq 0} \times \mathbb{R}^3, \quad (2.3.2)$$

as the state of and the input to the quadrotor system, and where

$$\Omega_x = \{(\mathbf{p}, \mathbf{v}, \mathcal{R}, \boldsymbol{\omega}) \in (\mathbb{R}^3)^2 \times \mathbb{R}^{3 \times 3} \times \mathbb{R}^3 : \mathcal{R}^T \mathcal{R} = \mathbf{I}, \mathcal{R} \mathcal{R}^T = \mathbf{I}\}, \quad (2.3.3)$$

$$T_z \Omega_x = \{(\delta \mathbf{p}, \delta \mathbf{v}, \delta \mathcal{R}, \delta \boldsymbol{\omega}) \in (\mathbb{R}^3)^2 \times \mathbb{R}^{3 \times 3} \times \mathbb{R}^3 : \delta \mathcal{R}^T \mathcal{R} + \mathcal{R}^T \delta \mathcal{R} = \mathbf{0}, \delta \mathcal{R} \mathcal{R}^T + \mathcal{R} \delta \mathcal{R}^T = \mathbf{0}\}, \quad (2.3.4)$$

denote, respectively, the state set and the tangent space of Ω_x at $\mathbf{z} \in \Omega_x$. Let $\mathbf{u}_z := (T, \boldsymbol{\tau}) : \mathbb{R}_{\geq 0} \mapsto \mathbb{R}^4$, and consider $\dot{\mathbf{z}} := (\mathbf{f}_z(\mathbf{z}(t), \mathbf{u}_z(t)), \mathbf{z}(0) \in \Omega_x)$ which evolves according to

$$\dot{\mathbf{z}}(t) = \mathbf{f}_z(\mathbf{z}(t), \mathbf{u}_z(t)), \mathbf{z}(0) \in \Omega_x, \quad (2.3.5)$$

where $\mathbf{f}_z : \Omega_z \times \mathbb{R}^4 \ni (\mathbf{z}, \mathbf{u}_z) \mapsto \mathbf{f}_z(\mathbf{z}, \mathbf{u}_z) \in T_{\mathbf{z}} \Omega_x$ is given by (consider \mathbf{z} as in (2.3.9) and \mathbf{u}_z as in (2.3.2))

$$\Omega_z \times \mathbb{R}^4 \ni (\mathbf{z}, \mathbf{u}_z) \mapsto \mathbf{f}_z(\mathbf{z}, \mathbf{u}_z) := \left(\mathbf{v}, \frac{T}{m} \mathcal{R} \mathbf{e}_3 - g \mathbf{e}_3, \mathcal{R} \mathcal{S}(\boldsymbol{\omega}), J^{-1}(\boldsymbol{\tau} - \mathcal{S}(\boldsymbol{\omega}) J \boldsymbol{\omega}) \right) \in T_{\mathbf{z}} \Omega_x. \quad (2.3.6)$$

Notice that $\mathbf{f}_z(\mathbf{z}, \mathbf{u}_z) \in T_{\mathbf{z}} \Omega_x$, for any $(\mathbf{z}, \mathbf{u}_z) \in \Omega_x \times \mathbb{R}^4$, implying that Ω_x is indeed positively invariant. In fact, if $(\delta \mathbf{p}, \delta \mathbf{v}, \delta \mathcal{R}, \delta \boldsymbol{\omega}) = \mathbf{f}_z(t, \mathbf{z}, \mathbf{u}_z)$ it follows that

$$\begin{aligned} \delta \mathcal{R}^T \mathcal{R} + \mathcal{R}^T \delta \mathcal{R} &\stackrel{(2.3.6)}{=} (\mathcal{R} \mathcal{S}(\boldsymbol{\omega}))^T \mathcal{R} + \mathcal{R}^T \mathcal{R} \mathcal{S}(\boldsymbol{\omega}) = -\mathcal{S}(\boldsymbol{\omega}) \mathcal{R}^T \mathcal{R} + \mathcal{R}^T \mathcal{R} \mathcal{S}(\boldsymbol{\omega}) \\ &\stackrel{(2.3.3)}{=} -\mathcal{S}(\boldsymbol{\omega}) + \mathcal{S}(\boldsymbol{\omega}) = \mathbf{0}, \end{aligned} \quad (2.3.7)$$

$$\begin{aligned} \delta \mathcal{R} \mathcal{R}^T + \mathcal{R} \delta \mathcal{R}^T &\stackrel{(2.3.6)}{=} \mathcal{R} \mathcal{S}(\boldsymbol{\omega}) \mathcal{R}^T + \mathcal{R} (\mathcal{R} \mathcal{S}(\boldsymbol{\omega}))^T = \mathcal{R} \mathcal{S}(\boldsymbol{\omega}) \mathcal{R}^T - \mathcal{R} \mathcal{S}(\boldsymbol{\omega}) \mathcal{R}^T \\ &\stackrel{(2.3.3)}{=} \mathcal{R} (\mathcal{S}(\boldsymbol{\omega}) - \mathcal{S}(\boldsymbol{\omega})) \mathcal{R}^T = \mathbf{0}, \end{aligned} \quad (2.3.8)$$

and thus $(\delta \mathbf{p}, \delta \mathbf{v}, \delta \mathbf{n}, \delta \boldsymbol{\omega}) = \mathbf{f}_z(\mathbf{z}, \mathbf{u}_z) \stackrel{(2.3.4)}{\in} T_{\mathbf{z}} \Omega_x$.

Problem 2.3.1. Given (2.3.6) and a desired position trajectory $\mathbf{p}^* \in \mathcal{C}^4(\mathbb{R}_{\geq 0}, \mathbb{R}^3)$, design $\mathbf{u}_z := (T, \boldsymbol{\tau}) : \mathbb{R}_{\geq 0} \mapsto \mathbb{R}^4$ such that $\lim_{t \rightarrow \infty} (\mathbf{p}(t) - \mathbf{p}^*(t)) = \mathbf{0}$ along solutions of (2.3.5).

2.3.4 Control Strategy

The control strategy here pursued is exactly that described in the beginning of this Chapter (see Figure 2.2, in page 14), and illustrated in Fig 2.7. In the particular case of the quadrotor system, the degree of freedom corresponds to rotations around the third body axis, $\mathcal{R} \mathbf{e}_3$, along which thrust is provided.

In order to pursue with the previous strategy, let us denote

$$\mathbf{x} := (\mathbf{e}, \mathbf{v}, \mathbf{r}, \boldsymbol{\omega}) \in \Omega_x, \quad (2.3.9)$$

$$\mathbf{u}_x := (a, \boldsymbol{\alpha}) \in \mathbb{R}^4 =: \mathcal{U}_x, \quad (2.3.10)$$

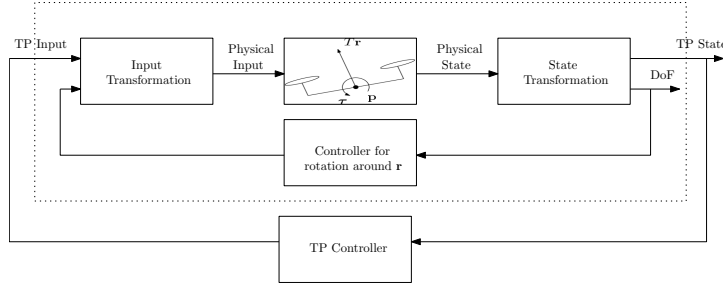


Figure 2.7: Control architecture as laid out in Fig. 2.1, but applied specifically to the quadrotor system.

with Ω_x as in (2.2.4). Let us then present the function, that is not a diffeomorphism between Ω_z and Ω_x , but rather a diffeomorphism between the set spanned by $\{(\mathbf{p}, \mathbf{v}, \mathcal{R}\mathbf{e}_3, \Pi(\mathcal{R}\mathbf{e}_3)\mathcal{R}\boldsymbol{\omega})\}_{\mathbf{z} \in \Omega_z}$ (which is in fact the set Ω_x) and Ω_x . Denote then, for each time instant $t \in \mathbb{R}_{\geq 0}$, $\mathbf{g}_z^x(t, \cdot) : \Omega_z \mapsto \Omega_x$, defined as

$$\mathbf{g}_z^x(t, \mathbf{z}) := (\mathbf{g}_z^e(t, \mathbf{z}), \mathbf{g}_z^v(t, \mathbf{z}), \mathbf{g}_z^r(t, \mathbf{z}), \mathbf{g}_z^\varpi(t, \mathbf{z})) \quad (2.3.11)$$

$$:= (\mathbf{p} - \mathbf{p}^*(t), \mathbf{v} - \dot{\mathbf{p}}^*(t), \mathcal{R}\mathbf{e}_3, \Pi(\mathcal{R}\mathbf{e}_3)\mathcal{R}\boldsymbol{\omega}). \quad (2.3.12)$$

Consider then also $\mathbf{u}_z^{cl} := (T^{cl}, \boldsymbol{\tau}^{cl}) : \Omega_z \times \mathcal{U}_x \times \mathbb{R} \ni (\mathbf{z}, \mathbf{u}_x, \tau_3) \mapsto \mathbf{u}_z^{cl}(\mathbf{z}, \mathbf{u}_x, \tau_3) \in \mathbb{R}^3$ defined as

$$\mathbf{u}_z^{cl}(\mathbf{z}, \mathbf{u}_x, \tau_3) := (T^{cl}(a), \boldsymbol{\tau}^{cl}(\mathbf{z}, \mathbf{u}_x, \tau_3)) \quad (2.3.13)$$

$$T^{cl}(a) := ma \quad (2.3.14)$$

$$\boldsymbol{\tau}^{cl}(\mathbf{z}, \mathbf{u}_x, \tau_3) := \mathcal{S}(\boldsymbol{\omega}) J\boldsymbol{\omega} + J\mathbf{e}_3\tau_3 + J(\mathcal{R}^T \boldsymbol{\alpha} - \mathcal{S}(\mathbf{e}_3)\boldsymbol{\omega}(\mathbf{e}_3^T \boldsymbol{\omega})), \quad (2.3.15)$$

with \mathbf{z} as in (2.3.1) and \mathbf{u}_x as in (2.3.10) (later a and $\boldsymbol{\alpha}$ will take the roll of thrust and torque of the thrust propelling system with state \mathbf{x} ; while τ_3 is a free input that can be used to control the degree of freedom).

For convenience, given a function $\mathbb{R}_{\geq 0} \times \Omega_z \ni (t, \mathbf{z}) \mapsto \mathbf{g}(t, \mathbf{z})$, denote (let $\tau_3 \in \mathbb{R}$)

$$\begin{aligned} \mathbb{R}_{\geq 0} \times \Omega_z \times \mathcal{U}_x \ni (t, \mathbf{z}, \mathbf{u}_x) &\mapsto (D_{f_z} \mathbf{g})(t, \mathbf{z}, \mathbf{u}_x) \\ (D_{f_z} \mathbf{g})(t, \mathbf{z}, \mathbf{u}_x) &:= \partial_t \mathbf{g}(\bar{t}, \mathbf{z})|_{\bar{t}=t} + \partial_{\mathbf{z}} \mathbf{g}(t, \bar{\mathbf{z}})|_{\mathbf{z}=\mathbf{z}} \mathbf{f}_z(\mathbf{z}, \mathbf{u}_z^{cl}(\mathbf{z}, \mathbf{u}_x, \tau_3)). \end{aligned}$$

It then follows from straightforward calculations that

$$(D_{f_z} \mathbf{g}_z^e)(t, \mathbf{z}, \mathbf{u}_x) = \mathbf{v} - \dot{\mathbf{p}}^*(t) = \mathbf{g}_z^v(t, \mathbf{z}); \quad (2.3.16)$$

$$(D_{f_z} \mathbf{g}_z^v)(t, \mathbf{z}, \mathbf{u}_x) = a \mathcal{R}\mathbf{e}_3 + \mathbf{g}\mathbf{e}_3 - \dot{\mathbf{p}}^*(t) = a \mathbf{g}_z^r(t, \mathbf{z}) + \mathbf{g}\mathbf{e}_3 - \dot{\mathbf{p}}^*(t); \quad (2.3.17)$$

$$\begin{aligned} (D_{f_z} \mathbf{g}_z^r)(t, \mathbf{z}, \mathbf{u}_x) &= \mathcal{R}\mathcal{S}(\boldsymbol{\omega}) \mathbf{e}_3 = \mathcal{S}(\mathcal{R}\boldsymbol{\omega}) \mathcal{R}\mathbf{e}_3 = \mathcal{S}(\Pi(\mathcal{R}\mathbf{e}_3)\mathcal{R}\boldsymbol{\omega}) \mathcal{R}\mathbf{e}_3 \\ &= \mathcal{S}(\mathbf{g}_z^\varpi(t, \mathbf{z})) \mathbf{g}_z^r(t, \mathbf{z}); \end{aligned} \quad (2.3.18)$$

and that

$$\begin{aligned}
 (D_{f_z} g_z^\varpi)(t, z, u_x) &= \Pi(\mathcal{R}\mathbf{e}_3)(\mathcal{R}\mathcal{S}(\omega)\mathbf{e}_3 + \mathcal{R}J^{-1}(\tau^{cl}(z, u_x, \tau_3) - \mathcal{S}(\omega)J\omega)) - \\
 &\quad ((\mathcal{R}\mathcal{S}(\omega)\mathbf{e}_3)(\mathcal{R}\mathbf{e}_3)^T + (\mathcal{R}\mathbf{e}_3)(\mathcal{R}\mathcal{S}(\omega)\mathbf{e}_3)^T)\mathcal{R}\omega \\
 &= \Pi(\mathcal{R}\mathbf{e}_3)(\mathcal{R}\mathcal{S}(\omega)\mathbf{e}_3 + \mathcal{R}J^{-1}(\tau^{cl}(z, u_x, \tau_3) - \mathcal{S}(\omega)J\omega)) + \\
 &\quad \mathcal{S}(\mathcal{R}\mathbf{e}_3)\mathcal{R}\omega\mathbf{e}_3^T\omega \\
 &\stackrel{(2.3.15)}{=} \Pi(\mathcal{R}\mathbf{e}_3)\alpha = \Pi(g_z^r(t, z))\alpha. \tag{2.3.19}
 \end{aligned}$$

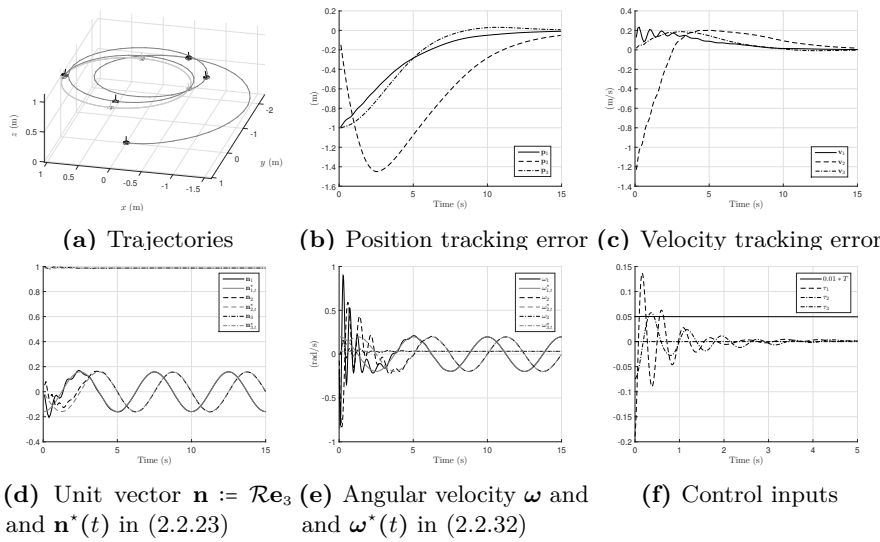
As such, combining results, it follows that (\mathbf{x} as in (2.3.9) and \mathbf{u}_x as in (2.3.10))

$$f_x(t, \mathbf{x}, \mathbf{u}_x) := (D_{f_z} g_z^x)(t, z, u_x) = (\mathbf{v}, ar - \mathbf{g}(t), \mathcal{S}(\varpi)\mathbf{r}_3, \Pi(\mathbf{r})\alpha), \tag{2.3.20}$$

and with $\mathbf{g}(t) := ge_3 + \ddot{\mathbf{p}}^*(t)$. The vector field f_x is that of a thrust-propelled system and, as such, the controller presented in Section 2.2 may be used to accomplish the goal as stated in Problem 2.3.1. Notice that τ_3 in the control law (2.3.13) does not interfere with (2.3.20). This means that we can use τ_3 to control the degree of freedom corresponding to the yaw motion of the quadrotor (more precisely, the degree of freedom corresponds to rotations around $\mathcal{R}\mathbf{e}_3$), and as illustrated in Fig 2.7.

2.3.5 Simulations

In Fig. 2.8, we present a simple solution to (2.3.5), with $\mathbf{z}(0) = (\mathbf{0}, \mathbf{0}, \mathbf{e}_3, \mathbf{0}) \in \Omega_z$, and by using the control law (2.3.15) composed with the control from a thrust-propelled system.



(d) Unit vector $\mathbf{n} := \mathcal{R}\mathbf{e}_3$ and $\mathbf{n}^*(t)$ in (2.2.23) and $\omega^*(t)$ in (2.2.32)

Figure 2.8: Simulation for $\mathbf{z}(0) = (\mathbf{0}, \mathbf{0}, \mathbf{e}_3, \mathbf{0}) \in \Omega_z$.

2.4 Controller for load lifting by a quadrotor

2.4.1 Introduction

Slung load transportation by a UAV is a challenging control problem, since the load sways with respect to the UAV and therefore it is desirable to reduce the relative motion between the UAV and the load. Different control strategies have been proposed for slung loads attached to one or several UAVs by cables. Differential flatness has been explored for the purposes of control and motion planning [30, 31], while dynamic programming has also been used for trajectory planning [53], with the goal of minimizing the load swing. Adaptive controllers have been proposed which compensate for different unknown parameters [29, 34, 54], such as a variable center of gravity, an unknown load mass or a constant input disturbance. A closed loop approach, where the motion of the load is tracked visually from the transporting helicopter, is found in [28], where the information from the visual tracking system is used to determine the frequency of the load sway and thereby the length of the rope. In [10], several quadrotors lift a single load, and the relations in static equilibrium between three quadrotors and a load are analyzed. In [30], differential flatness of the quadrotor-load system is explored for the purposes of trajectory planning.

Regarding the modeling of the slung load system, it is important to emphasize that the system's dynamics change according to whether the cable connecting the load and the quadrotor is under tension or compression, and such a modeling is found in [30].

In this section, we show that system quadrotor-load may be transformed into a thrust-propelled system, and we describe and impose conditions on the desired trajectory that guarantee that the cable remains under tension. Another contribution concerns a disturbance estimator that guarantees that the load tracks a desired trajectory under a constant thrust input disturbance. The results here presented are based on those in [54].

The remainder of this section is structured as follows. In subsection 2.4.3, the model of the quadrotor-load system is presented. In subsection 2.4.4, we provide a coordinate transformation that transforms the quadrotor-load system into the thrust-propelled system. In subsection 2.4.5, a disturbance removal controller is proposed. Finally, in subsection 2.4.6, illustrative simulations and preliminary experimental results are presented.

2.4.2 Notation

For brevity, denote quadrotor by UAV.

$M, m > 0$ UAV's and load's masses

$L > 0$ Cable's length

$\mathbf{P}, \mathbf{p} \in \mathbb{R}^3$ UAV's and the load's center of mass positions

$\mathbf{V}, \mathbf{v} \in \mathbb{R}^3$ UAV's and the load's center of mass velocities

$\mathbf{z} = (\mathbf{p}, \mathbf{v}, \mathbf{P}, \mathbf{V})$	State of the UAV-manipulator system
$U \in \mathbb{R}$	UAV's input thrust/propelling force
$\mathbf{r} \in \mathbb{S}^2$	UAV's input attitude
$\mathbf{u}_z = (U, \mathbf{r})$	Input to the UAV-manipulator system

2.4.3 Modeling

Consider a quadrotor vehicle and a point mass load attached to each other by a cable, as illustrated in Fig. 2.9. One of the cable's end-point coincides with the quadrotor's center of mass, while the other end-point coincides with the load's center of mass. When the cable is not under tension, the load behaves as a free falling (un-actuated) point mass, while the quadrotor behaves as a *standard* quadrotor. On the other hand, when the cable is under tension, it forces the distance between the quadrotor and the load to be identical to the cable length, and for as long as the cable remains under tension. As such, a taut cable *links* the quadrotor and the load, and the load is no longer un-actuated. In fact, the system quadrotor-load may be modeled as a hybrid system, with its (open-loop) vector field switching according to some function of the state and the input. Such modeling is performed in [30], where differential flatness of the system with respect to the load's position is verified, and exploited so as to plan a trajectory for the quadrotor. Consider the constants and variables as defined in the previous Notation section. Denote then

$$\mathbf{z} = (\mathbf{p}, \mathbf{v}, \mathbf{P}, \mathbf{V}) \in \Omega_z, \quad (2.4.1)$$

$$\mathbf{u}_z = (U, \mathbf{r}) \in \mathbb{R} \times \mathbb{S}^2 =: \mathcal{U}_z, \quad (2.4.2)$$

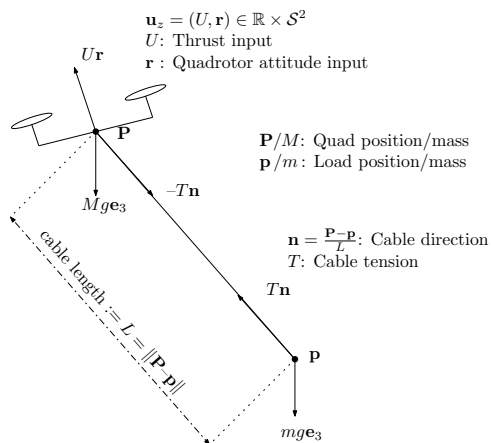


Figure 2.9: Modeling of quadrotor-load system

as the state of and input to the quadrotor-load system, where

$$\Omega_z = \{(\mathbf{p}, \mathbf{v}, \mathbf{P}, \mathbf{V}) \in \mathbb{R}^{12} : (\mathbf{P} - \mathbf{p})^T(\mathbf{P} - \mathbf{p}) = L^2, (\mathbf{P} - \mathbf{p})^T(\mathbf{V} - \mathbf{v}) = 0\}. \quad (2.4.3)$$

$$T_z\Omega_z = \{(\delta\mathbf{p}, \delta\mathbf{v}, \delta\mathbf{P}, \delta\mathbf{V}) \in \mathbb{R}^{12} : (\mathbf{P} - \mathbf{p})^T(\delta\mathbf{P} - \delta\mathbf{p}) = 0,$$

$$(\delta\mathbf{P} - \delta\mathbf{p})^T(\mathbf{V} - \mathbf{v}) + (\mathbf{P} - \mathbf{p})^T(\delta\mathbf{V} - \delta\mathbf{v}) = 0\}. \quad (2.4.4)$$

with Ω_z as the state set and $T_z\Omega_z$ as the tangent space to Ω_z at \mathbf{z} . Given an appropriate $\mathbf{u}_z : \mathbb{R}_{\geq 0} \mapsto \mathbb{R}^3$, the state of the quadrotor-load system $\mathbf{z} : \mathbb{R}_{\geq 0} \mapsto \Omega_z$ evolves according to

$$\dot{\mathbf{z}}(t) = \mathbf{f}_z(\mathbf{z}(t), \mathbf{u}_z(t) + b\mathbf{e}_1), \mathbf{z}(0) \in \Omega_z \quad (2.4.5)$$

where b is a constant unknown thrust input disturbance, and where $\mathbf{f}_z : \Omega_z \times \mathcal{U}_z \ni (\mathbf{z}, \mathbf{u}_z) \mapsto \mathbf{f}_z(\mathbf{z}, \mathbf{u}_z) \in T_z\Omega_z \subset \mathbb{R}^{12}$ is given by

$$\mathbf{f}_z(\mathbf{z}, \mathbf{u}_z) := \left(\mathbf{v}, \frac{\bar{T}(\mathbf{z}, \mathbf{u}_z)}{m} \bar{\mathbf{n}}(\mathbf{z}) - g\mathbf{e}_3, \mathbf{V}, \frac{U\mathbf{r}}{M} - \frac{\bar{T}(\mathbf{z}, \mathbf{u}_z)}{M} \bar{\mathbf{n}}(\mathbf{z}) - g\mathbf{e}_3 \right), \quad (2.4.6)$$

with \mathbf{z} as in (2.4.1), \mathbf{u}_z as in (2.4.2), and where g is the acceleration due to gravity; and where $\bar{\mathbf{n}} : \Omega_z \ni \mathbf{z} \mapsto \bar{\mathbf{n}}(\mathbf{z}) \in \mathbb{S}^2$, $\bar{\omega} : \Omega_z \ni \mathbf{z} \mapsto \bar{\omega}(\mathbf{z}) \in \mathbb{R}^3$ and $\bar{T} : \Omega_z \times \mathcal{U}_z \ni (\mathbf{z}, \mathbf{u}_z) \mapsto \bar{T}(\mathbf{z}, \mathbf{u}) \in \mathbb{R}$ are defined as

$$\bar{\mathbf{n}}(\mathbf{z}) := \frac{\mathbf{P} - \mathbf{p}}{\|\mathbf{P} - \mathbf{p}\|} = \frac{\mathbf{P} - \mathbf{p}}{L}, \quad (2.4.7)$$

$$\bar{\omega}(\mathbf{z}) := \mathcal{S}(\bar{\mathbf{n}}(\mathbf{z})) \frac{\partial \bar{\mathbf{n}}(\mathbf{z})}{\partial \mathbf{z}} \mathbf{f}_z(\mathbf{z}, \cdot) = \mathcal{S}(\bar{\mathbf{n}}(\mathbf{z})) \frac{\mathbf{V} - \mathbf{v}}{L}, \quad (2.4.8)$$

$$\bar{T}(\mathbf{z}, \mathbf{u}) := \frac{m}{M+m} (\mathbf{u}^T \bar{\mathbf{n}}(\mathbf{z}) + ML\|\mathbf{V} - \mathbf{v}\|^2). \quad (2.4.9)$$

Physically, the functions $\bar{\mathbf{n}}$, $\bar{\omega}$ and \bar{T} relate to the cable's unit vector, the cable's angular velocity and to the tension on the cable, respectively (see Fig. 2.9). It can now be verified that for any $(\mathbf{z}, \mathbf{u}_z) \in \Omega_z \times \mathcal{U}_z$, it holds that indeed $\mathbf{f}_z(\mathbf{z}, \mathbf{u}_z) \in T_z\Omega_z$. For that purpose, if we denote $(\delta\mathbf{p}, \delta\mathbf{v}, \delta\mathbf{P}, \delta\mathbf{V}) = \mathbf{f}_z(\mathbf{z}, \mathbf{u}_z)$, it follows that

$$(\mathbf{P} - \mathbf{p})^T(\delta\mathbf{P} - \delta\mathbf{p}) \stackrel{(2.4.6)}{=} (\mathbf{P} - \mathbf{p})^T(\mathbf{V} - \mathbf{v}) \stackrel{(2.4.3)}{=} 0, \quad (2.4.10)$$

$$(\delta\mathbf{P} - \delta\mathbf{p})^T(\mathbf{V} - \mathbf{v}) + (\mathbf{P} - \mathbf{p})^T(\delta\mathbf{V} - \delta\mathbf{v}) = \quad (2.4.11)$$

$$\stackrel{(2.4.6)}{=} (\mathbf{V} - \mathbf{v})^T(\mathbf{V} - \mathbf{v}) + (\mathbf{P} - \mathbf{p})^T \left(\frac{U\mathbf{r}}{M} - \bar{T}(\mathbf{z}, \mathbf{u}) \frac{m+M}{M+m} \bar{\mathbf{n}}(\mathbf{z}) \right) \stackrel{(2.4.7), (2.4.9), (2.4.3)}{=} 0. \quad (2.4.12)$$

As such, given the vector field in (2.4.6), it follows that a trajectory of (2.4.5) that starts in Ω_z remains in Ω_z ; and, consequently, the distance between the UAV and load remains constant and equal to the cable length. An approach for obtaining the vector field in (2.4.6) by means of the Euler-Lagrange formalism is found in [30].

Problem 2.4.1. *Given the system (2.4.5) and a desired trajectory $\mathbf{p}^* \in \mathcal{C}^4(\mathbb{R}_{\geq 0}, \mathbb{R}^3)$, design $\mathbf{u}_z = (U, \mathbf{r}) : \mathbb{R}_{\geq 0} \mapsto \mathbb{R} \times \mathbb{S}^2$ such that $\lim_{t \rightarrow \infty} (\mathbf{p}(t) - \mathbf{p}^*(t)) = \mathbf{0}$.*

Notice that if $U : \mathbb{R}_{\geq 0} \mapsto \mathbb{R}$ and $\mathbf{r} : \mathbb{R}_{\geq 0} \mapsto \mathbb{S}^2$ are control inputs then the quadrotor system itself is fully-actuated; however, for the same inputs, the system quadrotor-load is under-actuated.

2.4.4 Change of Coordinates

We now provide the diffeomorphism, and the control law function, which are used in the control architecture explained in beginning of this chapter (see page 13). With the help of Proposition 1.3.10, in page 11, it follows that

$$\Omega_z \times \mathcal{U}_z \ni (\mathbf{z}, \mathbf{u}_z) \mapsto \bar{\tau}(\mathbf{z}, \mathbf{u}_z) := d\bar{\omega}(\mathbf{z})\mathbf{f}_z(\mathbf{z}, \mathbf{u}_z) = \frac{1}{ML}\Pi(\bar{\mathbf{n}}(\mathbf{z}))U\mathbf{r}. \quad (2.4.13)$$

Notice that $U\mathbf{r} = (U\mathbf{r}^T\bar{\mathbf{n}}(\mathbf{z}))\bar{\mathbf{n}}(\mathbf{z}) + \Pi(\bar{\mathbf{n}}(\mathbf{z}))U\mathbf{r} =: U_1\bar{\mathbf{n}}(\mathbf{z}) + \mathbf{U}_2$. Moreover, notice that $U_1 = U\mathbf{r}^T\bar{\mathbf{n}}(\mathbf{z})$ acts on the tension function in (2.4.9), while $\mathbf{U}_2 = \Pi(\bar{\mathbf{n}}(\mathbf{z}))U\mathbf{r}$ acts on the angular acceleration (torque) of the cable's unit vector in (2.4.13). This insight suggests a path for designing the control law, namely, U_1 is designed so as to control the cable tension, and guaranteeing it remains positive; while \mathbf{U}_2 is designed so as to control the cable's unit vector.

Define then the transformed state as (this will be the thrust-propelled state)

$$\mathbf{x} = (\mathbf{e}, \mathbf{v}, \mathbf{n}, \boldsymbol{\omega}) \in \{(\tilde{\mathbf{e}}, \tilde{\mathbf{v}}, \tilde{\mathbf{n}}, \tilde{\boldsymbol{\omega}}) \in \mathbb{R}^3 \times \mathbb{R}^3 \times \mathcal{S}^2 \times \mathbb{R}^3 : \tilde{\mathbf{n}}^T \tilde{\boldsymbol{\omega}} = 0\} =: \Omega_x, \quad (2.4.14)$$

and with a physical interpretation for the state components that we provide later. We can now define, for each time instant $t \in \mathbb{R}_{\geq 0}$, the diffeomorphism $\mathbf{g}_z^x(t, \cdot) : \Omega_z \ni \mathbf{z} \mapsto \mathbf{g}_z^x(t, \mathbf{z}) \in \Omega_x$ – with $\mathbf{g}_z^x(t, \cdot) := (\mathbf{g}_z^x(t, \cdot))^{-1} : \Omega_x \ni \mathbf{x} \mapsto \mathbf{g}_z^x(t, \mathbf{x}) \in \Omega_z$ – defined as (\mathbf{z} as in (2.4.1) and \mathbf{x} as in (2.4.14))

$$\mathbf{g}_z^x(t, \mathbf{z}) := (\mathbf{p} - \mathbf{p}^*(t), \mathbf{v} - \dot{\mathbf{p}}^*(t), \bar{\mathbf{n}}(\mathbf{z}), \bar{\omega}(\mathbf{z})), \quad (2.4.15)$$

$$\mathbf{g}_z^x(t, \mathbf{x}) := (\mathbf{e} + \mathbf{p}^*(t), \mathbf{v} + \dot{\mathbf{p}}^*(t), L\mathbf{n} + \mathbf{e} + \mathbf{p}^*(t), L\mathcal{S}(\boldsymbol{\omega})\mathbf{n} + \mathbf{v} + \dot{\mathbf{p}}^*(t)). \quad (2.4.16)$$

Let us now provide a physical interpretation for the previous variables. Consider a $\mathbf{z} \in \Omega_z$ and a desired position trajectory $\mathbf{p}^* \in \mathcal{C}^4(\mathbb{R}_{\geq 0}, \mathbb{R}^3)$. Then $\mathbf{e} = \mathbf{p} - \mathbf{p}^*$ and corresponds to the position tracking error (as such, the goal of Problem 2.4.1 may be restated as $\lim_{t \rightarrow \infty} \mathbf{e}(t) = \mathbf{0}$); $\mathbf{v} = \mathbf{v} - \dot{\mathbf{p}}^*$ corresponds to the velocity tracking error; $\mathbf{n} = \bar{\mathbf{n}}(\mathbf{z})$ corresponds to the unit vector associated to the cable direction, as illustrated in Fig. 2.9; and $\boldsymbol{\omega} = \bar{\omega}(\mathbf{z})$ corresponds to the angular velocity of \mathbf{n} .

For convenience, denote

$$\mathbf{u}_x := (T, \boldsymbol{\tau}) \in \mathbb{R}^4 \quad (2.4.17)$$

where $T \in \mathbb{R}$ stands for the tension in the cable, and $\boldsymbol{\tau} \in \mathbb{R}^3$ stands for the torque input to control the cable direction, and which will be the inputs once the system is transformed into the thrust-propelled form. Additionally, denote $\mathbf{U}_x : \Omega_x \times \mathbb{R}^4 \ni (\mathbf{x}, \mathbf{u}_x) \mapsto \mathbf{U}_x(\mathbf{x}, \mathbf{u}_x) \in \mathbb{R}^3$ defined as

$$\mathbf{U}_x(\mathbf{x}, \mathbf{u}_x) = \mathbf{n}((M+m)T - md\|\boldsymbol{\omega}\|^2) + ML\Pi(\mathbf{n})\boldsymbol{\tau}, \quad (2.4.18)$$

and $\Gamma = \{(\mathbf{x}, \mathbf{u}_x) \in \Omega_x \times \mathbb{R}^4 : \mathbf{U}_x(\mathbf{x}, \mathbf{u}_x) \neq \mathbf{0}\}$. Let us now provide the control input transformation mapping, namely

$$\mathbf{u}_z^{cl} : \Gamma \ni (\mathbf{x}, \mathbf{u}_x) \mapsto \mathbf{u}_z^{cl}(\mathbf{x}, \mathbf{u}_x) := \left(\|\mathbf{U}_x(\mathbf{x}, \mathbf{u}_x)\|, \frac{\mathbf{U}_x(\mathbf{x}, \mathbf{u}_x)}{\|\mathbf{U}_x(\mathbf{x}, \mathbf{u}_x)\|} \right) \in \mathbb{R}_{>0} \times \mathcal{S}^2. \quad (2.4.19)$$

Consider a time instant $t \in \mathbb{R}_{\geq 0}$ and a $\mathbf{x} \in \Omega_x$. Then, let $\mathbf{z} = \mathbf{g}_x^z(t, \mathbf{x})$ and $\mathbf{u}_z = \mathbf{u}_z^{cl}(\mathbf{x}, \mathbf{u}_x)$. For this, it follows that the tension in the cable, given in (2.4.9), becomes

$$\bar{T}(\mathbf{z}, \mathbf{u}_z + b\mathbf{e}_1) \stackrel{(2.4.16),(2.4.18),(2.4.19)}{=} mT + \frac{m}{M+m} b \frac{\mathbf{n}^T \mathbf{U}_x(\mathbf{x}, \mathbf{u}_x)}{\|\mathbf{U}_x(\mathbf{x}, \mathbf{u}_x)\|}, \quad (2.4.20)$$

while the torque in the cable, given in (2.4.13), becomes

$$\bar{\tau}(\mathbf{z}, \mathbf{u}_z + b\mathbf{e}_1) \stackrel{(2.4.16),(2.4.18),(2.4.19)}{=} \Pi(\mathbf{n}) \boldsymbol{\tau} + \frac{b}{ML} \Pi(\mathbf{n}) \frac{\mathbf{U}_x(\mathbf{x}, \mathbf{u}_x)}{\|\mathbf{U}_x(\mathbf{x}, \mathbf{u}_x)\|}. \quad (2.4.21)$$

An interpretation for $\mathbf{u}_x = (T, \boldsymbol{\tau}) \in \mathbb{R}^4$ is now clearer from (2.4.20) and (2.4.21). Indeed, in the absence of a disturbance, i.e., $b = 0$, T yields the tension in the cable, apart from a positive multiplicative constant, namely the load's mass; while $\boldsymbol{\tau}$ yields the torque in the cable.

We now transform the vector field (2.4.6) into that of the thrust-propelled system. Given the mappings (2.4.16) and (2.4.19), it follows that (denote $\mathbf{g}(t) := g\mathbf{e}_3 + \dot{\mathbf{p}}^*(t)$)

$$\begin{aligned} & (\partial_{\bar{t}} \mathbf{g}_z^x(\bar{t}, \mathbf{z})|_{\bar{t}=t} + \partial_{\mathbf{z}} \mathbf{g}_z^x(t, \mathbf{z})|_{\mathbf{z}=\mathbf{z}} \mathbf{f}_z(\mathbf{z}, \mathbf{u}_z^{cl}(\mathbf{x}, \mathbf{u}_x) + b\mathbf{e}_1))|_{\mathbf{x}=\mathbf{g}_z^x(t, \mathbf{z})} = \\ &= (\mathbf{v}, T\mathbf{n} - \mathbf{g}(t), \mathcal{S}(\boldsymbol{\omega})\mathbf{n}, \mathcal{S}(\mathbf{n})\boldsymbol{\tau}) + \\ & \quad \left(\mathbf{0}, \frac{1}{M+m} \mathbf{n}\mathbf{n}^T \frac{\mathbf{U}_x(\mathbf{x}, \mathbf{u}_x)}{\|\mathbf{U}_x(\mathbf{x}, \mathbf{u}_x)\|}, \mathbf{0}, \frac{1}{ML} \Pi(\mathbf{n}) \frac{\mathbf{U}_x(\mathbf{x}, \mathbf{u}_x)}{\|\mathbf{U}_x(\mathbf{x}, \mathbf{u}_x)\|} \right) b \end{aligned} \quad (2.4.22)$$

$$=: \mathbf{f}_x(t, \mathbf{x}, \mathbf{u}_x) + \Phi(\mathbf{x}, \mathbf{u}_x)b \quad (2.4.23)$$

where \mathbf{f}_x is the thrust-propelled vector field (as defined in (2.2.10)). As such, in the absence of a disturbance, any controller for a thrust-propelled system may be used in accomplishing the goal as stated in Problem 2.4.1.

2.4.5 Disturbance Estimator

In this section, we provide a solution that accomplishes the goal described in Problem 2.4.1, when a constant unknown disturbance $b \in \{\beta \in \mathbb{R}^3 : |\beta| \leq b^{\max}\} =: \Omega_b$ exists, for some known $b^{\max} \geq 0$. Denote $\hat{b} : \mathbb{R}_{\geq 0} \mapsto \mathbb{R}$ as a disturbance estimate whose dynamics are designed next such that the goal described in Problem 2.4.1 is accomplished. For convenience, and since the disturbance estimate is dynamic, denote $\tilde{\mathbf{x}} = (\mathbf{x}, \hat{b}) \in \Omega_x \times \mathbb{R} =: \Omega_{\tilde{x}}$ as an extended state. Also, $\dot{\tilde{b}}(t) = f_b(t, \tilde{\mathbf{x}}(t))$, where $f_b \in \mathcal{C}(\mathbb{R}_{\geq 0} \times \Omega_{\tilde{x}}, \mathbb{R})$ is a vector field that is constructed next. With the previous notions in mind, it follows that $\dot{\tilde{\mathbf{x}}}(t) = \mathbf{f}_{\tilde{x}}(t, \tilde{\mathbf{x}}(t), \mathbf{u}_x(t))$, where

$$\mathbf{f}_{\tilde{x}}(t, \tilde{\mathbf{x}}, \mathbf{u}_x) = (\mathbf{f}_x(t, \mathbf{x}, \mathbf{u}_x) + \Phi(\mathbf{x}, \mathbf{u}_x)b, f_b(t, \tilde{\mathbf{x}})) \quad (2.4.24)$$

and, it is straightforward to verify that,

$$\begin{aligned} & (\partial_{\bar{t}} \mathbf{g}_z^x(\bar{t}, \mathbf{z})|_{\bar{t}=t} + \partial_{\mathbf{z}} \mathbf{g}_z^x(t, \mathbf{z})|_{\mathbf{z}=\mathbf{z}} \mathbf{f}_z(\mathbf{z}, \mathbf{u}_z))|_{\mathbf{x}=\mathbf{g}_z^x(t, \mathbf{z}), \mathbf{u}_z=\mathbf{u}_z^{cl}(\mathbf{x}, \mathbf{u}_x)-\hat{b}\mathbf{e}_1} = \\ &= (\mathbf{f}_x(t, \mathbf{x}, \mathbf{u}_x^{cl}(t, \mathbf{x})) + \Phi(\mathbf{x}, \mathbf{u}_x^{cl})(b - \hat{b}), f_b(t, \tilde{\mathbf{x}})). \end{aligned} \quad (2.4.25)$$

with $\mathbf{e}_1 \in \mathbb{R}^4$. If the disturbance b were known, it would suffice to choose $\hat{b}(0) = b$, and $f_b = 0$, in order to accomplish the goal in Problem 2.4.1. Since b is unknown, a different strategy is pursued, namely the disturbance estimate is updated with a projector operator that guarantees that the disturbance estimate remains in $\Omega_{\hat{b}} := \{\beta \in \mathbb{R}^3 : |\beta| \leq b^{\max} + \epsilon\}$, where $\epsilon > 0$ is a design parameter that can be chosen as small as desired; and provided that $\hat{b}(0) \in \Omega_{\hat{b}}$ (which is satisfied if $\hat{b}(0) = 0$). Consider then a Lyapunov function for the thrust-propelled system $V_x \in \mathcal{C}^1(\mathbb{R}_{\geq 0} \times \Omega_x, \mathbb{R}_{\geq 0})$ (the one in (2.2.43) is a possible one, if the control law (2.2.47) is chosen). Consider then the vector field

$$f_b(t, \tilde{\mathbf{x}}) = \text{Proj} \left(\Phi^T(\mathbf{x}, \mathbf{u}_x^{cl}(t, \mathbf{x})) \frac{\partial V_x(t, \mathbf{x})}{\partial \mathbf{x}}, \hat{b} \right), \quad (2.4.26)$$

whose choice will be clear next (Proj as defined in [55]). Consider then the Lyapunov function $V_{\tilde{x}} \in \mathcal{C}^1(\mathbb{R}_{\geq 0} \times \Omega_{\tilde{x}}, \mathbb{R}_{\geq 0})$, defined as

$$V_{\tilde{x}}(t, \tilde{\mathbf{x}}) = V_x(t, \mathbf{x}) + \frac{1}{k_b} \frac{(b - \hat{b})}{2}, \quad (2.4.27)$$

where $k_b > 0$. Given (2.4.25) and (2.4.26), it follows that

$$W_{\tilde{x}}(t, \tilde{\mathbf{x}}) = W_x(t, \mathbf{x}) - k_b(b - \hat{b}) \left(f_b(t, \tilde{\mathbf{x}}) - \Phi^T(\mathbf{x}, \mathbf{u}_x^{cl}(t, \mathbf{x})) \frac{\partial V_x(t, \mathbf{x})}{\partial \mathbf{x}} \right) \geq 0. \quad (2.4.28)$$

We may then use the Lyapunov function in (2.4.27) to conclude that $\lim_{t \rightarrow \infty} W_x(t, \mathbf{x}(t)) = 0$, and conclude asymptotic tracking of the desired position trajectory by the load.

2.4.6 Simulations

Consider a quadrotor with mass $M = 1.442$ kg, a load with mass $m = 0.144$ kg, a cable with length $L = 0.5$ m, and a disturbance $b = 0.2$ N. Consider the control law (2.2.53) with $\sigma(s) = 0.25 \frac{s}{\sqrt{1+s^2}}$, $\rho(s) = 0.70 \frac{s}{\sqrt{1+s^2}}$, $k = 1$ and $\Omega(\cdot)$ as an odd function and as the solution to the differential equation $\Omega'''(s) = 0$ for $s \in [0, 1]$, $\Omega'''(s) = s - 1$ for $s \in [1, 2]$ and $\Omega'''(s) = 1$ for $s > 2$ and initial conditions $\Omega(0) = 0$, $\Omega'(0) = 1$ and $\Omega''(0) = 0$. Consider the control law $\mathbf{u}_x^{cl}(\cdot, \cdot)$, in (2.2.47), with gains $v_\theta = 50$, $k_\theta = 1$, $v_\omega = 50$, $k_\omega = 1$; and the estimator vector field, in (2.4.25), with $k_b = 5$ and $\epsilon = 0.3$. For these choices, we provide a simulation in Fig. 2.10, as a solution of (2.4.5) with $\mathbf{z}(0) = (\mathbf{0}, \mathbf{0}, L\mathbf{e}_3, \mathbf{0}) \in \Omega_z$. In Fig. 2.10a, one can visualize in blue the desired trajectory, namely one with the load describing a circular motion of 1 m of radius, and an angular velocity of 0.1 rev/sec; and in black, the actual trajectory of the quadrotor-load system, where convergence to the desired trajectory is verified. In Fig. 2.10b, the position tracking error is presented, and its convergence to $\mathbf{0}$ indicates convergence of the system's trajectory to the desired trajectory. In Fig. 2.10d, the cable's unit vector and its equilibrium are presented, and $\mathbf{n}(\cdot)$ converges to its equilibrium $\mathbf{n}^*(\cdot)$ as defined in (2.2.23). Finally, in Fig. 2.10f, the thrust input, U , is

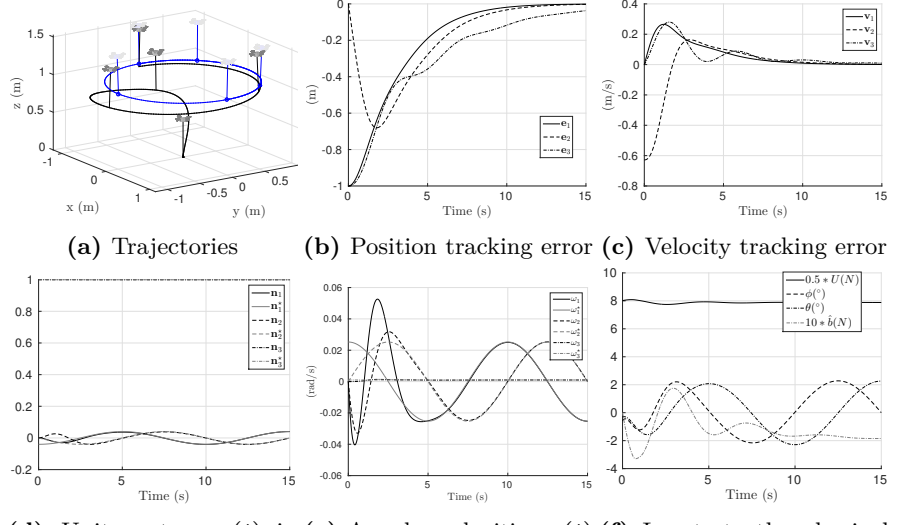


Figure 2.10: Simulation for $\mathbf{z}(0) = (\mathbf{0}, \mathbf{0}, L\mathbf{e}_3, \mathbf{0}) \in \Omega_z$ (In Fig. 2.10f, $\mathbf{r} = (c(\phi)s(\theta), -s(\phi), c(\phi)c(\phi))$).

presented, and the attitude input, \mathbf{r} , is also presented, where the attitude unit vector has been parametrized in pitch and roll angles (recall that $\mathbf{u}_z = (T, \mathbf{r}) = \mathbf{u}_z^{cl}(\mathbf{x}, \mathbf{u}_x^{cl})$). The thrust input stabilizes around a value that cancels the accumulated weight of the quadrotor and the load; while the pitch and roll oscillate around zero, since the load is describing a circle, and therefore the cable must rotate so as to point inwards the circular trajectory. In Fig. 2.10f, the disturbance estimate is also presented, and it converges to the real unknown disturbance, thus canceling its effect. Preliminary experimental results are presented in Fig. 2.11, where a quadrotor-load system is first commanded to hover over a green pen, and afterwards is commanded to hover over a blue pen. The quadrotor was a commercial one, namely an IRIS+ from 3D Robotics; the load weighted about 144 g; the cable had a length of approximately 0.5 m; and position measurements were obtained from a Qualisys motion capture system. A video of this experiment is found in [56].

2.5 Load lifting stability under attitude control delay

2.5.1 Introduction

In this Section, we propose a control law with the objective of steering the load to a desired point in the three dimensional space. Linearization around the equilibrium is used to infer exponential stability of the same equilibrium, and conditions on the



(a) Load hovering over green pen (b) Load hovering over blue pen

Figure 2.11: Preliminary experimental result: load hovering over green pen.

gains are provided for which exponential stability is preserved, in a similar approach to [19]. We modify the control law so as to provide a strategy for augmenting stability [57, Chapter 7], and we study the effect of the delay introduced by the attitude inner loop on the stability of the equilibrium. Finally, we also include an integral action term in the control law for compensating for battery drainage and model mismatches, such as an unknown load mass. The proposed control law may be used to find an initial guess for gains of control laws that are harder to tune but that work for a larger subset of the state space domain, such as that proposed in [54]. The results here presented are based on those in [58].

The remainder of this section is structured as follows. In subsection 2.5.3, the problem statement is described. In subsection 2.5.4, we provide a coordinate transformation, useful for the stability analysis. In subsection 2.5.5, a control law is presented which provides closed loop stability. In subsection 2.5.6, we model the quadrotor attitude inner loop, and provide conditions for which stability is preserved under the previous control law. Finally, in subsection 2.5.7, we present illustrative experimental results.

2.5.2 Notation

We refer the reader to the notation in Section 2.4.2. Given $\bar{\sigma} > 0$, we denote $\sigma(\cdot, \bar{\sigma}) : \mathbb{R} \ni x \mapsto \sigma(x, \bar{\sigma}) := \bar{\sigma} \frac{x}{\sqrt{\bar{\sigma}^2 + x^2}} \in (-\bar{\sigma}, \bar{\sigma})$, as a saturation function bounded by $\bar{\sigma}$ (i.e, $\sup_{x \in \mathbb{R}} |\sigma(x, \bar{\sigma})| = \bar{\sigma}$); we also denote $\sigma^{-1}(\cdot, \bar{\sigma}) : (-\bar{\sigma}, \bar{\sigma}) \ni y \mapsto \sigma^{-1}(y, \bar{\sigma}) = \bar{\sigma} \frac{y}{\sqrt{\bar{\sigma}^2 - y^2}} \in \mathbb{R}$ as the inverse mapping.

2.5.3 Problem Description

We consider the same set-up as in Section 2.4. However, in this Section we focus on local stability results.

Problem 2.5.1. *Given the vector field (2.4.6), design a control law $\mathbf{u}_z^{cl} : \Omega_x \rightarrow \mathbb{R}^3$ such that $\mathbf{z}^* = (\mathbf{p}^*, \mathbf{v}^*, \mathbf{P}^*, \mathbf{V}^*) = (\mathbf{0}, \mathbf{0}, L\mathbf{e}_3, \mathbf{0}) = L\mathbf{e}_9 \in \Omega_z \subset \mathbb{R}^{12}$ is a (locally) exponentially stable equilibrium of $\mathbf{f}_z^{cl} : \Omega_z \ni \mathbf{z} \mapsto \mathbf{f}_z^{cl}(\mathbf{x}) := \mathbf{f}_z(\mathbf{z}, \mathbf{u}_z^{cl}(\mathbf{z})) \in T_z \Omega_z$.*

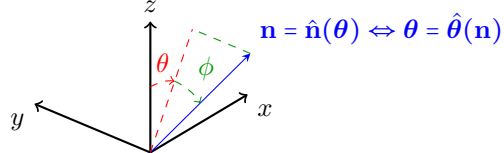


Figure 2.12: Geometric interpretation of (2.5.2) for $\mathbf{n} \in \tilde{\mathbb{S}}^2$ and $\boldsymbol{\theta} = (\phi, \theta) \in \Omega_\theta$

Remark 2.5.2. In general, we may require the load to track a trajectory of constant velocity. Let $\mathbf{p}^* : \mathbb{R}_{\geq 0} \ni t \mapsto \mathbf{p}^*(t) := \tilde{\mathbf{p}}^* + \tilde{\mathbf{v}}^* t \in \mathbb{R}^3$, for some constants $\tilde{\mathbf{p}}^*, \tilde{\mathbf{v}}^* \in \mathbb{R}^3$. Consider any $t \in \mathbb{R}$, $\mathbf{z} = (\mathbf{p}, \mathbf{v}, \mathbf{P}, \mathbf{V}) \in \Omega_x$ and $\mathbf{e} = (\tilde{\mathbf{p}}, \tilde{\mathbf{v}}, \tilde{\mathbf{P}}, \tilde{\mathbf{V}}) \in \Omega_x$; and denote $\phi(t, \cdot) : \Omega_x \ni \mathbf{x} \mapsto \phi(t, \mathbf{z}) \in \Omega_x$ defined as $\phi(t, \mathbf{z}) = (\mathbf{p} - \mathbf{p}^*(t), \mathbf{v} - \tilde{\mathbf{v}}^*, \mathbf{P}, \mathbf{V})$, and $\phi^{-1}(t, \cdot) : \Omega_x \ni \mathbf{e} \mapsto \phi^{-1}(t, \mathbf{e}) \in \Omega_x$ defined as $\phi^{-1}(t, \mathbf{e}) = (\tilde{\mathbf{p}} + \mathbf{p}^*(t), \tilde{\mathbf{v}} + \tilde{\mathbf{v}}^*, \tilde{\mathbf{P}}, \tilde{\mathbf{V}})$. It holds that $\mathbf{f}_x(\mathbf{e}, \mathbf{u}) = (\frac{\partial \phi(t, \mathbf{z})}{\partial t} + \frac{\partial \phi(t, \mathbf{z})}{\partial \mathbf{z}} \mathbf{f}_x(\mathbf{z}, \mathbf{u}))|_{\mathbf{z}=\phi^{-1}(t, \mathbf{e})}$, for any $\mathbf{e} \in \Omega_x$ and $\mathbf{u} \in \mathbb{R}^3$. As such, Problem 2.5.1 may be reformulated so as to consider tracking of constant velocity trajectories.

2.5.4 Coordinate Change

We wish to study the stability properties of $\mathbf{z}^* = L\mathbf{e}_9 \in \Omega_x$ (after a control law has been chosen). However, it proves convenient to study the stability in a different coordinate system, which we associate to the letter x from now. In summary, we provide a coordinate transformation, and study the stability properties in the new coordinate system.

To start with, let us provide some useful functions. Denote, for convenience, $\Omega_\theta = (-\frac{\pi}{2}, \frac{\pi}{2}) \times (-\pi, \pi)$, and $\tilde{\mathbb{S}}^2 = \mathbb{S}^2 \setminus \{(n_x, n_y, n_z) \in \mathbb{S}^2 : n_x = 0, n_z \leq 0\}$. Consider the unit vector parametrization $\hat{\mathbf{n}} : \Omega_\theta \ni \boldsymbol{\theta} \mapsto \hat{\mathbf{n}}(\boldsymbol{\theta}) \in \tilde{\mathbb{S}}^2$ and $\hat{\theta} : \tilde{\mathbb{S}}^2 \ni \mathbf{n} \mapsto \hat{\theta}(\mathbf{n}) \in \Omega_\theta$, defined as

$$\hat{\mathbf{n}}(\boldsymbol{\theta}) := (\cos(\phi) \sin(\theta), -\sin(\phi), \cos(\phi) \cos(\theta)), \quad (2.5.1)$$

$$\hat{\theta}(\mathbf{n}) := \left(\arctan \left(\frac{\mathbf{e}_1^T \mathbf{n}}{\mathbf{e}_3^T \mathbf{n}} \right), -\arcsin(\mathbf{e}_2^T \mathbf{n}) \right), \quad (2.5.2)$$

where $\boldsymbol{\theta} = (\phi, \theta) \in \Omega_\theta$. Figure 2.12 illustrates geometrically the choice of angles and the mappings (2.5.2) (in essence, we associate two angles $(\phi, \theta) \in \Omega_\theta$ to the cable unit vector – see Fig. 2.9). We emphasize that $\hat{\mathbf{n}}(\mathbf{0}_2) = \mathbf{e}_3$, which will allow the equilibrium in the new coordinate system to be at zero. Consider also $\hat{\omega} : \Omega_\theta \times \mathbb{R}^2 \ni (\boldsymbol{\theta}, \boldsymbol{\omega}_\theta) \mapsto \hat{\omega}(\boldsymbol{\theta}, \boldsymbol{\omega}_\theta) \in \mathbb{R}^3$ and $\boldsymbol{\omega}_\theta : \tilde{\mathbb{S}}^2 \times \mathbb{R}^3 \ni (\mathbf{n}, \boldsymbol{\omega}) \mapsto \boldsymbol{\omega}_\theta(\mathbf{n}, \boldsymbol{\omega}) \in \mathbb{R}^2$, defined as

$$\hat{\omega}(\boldsymbol{\theta}, \boldsymbol{\omega}_\theta) := d\hat{\mathbf{n}}(\boldsymbol{\theta}) \boldsymbol{\omega}_\theta = \begin{bmatrix} -\sin(\phi) \sin(\theta) & \cos(\phi) \cos(\theta) \\ -\cos(\phi) & 0 \\ -\sin(\phi) \cos(\theta) & -\cos(\phi) \sin(\theta) \end{bmatrix} \begin{bmatrix} \omega_\phi \\ \omega_\theta \end{bmatrix}, \quad (2.5.3)$$

$$\boldsymbol{\omega}_{\hat{\theta}}(\mathbf{n}, \boldsymbol{\omega}) := d\hat{\theta}(\mathbf{n})\mathcal{S}(\boldsymbol{\omega})\mathbf{n} = \begin{bmatrix} 0 & \frac{-1}{\sqrt{1-(\mathbf{e}_2^T \mathbf{n})^2}} & 0 \\ \frac{(\mathbf{e}_3^T \mathbf{n})}{1-(\mathbf{e}_2^T \mathbf{n})^2} & 0 & \frac{-(\mathbf{e}_1^T \mathbf{n})}{1-(\mathbf{e}_2^T \mathbf{n})^2} \end{bmatrix} \mathcal{S}(\boldsymbol{\omega})\mathbf{n}, \quad (2.5.4)$$

where $\boldsymbol{\theta} = (\phi, \theta)$ and $\boldsymbol{\omega}_{\theta} = (\omega_{\phi}, \omega_{\theta})$ (later, we let $\dot{\boldsymbol{\theta}} = \boldsymbol{\omega}_{\theta}$).

We are now in position to provide the mapping between coordinates. Denote

$$\mathbf{x} = (\mathbf{p}, \mathbf{v}, \boldsymbol{\theta}, \boldsymbol{\omega}_{\theta}) = ((p_x, p_y, p_z), (v_x, v_y, v_z), (\phi, \theta), (\omega_{\phi}, \omega_{\theta})) \in \Omega_z, \quad (2.5.5)$$

$$\Omega_z = \mathbb{R}^3 \times \mathbb{R}^3 \times \Omega_{\theta} \times \mathbb{R}^2, \quad (2.5.6)$$

and consider the diffeomorphism $\mathbf{g}_z^x : \Omega_z \ni \mathbf{z} \mapsto \mathbf{g}_z^x(\mathbf{z}) \in \Omega_x$, and $\mathbf{g}_x^z : \Omega_x \ni \mathbf{x} \mapsto \mathbf{g}_x^z(\mathbf{x}) \in \Omega_z$, defined as

$$\mathbf{g}_z^x(\mathbf{z}) := (\mathbf{p}, \mathbf{v}, \hat{\boldsymbol{\theta}}(\bar{\mathbf{n}}(\mathbf{z})), \boldsymbol{\omega}_{\theta}(\bar{\mathbf{n}}(\mathbf{z}), \bar{\boldsymbol{\omega}}(\mathbf{z}))) \quad (2.5.7)$$

$$\mathbf{g}_x^z(\mathbf{x}) := (\mathbf{p}, \mathbf{v}, \mathbf{p} + L\hat{\mathbf{n}}(\boldsymbol{\theta}), \mathbf{v} + L\mathcal{S}(\hat{\boldsymbol{\omega}}(\boldsymbol{\theta}, \boldsymbol{\omega}_{\theta}))\hat{\mathbf{n}}(\boldsymbol{\theta})), \quad (2.5.8)$$

with \mathbf{x} as in (2.5.5) and \mathbf{z} as in (2.4.1); and with $\hat{\mathbf{n}}, \hat{\boldsymbol{\theta}}$ and $\hat{\boldsymbol{\omega}}, \boldsymbol{\omega}_{\theta}$ as defined in (2.5.2) and (2.5.3), respectively. Notice that $\mathbf{g}_z^x(\mathbf{z}^*) = \mathbf{0} \Leftrightarrow \mathbf{g}_x^z(\mathbf{0}) = \mathbf{z}^*$, and thus in the new coordinate system $\mathbf{x}^* = \mathbf{0} \in \mathbb{R}^{10}$ is the equilibrium we wish to render exponentially stable (see Problem 2.5.1). The open loop vector field in the new coordinate system is given by

$$\mathbf{f}_x : \Omega_z \times \mathbb{R}^3 \ni (\mathbf{x}, \mathbf{u}) \mapsto \mathbf{f}_x(\mathbf{x}, \mathbf{u}) = dg_z^x(\mathbf{z})\mathbf{f}_z(\mathbf{z}, \mathbf{u})|_{\mathbf{z}=g_x^z(\mathbf{x})} \in \mathbb{R}^{10}. \quad (2.5.9)$$

In the new coordinates, it follows that $\mathbf{f}_x(\mathbf{0}, (M+m)g\mathbf{e}_3) = \mathbf{0}$, which means (as shall be seen later) that $\mathbf{x}^* = \mathbf{0}$ is an equilibrium point for the closed loop vector field (intuition suggests that the equilibrium control input is $(M+m)g\mathbf{e}_3$, which corresponds to the total weight that needs to be canceled). It is easier to study stability properties for (2.5.9) than for (2.4.6), however, (2.5.9) is considerably lengthier to write explicitly when compared to (2.4.6), which is why it is omitted here.

2.5.5 Simple Control Law

We are now in position to present the control law. For convenience, we use three subscripts $\{x, y, z\}$, with $k \in \{x, y, z\}$ standing for the motion in the k -direction. For each $k \in \{x, y, z\}$, consider then

$$u_k : \mathbb{R}^2 \ni (p, v) \mapsto u_k(p, v) := -k_{p,k}\sigma(p, \sigma_{p,k}) - k_{v,k}\sigma(v, \sigma_{v,k}) \in \mathbb{R} \quad (2.5.10)$$

where $\sigma(\cdot, \cdot)$ is a saturation function (see Notation); $k_{p,k}$ and $k_{v,k}$ are positive gains related to the position and velocity feedback, respectively; and $\sigma_{p,k}$ and $\sigma_{v,k}$ are saturations related to the position and velocity feedback, respectively (note that $\sup_{(p,v) \in \mathbb{R}^2} |u_k(p, v)| = k_{p,k}\sigma_p + k_{v,k}\sigma_v$).

Consider then the control law $\mathbf{u}_z^{cl} : \Omega_x \ni \mathbf{z} \mapsto \mathbf{u}_z^{cl}(\mathbf{z}) \in \mathbb{R}^3$ defined as

$$\mathbf{u}_z^{cl}(\mathbf{z}) := \begin{bmatrix} Mu_x(\mathbf{e}_1^T \mathbf{P}, \mathbf{e}_1^T \mathbf{V}) + MLk_\theta \mathbf{e}_1^T \bar{\mathbf{n}}(\mathbf{z}) \\ Mu_y(\mathbf{e}_2^T \mathbf{P}, \mathbf{e}_2^T \mathbf{V}) + MLk_\theta \mathbf{e}_2^T \bar{\mathbf{n}}(\mathbf{z}) \\ (M+m)(g + u_z(\mathbf{e}_3^T \mathbf{p}, \mathbf{e}_3^T \mathbf{v})) \end{bmatrix}, \quad (2.5.11)$$

with u_x , u_y and u_z defined in (2.5.10) for $k \in \{x, y, z\}$. Given the control law (2.5.11), the closed loop vector field becomes

$$\mathbf{f}_x^{cl} : \Omega_x \ni \mathbf{x} \mapsto \mathbf{f}_x^{cl}(\mathbf{x}) := \mathbf{f}_x(\mathbf{x}, \mathbf{u}_z^{cl}(\mathbf{z}))|_{\mathbf{z}=g_x^z(\mathbf{x})} \in \mathbb{R}^{10}, \quad (2.5.12)$$

and $\mathbf{x}^* = \mathbf{0}$ is indeed an equilibrium of (2.5.12), since $\mathbf{u}_z^{cl}(\mathbf{z}^*) = (M+m)g\mathbf{e}_3$. Linearizing (2.5.12) around $\mathbf{0}_{10}$ yields the matrix $A = d\mathbf{f}_x^{cl}(\mathbf{0}_{10})$, which can be transformed into a block diagonal (A is not a block diagonal matrix) via an appropriate similarity transformation. For that purpose, consider

$$P := [P_x \ P_y \ P_z]^T \in \mathbb{R}^{10 \times 10}, \quad (2.5.13)$$

$$P_x := [\mathbf{e}_1 \ \mathbf{e}_3 \ g\mathbf{e}_8 \ g\mathbf{e}_{10}] \in \mathbb{R}^{10 \times 4}, \quad (2.5.14)$$

$$P_y := [\mathbf{e}_2 \ \mathbf{e}_4 \ -g\mathbf{e}_7 \ -g\mathbf{e}_9] \in \mathbb{R}^{10 \times 4}, \quad (2.5.15)$$

$$P_z := [\mathbf{e}_3 \ \mathbf{e}_6] \in \mathbb{R}^{10 \times 2}. \quad (2.5.16)$$

It follows that $PAP^{-1} = A_x \oplus A_y \oplus A_z$ (see Notation), where (let $h \in \{x, y\}$)

$$A_z = \begin{bmatrix} 0 & 1 \\ -k_{p,z} & -k_{p,z} \end{bmatrix}, A_h = \begin{bmatrix} 0 & 1 & 0 & 0 \\ 0 & 0 & 1 & 0 \\ 0 & 0 & 0 & 1 \\ -\frac{g}{L}k_{p,h} & -\frac{g}{L}k_{v,h} & -(k_{p,h} + k_\theta + \frac{g}{L}\frac{M+m}{M}) & -k_{v,h} \end{bmatrix}. \quad (2.5.17)$$

We have thus one chain of two integrators, related to the z motion of the load; and two chains of four integrators, related to the horizontal motion of the load. Indeed, denoting,

$$\boldsymbol{\xi}_x(\mathbf{z}) = P_x^T \mathbf{z} \stackrel{(2.5.15)}{=} (p_x, v_x, g\theta, g\omega_\theta) \quad (2.5.18)$$

$$\boldsymbol{\xi}_y(\mathbf{z}) = P_y^T \mathbf{z} \stackrel{(2.5.15)}{=} (p_y, v_y, -g\phi, -g\omega_\phi) \quad (2.5.19)$$

$$\boldsymbol{\xi}_z(\mathbf{z}) = P_z^T \mathbf{z} \stackrel{(2.5.15)}{=} (p_z, v_z) \quad (2.5.20)$$

(with \mathbf{z} as in (2.4.1)), it follows that $\dot{\mathbf{z}}(t) = A\mathbf{z}(t)$ implies that

$$\frac{d^4 p_h(t)}{dt^4} = \mathbf{e}_4^T A_h \boldsymbol{\xi}_h(\mathbf{z}(t)) = \mathbf{e}_4^T A_h \left[\frac{d^0 p_h(t)}{dt^0} \dots \frac{d^3 p_h(t)}{dt^3} \right]^T, h \in \{x, y\}, \quad (2.5.21)$$

$$\frac{d^2 p_z(t)}{dt^2} = \mathbf{e}_2^T A_z \boldsymbol{\xi}_z(\mathbf{z}(t)) = \mathbf{e}_5^T A_z \left[\frac{d^0 p_z(t)}{dt^0} \frac{d^1 p_z(t)}{dt^1} \right]^T. \quad (2.5.22)$$

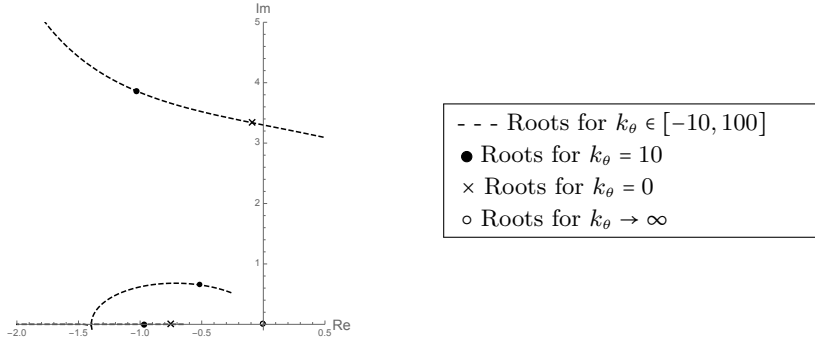


Figure 2.13: Roots of characteristic polynomial of A_x , in (2.5.17), in the complex plane (conjugate poles are omitted); all other constants are those provided in Section 2.5.7.

For the roots of the characteristic polynomial of A_z in (2.5.17) to have negative real part, it suffices that $k_{p,z} > 0$ and $k_{v,z} > 0$. For finding the location of the roots of the characteristic polynomial of A_h in (2.5.17) w.r.t. the imaginary axis, we apply the Routh's criterion to (2.5.17) [57, Chapter 7], and obtain (these are the numbers in the first column of the Routh's table)

$$\left[1 \quad k_{v,h} \quad k_{v,h} \left(\frac{g}{L} \frac{m}{M} + k_\theta + k_{p,h} \right) \quad \frac{g}{L} \left(\frac{g}{L} \frac{m}{M} + k_\theta \right) k_{v,h}^2 \quad \frac{g}{L} k_{p,h} \right], \quad (2.5.23)$$

which guarantees that exponential stability is preserved for as long as $k_\theta > -\left(\frac{g}{L} \frac{m}{M} + k_{p,h}\right)$ for $h \in \{x, y\}$ (in this case, all entries are positive). More importantly, we can look at the roots of the characteristic polynomial of A_h (in (2.5.17)) for different values of k_θ , as done in Fig. 2.13. As inferred from that figure, increasing k_θ (for example, from 0 to 10 see Fig. 2.13) has the benefit of making the system faster, i.e., of increasing the speed of convergence to the equilibrium. As such, k_θ can be tuned so as to augment the stability of the closed loop.

2.5.6 Attitude Control Delay

Previously, in subsection 2.5.3, we assumed that the UAV provides the requested input without delay. However, that is not the case in a real physical system, and it is important to study the effect of delays in the closed loop stability for the proposed control law. From here on, we work with augmented states and use a bar notation to denote those. Consider then the augmented state

$$\bar{\mathbf{z}} = (\mathbf{z}, \mathbf{r}) \in \Omega_z \times \mathbb{S}^2 =: \Omega_{\bar{z}} \quad (2.5.24)$$

where $\mathbf{r} \in \mathbb{S}^2$ is the quadrotor's direction where input thrust is provided (see Fig. 2.9). The state $\bar{\mathbf{z}} : \mathbb{R}_{\geq 0} \ni t \mapsto \bar{\mathbf{z}}(t) \in \Omega_{\bar{z}}$ evolves according to

$$\dot{\bar{\mathbf{z}}}(t) = \mathbf{f}_{\bar{z}}(\bar{\mathbf{z}}(t), \mathbf{u}(t)), \bar{\mathbf{z}}(0) \in \Omega_{\bar{z}} \quad (2.5.25)$$

where

$$\begin{aligned}\mathbf{f}_{\bar{z}} : \Omega_{\bar{z}} \times \mathbb{R}^3 \setminus \{\mathbf{0}\} &\ni (\bar{\mathbf{z}}, \mathbf{u}) \mapsto \mathbf{f}_{\bar{z}}(\bar{\mathbf{z}}, \mathbf{u}) := (\mathbf{f}_z(\mathbf{z}, \mathbf{u}^T \mathbf{r} \mathbf{r}), \mathbf{f}_r(\mathbf{r}, \mathbf{u})) \\ &:= \left(\mathbf{f}_x(\mathbf{z}, \mathbf{u}^T \mathbf{r} \mathbf{r}), k_{\bar{\theta}} \Pi(\mathbf{r}) \frac{\mathbf{u}}{\|\mathbf{u}\|} \right) \in T_{\bar{\mathbf{z}}} \Omega_{\bar{z}},\end{aligned}\quad (2.5.26)$$

with \mathbf{f}_x as in (2.4.6), and with $k_{\bar{\theta}}$ as a positive gain that relates to the delay ($\frac{1}{k_{\bar{\theta}}}$ may be interpreted as a time constant of a first order system).

Let us provide some intuition for (2.5.26). Consider a constant $\mathbf{r}^* \in \mathbb{S}^2$ and the function $V : \mathbb{S}^2 \ni \mathbf{r} \mapsto V(\mathbf{r}) = 1 - \mathbf{r}^T \mathbf{r}^* \in [0, 2]$: then, along a solution $\mathbb{R}_{\geq 0} \ni t \mapsto \mathbf{r}(t) := \mathbf{r}_0 + \int_0^t \mathbf{f}_r(\mathbf{r}(\tau), \mathbf{r}^*) \tau d\tau = \mathbf{r}_0 + k_{\bar{\theta}} \int_0^t \Pi(\mathbf{r}(\tau)) \mathbf{r}^* d\tau$ (for some $\mathbf{r}_0 \in \mathbb{S}^2$), it follows that $\dot{V}(\mathbf{r}(t)) = -W(\mathbf{r}(t))$ where $\mathbb{S}^2 \ni \mathbf{r} \mapsto W(\mathbf{r}) := -dV(\mathbf{r}) \mathbf{f}_r(\mathbf{r}, \mathbf{r}^*) = k_{\bar{\theta}} \mathbf{r}^{*T} \Pi(\mathbf{r}) \mathbf{r}^* = k_{\bar{\theta}} \|\Pi(\mathbf{r}) \mathbf{r}^*\|^2 = k_{\bar{\theta}} V(\mathbf{r})(2 - V(\mathbf{r}))$; this suffices to conclude that $V(\mathbf{r}(\cdot))$ converges to either 0 or 2. In fact, it converges to 0 as long as $\mathbf{r}_0 \neq -\mathbf{r}^*$, and it converges exponential fast. For a time-varying $\mathbf{r}^* : \mathbb{R}_{\geq 0} \mapsto \mathbb{S}^2$, the same conclusion follows if $\dot{\mathbf{r}}(t) = \dot{\mathbf{r}}^*(t) + k_{\bar{\theta}} \Pi(\mathbf{r}(t)) \mathbf{r}^*$, with $\dot{\mathbf{r}}^*(\cdot)$ as a feedforward term. In (2.5.26), a feedforward term is not included, since the desired attitude at the equilibrium is constant. Thus, loosely speaking, if $k_{\bar{\theta}}$ is *big* and $\mathbf{u}(\cdot)$ is slow varying, $\mathbf{r}(\cdot)$ converges exponentially fast to $\frac{\mathbf{u}(\cdot)}{\|\mathbf{u}(\cdot)\|}$; this in turn guarantees that $\mathbf{u}^T(\cdot) \mathbf{r}(\cdot) \mathbf{r}(\cdot)$ converges to $\mathbf{u}(\cdot)$, in which case the model in Section 2.4.3 is recovered (see (2.4.6), in page 34). Note also that \mathbf{f}_r models the attitude inner loop of the quadrotor in (2.5.26), but there are more ways of modeling that inner loop.

As done in previous subsection, it is convenient to work in a new coordinate system. For that reason, denote

$$\bar{\mathbf{x}} = (\mathbf{x}, \bar{\boldsymbol{\theta}}) = (\mathbf{x}, (\bar{\phi}, \bar{\theta})) \in \Omega_{\bar{x}} \stackrel{\mathbf{x} \text{ as in (2.5.5)}}{=} \Omega_x \times \Omega_{\theta}, \quad (2.5.27)$$

and consider $g_{\bar{z}}^{\bar{x}} : \Omega_{\bar{z}} \ni \bar{\mathbf{z}} \mapsto g_{\bar{z}}^{\bar{x}}(\bar{\mathbf{z}}) \in \Omega_{\bar{x}}$ and $g_{\bar{x}}^{\bar{z}} : \Omega_{\bar{x}} \ni \bar{\mathbf{x}} \mapsto g_{\bar{x}}^{\bar{z}}(\bar{\mathbf{x}}) \in \Omega_{\bar{z}}$ defined as

$$g_{\bar{z}}^{\bar{x}}(\bar{\mathbf{z}}) := (g_z^x(\mathbf{z}), \hat{\boldsymbol{\theta}}(\mathbf{r})), g_{\bar{x}}^{\bar{z}}(\bar{\mathbf{x}}) := (g_z^x(\mathbf{x}), \hat{\mathbf{n}}(\bar{\boldsymbol{\theta}})), \quad (2.5.28)$$

with $\bar{\mathbf{z}}$ and $\bar{\mathbf{x}}$ as in (2.5.24) and (2.5.27), respectively; and with $\hat{\boldsymbol{\theta}}$ and $\hat{\mathbf{n}}$ as in (2.5.2). Geometrically, we parametrize the quadrotor unit vector \mathbf{r} (see Fig. 2.9) by two angles $\bar{\boldsymbol{\theta}} = (\bar{\phi}, \bar{\theta}) \in \Omega_{\theta}$ similarly to the parametrization of the cable unit vector \mathbf{n} by $\boldsymbol{\theta} = (\phi, \theta) \in \Omega_{\theta}$ (see Fig. 2.12)

From (2.5.28), one can construct the open loop vector field for the augmented system, $\mathbf{f}_{\bar{x}}(\bar{\mathbf{x}}, \mathbf{u}) \stackrel{(2.5.27)}{=} dg_{\bar{z}}^{\bar{x}}(\bar{\mathbf{z}}) \mathbf{f}_z(\bar{\mathbf{z}}, \mathbf{u})|_{\bar{\mathbf{x}}=g_{\bar{z}}^{\bar{x}}(\bar{\mathbf{z}})}$, for which it follows that $\mathbf{f}_{\bar{x}}(\mathbf{0}_{12}, (M+m)g\mathbf{e}_3) = \mathbf{0}_{12}$ (and thus zero is an equilibrium).

Consider then the control law (2.5.11), which leads to the closed loop vector field $\mathbf{f}_{\bar{x}}^{cl} : \Omega_{\bar{x}} \ni \bar{\mathbf{x}} \mapsto \mathbf{f}_{\bar{x}}^{cl}(\bar{\mathbf{x}}) := \mathbf{f}_{\bar{x}}(\bar{\mathbf{x}}, \mathbf{u}^{cl}(\mathbf{z}))|_{\mathbf{z}=g_{\bar{x}}^{\bar{z}}(\bar{\mathbf{x}})} \in \mathbb{R}^{12}$ and to the linearization matrix $\bar{A} = d\mathbf{f}_{\bar{x}}^{cl}(\mathbf{0}_{12})$. Similarly to the previous subsection, consider $\bar{P} = [\bar{P}_x \bar{P}_y \bar{P}_z]^T \in \mathbb{R}^{12 \times 12}$ where

$$\bar{P}_x = \begin{bmatrix} P_x & \frac{g^2}{L} \frac{M+m}{M} (\mathbf{e}_8 - \mathbf{e}_{11}) \\ \mathbf{0}_{2 \times 4} & \end{bmatrix} \in \mathbb{R}^{12 \times 5}, \quad (2.5.29)$$

$$\bar{P}_y = \begin{bmatrix} P_y \\ \mathbf{0}_{2 \times 4} \end{bmatrix} - \frac{g^2}{L} \frac{M+m}{M} (\mathbf{e}_9 - \mathbf{e}_{12}) \in \mathbb{R}^{12 \times 5}, \quad (2.5.30)$$

$$\bar{P}_z = \begin{bmatrix} P_z \\ \mathbf{0}_{2 \times 2} \end{bmatrix} \in \mathbb{R}^{12 \times 2}, \quad (2.5.31)$$

for which it follows that $\bar{P} \bar{A} \bar{P}^{-1} = \bar{A}_x \oplus \bar{A}_y \oplus \bar{A}_z$, where $\bar{A}_z = A_z$ and, for $h \in \{x, y\}$,

$$\bar{A}_h = \begin{bmatrix} \begin{bmatrix} 0 & 1 & 0 & 0 \\ 0 & 0 & 1 & 0 \\ 0 & 0 & 0 & 1 \\ 0 & 0 & 0 & 0 \end{bmatrix} & \begin{bmatrix} 0 \\ 0 \\ 0 \\ 1 \end{bmatrix} \\ k_{\bar{\theta}} \mathbf{e}_4^T A_h - \frac{g}{L} \frac{M+m}{M} \mathbf{e}_4^T & -k_{\bar{\theta}} \end{bmatrix} \quad (2.5.32)$$

As such, when considering the system (2.5.26) with a delay, we have one chain of two integrators, related to the z motion of the load (as in previous subsection); and two chains of five integrators, related to the horizontal motion of the load (as opposed to four, as in the previous subsection). Indeed, denoting (for brevity, we omit for the y coordinate)

$$\begin{aligned} \bar{\xi}_x(\bar{\mathbf{z}}) &\stackrel{(2.5.27)}{=} (\xi_x(\mathbf{z}), \frac{g^2}{L} \frac{M+m}{M} (\theta - \bar{\theta})), \\ &\stackrel{(2.5.19)}{=} (p_x, v_x, g\theta, g\omega_\theta, \frac{g^2}{L} \frac{M+m}{M} (\theta - \bar{\theta})), \end{aligned} \quad (2.5.33)$$

it follows that $\dot{\bar{\mathbf{z}}}(t) = \bar{A}\bar{\mathbf{z}}(t)$ implies that

$$\frac{d^5 p_x(t)}{dt^5} = \mathbf{e}_5^T \bar{A}_x \bar{\xi}_x(\bar{\mathbf{z}}(t)) = \mathbf{e}_5^T \bar{A}_x \left[\frac{d^0 p_x(t)}{dt^0} \dots \frac{d^4 p_x(t)}{dt^4} \right]^T. \quad (2.5.34)$$

For finding the location of the roots of the characteristic polynomial of (2.5.32) w.r.t. the imaginary axis, we apply the Routh's criterion with $k_{\theta} = 0$, and obtain (for convenience, denote $\gamma = k_{\bar{\theta}} k_{v,h} - k_{p,h}$)

$$\begin{bmatrix} 1 & k_{\bar{\theta}} & k_{\bar{\theta}}\gamma & k_{\bar{\theta}}^2\gamma \left(\frac{g}{L} \frac{m}{M} + k_{p,h} \right) & k_{\bar{\theta}}^2 \frac{g^2}{L^2} \frac{m}{M} \gamma^2 & \frac{g}{L} k_{p,h} \end{bmatrix}. \quad (2.5.35)$$

Thus exponential stability of the equilibrium is preserved for as long as $\gamma > 0 \Leftrightarrow k_{\bar{\theta}} > \frac{k_{p,h}}{k_{v,h}}$, i.e., provided that the attitude gain is *big enough*. Since, we do not have control over $k_{\bar{\theta}}$, preserving stability amounts to guaranteeing that $\frac{k_{p,h}}{k_{v,h}}$, for $h \in \{x, y\}$, remains *small enough*.

Theorem 2.5.3. Consider the quadrotor-load system with the open loop vector field (2.5.26), and the control law (2.5.11). Then, the equilibrium $\bar{\mathbf{z}}^* = (L\mathbf{e}_9, \mathbf{e}_3) \in \Omega_z \times \mathbb{S}^2$ of $\mathbf{f}_z^{cl}(\bar{\mathbf{z}}) \stackrel{(2.5.24)}{=} \mathbf{f}_z(\bar{\mathbf{z}}, \mathbf{u}^{cl}(\mathbf{z}))$ is exponentially stable if and only if $k_{\bar{\theta}} > \max_{h \in \{x, y\}} \frac{k_{p,h}}{k_{v,h}}$, i.e., iff the attitude inner loop is sufficiently fast.

Proof. Linearizing $\mathbf{f}_{\bar{x}}^{cl}(\bar{\mathbf{x}}) = dg_{\bar{z}}^{\bar{x}}(\bar{\mathbf{z}})\mathbf{f}_{\bar{z}}^{cl}(\bar{\mathbf{z}})|_{\bar{\mathbf{z}}=g_{\bar{x}}^{\bar{z}}(\bar{\mathbf{x}})}$ around $\bar{\mathbf{x}}^* = g_{\bar{z}}^{\bar{x}}(\bar{\mathbf{z}}^*) = \mathbf{0}_{12}$ yields the matrix (2.5.32) with $k_\theta = 0$. Exponential stability of the equilibrium follows from the Routh's criterion inferred from (2.5.35). \square

If we apply the Routh's criterion for an arbitrary k_θ , we obtain

$$\begin{bmatrix} 1 & k_{\bar{\theta}} & k_{\bar{\theta}}(k_{\bar{\theta}}k_{v,h} - (k_{p,h} + k_\theta)) & \gamma_1 & \gamma_2 & \frac{g}{L}k_{p,h} \end{bmatrix} \quad (2.5.36)$$

where γ_1 and γ_2 are quadratic expressions on k_θ and $k_{\bar{\theta}}$, and which we omit for brevity. Thus the equilibrium is exponentially stable only if

$$k_{\bar{\theta}} > (k_{p,h} + k_\theta)k_{v,h}^{-1} \Leftrightarrow k_\theta < k_{\bar{\theta}}k_{v,h} - k_{p,h}. \quad (2.5.37)$$

The previous condition is necessary, but not sufficient: for sufficiency, positiveness of all entries in (2.5.36) must be guaranteed.

Recall that the control law (2.5.11) sufficed to render the equilibrium stable, and the same conclusion holds as long as $k_{\bar{\theta}} > \frac{k_{p,h}}{k_{v,h}}$. As such, a large proportional gain (w.r.t. the derivative gain) requires a fast attitude inner loop.

In Section 2.5.5, it was deduced that choosing a positive k_θ augmented the closed loop stability; however, notice from (2.5.37) that a larger k_θ requires a larger $k_{\bar{\theta}}$, and, consequently, for a *slow* attitude inner loop (*small* $k_{\bar{\theta}}$), choosing a *large* positive k_θ , instead of augmenting stability, may actually render the equilibrium unstable.

In Fig. 2.14a, the roots of the characteristic polynomial of (2.5.32) are plotted for different delays and for $k_\theta \in [-40, 37] \text{ s}^{-2}$. For example, for $k_{\bar{\theta}} = \frac{1}{0.6} \text{ s}^{-1}$, $k_\theta = -1.5 \text{ s}^{-2} < 0$ is better than $k_\theta = 0 \text{ s}^{-2}$ in the sense that it provides a better distribution of roots. In fact, for each $k_{\bar{\theta}} > 0$ there is an interval for k_θ where exponential stability is preserved. In Fig. 2.14b, the roots are plotted for different k_θ and for $k_{\bar{\theta}} \in [\frac{1}{10}, 10] \text{ s}^{-1}$. As can be seen, choosing a positive k_θ may actually render the equilibrium unstable (see Fig. 2.14b with $k_\theta = 2 \text{ s}^{-2}$). As expected, notice that the equilibrium becomes unstable when $k_{\bar{\theta}} \rightarrow 0$, i.e., when the attitude inner loop becomes *too slow*.

Remark 2.5.4. *Adding an integral action adds robustness again disturbances and model mismatches, such as an unknown load that is picked-up by the aerial vehicle. In [58], an integral action term is included in the control law, and the stability of the equilibrium is still guaranteed.*

2.5.7 Experimental Results

For the experiments, a commercial quadrotor was used, namely an IRIS+ from 3D Robotics, weighting $M = 1.442 \text{ kg}$, with a maximum payload of 0.4 kg . For the load, a wood block weighting $m = 0.145 \text{ kg}$ (corresponding to $\approx 10\%$ of the UAV's weight) was chosen, attached to the UAV by a cable of $L = 0.9 \text{ m}$. The commands for controlling the quadrotor are processed on a ground station, developed in a ROS environment, and sent to the on-board autopilot, which allows for remotely controlling the aerial vehicle through a desired three dimensional force input. A

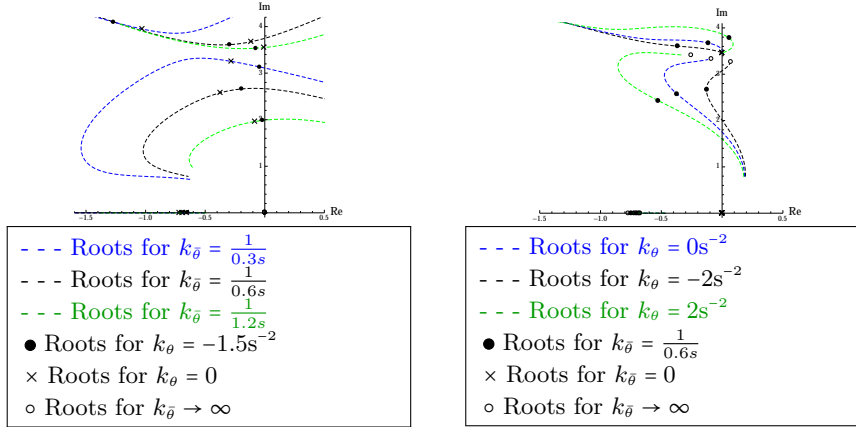


Figure 2.14: Roots of characteristic polynomial of \bar{A}_x , in (2.5.32), in the complex plane (conjugate poles are omitted, and all other constants are those in subsection 2.5.7.).

wireless radio communication between ground station and autopilot is established through a telemetry radio, using a MAVLink protocol that directly overrides the signals sent from the radio transmitter. The quadrotor's and load's position and velocity are estimated by 12 cameras from a Qualisys motion capture system.

The control law (2.5.11) is applied, with $k_{i,z} = 0.25\text{s}^{-3}$ and $\sigma_{i,z} = 0.5\text{ms}^{-2}$ (these are gains for the integral action [58]); with $k_\theta = -2\text{s}^{-2}$; with $k_{p,x} = k_{p,y} = 3.5\text{s}^{-2}$, $k_{v,x} = k_{v,y} = 5.5\text{s}^{-1}$, $\sigma_{p,x} = \sigma_{p,y} = 0.5\text{m}$ and $\sigma_{v,x} = \sigma_{v,y} = 0.5\text{ms}^{-1}$; with $k_{p,z} = 1.0\text{s}^{-2}$, $k_{v,z} = 1.2\text{s}^{-1}$, $\sigma_{p,z} = 0.5\text{m}$ and $\sigma_{v,z} = 0.5\text{ms}^{-1}$ (see (2.5.11)). We provide three experiments, in Figs. 2.15–2.17.

In Fig 2.15, the load is required to hover at $\tilde{\mathbf{p}}^* = 0.5\mathbf{e}_3\text{m}$ (see Remark 2.5.2), and the control law is tested for robustness with respect to disturbances; first, the load is disturbed in the x -direction (at $t \approx 8\text{s}$); then disturbed in the y -direction (at $t \approx 18\text{s}$); and, finally, the UAV is disturbed in the x -direction (at $t \approx 28\text{s}$). The effect of these disturbances is seen in all Figs. 2.15a–2.15d. All these disturbances are well damped, as seen in Fig. 2.15c. In Fig 2.16, the load is required to hover at the consecutive points $\tilde{\mathbf{p}}^* \in \{(0, 0, 0.5), (1.2, 1.2, 0.5), (1.2, -1.2, 0.5), (-1.2, -1.2, 0.5), (-1.2, 1.2, 0.5), (0, 0, 0.5)\}\text{m}$. There is an interval of ten seconds between consecutive points, which correspond to the corners of a square (see Fig. 2.16a). The tracking performance is shown in Fig. 2.16b, and the larger standard deviation of the cable angles is around 3.2° – see Fig. 2.16c. In Fig 2.17, the load is required to describe a circle on the horizontal plane centered around $0.5\mathbf{e}_3\text{m}$, with radius of 1.04m and at 0.1rev/s ; this, in turn, implies that the quadrotor is required to describe a circle on the horizontal plane centered around $1.4\mathbf{e}_3\text{m}$, with radius of 1m and at 0.1rev/s . The tracking performance is shown in Fig. 2.17b, and the larger standard deviation of the cable angles is around 5° – see Fig. 2.16c; perfect tracking of the circle would lead to a standard deviation of 1.6° .

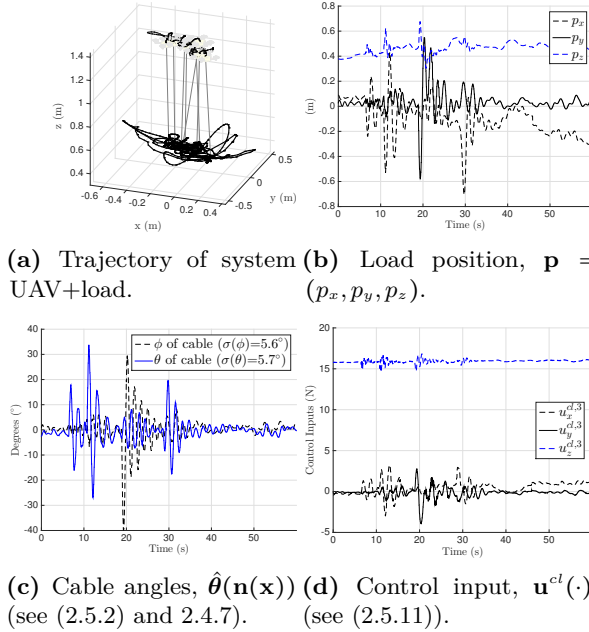


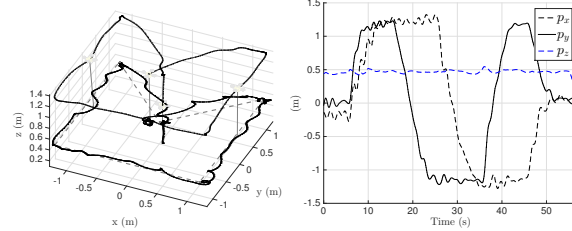
Figure 2.15: Impulse disturbances on UAV+load system (disturbance on load in the x and y directions, at $t \approx 8s$ and $t \approx 18s$; and disturbance on UAV in the x -direction, at $t \approx 27s$).

2.6 Decoupled design of controllers for aerial manipulation with quadrotors

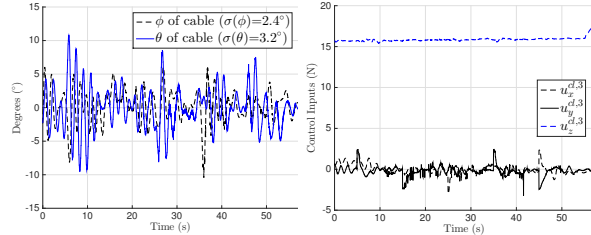
2.6.1 Introduction

When combining a UAV and a robotic manipulator, their dynamics are coupled, and controllers that consider the complete dynamics are found. In [59], cartesian impedance control is studied, while [60] designs a passivity-based controller. Robust and/or adaptive controllers are developed in [61, 62] that control the motion of a multirotor while the manipulator is driven to a desired position carrying a load.

In this work, we also consider the complete quadrotor-manipulator system's dynamics in the control design and analysis. We provide a change of coordinates which splits the system into two decoupled subsystems, one concerning the dynamics of the center of mass of the quadrotor-manipulator system; and another concerning the manipulator's orientation dynamics. These subsystems' dynamics are similar to those of quadrotor's dynamics, and we propose controllers that guarantee that the quadrotor tracks a desired position trajectory, while the manipulator's orientation tracks a desired orientation. Finally, we also consider an input disturbance on the thrust of the quadrotor, and one of our main contributions concerns a disturbance

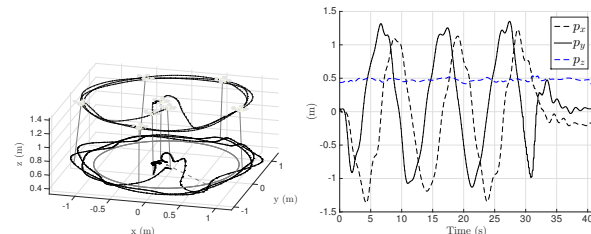


(a) Trajectory of system UAV+load.
(b) Load position, $\mathbf{p} = (p_x, p_y, p_z)$.

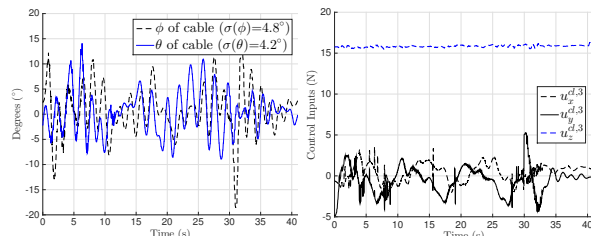


(c) Cable angles, $\hat{\theta}(\mathbf{n}(\mathbf{x}))$
(d) Control input, $\mathbf{u}^{cl}(\cdot)$
(see (2.5.2) and 2.4.7).
(see (2.5.11)).

Figure 2.16: System UAV+load, with load required to move to the corners of a square of length 1.2m, at intervals of 10s.



(a) Trajectory of system UAV+load.
(b) Load position, $\mathbf{p} = (p_x, p_y, p_z)$.



(c) Cable angles, $\hat{\theta}(\mathbf{n}(\mathbf{x}))$
(d) Control input, $\mathbf{u}^{cl}(\cdot)$
(see (2.5.2) and 2.4.7).
(see (2.5.11)).

Figure 2.17: System UAV+load, with load required to describe a circle of radius 1.04m, and at 0.1rev/s.

estimate method that guarantees that the previous tracking objectives are still accomplished; and where the disturbance estimate depends on the position tracking error and the orientation tracking error according to different gains, owing to the decoupling. The results here presented are based on those in [15].

The remainder of this section is structured as follows. In subsection 2.6.3, we provide a model of the quadrotor-manipulator system, and we describe the tracking problem. In subsections 2.6.4, we provide the diffeomorphism used in converting the system into two separate thrust propelled systems. Finally, in subsection 2.6.5, simulations and experiments are provided that validate the proposed algorithms.

2.6.2 Notation

For brevity, denote quadrotor by UAV.

$M, m > 0$	UAV's and load's masses
$L > 0$	Manipulator's length
$\mathbf{P}, \mathbf{p} \in \mathbb{R}^3$	UAV's and the load's center of mass positions
$\mathbf{V}, \mathbf{v} \in \mathbb{R}^3$	UAV's and the load's center of mass velocities
$\mathcal{R} \in \mathbb{SO}(3)$	UAV's rotation matrix
$\mathbf{r} := \mathcal{R}\mathbf{e}_3 \in \mathbb{S}^2$	UAV's direction along which input thrust is provided
$\mathbf{z} = (\mathbf{p}, \mathbf{v}, \mathbf{P}, \mathbf{V}, \mathbf{r})$	State of the UAV-manipulator system
$U \in \mathbb{R}$	UAV's input thrust/propelling force
$\boldsymbol{\omega} \in \mathbb{R}^3$	UAV's input angular velocity, expressed in the inertial frame
$\boldsymbol{\tau} \in \mathbb{R}^3$	Input torque on the manipulator
$\mathbf{u}_z = (U, \boldsymbol{\omega}, \boldsymbol{\tau})$	Input to the UAV-manipulator system

2.6.3 Modeling

Consider a quadrotor vehicle and a point mass load attached to each other by a rigid manipulator, as illustrated in Fig. 2.18. The manipulator end-points coincide with the quadrotor's and the load's center of mass. Moreover, we assume there is a ball joint connecting the quadrotor's center of mass and one of the manipulator's end-point, which overlap; and finally we assume that an input torque on the manipulator is available. Under the absence of such an input torque, the load attached to one of the manipulator's end-point behaves as a slung load, that can swing with respect to the quadrotor. When the ball joint is locked, the input torque is determined from this constraint, and the manipulator moves rigidly with the quadrotor. Also, notice that the manipulator imposes a kinematic constraint on the system, namely it enforces the distance between the quadrotor's and load's positions to be constant and equal to the manipulator's length, which we assume is constant. Later, we prove the quadrotor-manipulator system is differentially flat with respect to the system's center of mass and the manipulator's orientation. With that in mind, the focus of

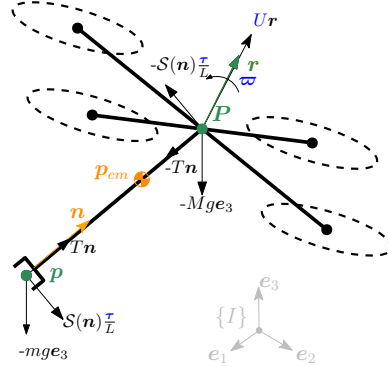


Figure 2.18: Modeling of quadrotor-manipulator system

this paper is on providing closed-loop control laws that guarantee that the system's center of mass follows a desired trajectory and that the manipulator's orientation follows a desired orientation.

Consider the constants and variables as defined in the previous Notation subsection. Denote then

$$\mathbf{z} = (\mathbf{p}, \mathbf{v}, \mathbf{P}, \mathbf{V}, \mathbf{r}) \in \Omega_z \quad (2.6.1)$$

$$\mathbf{u}_z = (U, \varpi, \boldsymbol{\tau}) \in \mathbb{R} \times \mathbb{R}^3 \times \mathbb{R}^3 =: \mathcal{U}_z \quad (2.6.2)$$

where \mathbf{z} and \mathbf{u}_z stand for the state of and input to the quadrotor-manipulator system and

$$\Omega_z := \{(\mathbf{p}, \mathbf{v}, \mathbf{P}, \mathbf{V}, \mathbf{r}) \in (\mathbb{R}^3)^5 : \mathbf{r}^T \mathbf{r} = 1, (\mathbf{P} - \mathbf{p})^T (\mathbf{P} - \mathbf{p}) = L, (\mathbf{V} - \mathbf{v})^T (\mathbf{P} - \mathbf{p}) = 0\}, \quad (2.6.3)$$

$$T_{\mathbf{z}} \Omega_z := \{(\delta \mathbf{p}, \delta \mathbf{v}, \delta \mathbf{P}, \delta \mathbf{V}, \delta \mathbf{r}) \in (\mathbb{R}^3)^5 : \mathbf{r}^T \delta \mathbf{r} = 0, (\delta \mathbf{P} - \delta \mathbf{p})^T (\mathbf{P} - \mathbf{p}) = 0, \quad (2.6.4)$$

$$(\delta \mathbf{V} - \delta \mathbf{v})^T (\mathbf{P} - \mathbf{p}) + (\mathbf{V} - \mathbf{v})^T (\delta \mathbf{P} - \delta \mathbf{p}) = 0\}, \quad (2.6.5)$$

where Ω_z is the state set and $T_{\mathbf{z}} \Omega_z$ the tangent space to Ω_z at $\mathbf{z} \in \Omega_z$. Given an appropriate $\mathbf{u}_z = (U, \varpi, \boldsymbol{\tau}) : \mathbb{R}_{\geq 0} \mapsto \mathcal{U}_z$, we consider the trajectory $\mathbf{z} : \mathbb{R}_{\geq 0} \mapsto \Omega_z$ evolving according to the dynamics

$$\dot{\mathbf{z}}(t) = \mathbf{f}_z(\mathbf{z}(t), \mathbf{u}_z(t)), \mathbf{z}(0) \in \Omega_z, \quad (2.6.6)$$

where $\mathbf{f}_z : \Omega_z \times \mathcal{U}_z \ni (\mathbf{z}, \mathbf{u}_z) \mapsto \mathbf{f}_z(\mathbf{z}, \mathbf{u}_z) \in T_{\mathbf{z}} \Omega_z$ is given by

$$\mathbf{f}_z(\mathbf{z}, \mathbf{u}_z) := (\mathbf{v}, \mathbf{a}(\mathbf{z}, \mathbf{u}_z), \mathbf{V}, \mathbf{A}(\mathbf{z}, \mathbf{u}_z), \mathcal{S}(\varpi) \mathbf{r}), \quad (2.6.7)$$

$$\mathbf{a}(\mathbf{z}, \mathbf{u}_z) := \frac{T(\mathbf{z}, \mathbf{u}_z + b \mathbf{e}_1)}{m} \bar{\mathbf{n}}(\mathbf{z}) + \mathcal{S}(\bar{\mathbf{n}}(\mathbf{z})) \frac{\boldsymbol{\tau}}{mL} - g \mathbf{e}_3, \quad (2.6.8)$$

$$\mathbf{A}(\mathbf{z}, \mathbf{u}_z) := \frac{U + b}{M} \mathbf{r} - \frac{T(\mathbf{z}, \mathbf{u}_z + b \mathbf{e}_1)}{M} \bar{\mathbf{n}}(\mathbf{z}) - \mathcal{S}(\bar{\mathbf{n}}(\mathbf{z})) \frac{\boldsymbol{\tau}}{ML} - g \mathbf{e}_3, \quad (2.6.9)$$

where g is the acceleration due to gravity, and where $\bar{\mathbf{n}} : \Omega_z \ni \mathbf{z} \mapsto \bar{\mathbf{n}}(\mathbf{z}) \in \mathbb{S}^2$, $\bar{\boldsymbol{\omega}} : \Omega_z \ni \mathbf{z} \mapsto \bar{\boldsymbol{\omega}}(\mathbf{z}) \in \mathbb{R}^3$ and $T : \Omega_z \times \mathcal{U}_z \ni (\mathbf{z}, \mathbf{u}_z) \mapsto T(\mathbf{z}, \mathbf{u}_z) \in \mathbb{R}$ are defined as

$$\bar{\mathbf{n}}(\mathbf{z}) = \frac{\mathbf{P} - \mathbf{p}}{\|\mathbf{P} - \mathbf{p}\|} = \frac{\mathbf{P} - \mathbf{p}}{L}, \bar{\boldsymbol{\omega}}(\mathbf{z}) := \mathcal{S}(\bar{\mathbf{n}}(\mathbf{z})) \frac{\mathbf{V} - \mathbf{v}}{L}, \quad (2.6.10)$$

$$T(\mathbf{z}, \mathbf{u}_z) = \frac{m}{M+m} \left(U \mathbf{r}^T \bar{\mathbf{n}}(\mathbf{z}) + \frac{M}{L} \|\mathbf{V} - \mathbf{v}\|^2 \right), \quad (2.6.11)$$

and where $b \in \mathbb{R}$ is a constant unknown disturbance acting on the thrust input (and $\mathbf{e}_1 \in \mathbb{R}^7$). The functions \mathbf{a} and \mathbf{A} are related to the loads' and the quadrotors acceleration; the functions $\bar{\mathbf{n}}$ and $\bar{\boldsymbol{\omega}}$ in (2.6.10) are related with the manipulator's orientation and angular velocity, respectively; and, finally, the function T in (2.6.11) is related with the tension/compression exerted on the manipulator.

Finding the vector field (2.6.7) may be accomplished by means of the Euler-Lagrange formalism. Here, however, that vector field was derived by considering the net force in each center of mass, where the tension is taken as an internal force. This internal force is then found by guaranteeing that

$$\mathbf{f}_z(\mathbf{z}, \mathbf{u}_z) \in T_z \Omega_z \quad \forall (\mathbf{z}, \mathbf{u}_z) \in \Omega_z \times \mathcal{U}_z, \quad (2.6.12)$$

which is indeed the case. This guarantees that Ω_z is in fact positively invariant, i.e., the tension in the manipulator guarantees that the distance between the quadrotor's and the load's center of mass remains constant and equal to the manipulator's length. Notice also that the tension on the manipulator does not depend on the torque input, since this torque does not attempt to drive the quadrotor away from the load; rather it only attempts to make the quadrotor and load rotate around each other.

Problem 2.6.1. Given the system (2.6.6), a desired trajectory $\mathbf{P}^* : \mathbb{R}_{\geq 0} \mapsto \mathbb{R}^3$ and a desired orientation $\bar{\mathbf{n}}^* : \mathbb{R}_{\geq 0} \mapsto \mathbb{S}^2$, design $\mathbf{u}_z = (U, \boldsymbol{\varpi}, \boldsymbol{\tau}) : \mathbb{R}_{\geq 0} \mapsto \mathcal{U}_z$, such that $\lim_{t \rightarrow \infty} (\mathbf{P}(t) - \mathbf{P}^*(t)) = \mathbf{0}$ and $\lim_{t \rightarrow \infty} (\bar{\mathbf{n}}(t) - \bar{\mathbf{n}}^*(t)) = \mathbf{0}$ along solutions of (2.6.6).

Problem 2.6.1 can be restated as finding a control law, such that the quadrotor follows a desired trajectory, while the manipulator follows a desired orientation. For example, we may want the quadrotor to describe a circular motion, while the manipulator is always pointing downwards. As shall be seen later, Problem 2.6.1 can also be restated as finding a control law, such that the center of mass of the quadrotor-manipulator system follows a desired trajectory given by $\mathbf{P}^* - L \frac{m}{M+m} \bar{\mathbf{n}}^*$, while the manipulator follows the desired orientation given by $\bar{\mathbf{n}}^*$.

2.6.4 Control Strategy

Coordinate transformation

In this subsection, we provide a coordinate transformation between the state as defined in Section 2.6.3 and the state of two separate thrust propelled systems. This

coordinate transformation has a clear physical interpretation and it corresponds to the diffeomorphism as explained in the beginning of the chapter (see Fig. 2.2, in page 14). For that purpose, consider $\mathbf{p}_{cm} : \Omega_z \ni \mathbf{z} \mapsto \mathbf{p}_{cm}(\mathbf{z}) \in \mathbb{R}^3$ and $\mathbf{v}_{cm} : \Omega_z \ni \mathbf{z} \mapsto \mathbf{v}_{cm}(\mathbf{z}) \in \mathbb{R}^3$ defined as

$$\mathbf{p}_{cm}(\mathbf{z}) = \frac{M\mathbf{P} + m\mathbf{p}}{M+m}, \mathbf{v}_{cm}(\mathbf{z}) = \frac{M\mathbf{V} + m\mathbf{v}}{M+m}, \quad (2.6.13)$$

where, physically, $\mathbf{p}_{cm}(\mathbf{z})$ and $\mathbf{v}_{cm}(\mathbf{z})$ stand, respectively, for the position and velocity of the center of mass of the quadrotor-manipulator system with state $\mathbf{z} \in \Omega_z$ (see Fig. 2.18). It follows from (2.6.13) and (2.6.10) that, for \mathbf{z} as in (2.6.1),

$$\mathbf{P} = \mathbf{p}_{cm}(\mathbf{z}) + \bar{\mathbf{n}}(\mathbf{z}) \frac{Lm}{M+m} \Leftrightarrow \mathbf{p}_{cm}(\mathbf{z}) = \mathbf{P} - \frac{Lm}{M+m} \bar{\mathbf{n}}(\mathbf{z}), \quad (2.6.14)$$

$$\mathbf{p} = \mathbf{p}_{cm}(\mathbf{z}) - \bar{\mathbf{n}}(\mathbf{z}) \frac{LM}{M+m} \Leftrightarrow \mathbf{p}_{cm}(\mathbf{z}) = \mathbf{p} + \frac{Lm}{M+m} \bar{\mathbf{n}}(\mathbf{z}). \quad (2.6.15)$$

Equation (2.6.14) motivates the definition $\mathbf{p}_{cm}^* : \mathbb{R}_{\geq 0} \ni t \mapsto \mathbf{p}_{cm}^*(t) := \mathbf{P}^*(t) - \frac{Lm}{M+m} \mathbf{n}^*(t) \in \mathbb{R}^3$ as the desired position trajectory for the system's center of mass.

Denote then

$$\mathbf{x}_1 = (\mathbf{e}, \mathbf{v}, \mathbf{r}) \in \mathbb{R}^3 \times \mathbb{R}^3 \times \mathbb{S}^2 =: \Omega_{x_1} \quad (2.6.16)$$

$$\mathbf{x}_2 = (\mathbf{n}, \boldsymbol{\omega}) \in \{(\tilde{\mathbf{n}}, \tilde{\boldsymbol{\omega}}) \in \mathbb{S}^2 \times \mathbb{R}^3 : \tilde{\boldsymbol{\omega}}^T \tilde{\mathbf{n}} = 0\} =: \Omega_{x_2} \quad (2.6.17)$$

$$\mathbf{x} = (\mathbf{x}_1, \mathbf{x}_2) \in \Omega_x := \Omega_{x_1} \times \Omega_{x_2} \quad (2.6.18)$$

where \mathbf{x}_1 and \mathbf{x}_2 are the states of the two decoupled systems we obtain after considering the diffeomorphism presented next. Physically, \mathbf{e} and \mathbf{v} correspond to the position and velocity tracking error of the center of mass, while \mathbf{r} is still the quadrotor direction along which thrust is provided; on the other hand, \mathbf{n} and $\boldsymbol{\omega}$ correspond to the manipulator unit vector and angular velocity. Consider then, for each positive time instant t , the diffeomorphism $g_z^x(t, \cdot) : \Omega_z \ni \mathbf{z} \mapsto g_z^x(t, \mathbf{z}) \in \Omega_x$ – with $g_x^z(t, \cdot) := (g_z^x)^{-1}(t, \cdot) : \Omega_x \ni \mathbf{x} \mapsto g_x^z(t, \mathbf{x}) \in \Omega_z$ – defined as

$$g_z^x(t, \mathbf{z}) := (g_z^{x_1}(t, \mathbf{z}), g_z^{x_2}(t, \mathbf{z})) \quad (2.6.19)$$

$$:= ((\mathbf{p}_{cm}(\mathbf{z}) - \mathbf{p}_{cm}^{*(0)}(t), \mathbf{v}_{cm}(\mathbf{z}) - \mathbf{p}_{cm}^{*(1)}(t), \mathbf{r}), (\bar{\mathbf{n}}(\mathbf{z}), \bar{\boldsymbol{\omega}}(\mathbf{z}))), \quad (2.6.20)$$

and

$$\begin{aligned} g_x^z(t, \mathbf{x}) &:= \left(\mathbf{e} + \mathbf{p}_{cm}^{*(0)}(t) - \mathbf{n} \frac{M}{M+m}, \mathbf{v} + \mathbf{p}_{cm}^{*(1)}(t) - \mathcal{S}(\boldsymbol{\omega}) \mathbf{n} \frac{M}{M+m}, \right. \\ &\quad \left. \mathbf{e} + \mathbf{p}_{cm}^{*(0)}(t) + \mathbf{n} \frac{m}{M+m}, \mathbf{v} + \mathbf{p}_{cm}^{*(1)}(t) + \mathcal{S}(\boldsymbol{\omega}) \mathbf{n} \frac{m}{M+m}, \mathbf{r} \right). \end{aligned} \quad (2.6.21)$$

Compare the map g_x^z as in (2.6.21) and \mathbf{z} as in (2.6.1), and recall the meaning of \mathbf{x} : this should provide some intuition for (2.6.21). Finally, denote

$$\mathbf{u}_{x_1} = (u, \boldsymbol{\varpi}) \in \mathbb{R} \times \mathbb{R}^3 \quad (2.6.22)$$

$$\mathbf{u}_x := (\mathbf{u}_{x_1}, \mathbf{u}_{x_2}) \in \mathbb{R}^7 =: \mathcal{U}_x \quad (2.6.23)$$

where \mathbf{u}_{x_1} and \mathbf{u}_{x_2} correspond to the input of the systems with states \mathbf{x}_1 and \mathbf{x}_2 , respectively. Finally, define $\mathbf{u}_z^{cl} : \Omega_x \times \mathcal{U}_x \ni (\mathbf{x}, \mathbf{u}_x) \mapsto \mathbf{u}_z^{cl}(\mathbf{x}, \mathbf{u}_x) \in \mathcal{U}_z$ as

$$\mathbf{u}_z^{cl}(\mathbf{x}, \mathbf{u}_x) := \left((M+m)u, \boldsymbol{\varpi}, L^2 \frac{Mm}{M+m} \mathcal{S}(\mathbf{n}) \left(\boldsymbol{\alpha} - \frac{(M+m)u}{LM} \mathbf{r} \right) \right), \quad (2.6.24)$$

which provides the necessary input transformation, as illustrated in Fig. 2.2. It then follows, from straightforward calculations, that

$$\begin{aligned} \mathbf{f}_x(t, \mathbf{x}, \mathbf{u}_x) &:= \left(\partial_{\bar{t}} \mathbf{g}_z^x(\bar{t}, \mathbf{z})|_{\bar{t}=t} + \partial_{\bar{\mathbf{z}}} \mathbf{g}_z^x(t, \bar{\mathbf{z}})|_{\mathbf{z}=\mathbf{z}} \mathbf{f}_z(\mathbf{z}, \mathbf{u}_z) \right) |_{\mathbf{z}=\mathbf{g}_z^x(t, \mathbf{x}), \mathbf{u}_z=\mathbf{u}_z^{cl}(\mathbf{x}, \mathbf{u}_x)} \\ &= ((\mathbf{v}, \mathbf{ur} - (g\mathbf{e}_3 + \mathbf{p}_{cm}^{*(2)}(t)), \mathcal{S}(\boldsymbol{\varpi}) \mathbf{r}), (\mathcal{S}(\boldsymbol{\omega}) \mathbf{n}, \mathcal{S}(\mathbf{n}) \boldsymbol{\alpha})) + \\ &\quad \left(\mathbf{0}, \frac{\mathbf{r}}{M+m}, \mathbf{0}, \mathbf{0}, \mathcal{S}(\mathbf{n}), \frac{\mathbf{r}}{LM} \right) b \\ &=: (\mathbf{f}_{x_1}(t, \mathbf{x}_1, \mathbf{u}_{x_1}), \mathbf{f}_{x_2}(t, \mathbf{x}_2, \mathbf{u}_{x_2})) + \Phi(\mathbf{x}_1)b. \end{aligned} \quad (2.6.25)$$

Attaining (2.6.25) follows from straightforward but lengthy computations [15]. Notice now that the coordinate change in (2.6.20) and the input change in (2.6.24) lead to a vector field (2.6.25), where the open-loop dynamics of the states \mathbf{x}_1 and \mathbf{x}_2 (see (2.6.18)) are not coupled. In fact, in the absence of a disturbance, i.e., if $b = 0$, we can design control laws for \mathbf{u}_{x_1} and \mathbf{u}_{x_2} that depend only on the respective states.

In the presence of an unknown disturbance, a similar approach to that presented in Subsection 2.4.5 may be pursued [15], where we introduce a disturbance estimator \hat{b} (and the extended state $\tilde{\mathbf{x}} = (\mathbf{x}, \hat{b}) \in \Omega_{\tilde{x}} := \Omega_x \times \mathbb{R}$) and design a vector field f_b for this estimator. Here we present a summary of the design steps, and we refer the reader to [15] for details. In summary, it suffices to construct a Lyapunov function $V_{\tilde{x}} : \mathbb{R}_{\geq 0} \times \Omega_{\tilde{x}} \ni (t, \tilde{\mathbf{x}}) \mapsto V_{\tilde{x}}(t, \tilde{\mathbf{x}}) \in \mathbb{R}_{\geq 0}$ given by

$$V_{\tilde{x}}(t, \tilde{\mathbf{x}}) = \sum_{i \in \{1, 2\}} k_{\hat{b}_i} V_{x_i}(t, \mathbf{x}_i) + \frac{(\hat{b} - b)^2}{2} \quad (2.6.26)$$

where $k_{\hat{b}_1}$ and $k_{\hat{b}_2}$ are positive gains and V_{x_1} and V_{x_2} are Lyapunov functions for which

$$W_{x_i}(t, \mathbf{x}_i) = - \left(\partial_{\bar{t}} V_{x_i}(\bar{t}, \mathbf{x}_i)|_{\bar{t}=t} + \partial_{\bar{\mathbf{x}}_i} V_{x_i}(t, \bar{\mathbf{x}}_i)|_{\bar{\mathbf{x}}_i=\mathbf{x}_i} \mathbf{f}_{x_i}(t, \mathbf{x}_i, \mathbf{u}_{x_i}^{cl}(t, \mathbf{x}_i)) \right) \geq 0 \quad (2.6.27)$$

given a control law $\mathbf{u}_{x_i}^{cl}$ and for $i \in \{1, 2\}$. Similarly to as in Subsection 2.4.5, the disturbance estimator vector field is then chosen as

$$\begin{aligned} f_b(t, \tilde{\mathbf{x}}) &= \text{Proj} \left(\Phi^T(\mathbf{x}) \partial_{\tilde{\mathbf{x}}} V_{\tilde{x}}(t, \tilde{\mathbf{x}})|_{\tilde{\mathbf{x}}=\tilde{\mathbf{x}}}, \hat{b} \right) \\ &= \text{Proj} \left(\Phi^T(\mathbf{x}) \left(\sum_{i \in \{1, 2\}} k_{\hat{b}_i} \partial_{\tilde{\mathbf{x}}_i} V_{x_i}(t, \bar{\mathbf{x}}_i)|_{\bar{\mathbf{x}}_i=\mathbf{x}_i} \right), \hat{b} \right), \end{aligned} \quad (2.6.28)$$

with $\text{Proj}(\cdot, \cdot)$ as defined in [63]. It then follows that

$$\begin{aligned} W_{\tilde{x}}(t, \tilde{\mathbf{x}}) &:= - \left(\partial_{\bar{t}} V_{\tilde{x}}(\bar{t}, \tilde{\mathbf{x}})|_{\bar{t}=t} + \partial_{\tilde{\mathbf{x}}} V_{\tilde{x}}(t, \tilde{\mathbf{x}})|_{\tilde{\mathbf{x}}=\tilde{\mathbf{x}}} (\mathbf{f}_x(t, \mathbf{x}, \mathbf{u}_x^{cl}(t, \mathbf{x}), f_b(t, \tilde{\mathbf{x}}))) \right), \\ (2.6.25), (2.6.28) &= \sum_{i \in \{1, 2\}} k_{\hat{b}_i} W_{x_i}(t, \mathbf{x}_i) + (b - \hat{b})(f_b(t, \tilde{\mathbf{x}}) - \Phi^T(\mathbf{x}) \partial_{\tilde{\mathbf{x}}} V_{\tilde{x}}(t, \tilde{\mathbf{x}})|_{\tilde{\mathbf{x}}=\tilde{\mathbf{x}}}) \geq 0. \end{aligned}$$

As such, we can invoke similar arguments as in Subsection 2.4.5 to conclude that $W_{\dot{x}}$, and thus W_{x_1} and W_{x_2} , converge to zero along solutions of the closed loop system. This in turn implies that the center of mass tracks the desired position trajectory and that the manipulator tracks the desired attitude.

Remark 2.6.2. *The gain k_{b_1} may be interpreted as a weight on the disturbance estimate vector field due to the tracking error of the center of mass – associated to \mathbf{x}_1 ; while the gain k_{b_2} may be interpreted as a weight on the disturbance estimate vector field due to the tracking error of the manipulator’s orientation – associated to \mathbf{x}_2 . In particular, the ratio k_{b_1}/k_{b_2} is important, in the sense that it determines how more/less important the tracking error of the center of mass is in estimating the disturbance than the tracking error of the manipulator’s orientation.*

To summarize, the proposed control law $\tilde{\mathbf{u}}_z^{cl}$ is given by (take $\tilde{\mathbf{z}} = (\mathbf{z}, \hat{b})$, with \mathbf{z} as in (2.6.1), and where \mathbf{z} is assumed measured at each time instant)

$$\tilde{\mathbf{u}}_z^{cl}(t, \tilde{\mathbf{z}}) = \mathbf{u}_z^{cl}(\mathbf{x}, \mathbf{u}_x(t, \mathbf{x}))|_{\mathbf{x}=\mathbf{g}_z^x(t, \mathbf{z})} - \hat{b}\mathbf{e}_1, \quad (2.6.29)$$

$$\mathbf{u}_x^{cl}(t, \mathbf{x}) = (\mathbf{u}_{x_1}^{cl}(t, \mathbf{x}_1), \mathbf{u}_{x_2}^{cl}(t, \mathbf{x}_2)), \quad (2.6.30)$$

$$\dot{\hat{b}} = f_{\hat{b}}(t, \tilde{\mathbf{x}})|_{\tilde{\mathbf{x}}=(\mathbf{x}, \hat{b})=(\mathbf{g}_z^x(t, \mathbf{z}), \hat{b})}, \quad \hat{b}(0) = 0, \quad (2.6.31)$$

which is a dynamic controller, not a static one.

2.6.5 Simulations and Experiments

In this section, we present a simulation and two experiments that validate the proposed algorithms.

2.6.6 Simulation

Consider a quadrotor with mass $M = 1.442$ kg, a load with mass $m = 0.35$ kg, a manipulator with length $L = 0.35$ m, and a disturbance $b = 0.1$ N. Consider the control law $\mathbf{u}_\xi(\cdot)$ (in [33]) with $\sigma(s) = 0.25\frac{s}{\sqrt{1+s^2}}$, $\rho(s) = 0.70\frac{s}{\sqrt{1+s^2}}$, $k = 1$ and $\Omega(\cdot)$ as an odd function and as the solution to the differential equation $\Omega'''(s) = 1$ for $s > 1$ and $\Omega'''(s) = 0$ for $0 \leq s \leq 1$ and initial conditions $\Omega(0) = 0$, $\Omega'(0) = 1$ and $\Omega''(0) = 0$. Consider the control law $\mathbf{u}_x^{cl}(\cdot, \cdot)$, as in (2.2.47), with gains $v_\theta = 50$ and $k_\theta = 1$; and another the control law $\mathbf{u}_{x_2}^{cl}(\cdot, \cdot)$, as in (2.2.47), with gains $v_\theta = 20$, $k_\theta = 1$, $v_\omega = 20$ and $k_\omega = 1$. and, finally, the estimator vector field, in (2.6.28), with $k_{b_1} = 1$, $k_{b_2} = 0.05$, $b^{\max} = 0.3$ and $\epsilon = 0.1$. For these choices, we provide a simulation in Fig. 2.19, as a solution of (2.6.6) with $\mathbf{z}(0) = (-L\mathbf{e}_3, \mathbf{0}, \mathbf{0}, \mathbf{0}, \mathbf{e}_3) \in \Omega_z$. In Fig. 2.19a, the desired trajectory is visualized in blue, specifically a quadrotor describing a circular motion of 1 m of radius and an angular velocity of 0.2 rev/sec, and with the manipulator describing a motion given by $\mathbf{n}^*(t) = [0 \sin(\gamma(t)) \cos(\gamma(t))]$ with $\gamma(t) = \frac{\pi}{4} \cos(\frac{\pi}{5}t)$; while the actual trajectory of the quadrotor-manipulator system is visualized in black, where convergence to the desired trajectory is verified.

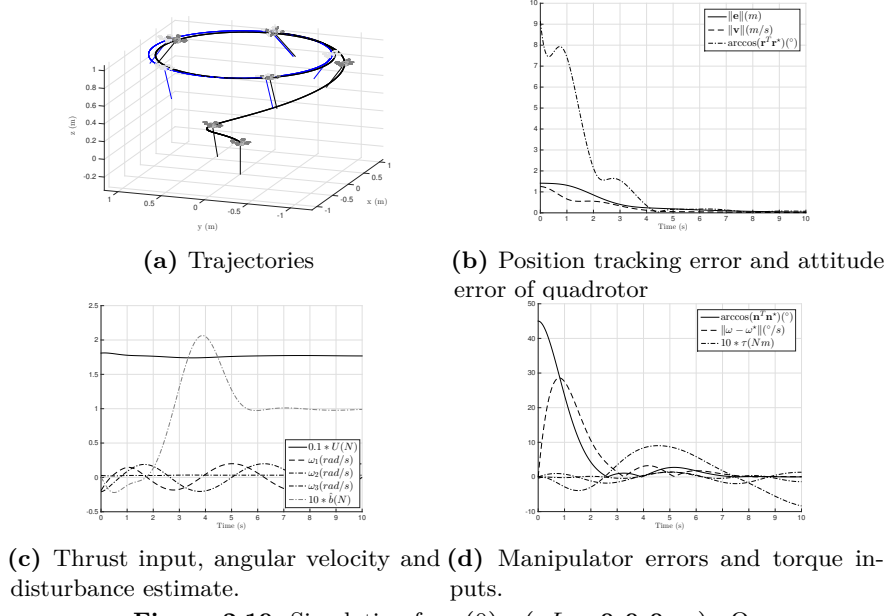


Figure 2.19: Simulation for $\mathbf{z}(0) = (-L\mathbf{e}_3, \mathbf{0}, \mathbf{0}, \mathbf{0}, \mathbf{e}_3) \in \Omega_z$.

In Fig. 2.19b, the position tracking error of the quadrotor is presented, and it converges to $\mathbf{0}$; in Fig. 2.19c, the thrust input, the quadrotor angular velocity and the disturbance estimate are presented; notice the disturbance estimate converges to the real unknown disturbance, namely 0.1N , thus canceling its effect. Finally, in Fig. 2.19d, the orientation tracking error of the manipulator is presented, and it converges to 0; the torque input, as defined in (2.6.29), is also presented.

2.6.7 Experimental Set-up and Experiments

For the experiments, a commercial quadrotor was used, namely an IRIS+ from 3D Robotics, weighting 1.442 kg, with a maximum payload of 0.4kg. The commands for controlling the quadrotor are processed on a ground station, developed in a ROS environment, and sent to the on-board autopilot, which allows to remotely control the aerial vehicle through the total thrust and the angular velocity. A wireless radio communication between ground station and autopilot is established through a telemetry radio, using a MAVLink protocol that directly overrides the signals sent from the radio transmitter. The quadrotor's pose is estimated by 12 cameras from a Qualisys motion capture system.

Three experiments were conducted, with a manipulator rigidly attached to the quadrotor. The manipulator consists of a rigid bar, of 0.35m of length and with a load at the extremity of 0.355kg – for this manipulator, the center of mass of the quadrotor-manipulator system shifts by approximately 7 cm away from the quadrotor center of mass. For the three experiments, the controller has the same structure,

specifically that in (2.6.29) and the desired trajectory is the same. In the first experiment, trajectory tracking of the center of mass of the quadrotor-manipulator system is performed – Fig. 2.20c; in the second, trajectory tracking of the center of mass of the quadrotor without manipulator is performed – Fig. 2.20d; and, in the third, trajectory tracking of the center of mass of the quadrotor, but where the manipulator is attached and where the controller is oblivious to its presence, is performed – Fig. 2.20b. For the first two experiments, the tracking performance and behavior is good as expected. However, for the third experiment, the tracking performance is slightly worse, with slower convergence to the steady state and some extra oscillations around the steady state, when compared to the previous two experiments; in this case, the manipulator is present but it is seen as a disturbance on the system, which explains the decrease in performance. This indicates that considering the manipulator presence, as done in the first experiment, can benefit the tracking performance.

A pick-and-place task experiment was also performed – Fig. 2.21. First, the quadrotor moves over the target point – target 1, it descends and it grasps the object at the picking position; once the object is grasped, the quadrotor goes back to the initial altitude and it moves to the target point – target 2; at the target point, the quadrotor descends and drops the object. When the load is grasped or released, the controller is updated, and the center of mass is recomputed before a new desired trajectory is set. Figure 2.21b shows that the task is successfully accomplished. During the descent phase the robot’s actual trajectory leaves the tolerance region in two occasions. In particular, when the vehicle is close to the picking or dropping place, the propellers airflow causes turbulence which disturbs the dynamics of the system. However, as seen in Figure 2.21b and Figure 2.21c, the algorithm pauses the descent phase until the position error returns within the tolerance region. A companion video with experiments – different runs but same conditions as the experiments described before – is found that illustrates both this and the previous experiment.

2.7 Controller for load lifting by two quadrotors

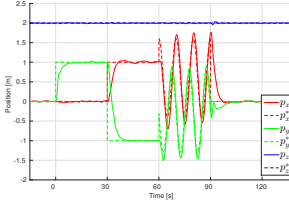
2.7.1 Introduction

In this Section, we focus on the problem of transporting a load in a system composed of one load and two quadrotors, and where each quadrotor is connected to the load by a cable of fixed length. Compared to cables, grippers and robotic arms are expensive and mechanically complex, which motivates the study of tethered transportation. Moreover, transportation with multiple aerial vehicles adds robustness for when one or more team members suffers a failure, such as an actuator failure [10].

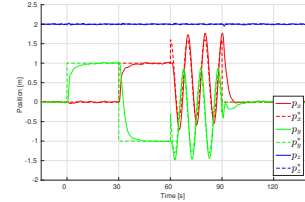
In this Section, we propose a controller that guarantees that the load asymptotically tracks a desired position trajectory. While in the literature specific control laws are found [10, 26, 32], we instead provide a general control framework that transforms the quadrotors-load system into three decoupled subsystems. In particu-



(a) Iris+ with aluminium bar of 350g and (b) CM of quadrotor system, with mass 35cm (CM of the whole system is 7cm) manipulator attached (control oblivious to away from CM of IRIS+).



(c) CM of quadrotor-manipulator system.

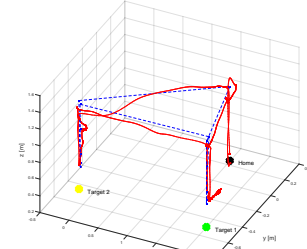


(d) CM of quadrotor system, without manipulator.

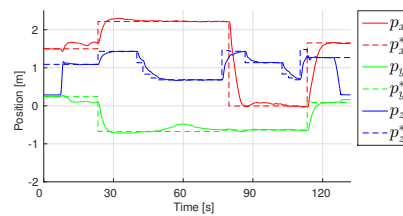
Figure 2.20: Position trajectory tracking of center of mass (CM) for different configurations, with controller defined in 2.6.29



(a) Iris+ with aluminum arm with a 1DOF revolute joint and a clamp gripper.



(b) Blue: desired trajectory. Red: real trajectory. Target 1 is the picking point, and Target 2 is the dropping point.



(c) Tracking error during flight.

Figure 2.21: Pick and place experiment

lar, one of these subsystems, concerning the load's position, has dynamics similar to those of an under-actuated aerial vehicle. This means that we may leverage different control strategies that have been proposed in the literature for under-actuated aerial vehicles [20]. Apart from this contribution, we also control the angle between the cables, rather than controlling the cable links to follow designed directions [32]. This makes it easier to design controllers that guarantee, for example, that the angle between the cables is always lower bounded by some desired angle, chosen such that the transporting vehicles remain safely apart from each other. Finally, we also control the rotation around the load and around a specific axis, exploring one of the degrees of freedom in the quadrotors-load system. The results here presented are based on those in [64].

The remainder of this Section is structured as follows. In Subsection 2.7.3, we describe the system's dynamics and present the problem statement. In Subsection 2.7.4, we present and explain the design steps for the controller that transforms the system into the three decoupled subsystems. In Subsection 2.7.5, we propose specific controllers for those subsystems. Finally, in Subsection 2.7.6, we provide simulations which illustrate the proposed algorithm in action.

2.7.2 Notation

Denote by $D(d_1, d_2, d_3) = D \in \mathbb{R}^{3 \times 3}$ the diagonal matrix with diagonal entries $D_{ii} = d_i \in \mathbb{R}$ for $i \in \{1, 2, 3\}$. Given functions f_1, f_2, g_1 and g_2 , we denote $\sum f_i := f_1 + f_2$ and $\sum f_i g_j := f_1 g_2 + f_2 g_1$.

2.7.3 Modeling and Problem Statement

Similarly to as in Section 2.4, we consider two aerial vehicles and a point mass load attached to each quadrotor by a cable, as illustrated in Fig. 2.22. We denote by $\mathbf{P}_1, \mathbf{P}_2, \mathbf{p} \in \mathbb{R}^3$ the quadrotors' and the load's center of mass positions, respectively; by $\mathbf{V}_1, \mathbf{V}_2, \mathbf{v} \in \mathbb{R}^3$ the quadrotor's and the load's center of mass velocities, respectively;

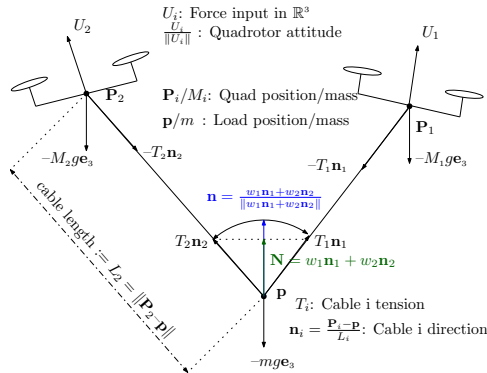


Figure 2.22: Modeling of quadrotors-load system

by $M_1, M_2, m > 0$ the quadrotor's and load's masses, respectively; and by $L_1, L_2 > 0$ the cables' lengths. Finally, we denote by $\mathbf{U}_1, \mathbf{U}_2 \in \mathbb{R}^3$ the quadrotors' input forces, which we assume are inputs to the quadrotors-load system. Consider then

$$\mathbf{z} = (\mathbf{p}, \mathbf{v}, \mathbf{P}_1, \mathbf{V}_1, \mathbf{P}_2, \mathbf{V}_2) \in \Omega_z, \quad (2.7.1)$$

$$\mathbf{u}_z = (\mathbf{U}_1, \mathbf{U}_2) \in (\mathbb{R}^3)^2, \quad (2.7.2)$$

where

$$\Omega_z = \{(\mathbf{p}, \mathbf{v}, \mathbf{P}_1, \mathbf{V}_1, \mathbf{P}_2, \mathbf{V}_2) \in (\mathbb{R}^3)^6 : i \in \{1, 2\}, (\mathbf{P}_i - \mathbf{p})^T(\mathbf{P}_i - \mathbf{p}) = L_i^2, (\mathbf{V}_i - \mathbf{v})^T(\mathbf{V}_i - \mathbf{v}) = 0\}, \quad (2.7.3)$$

$$T_{\mathbf{z}}\Omega_z = \{(\delta\mathbf{p}, \delta\mathbf{v}, \delta\mathbf{P}_1, \delta\mathbf{V}_1, \delta\mathbf{P}_2, \delta\mathbf{V}_2) \in (\mathbb{R}^3)^6 : i \in \{1, 2\}, \quad (2.7.4)$$

$$(\mathbf{P}_i - \mathbf{p})^T(\delta\mathbf{P}_i - \delta\mathbf{p}) = 0, (\delta\mathbf{V}_i - \delta\mathbf{v})^T(\mathbf{P}_i - \mathbf{p}) + (\mathbf{V}_i - \mathbf{v})^T(\delta\mathbf{P}_i - \delta\mathbf{p}) = 0\}, \quad (2.7.5)$$

where $T_{\mathbf{z}}\Omega_z$ denotes the tangent space of Ω_z at $\mathbf{z} \in \Omega_z$. We make use of (2.7.1) to denote the state of the quadrotors-load system, and of (2.7.2) to denote the control input, and as illustrated in Fig 2.22. Given an appropriate $\mathbf{u}_z : \mathbb{R}_{\geq 0} \mapsto \mathbb{R}^6$, a system's trajectory $\mathbf{z} : \mathbb{R}_{\geq 0} \mapsto \Omega_z$ evolves according to

$$\dot{\mathbf{z}}(t) = \mathbf{f}_z(\mathbf{z}(t), \mathbf{u}_z(t)), \mathbf{z}(0) \in \Omega_z, \quad (2.7.6)$$

where $\mathbf{f}_z : \Omega_z \times \mathbb{R}^6 \ni (\mathbf{z}, \mathbf{u}_z) \mapsto \mathbf{f}_z(\mathbf{z}, \mathbf{u}_z) \in T_{\mathbf{z}}\Omega_z$ is given by

$$\mathbf{f}_z(\mathbf{z}, \mathbf{u}_z) = (\mathbf{v}, \mathbf{a}(\mathbf{z}, \mathbf{u}_z), \mathbf{V}_1, \mathbf{A}_1(\mathbf{z}, \mathbf{u}_z), \mathbf{V}_2, \mathbf{A}_2(\mathbf{z}, \mathbf{u}_z)), \quad (2.7.7)$$

with \mathbf{z} as in (2.7.1); and with the functions \mathbf{A}_1 , \mathbf{A}_2 and \mathbf{a} , as, respectively, the quadrotors' and the load's acceleration (net force divided by respective mass). To be specific, $\mathbf{a}, \mathbf{A}_1, \mathbf{A}_2 : \Omega_z \times \mathbb{R}^6 \ni (\mathbf{z}, \mathbf{u}_z) \mapsto \mathbf{a}(\mathbf{z}, \mathbf{u}_z), \mathbf{A}_1(\mathbf{z}, \mathbf{u}_z), \mathbf{A}_2(\mathbf{z}, \mathbf{u}_z) \in \mathbb{R}^3$ are given by

$$\mathbf{a}(\mathbf{z}, \mathbf{u}_z) = \sum \frac{T_i(\mathbf{z}, \mathbf{u}_z)}{m} \mathbf{n}_i(\mathbf{z}) - g\mathbf{e}_3, \quad (2.7.8)$$

$$\mathbf{A}_i(\mathbf{z}, \mathbf{u}_z) = \frac{\mathbf{U}_i}{M_i} - \frac{T_i(\mathbf{z}, \mathbf{u}_z)}{M_i} \mathbf{n}_i(\mathbf{z}) - g\mathbf{e}_3, i \in \{1, 2\}, \quad (2.7.9)$$

where g is the acceleration due to gravity, with \mathbf{u}_z as in (2.7.2), and where $\mathbf{n}_1, \mathbf{n}_2 : \Omega_z \ni \mathbf{z} \mapsto \mathbf{n}_1(\mathbf{z}), \mathbf{n}_2(\mathbf{z}) \in \mathbb{S}^2$ and $T_1, T_2 : \Omega_z \times \mathbb{R}^6 \ni (\mathbf{z}, \mathbf{u}_z) \mapsto T_1(\mathbf{z}, \mathbf{u}_z), T_2(\mathbf{z}, \mathbf{u}_z) \in \mathbb{R}$ are defined as, for $i \in \{1, 2\}$,

$$\mathbf{n}_i(\mathbf{z}) = \frac{\mathbf{P}_i - \mathbf{p}}{\|\mathbf{P}_i - \mathbf{p}\|} \stackrel{(2.7.3)}{=} \frac{\mathbf{P}_i - \mathbf{p}}{L_i} \quad (2.7.10)$$

$$T_i(\mathbf{z}, \mathbf{u}_z) = \mathbf{e}_i^T M^{-1}(\mathbf{z}) \begin{bmatrix} \frac{m}{M_1} \mathbf{n}_1^T(\mathbf{z}) \mathbf{U}_1 + mL_1 \|\mathbf{V}_1 - \mathbf{v}\|^2 \\ \frac{m}{M_2} \mathbf{n}_2^T(\mathbf{z}) \mathbf{U}_2 + mL_2 \|\mathbf{V}_2 - \mathbf{v}\|^2 \end{bmatrix}, \quad (2.7.11)$$

with \mathbf{u}_z as in (2.7.2) and where

$$M(\mathbf{z}) = m \begin{bmatrix} M_1^{-1} & 0 \\ 0 & M_2^{-1} \end{bmatrix} + \begin{bmatrix} \mathbf{n}_1^T(\mathbf{z}) \\ \mathbf{n}_2^T(\mathbf{z}) \end{bmatrix} \begin{bmatrix} \mathbf{n}_1(\mathbf{z}) & \mathbf{n}_2(\mathbf{z}) \end{bmatrix}. \quad (2.7.12)$$

We also define $\omega_1, \omega_2 : \Omega_z \ni \mathbf{z} \mapsto \omega_1(\mathbf{z}), \omega_2(\mathbf{z}) \in \mathbb{R}^3$ as

$$\omega_i(\mathbf{z}) = \mathcal{S}(\mathbf{n}_i(\mathbf{z})) \frac{\partial \mathbf{n}_i(\mathbf{z})}{\partial \mathbf{z}} \mathbf{f}_z(\mathbf{z}, \cdot) = \mathcal{S}(\mathbf{n}_i(\mathbf{z})) \frac{\mathbf{V}_i - \mathbf{v}}{L_i}, \quad (2.7.13)$$

for $i \in \{1, 2\}$. Physically, the functions \mathbf{n}_i , ω_i and T_i are related to the cable's $i \in \{1, 2\}$ unit vector, angular velocity and tension, respectively, and as illustrated in Fig. 2.22. Equations (2.7.8) and (2.7.9) are found by considering the net contribution of all forces applied on the load's and the quadrotors' centers of mass; while (2.7.11) is found by guaranteeing that $\mathbf{f}_z(\mathbf{z}, \mathbf{u}_z) \in T_{\mathbf{z}}\Omega_z$, for all $\mathbf{z} \in \Omega_z$ and $\mathbf{u}_z \in \mathbb{R}^6$, which is indeed the case. The vector field (2.7.7) may also be derived by means of the Euler-Lagrange formalism [30]. Let us now state the problem to be solved in this paper.

Problem 2.7.1. *Given a desired position trajectory $\mathbf{p}^* \in \mathcal{C}^4(\mathbb{R}_{\geq 0}, \mathbb{R}^3)$, design $\mathbf{u}_z = (\mathbf{U}_1, \mathbf{U}_2) : \mathbb{R}_{\geq 0} \mapsto \mathbb{R}^6$ such that $\lim_{t \rightarrow \infty} (\mathbf{p}(t) - \mathbf{p}^*(t)) = \mathbf{0}$ along trajectories of (2.7.6).*

Notice that if $\mathbf{U}_1, \mathbf{U}_2 : \mathbb{R}_{\geq 0} \mapsto \mathbb{R}^3$ are control inputs then the quadrotors themselves are fully-actuated in the absence of tension in the cables; however, for the same inputs, the quadrotors-load system is under-actuated. In fact, note that the quadrotors-load system may be described by a 7th dimensional generalized coordinate, with three coordinates for the load's position, and two coordinates for each cable unit vector ($3 + 2 \times 2$); while the input to the system is only 6th dimensional. On the other hand, a system composed of three (or more) quadrotors and a load is fully actuated, since a 9th dimensional generalized coordinate ($3 + 3 \times 2$) describes the system, while a 9th dimensional input is available. Given that the jacobian associated to that system has full rank, then the system is fully-actuated and impedance control strategies are applicable. This, however, is not the case for the system considered in this paper, which is under-actuated.

2.7.4 Control Law Design

Preliminary Definitions

Let us provide some definitions and relations, useful in the following sections. For brevity and when stated, we use the shorthand notation

$$\mathbf{n}_i = \mathbf{n}_i(\mathbf{z}), \omega_i = \omega_i(\mathbf{z}), \text{ for } i \in \{1, 2\}, \quad (2.7.14)$$

with $\mathbf{n}_i(\cdot)$ and $\omega_i(\cdot)$ as in (2.7.10) and (2.7.13), respectively. Note that for $i \in \{1, 2\}$,

$$(-1)^i = \pm 1, (-1)^{i+1} = \mp 1, \quad (2.7.15)$$

which is made use of in later sections. Let $\mathbf{N} : \Omega_z \mapsto \mathbb{R}^3$ be defined as

$$\mathbf{N}(\mathbf{z}) = \sum w_i \mathbf{n}_i(\mathbf{z}), \text{ with } \sum w_i = 1 \text{ and } w_1, w_2 > 0, \quad (2.7.16)$$

and corresponding to the convex combination of $\mathbf{n}_1(\cdot)$ and $\mathbf{n}_2(\cdot)$ (see Fig. 2.22). Consider also

$$\tilde{\Omega}_z = \left\{ \mathbf{z} \in \Omega_z : \mathbf{n}_1^T(\mathbf{z})\mathbf{n}_2(\mathbf{z}) \notin \left\{ \pm 1, -\frac{w_1}{w_2}, -\frac{w_2}{w_1} \right\} \right\}, \quad (2.7.17)$$

which is a subset of Ω_z and the domain of several functions presented next. Denote then $\mathbf{n} : \tilde{\Omega}_z \mapsto \mathcal{S}^2$ and $\boldsymbol{\omega} : \tilde{\Omega}_z \mapsto \mathbb{R}^3$, defined as

$$\mathbf{n}(\mathbf{z}) = \frac{\mathbf{N}(\mathbf{z})}{\|\mathbf{N}(\mathbf{z})\|} \stackrel{(2.7.16)}{=} \frac{\sum w_i \mathbf{n}_i(\mathbf{z})}{\|\sum w_i \mathbf{n}_i(\mathbf{z})\|} \quad (2.7.18)$$

$$\boldsymbol{\omega}(\mathbf{z}) = \mathcal{S}(\mathbf{n}(\mathbf{z})) d\mathbf{n}(\mathbf{z}) \mathbf{f}_z(\mathbf{z}, \cdot) = \mathcal{S}(\mathbf{n}(\mathbf{z})) \frac{\sum w_i \mathcal{S}(\boldsymbol{\omega}_i(\mathbf{z})) \mathbf{n}_i(\mathbf{z})}{\|\mathbf{N}(\mathbf{z})\|}. \quad (2.7.19)$$

For brevity and when stated, we use the shorthand notation

$$\mathbf{n} = \mathbf{n}(\mathbf{z}), \mathbf{N} = \mathbf{N}(\mathbf{z}), \boldsymbol{\omega} = \boldsymbol{\omega}(\mathbf{z}). \quad (2.7.20)$$

Given (2.7.18) and (2.7.19), and along solutions of (2.7.6), it follows that $\dot{\mathbf{n}}(\mathbf{z}(t)) = \mathcal{S}(\boldsymbol{\omega}(\mathbf{z}(t))) \mathbf{n}(\mathbf{z}(t))$. The unit vector (2.7.18) is illustrated in Fig. 2.22 and, physically, it represents the direction along which a propelling force is applied on the load. The coefficients w_1 and w_2 provide a means of distributing the load's weight onto each UAV; in particular, and loosely speaking, for $(i, j) \in \{(1, 2), (2, 1)\}$, if $(w_i, w_j) \approx (1, 0)$, then $\mathbf{n}(\cdot) \stackrel{(2.7.18)}{\approx} \mathbf{n}_i(\cdot)$ and, consequently, most of the load's weight is carried by the UAV i . To be more precise, consider Problem 2.7.1 with $\mathbf{p}^*(t) = \bar{\mathbf{p}} \in \mathbb{R}^3$ for all $t \geq 0$, i.e., suppose we wish the load to be at a constant position, namely $\bar{\mathbf{p}}$. For this scenario, choose weights w_1 and w_2 (as in (2.7.16)), and an angle $\bar{\theta} \in (0, \frac{\pi}{2})$; then consider

$$\bar{\mathbf{n}}_1 = (\sin(-\bar{\theta}_1), 0, \cos(-\bar{\theta}_1)) \in \mathcal{S}^2, \quad (2.7.21)$$

$$\bar{\mathbf{n}}_2 = (\sin(-\bar{\theta}_2), 0, \cos(-\bar{\theta}_2)) \in \mathcal{S}^2, \quad (2.7.22)$$

$$\bar{\mathbf{z}} = (\bar{\mathbf{p}}, \mathbf{0}, \bar{\mathbf{p}} + L_1 \bar{\mathbf{n}}_1, \mathbf{0}, \bar{\mathbf{p}} + L_2 \bar{\mathbf{n}}_2, \mathbf{0}) \in \Omega_z, \quad (2.7.23)$$

$$\text{s.t. } \bar{\theta}_1 + \bar{\theta}_2 = \bar{\theta}, w_1 \sin(\bar{\theta}_1) = w_2 \sin(\bar{\theta}_2). \quad (2.7.24)$$

Then, for $\bar{\mathbf{u}}_z = (\bar{\mathbf{U}}_1, \bar{\mathbf{U}}_2) = (M_1 g \mathbf{e}_3 + \bar{T}_1 \bar{\mathbf{n}}_1, M_2 g \mathbf{e}_3 + \bar{T}_2 \bar{\mathbf{n}}_2)$ with

$$\begin{bmatrix} \bar{T}_1 \\ \bar{T}_2 \end{bmatrix} = mg \begin{bmatrix} \frac{\sin(\bar{\theta}_2)}{\sin(\bar{\theta}_1 + \bar{\theta}_2)} \\ \frac{\sin(\bar{\theta}_1)}{\sin(\bar{\theta}_1 + \bar{\theta}_2)} \end{bmatrix} \stackrel{(2.7.24)}{=} mg \frac{\sin(\bar{\theta}_1)}{\sin(\bar{\theta})} \begin{bmatrix} \frac{w_1}{w_2} \\ 1 \end{bmatrix} \stackrel{(2.7.24)}{=} mg \frac{\sin(\bar{\theta}_2)}{\sin(\bar{\theta})} \begin{bmatrix} 1 \\ \frac{w_2}{w_1} \end{bmatrix}, \quad (2.7.25)$$

it follows that $\mathbf{f}_z(\bar{\mathbf{z}}, \bar{\mathbf{u}}_z) = \mathbf{0}$ and, consequently, $\bar{\mathbf{z}}$ is an equilibrium state and $\bar{\mathbf{u}}_z$ an equilibrium input. It follows from (2.7.25) that $\frac{\bar{T}_1}{\bar{T}_2} = \frac{w_1}{w_2}$ and, thus, the ratio $\frac{w_1}{w_2}$ may be chosen so as to distribute the weight of the load on each UAV in a desirable way.

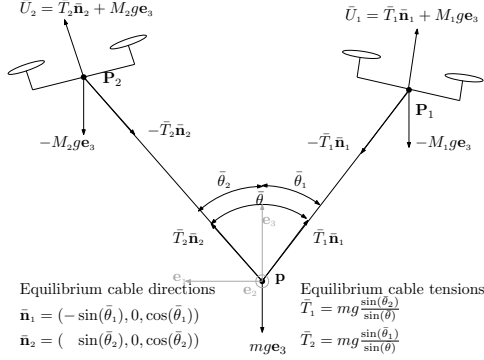


Figure 2.23: After choosing weights w_1 and w_2 (as in (2.7.16)) and an angle $\bar{\theta} \in (0, \frac{\pi}{2})$, an equilibrium configuration exists where $\frac{\bar{T}_1}{\bar{T}_2} = \frac{w_1}{w_2}$ and, thus, the ratio $\frac{w_1}{w_2}$ regulates the distribution of the load's weight onto each UAV.

Denote $\Gamma^1, \Gamma^2, \Gamma_n^1, \Gamma_n^2 : \tilde{\Omega}_z \mapsto \mathbb{R}^{3 \times 3}$ defined as

$$\Gamma^i(\mathbf{z}) = \begin{bmatrix} 1 & 0 & 0 \\ \tan(\theta) & -\frac{1}{\cos(\theta)} & 0 \\ 0 & 0 & 1 \end{bmatrix}, \Gamma_n^i(\mathbf{z}) = \begin{bmatrix} \frac{1}{\cos(\theta)} & -\tan(\theta) & 0 \\ 0 & 1 & 0 \\ 0 & 0 & 1 \end{bmatrix} \Big|_{\theta=\arccos(\mathbf{n}_i^T(\mathbf{z})\mathbf{n}(\mathbf{z}))}, \quad (2.7.26)$$

for $i \in \{1, 2\}$ (the latter are well defined owing to (2.7.17) and since $\mathbf{n}_i^T(\cdot)\mathbf{n}(\cdot) = 0 \Rightarrow \mathbf{n}_i^T(\cdot)\mathbf{n}_j(\cdot) = -\frac{w_i}{w_j}$, for $(i, j) \in \{(1, 2), (2, 1)\}$). Let us now provide four orientation frames (two for each UAV), namely $\mathcal{R}^1, \mathcal{R}^2, \mathcal{R}_n^1, \mathcal{R}_n^2 : \tilde{\Omega}_z \mapsto \mathcal{O}(3)$ defined as

$$\mathcal{R}^i(\mathbf{z}) = \left[\mathbf{n}_i \quad \frac{\Pi(\mathbf{n}_i)\mathbf{n}}{\|\Pi(\mathbf{n}_i)\mathbf{n}\|} \quad \frac{\mathcal{S}(\mathbf{n})\mathbf{n}_i}{\|\mathcal{S}(\mathbf{n})\mathbf{n}_i\|} \right] \Big|_{\substack{\mathbf{n} = \mathbf{n}(\mathbf{z}), \\ \mathbf{n}_i = \mathbf{n}_i(\mathbf{z})}}, i \in \{1, 2\}, \quad (2.7.27)$$

$$\mathcal{R}_n^i(\mathbf{z}) = \left[\mathbf{n} \quad \frac{\Pi(\mathbf{n})\mathbf{n}_i}{\|\Pi(\mathbf{n})\mathbf{n}_i\|} \quad \frac{\mathcal{S}(\mathbf{n})\mathbf{n}_i}{\|\mathcal{S}(\mathbf{n})\mathbf{n}_i\|} \right] \Big|_{\substack{\mathbf{n} = \mathbf{n}(\mathbf{z}), \\ \mathbf{n}_i = \mathbf{n}_i(\mathbf{z})}}, i \in \{1, 2\}, \quad (2.7.28)$$

illustrated in Fig. 2.24. We emphasize that, for any $\mathbf{z} \in \tilde{\Omega}_z$,

$$\mathcal{R}^i(\mathbf{z})\Gamma^i(\mathbf{z}) = \mathcal{R}_n^i(\mathbf{z})\Gamma_n^i(\mathbf{z}), i \in \{1, 2\}, \quad (2.7.29)$$

$$\mathcal{R}_n^2(\mathbf{z}) = \mathcal{R}_n^1(\mathbf{z})\mathcal{R}_x(\pi) = \mathcal{R}_n^1(\mathbf{z})D(1, -1, -1). \quad (2.7.30)$$

The orientation frames (2.7.27) and (2.7.28) are convenient at different design steps, and (2.7.29) provides a conversion between the two. Notice that \mathcal{R}^i and \mathcal{R}_n^i differ from a rotation around the third axis, and thus it is easy to verify that $\mathcal{R}^i(\cdot)(\Gamma_n^i(\cdot))^{-1} = \mathcal{R}_z(\arccos(\mathbf{n}_i^T(\cdot)\mathbf{n}(\cdot)))D(1, -1, 1)$.

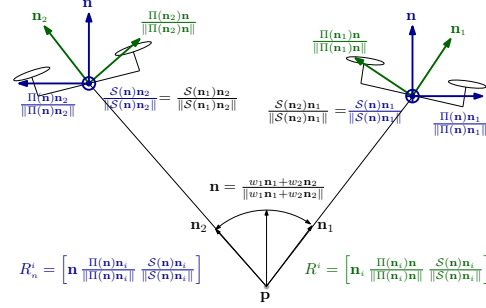


Figure 2.24: Orientation frames as defined in (2.7.27) (in green) and (2.7.28) (in blue).

Control Law

In this section, we present the control law, and in the following sections, we explain how the control law is designed. Let

$$\mathbf{u}_x = (\mathbf{u}_{\bar{x}}, \tau_\theta, \tau_\psi) = ((T, \boldsymbol{\tau}), \tau_\theta, \tau_\psi) \in \mathbb{R} \times \mathbb{R}^3 \times \mathbb{R} \times \mathbb{R} =: \mathcal{U}_x, \quad (2.7.31)$$

which corresponds to an input we design later. In particular, $\mathbf{u}_{\bar{x}}$, composed of T and $\boldsymbol{\tau}$, is designed such that the load tracks a desired position trajectory; τ_θ is designed such that the cables remain apart by a given desired, possibly time-varying, angle – this in turn guarantees that the cables do not overlap, and that the two UAV's remain apart from each other; and τ_ψ is designed so as to control the rotation of the two transporting quadrotors around the load. Physically, T has the dimensions of an acceleration, while $\boldsymbol{\tau}$, τ_θ and τ_ψ have the dimensions of an acceleration per length.

We start by presenting the complete control law, and later we provide details on how this control law is obtained. Consider then the individual control laws $\mathbf{U}_1^{cl}, \mathbf{U}_2^{cl} : \Omega_z \times \mathbb{R}^6 \mapsto \mathbb{R}^3$ defined as, for $i \in \{1, 2\}$,

$$\mathbf{U}_i^{cl}(\mathbf{z}, \mathbf{u}_x) = M_i L_i \mathcal{R}^i(\mathbf{z}) \Gamma^i(\mathbf{z}) \alpha_i(\mathbf{z}, \mathbf{u}_x) \quad (2.7.32)$$

$$\stackrel{(2.7.29)}{=} M_i L_i \mathcal{R}_n^i(\mathbf{z}) \Gamma_n^i(\mathbf{z}) \alpha_i(\mathbf{z}, \mathbf{u}_x), \quad (2.7.33)$$

and the complete control law $\mathbf{u}_z^{cl} : \Omega_z \times \mathcal{U}_x \mapsto \mathcal{U}_z$ defined as

$$\mathbf{u}_z^{cl}(\mathbf{z}, \mathbf{u}_x) = (\mathbf{U}_1^{cl}(\mathbf{z}, \mathbf{u}_x), \mathbf{U}_2^{cl}(\mathbf{z}, \mathbf{u}_x)), \quad (2.7.34)$$

where (\mathbf{u}_x as in (2.7.31))

$$\alpha_i(\mathbf{z}, \mathbf{u}_x) = \begin{bmatrix} \frac{[w_1 w_2] M(\mathbf{z}) \mathbf{e}_i}{L_i \|\mathbf{N}(\mathbf{z})\|} T - \|\boldsymbol{\omega}_i(\mathbf{z})\|^2 \\ \frac{1}{w_i} \bar{\tau}_\theta(\mathbf{z}, \mathbf{u}_{\bar{x}}, \tau_\theta) \\ \frac{1}{w_i} \bar{\tau}_\psi(\mathbf{z}, \mathbf{u}_{\bar{x}}, \tau_\psi) \end{bmatrix} - \frac{\|\mathbf{N}(\mathbf{z})\|}{2w_i} \mathcal{S}(\mathbf{e}_1) \mathcal{R}_n^{i,T}(\mathbf{z}) \bar{\tau}(\mathbf{z}, \mathbf{u}_{\bar{x}}), \quad (2.7.35)$$

with

$$\bar{\tau}(\mathbf{z}, \mathbf{u}_{\bar{x}}) = \tau - \tilde{\tau}_2(\mathbf{z}, T), \quad (2.7.36)$$

$$\bar{\tau}_\theta(\mathbf{z}, \mathbf{u}_{\bar{x}}, \tau_\theta) = \left(\sum \frac{1}{w_i \mathbf{n}_i^T(\mathbf{z}) \mathbf{n}(\mathbf{z})} \right)^{-1} (\tau_\theta - \tilde{\tau}_{\theta,4}(\mathbf{z}, \mathbf{u}_{\bar{x}})), \quad (2.7.37)$$

$$\bar{\tau}_\psi(\mathbf{z}, \mathbf{u}_{\bar{x}}, \tau_\psi) = \left(\sum \frac{\mathbf{n}_j^T(\mathbf{z}) \mathbf{n}(\mathbf{z})}{w_i \|\mathcal{S}(\mathbf{n}_1(\mathbf{z})) \mathbf{n}_2(\mathbf{z})\|} \right)^{-1} (\tau_\psi - \tilde{\tau}_{\psi,3}(\mathbf{z}, \mathbf{u}_{\bar{x}})), \quad (2.7.38)$$

and where the functions $\tilde{\tau}_2$, $\tilde{\tau}_{\theta,4}$ and $\tilde{\tau}_{\psi,3}$ are omitted for brevity. In what follows, given an appropriate $\mathbf{u}_x = (T, \boldsymbol{\tau}, \tau_\theta, \tau_\psi) : \mathbb{R}_{\geq 0} \mapsto \mathbb{R}^6$, we consider trajectories $\mathbf{z} : \mathbb{R}_{\geq 0} \mapsto \Omega_z$ satisfying

$$\dot{\mathbf{z}}(t) = \mathbf{f}_z(\mathbf{z}(t), \mathbf{u}_z^{cl}(\mathbf{z}(t), \mathbf{u}_x(t))), \mathbf{z}(0) \in \Omega_z. \quad (2.7.39)$$

Let us provide some intuition into (2.7.32)–(2.7.33), and, for that purpose, consider a \mathbf{z} as in (2.7.1), a \mathbf{u}_x as in (2.7.31) and $i \in \{1, 2\}$. We design $\mathbf{n}_i^T(\mathbf{z}) \mathbf{U}_i(\mathbf{z}, \mathbf{u}_x)$ so as to control the tension in the cables and to provide a thrust force T on the load and along the direction $\mathbf{n}(\mathbf{z})$ – see left side in Fig. 2.25a. Notice that for $(k, \gamma) \in \{(2, \theta), (3, \psi)\}$,

$$\sum_{i \in \{1, 2\}} \frac{(-1)^{i+1} w_i}{\|\mathbf{N}(\mathbf{z})\|} \frac{(\mathcal{R}_n^i(\mathbf{z}) \mathbf{e}_k)^T \mathbf{U}_i^{cl}(\mathbf{z}, \mathbf{u}_x)}{M_i L_i} \stackrel{(2.7.35)}{=} (\mathcal{R}_n^2(\mathbf{z}) \mathbf{e}_k)^T \bar{\tau}(\mathbf{z}, \mathbf{u}_{\bar{x}}), \quad (2.7.40)$$

$$\sum_{i \in \{1, 2\}} \frac{w_i}{2} \frac{(\mathcal{R}_n^i(\mathbf{z}) \mathbf{e}_k)^T \mathbf{U}_i^{cl}(\mathbf{z}, \mathbf{u}_x)}{M_i L_i} \stackrel{(2.7.35)}{=} \bar{\tau}_\gamma(\mathbf{z}, \mathbf{u}_{\bar{x}}, \tau_\gamma). \quad (2.7.41)$$

Thus, loosely speaking, it follows from (2.7.40) that we design (2.7.37) by creating concurrent forces in the space orthogonal to (2.7.18), and producing a torque that acts on the unit vector (2.7.18) – see right side in Fig. 2.25a. On the other hand, it follows from (2.7.41), that we design $\bar{\tau}_\theta$ by producing a differential of forces along $\mathcal{R}_n^1(\mathbf{z}) \mathbf{e}_2 \stackrel{(2.7.30)}{=} -\mathcal{R}_n^2(\mathbf{z}) \mathbf{e}_2$, which results in a torque that brings the cables' unit vectors closer or further apart – see right side in Fig. 2.25b. It also follows from (2.7.41), that we design $\bar{\tau}_\psi$ by producing a differential of forces along $\mathcal{R}_n^1(\mathbf{z}) \mathbf{e}_3 \stackrel{(2.7.30)}{=} -\mathcal{R}_n^2(\mathbf{z}) \mathbf{e}_3$, which results in a torque that makes the plane spanned by both cables rotate – see left side in Fig. 2.25b. The detailed design steps are here omitted for brevity.

2.7.5 Control Design for \mathbf{u}_x

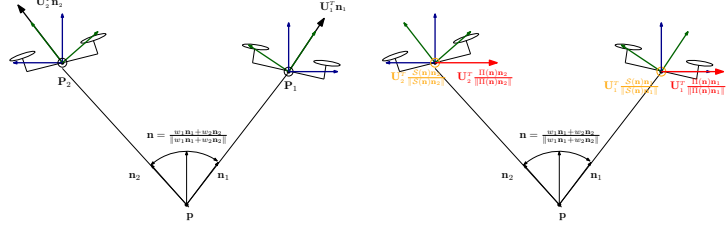
In this section we describe how to design the controllers for the input \mathbf{u}_x as in (2.7.31). Consider then

$$\tilde{\mathbf{x}} = (\mathbf{p}, \mathbf{v}, \mathbf{n}, \boldsymbol{\omega}) \in \Omega_{\bar{x}}, \quad (2.7.42)$$

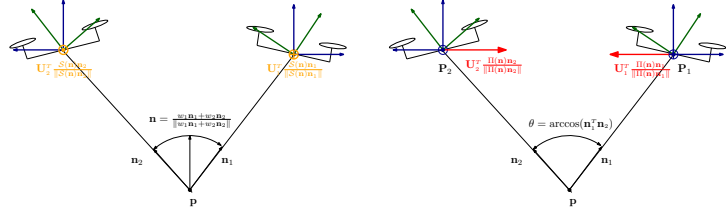
$$\Omega_{\bar{x}} = \{(\mathbf{p}, \mathbf{v}, \mathbf{n}, \boldsymbol{\omega}) \in (\mathbb{R}^3)^4 : \mathbf{n}^T \mathbf{n} = 1, \mathbf{n}^T \boldsymbol{\omega} = 0\}, \quad (2.7.43)$$

$$\boldsymbol{\theta} = (\theta, \omega_\theta) \in \Omega_\theta = [-\pi, \pi] \times \mathbb{R}, \quad (2.7.44)$$

$$\mathbf{x} = (\tilde{\mathbf{x}}, \boldsymbol{\theta}, \omega_\psi) \in \Omega_x = \Omega_{\bar{x}} \times \Omega_\theta \times \mathbb{R}. \quad (2.7.45)$$



(a) Input along cable direction to control tension in cables (left). Concurrent inputs along directions orthogonal to \mathbf{n} to control torque on \mathbf{n} (right).



(b) Differential inputs along direction orthogonal to both cables to control rotation around \mathbf{n} (left). Differential inputs along direction orthogonal to \mathbf{n} to control angle between cables (right).

Figure 2.25: Intuition for control law design along different directions.

Physically, $\tilde{\mathbf{x}}$ specifies the state a thrust propelled system, with error position \mathbf{p} , error velocity \mathbf{v} , propelling attitude direction \mathbf{n} and propelling attitude angular velocity $\boldsymbol{\omega}$; θ specifies the error angular displacement, with θ as the error between the angle formed by the cables and its desired value, and ω_θ as the corresponding error angular velocity; and finally ω_ψ specifies the angular velocity around the unit vector (2.7.18). Under the proposed control law (2.7.34), these three states have uncoupled vector fields, as verified next.

Consider then a desired position trajectory $\mathbf{p}^* \in \mathcal{C}^4(\mathbb{R}_{\geq 0}, \mathbb{R}^3)$, as in Problem 2.7.1, and a desired angle trajectory between the cables $\theta^* \in \mathcal{C}^2(\mathbb{R}_{\geq 0}, (0, \pi))$. Consider also, for each time instant $t \geq 0$, the mapping $\mathbf{g}_z^x(t, \cdot) : \Omega_z \mapsto \Omega_x$ defined as

$$\mathbf{g}_z^x(t, \mathbf{z}) = (\mathbf{g}_z^{\tilde{x}}(t, \mathbf{z}), \mathbf{g}_z^\theta(t, \mathbf{z}), \omega_\psi(\mathbf{z})), \quad (2.7.46)$$

$$\mathbf{g}_z^{\tilde{x}}(t, \mathbf{z}) = (\mathbf{p} - \mathbf{p}^*(t), \mathbf{v} - \dot{\mathbf{p}}^*(t), \mathbf{n}(\mathbf{z}), \boldsymbol{\omega}(\mathbf{z})), \quad (2.7.47)$$

$$\mathbf{g}_z^\theta(t, \mathbf{z}) = (\theta(\mathbf{z}) - \theta^*(t), \omega_\theta(\mathbf{z}) - \dot{\theta}^*(t)), \quad (2.7.48)$$

with \mathbf{z} as in (2.7.1) and the functions \mathbf{n} , $\boldsymbol{\omega}$ as in (2.7.18), (2.7.19), respectively (the functions θ , ω_θ , ω_ψ are found in [64]). It follows that, along trajectories of (2.7.39), if $\mathbf{x}(t) = \phi(t, \mathbf{z}(t))$ for all $t \geq 0$, then

$$\dot{\mathbf{x}}(t) = \mathbf{f}_x(t, \mathbf{x}(t), \mathbf{u}_x(t)) \quad (2.7.49)$$

with (next, \mathbf{x} is as in (2.7.45) and \mathbf{u}_x is as in (2.7.31))

$$\mathbf{f}_x(t, \mathbf{x}, \mathbf{u}_x) = (\mathbf{f}_{\bar{x}}(t, \tilde{\mathbf{x}}, \mathbf{u}_{\bar{x}}), \mathbf{f}_\theta(t, \boldsymbol{\theta}, \tau_\theta), \mathbf{f}_\psi(\tau_\psi)) \quad (2.7.50)$$

$$\mathbf{f}_{\bar{x}}(t, \tilde{\mathbf{x}}, \mathbf{u}_{\bar{x}}) = (\mathbf{v}, T\mathbf{n} - (g\mathbf{e}_3 + \dot{\mathbf{p}}^*(t)), \mathcal{S}(\boldsymbol{\omega})\mathbf{n}, \Pi(\mathbf{n})\boldsymbol{\tau}), \quad (2.7.51)$$

$$\mathbf{f}_\theta(t, \boldsymbol{\theta}, \tau_\theta) = (\omega_\theta, \ddot{\theta}^*(t) + \tau_\theta), \quad (2.7.52)$$

$$\mathbf{f}_{\omega_\psi}(\tau_\psi) = \tau_\psi, \quad (2.7.53)$$

We note that the mapping in (2.7.46) is not a diffeomorphism, since, at any time instant $t \geq 0$, we cannot reconstruct a state $\mathbf{z} \in \Omega_z$ given a state $\mathbf{x} \in \Omega_x$, but that does not pose a problem with respect to computing (2.7.49). See Section 2.3, on the quadrotor control.

The vector field (2.7.51) is that of a thrust propelled system, and thus the controller in Section 2.2 may be used. The vector field (2.7.52) is that of a double integrator for which controllers are also found in the literature [65]. In particular, given a desired angle trajectory $\theta^* \in \mathcal{C}^2(\mathbb{R}_{\geq 0}, (0, \pi))$ and positive constants k_θ and k_{ω_θ} , we choose the control law

$$\tau_\theta^{cl}(t, \boldsymbol{\theta}) = \ddot{\theta}^*(t) - k_{\omega_\theta}\omega_\theta - k_\theta \sin(\theta), \quad (2.7.54)$$

with $\boldsymbol{\theta}$ as in (2.7.44). The vector field (2.7.53) is that of a single integrator for which controllers are also found in the literature. In particular, given a desired angular velocity $\omega_\psi^* \in \mathcal{C}^1(\mathbb{R}_{\geq 0}, \mathbb{R})$ and a positive constant k_{ω_ψ} , we choose the control law

$$\tau_\psi^{cl}(t, \omega_\psi) = \dot{\omega}_\psi^*(t) - k_{\omega_\psi}(\omega_\psi - \omega_\psi^*(t)). \quad (2.7.55)$$

2.7.6 Simulations

Consider two quadrotors with masses $M_1 = M_2 = 1.442$ kg; cables with lengths $L_1 = L_2 = 1.2$ m; and a load with mass $m = 1.1$ kg. The desired position trajectory is $\mathbf{p}^*(t) = (\cos(0.5t), \sin(0.5t), 1)\text{m}$, i.e., a circular trajectory with radius of 1m and describing a revolution every 12 s; and the desired angle between the cables is $\theta^*(t) = 30^\circ$; The weights in (2.7.16) are chosen as $w_1 = w_2 = \frac{1}{2}$. The control law $\mathbf{u}_{\bar{x}}^{cl}(\cdot, \cdot)$ is that presented in [66], and the controllers $\tau_\theta^{cl}(\cdot, \cdot)$ and $\tau_\psi^{cl}(\cdot, \cdot)$ are those in (2.7.54) and (2.7.55), with $k_{\omega_\theta} = 6$, $k_\theta = 4$ and $k_{\omega_\psi} = 1$. For these choices, we provide a simulation in Fig. 2.26, as a solution of $\dot{\mathbf{z}}(t) = \mathbf{f}_z(\mathbf{z}(t), \mathbf{u}_z(t))$ with $\mathbf{u}_z(t) = \mathbf{u}_z^{cl}(\mathbf{z}(t), \mathbf{u}_x^{cl}(t, \phi(t, \mathbf{z}(t))))$ and where $\mathbf{z}(0) = (\mathbf{0}, \mathbf{0}, L_1\mathbf{q}(40^\circ, 40^\circ), \mathbf{0}, L_2\mathbf{q}(-40^\circ, 40^\circ), \mathbf{0}) \in \Omega_z$, and with $\mathbf{q}(\theta, \psi) := -(\sin(\theta)\cos(\psi), \sin(\theta)\sin(\psi), \cos(\theta)) \in \mathcal{S}^2$. In Fig. 2.26a, one visualizes in light gray the desired trajectory, and in dark bold the actual trajectory, which visually suggests position tracking. In Fig. 2.26b, the position tracking error is presented, and the convergence to $\mathbf{0}$ indicates convergence of the load's trajectory to the desired trajectory. In Fig. 2.26d, the angle between the cables is presented, and one verifies convergence of this angle to the desired angle trajectory of 30° . Finally, in Fig. 2.26c, the inputs as computed from the proposed control law – namely, $\mathbf{u}_z(t) = \mathbf{u}_z^{cl}(\mathbf{z}(t), \mathbf{u}_x^{cl}(t, \phi(t, \mathbf{z}(t))))$ – are presented.

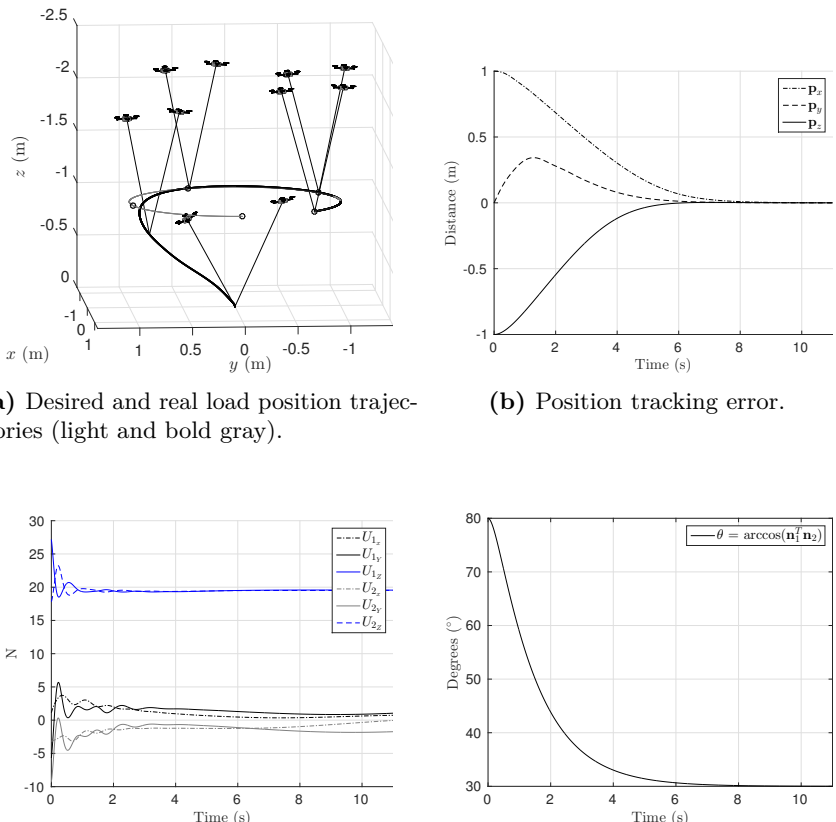


Figure 2.26: Two fully actuated aerial vehicles transporting a load with the proposed control law in (2.7.34)

Chapter 3

Attitude Synchronization

In this chapter, we consider the problem of attitude synchronization among a group of agents in the group of unit vectors, or a group of agents in group of rotation matrices. This is particularly motivated by applications such as those illustrated in Fig. 3.1, where one wishes multiple cables to point in a common direction, or equivalently one wishes multiple cables to synchronize. Firstly, in Section 3.3, we consider agents controlled at the angular velocity level, which are similar to first order integrators, and where the network graph is allowed to change as time progresses. By transforming the problems of synchronization on the group of unit vectors and of synchronization on the group rotation matrices into a common form, we are able to study synchronization under a common framework. Secondly, in Section 3.4, we consider agents in the group of unit vectors controlled at the torque level, which are similar to second order integrators, and this time the network graph is assumed static. We propose constrained torque control laws, which do not require torque on the space orthogonal to the unit vector each agent is supposed to synchronize.

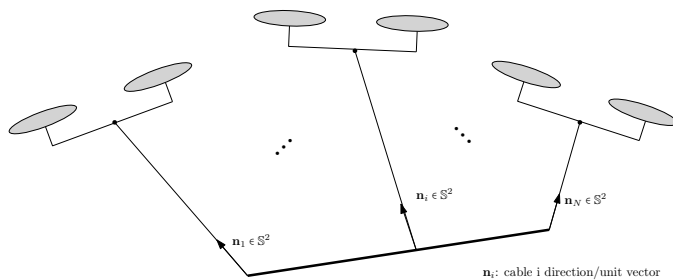


Figure 3.1: When N UAVs lift a common object attached to the latter by cables, it might be of interest to align those cables, which corresponds to a problem of attitude synchronization. When the cables are aligned, control techniques from Chapter 2 may be leveraged.

3.1 Background

Decentralized control in multi-agent systems is a topic of active research, with applications in large scale robotic systems. Attitude synchronization in satellite formations is one of the relevant applications [67, 68], where the control goal is to guarantee that a network of fully actuated rigid bodies acquires a common attitude. Coordination of underwater vehicles in ocean exploration missions [69], and of unmanned aerial vehicles in aerial exploration missions, may also be casted as attitude synchronization problems.

In the literature, attitude synchronization strategies for elements in the special orthogonal group are found in [70–78], which focus on *complete* attitude synchronization; and in [79–89], which focus on *incomplete* attitude synchronization. In this chapter, we focus on both *complete* and *incomplete* attitude synchronization. We refer to *incomplete* attitude synchronization when the agents are unit vectors in the three dimensional space; and we refer to *complete* attitude synchronization, when the agents are three dimensional rotation matrices. Incomplete synchronization represents a relevant practical problem, when the goal among multiple agents is to share a common direction. In flocking, for example, moving along a common direction is a requirement. Also, in a network of satellites whose antennas are to point in a common direction, incomplete synchronization may be more important than complete.

In [71–74, 76–78], state dependent control laws for torques are presented which guarantee synchronization for elements in the group of three dimensional rotation matrices, while in [82, 83, 90] state dependent control laws for torques are presented which guarantee synchronization for elements in the group of three dimensional unit vectors. With respect to complete attitude synchronization, different solutions for consensus in the special orthogonal group are found [67, 72, 73, 77, 78, 91–94]. *Incomplete* attitude synchronization, however, has not received the same attention. In this scenario, a rigid body has a main direction and the global objective is to guarantee alignment of all rigid bodies' main directions. The space orthogonal to each main direction can be left free of actuation or controlled to accomplish some other goals. Complete attitude synchronization requires more measurements when compared to incomplete attitude synchronization, and it might be the case that a rigid body is not fully actuated but rather only actuated in the space orthogonal to a specific direction, in which case incomplete attitude synchronization is still feasible. *Incomplete* attitude synchronization is also denoted synchronization on the sphere in [80–84, 86], where the focus has been on kinematic or point mass dynamic agents, i.e., dynamical agents without moment of inertia.

In [73], attitude control in a leader-follower network of rigid bodies has been studied, with the special orthogonal group being parametrized with Modified Rodrigues Parameters. The proposed solution guarantees attitude synchronization for connected graphs, but it requires all rigid bodies to be aware of a common and global orientation frame. In [77, 78], a controller for a single-leader single-follower network is proposed that guarantees global attitude synchronization at the cost of

introducing a discontinuity in the control laws. In [91], attitude synchronization in a leader-follower network is accomplished by designing a non-linear distributed observer for the leader. In [76, 95], a combination of a tracking input and a synchronization input is used; the tracking input adds robustness if connectivity is lost and it is designed in the spirit of leader-following, where the leader is a virtual one and it encapsulates a desired trajectory; however, this strategy requires all agents to be aware of a common and global reference frame. In another line of work, in [72, 92], attitude synchronization is accomplished without the need of a common orientation frame among agents. Additionally, in [72], a controller for switching and directed network topologies is proposed, and local stability of consensus in connected graphs is guaranteed, provided that the control gain is sufficiently high. In [67], attitude synchronization is accomplished with controllers based on behavior based approaches and for a bidirectional ring topology. The special orthogonal group is parametrized with quaternions, and the proposed strategy also requires a common attitude frame among agents. In [96], a quaternion based controller is proposed that guarantees a synchronized network of rigid bodies is a global equilibrium configuration, provided that the network graph is acyclic. This comes at the cost of having to design discontinuous (hybrid) controllers. A discrete time protocol for complete synchronization of kinematic agents is found in [75], and the notion of *reshaping function* is introduced there. The protocol provides almost global convergence to a synchronized configuration, which relies on proving that all other equilibria configurations, apart from the equilibria configuration where agents are synchronized, are unstable. In [93], controllers for complete attitude synchronization and for switching topologies are proposed, but this is accomplished at the kinematic level, i.e., by controlling the agents' angular velocity (rather than their torque). This work is extended in [94] by providing controllers at the torque level, and similarly to [67], stability properties rely of high gain controllers.

In [80, 81], incomplete synchronization of kinematic agents on the sphere is studied, with a constant edge weight function for all edges. In particular, in [81], incomplete synchronization is used for accomplishing a flocking behavior, where a group of agents moves in a common direction. In [82], dynamic agents, which move at constant speed on a sphere, are controlled by a state feedback control law that steers their velocity vector so as to force the agents to attain a collective circular motion; since the agents are mass points, the effect of the moment of inertia is not studied. In [83], dynamic point mass agents, constrained to move on a sphere, are controlled to form patterns on the sphere, by constructing attractive and repelling forces; in the absence of repelling forces, synchronization is achieved. Also, the closed-loop dynamics of these agents are invariant to rotations, or symmetry preserving, as those in [80, 81], in the sense that two trajectories, whose initial condition – composed of position and velocity – differs only on a rotation, are the same at each time instant apart from the previous rotation. In Section 3.4, this property does not hold, since our dynamic agents have a moment of inertia, unlike the agents in [80, 81, 83].

3.2 Preliminaries

3.2.1 Visualization of synchronization

Let us explain next the meaning of complete and incomplete synchronization, with the help of meaningful illustrations.

Complete Synchronization

Consider a group of $N \in \mathbf{N}$ rotations matrices

$$\mathcal{R}_1, \dots, \mathcal{R}_N \in \mathbb{SO}(3) = \{\mathcal{R} \in \mathbb{R}^{3 \times 3} : \mathcal{R}^T \mathcal{R} = \mathbf{I}, \mathcal{R} \mathcal{R}^T = \mathbf{I}, \det(\mathcal{R}) = 1\}. \quad (3.2.1)$$

We say that the agents are synchronized if they all share the same *complete* orientation, i.e., if $\mathcal{R}_1 = \dots = \mathcal{R}_N$, as illustrated in Fig. 3.4, in page 74, for $N = 2$. The term *complete* synchronization is used in juxtaposition with *incomplete* synchronization as described in the next subsection. In *incomplete* synchronization, rather than synchronizing all three bodies axes, the agents synchronize only one body direction.

Let $\tilde{\mathbb{SO}}(3) := \mathbb{SO}(3) \setminus \{\mathcal{R} \in \mathbb{SO}(3) : \mathcal{R} \neq 2\mathbf{n}\mathbf{n}^T - \mathbf{I}, \mathbf{n} \in \mathbb{S}^2\}$. For ease of visualization, we define $\mathbf{v} : \tilde{\mathbb{SO}}(3) \ni \mathcal{R} \mapsto \mathbf{v}(\mathcal{R}) \in \{\mathbf{x} \in \mathbb{R}^3 : \|\mathbf{x}\| < 1\}$ as

$$\mathbf{v}(\mathcal{R}) := \frac{\theta(\mathcal{R})}{\pi} \mathcal{S}^{-1} \left(\frac{\mathcal{R} - \mathcal{R}^T}{2 \sin(\theta(\mathcal{R}))} \right), \mathcal{R} \neq \mathbf{I}, \text{ and } \mathbf{v}(\mathbf{I}) := \mathbf{0}, \quad (3.2.2)$$

where $\theta : \mathbb{SO}(3) \ni \mathcal{R} \mapsto \theta(\mathcal{R}) := \arccos\left(\frac{\text{tr}(\mathcal{R}) - 1}{2}\right) \in [0, \pi]$. As such, given a rotation matrix $\mathcal{R} \in \tilde{\mathbb{SO}}(3)$, we can visualize it in a sphere of unitary radius (excluding its surface), as illustrated in Fig. 3.3. For $\mathcal{R} \in \{\tilde{\mathcal{R}} \in \mathbb{SO}(3) : \tilde{\mathcal{R}} \neq 2\mathbf{n}\mathbf{n}^T - \mathbf{I}, \mathbf{n} \in \mathbb{S}^2\}$, \mathbf{v} is not well defined in the sense that the limit $\lim_{\tilde{\mathcal{R}} \rightarrow \mathcal{R}} \mathbf{v}(\tilde{\mathcal{R}})$ does not exist. This is related to the fact that $\mathcal{R} = 2(+\mathbf{n})(+\mathbf{n})^T - \mathbf{I} = 2(-\mathbf{n})(-\mathbf{n})^T - \mathbf{I}$, where both $+\mathbf{n}, -\mathbf{n} \in \mathbb{S}^2$. In fact, under appropriate constraints (namely, on how $\tilde{\mathcal{R}} \rightarrow \mathcal{R}$), the previous limit is either $+\mathbf{n}$ or $-\mathbf{n}$. This corresponds to the surface of the sphere of unitary radius, where each diametrically opposed point, represents the same rotation matrix.

Incomplete Synchronization

Consider again a group of N rotations matrices as in (3.2.1), representing N orientation frames (w.r.t. an unknown inertial orientation frame). Consider also N unit vectors $\bar{\mathbf{n}}_1, \dots, \bar{\mathbf{n}}_N \in \mathbb{S}^2 = \{\mathbf{x} \in \mathbb{R}^3 : \mathbf{x}^T \mathbf{x} = 1\}$, and finally the unit vectors $\mathbf{n}_1 := \mathcal{R}_1 \bar{\mathbf{n}}_1 \in \mathbb{S}^2, \dots, \mathbf{n}_N := \mathcal{R}_N \bar{\mathbf{n}}_N \in \mathbb{S}^2$. Intuitively, for each $i \in \{1, \dots, N\}$, \mathbf{n}_i represents a direction on the i^{th} orientation frame. While in *complete* synchronization it is required that $\mathcal{R}_1 = \dots = \mathcal{R}_N$, i.e., that all orientation frames are the same, in *incomplete* synchronization it is required that $\mathbf{n}_1 = \dots = \mathbf{n}_N \Leftrightarrow \mathcal{R}_1 \bar{\mathbf{n}}_1 = \dots = \mathcal{R}_N \bar{\mathbf{n}}_N$. Figures 3.4 and 3.5 illustrate the concept of incomplete synchronization for two agents. We emphasize that (let $N = 2$) if $\bar{\mathbf{n}}_1 = \bar{\mathbf{n}}_2$ then $\mathcal{R}_1 = \mathcal{R}_2 \Rightarrow \mathbf{n}_1 = \mathbf{n}_2$, but

the reverse is not true, as exemplified in Fig. 3.5. On the other hand if $\bar{\mathbf{n}}_1 \neq \bar{\mathbf{n}}_2$ then $\mathcal{R}_1 = \mathcal{R}_2 \not\rightarrow \mathbf{n}_1 = \mathbf{n}_2$, which means incomplete synchronization *is not* a subcase of complete synchronization, i.e., complete synchronization does not guarantee incomplete synchronization. See Fig. 3.4 for an illustration.

3.2.2 Output Feedback

Let us explain next the concept of decentralized output feedback in the setting of multi-agents systems, which is illustrated in Fig. 3.6, in page 75.

Let $N, m \in \mathbb{N}$ and consider

$$\mathbf{x} = (\mathbf{x}_1, \dots, \mathbf{x}_N) \in (\Omega_x)^N, \quad (3.2.3)$$

$$\mathbf{u} = (\mathbf{u}_1, \dots, \mathbf{u}_N) \in (\mathbb{R}^m)^N, \quad (3.2.4)$$

with \mathbf{x} as a state, \mathbf{u} as a input, and where Ω_x is some set and $T_y \Omega_x$ is the tangent space of Ω_x at $y \in \Omega_x$. Let $i \in \{1, \dots, N\}$. Given an appropriate $\mathbf{u}_i : \mathbb{R}_{\geq 0} \mapsto \mathbb{R}^m$, a trajectory $\mathbf{x}_i : \mathbb{R}_{\geq 0} \ni t \mapsto \mathbf{x}_i(t) \in \Omega_x$ is given by

$$\mathbf{x}_i(t) = \mathbf{x}_{i,0} + \int_0^t \mathbf{f}_{x_i}(\mathbf{x}_i(\tau), \mathbf{u}_i(\tau)) d\tau, \quad \mathbf{x}_{i,0} \in \Omega_x, \quad (3.2.5)$$

where $\mathbf{f}_{x_i}(\mathbf{x}_i, \mathbf{u}_i) \in T_{\mathbf{x}_i} \Omega_x$ for any $(\mathbf{x}_i, \mathbf{u}_i) \in \Omega_x \times \mathbb{R}^m$. Given an appropriate $\mathbf{u} = (\mathbf{u}_1, \dots, \mathbf{u}_N) : \mathbb{R}_{\geq 0} \mapsto (\mathbb{R}^m)^N$, $\mathbf{x} = (\mathbf{x}_1, \dots, \mathbf{x}_N) := \mathbb{R}_{\geq 0} \ni t \mapsto \mathbf{x}(t) \in (\Omega_x)^N$ evolves according to

$$\begin{aligned} \dot{\mathbf{x}}(t) &= (\mathbf{f}_{x_1}(\mathbf{x}_1(t), \mathbf{u}_1(t)), \dots, \mathbf{f}_{x_N}(\mathbf{x}_N(t), \mathbf{u}_N(t))), \quad \mathbf{x}(0) = (\mathbf{x}_1(0), \dots, \mathbf{x}_N(0)) \in (\Omega_x)^N, \\ &=: \mathbf{F}_x(\mathbf{x}(t), \mathbf{u}(t)), \quad \mathbf{x}(0) \in (\Omega_x)^N, \end{aligned} \quad (3.2.6)$$

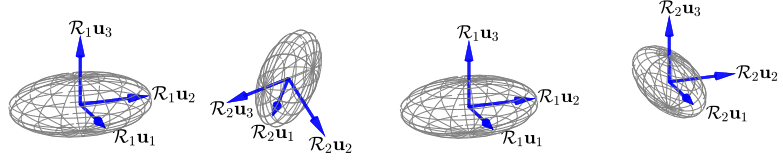
where $\mathbf{F}_x(\mathbf{x}, \mathbf{u}) \in T_{\mathbf{x}}(\Omega_x)^N := T_{\mathbf{x}_1} \Omega_x \times \dots \times T_{\mathbf{x}_N} \Omega_x$ for any $(\mathbf{x}, \mathbf{u}) \in (\Omega_x)^N \times (\mathbb{R}^m)^N$. In the setting of multi-agent systems, it is common to assume that the open-loop vector field of all agents is the same (same function), but this assumption is not necessary, as exemplified in Section 3.3 (where the agents have different moments of inertia).

Consider then the *non-injective* output functions

$$\mathbf{h}_i : (\Omega_x)^N \mapsto (\mathcal{H})^{p_i}, \quad i \in \{1, \dots, N\} \quad (3.2.7)$$

with \mathcal{H} as the measurement set. In the setting of multi-agent systems, \mathbf{h}_i corresponds to the measurement function of agent $i \in \{1, \dots, N\}$, which makes $p_i \in \mathbb{N}$ measurements, and with \mathcal{H} as the measurement set. Since, for any $i \in \{1, \dots, N\}$, \mathbf{h}_i is non-injective, it follows that given a measurement $\mathbf{y} \in \mathbf{h}_i((\Omega_x)^N) \subseteq (\mathcal{H})^{p_i}$ one cannot necessarily recover one single $\mathbf{x} \in (\Omega_x)^N$ such that $\mathbf{h}_i(\mathbf{x}) = \mathbf{y}$. Consider also the combined output function (which may be injective)

$$\mathbf{H} : (\Omega_x)^N \ni \mathbf{x} \mapsto \mathbf{H}(\mathbf{x}) := (\mathbf{h}_1(\mathbf{x}), \dots, \mathbf{h}_N(\mathbf{x})) \in (\mathcal{H})^{p_1} \times \dots \times (\mathcal{H})^{p_N}. \quad (3.2.8)$$



(a) Two rotation matrices not synchronized, i.e., $\mathcal{R}_1 \neq \mathcal{R}_2$
(b) Two rotation matrices synchronized, i.e., $\mathcal{R}_1 = \mathcal{R}_2$

Figure 3.2: In complete synchronization, N agents synchronize their rotation matrices ($\mathbf{u}_1, \mathbf{u}_2$ and \mathbf{u}_3 stand for the canonical basis vectors in \mathbb{R}^3).

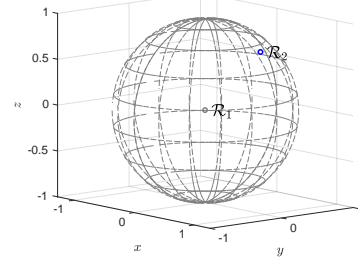
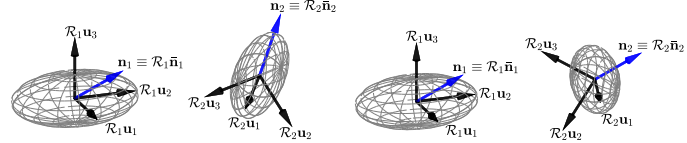
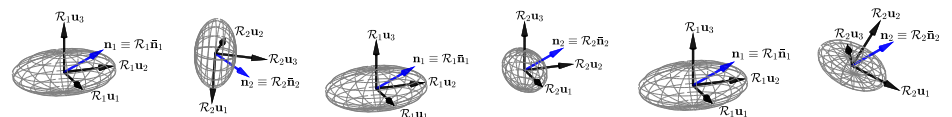


Figure 3.3: Representation using (3.2.2) for rotation matrices in Fig. 3.2a.



(a) Not synchronized, $\mathbf{n}_1 \neq \mathbf{n}_2$. (b) Synchronized, $\mathbf{n}_1 = \mathbf{n}_2$.

Figure 3.4: In incomplete synchronization, N unit vectors $\mathbf{n}_1 = \mathcal{R}_1\bar{\mathbf{n}}_1, \dots, \mathbf{n}_N = \mathcal{R}_N\bar{\mathbf{n}}_N$ are required to align with each other. In Figs. 3.4a-3.4b, $\bar{\mathbf{n}}_1 = -\bar{\mathbf{n}}_2 = \sqrt{3}^{-1}\mathbf{1}_3$ ($\mathbf{u}_1, \mathbf{u}_2$ and \mathbf{u}_3 stand for the canonical basis vectors of \mathbb{R}^3).



(a) Not synchronized $\mathbf{n}_1 \neq \mathbf{n}_2$. (b) Synchronized $\mathbf{n}_1 = \mathbf{n}_2$ (and $\mathcal{R}_1 = \mathcal{R}_2$) (c) Synchronized $\mathbf{n}_1 = \mathbf{n}_2$ (and $\mathcal{R}_1 \neq \mathcal{R}_2$)

Figure 3.5: In incomplete synchronization, N unit vectors $\mathbf{n}_1 = \mathcal{R}_1\bar{\mathbf{n}}_1, \dots, \mathbf{n}_N = \mathcal{R}_N\bar{\mathbf{n}}_N$ are required to align with each other. In Figs. 3.5a-3.5c, $\bar{\mathbf{n}}_1 = \bar{\mathbf{n}}_2 = \sqrt{3}^{-1}\mathbf{1}_3$ ($\mathbf{u}_1, \mathbf{u}_2$ and \mathbf{u}_3 stand for the canonical basis vectors of \mathbb{R}^3).

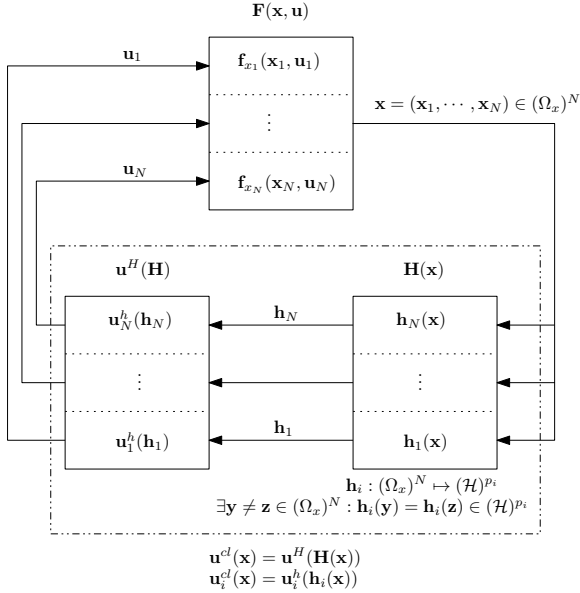


Figure 3.6: Decentralized output feedback in the setting of multi-agents systems: each agent $i \in \{1, \dots, N\}$ makes p_i measurements, in the measurement set \mathcal{H} ; also, the measurement functions $\mathbf{h}_1, \dots, \mathbf{h}_N$ are non-injective, and thus no agent i can reconstruct the state \mathbf{x} by measuring $\mathbf{h}_i(\mathbf{x})$.

Given all the above, and in the setting of multi-agent systems, we call a function $\mathbf{u}^H : (\mathcal{H})^{p_1} \times \dots \times (\mathcal{H})^{p_N} \ni (\mathbf{h}_1, \dots, \mathbf{h}_N) = \mathbf{H} \mapsto \mathbf{u}^H(\mathbf{H}) \in (\mathbb{R}^m)^N$ an output feedback control law if

$$\mathbf{u}^H(\mathbf{H}) := (\mathbf{u}_1^h(\mathbf{h}_1), \dots, \mathbf{u}_N^h(\mathbf{h}_N)), \quad (3.2.9)$$

for some $\mathbf{u}_i^h : (\mathcal{H})^{p_i} \mapsto \mathbb{R}^m$ and for each $i \in \{1, \dots, N\}$. Then, given an output feedback control law \mathbf{u}^H , $\mathbf{x} = (\mathbf{x}_1, \dots, \mathbf{x}_N) := \mathbb{R}_{\geq 0} \ni t \mapsto \mathbf{x}(t) \in \Omega_x$ evolves according to

$$\dot{\mathbf{x}}(t) = (\mathbf{f}_{x_1}(\mathbf{x}_1(t), \mathbf{u}_1^h(\mathbf{h}_1(\mathbf{x}(t)))), \dots, \mathbf{f}_{x_N}(\mathbf{x}_N(t), \mathbf{u}_N^h(\mathbf{h}_N(\mathbf{x}(t))))), \mathbf{x}(0) \in (\Omega_x)^N, \quad (3.2.10)$$

$$=: \mathbf{F}_x(\mathbf{x}(t), \mathbf{u}^H(\mathbf{H}(\mathbf{x}(t)))), \mathbf{x}(0) \in (\Omega_x)^N. \quad (3.2.11)$$

and we call $\mathbf{u}^{cl} : (\Omega_x)^N \ni \mathbf{x} \mapsto \mathbf{u}^{cl}(\mathbf{x}) := \mathbf{u}^H(\mathbf{H}(\mathbf{x})) \in (\mathbb{R}^m)^N$, with \mathbf{H} as in (3.2.8), a decentralized output feedback control law if the functions (3.2.7) are non-injective. In the next two sections, namely Section 3.3 and Section 3.4, we make use of this concept of decentralized output feedback control law.

3.2.3 Graph Theory

In this subsection, we present some definitions and results from graph theory that are used in following sections, and we refer the reader to [97] for further details. A

graph $\mathcal{G} = \{\mathcal{N}, \mathcal{E}\}$ is said to be connected if there exists a path between any two vertices in \mathcal{N} . \mathcal{G} is a tree if it is connected and it contains no cycles. An orientation on the graph \mathcal{G} is the assignment of a direction to an each edge $(i, j) \in \mathcal{E}$, where each edge vertex is either the tail or the head of the edge. For brevity, we denote $N = |\mathcal{N}|$, $M = |\mathcal{E}|$ and $\mathcal{M} = \{1, \dots, M\}$. Additionally, and for notational convenience in the analysis that follows, consider the sets $\mathcal{E} = \{(i, j) \in \mathcal{N} \times \mathcal{N} : j \in \mathcal{N}_i\}$ (i.e., the set of edges of the graph \mathcal{G}) and $\bar{\mathcal{E}} = \{(i, j) \in \mathcal{E} : j > i\}$. For undirected network graphs, we can construct an injective function $\bar{\kappa} : \bar{\mathcal{E}} \mapsto \mathcal{M}$ from which it is possible to construct a second, now surjective, function $\kappa : \mathcal{E} \mapsto \mathcal{M}$, which satisfies $\kappa(i, j) = \bar{\kappa}(j, i)$ when $j > i$ and $\kappa(i, j) = \bar{\kappa}(j, i)$ when $j < i$. As such, by construction, for every $(i, j) \in \mathcal{E}$, $\kappa(i, j) = \kappa(j, i)$, since we consider undirected graphs. The function $\kappa(\cdot, \cdot)$ thus assigns an edge index to every unordered pair of neighbors. The incidence matrix $B \in \mathbb{R}^{N \times M}$ of \mathcal{G} is such that, for every $k \in \mathcal{M}$ and for $(i, j) = \bar{\kappa}^{-1}(k)$, $B_{ik} = 1$, $B_{jk} = -1$ and $B_{lk} = 0$ for all $l \in \mathcal{N} \setminus \{i, j\}$. Finally, for each edge $k \in \mathcal{M}$ and $(i, j) = \bar{\kappa}^{-1}(k)$, we denote ${}_i \mathbf{n} := \mathbf{n}_i$ and ${}_k \mathbf{n} := \mathbf{n}_j$, i.e., we identify an agent by its node index but also by its edges' indexes (${}_k \mathbf{n}$ if \mathbf{n}_i is the tail of edge k , and ${}_k \mathbf{n}$ if \mathbf{n}_i is the head of edge k).

Proposition 3.2.1. If \mathcal{G} is a tree, then $B^T B$ and $(B \otimes \mathbf{I})^T (B \otimes \mathbf{I})$ are positive definite [98].

Proposition 3.2.2. If \mathcal{G} is connected but not a tree, then the null space of the incidence matrix, i.e., $\mathcal{N}(B)$, is non-empty, and it corresponds to the cycle space of \mathcal{G} [99, Lemma 3.2].

3.3 A common framework for attitude synchronization of unit vectors in networks with switching topology

3.3.1 Introduction

In this Section, we consider kinematic agents and we design decentralized output feedback control laws (see Section 3.2.2), for the agents' angular velocities, which are not exclusively state dependent, but are also time dependent, with the time dependency encapsulating the case of a switching network topology.

We note that, regarding synchronization in $\mathbb{SO}(3)$, relevant results are found in [86, 93, 100–102]. In e.g. [93], two control laws are proposed, one requiring a common orientation frame among agents, and one with no such requirement. In [86, 101–103], consensus on non-linear spaces is analyzed with the help of a common weak non-smooth Lyapunov function, i.e., a Lyapunov function which is non-increasing along solutions. Also, in [93], control laws which guarantee synchronization under a switching topology are presented, under the hypothesis of a dwell time between consecutive switches.

In the framework of this section, we relax the assumption of dwell time and provide conditions for synchronization under arbitrary switching. Our approach is based on the construction of a common weak non-smooth Lyapunov function

for analyzing synchronization in \mathbb{S}^n , for any $n \in \mathbb{N}$. In order to handle the non-smoothness of the proposed Lyapunov function, we present an invariance-like result which does not require any dwell time assumptions for the switching dynamics (see also [104–107] for invariance like theorems for switched systems). We propose control laws for angular velocities of unit vectors in \mathbb{R}^3 and 3D rotation matrices that guarantee synchronization for a network of agents with switching topology. The control laws devised for unit vectors and rotation matrices achieve different goals, and differ in two aspects worth emphasizing. First, controlling rotation matrices requires more measurements when compared with controlling unit vectors; secondly, while controlling rotation matrices requires full actuation, i.e., all body components of the angular velocity need to be controllable, controlling unit vectors does not. Our main contribution compared to the aforementioned literature lies in analyzing both problems under a common framework, in order to allow for a unified stability analysis under arbitrary switching using the same common weak Lyapunov function. Particularly both problems are transformed into synchronization problems in \mathbb{S}^m for an appropriate $m \in \mathbb{N}$. Since rotation matrices can be parametrized by unit quaternions [108], which are unit vectors in \mathbb{R}^4 , i.e., \mathcal{S}^3 , these are chosen for the analysis of the proposed control law. We also note that consensus in \mathbb{R}^n can be casted as a synchronization problem in \mathbb{S}^n , and that under our framework, we do not require a dwell time between consecutive The results here presented are based on those in [109].

The remainder of this section is structured as follows. In Section 3.3.2, we describe the conditions on vector fields that guarantee convergence to the consensus set. In Section 3.3.4, we describe the common framework for analysis of both synchronization in \mathbb{S}^2 and $\mathbb{SO}(3)$. In Sections 3.3.6 and 3.3.5, the control laws for synchronization in $\mathbb{SO}(3)$ and \mathbb{S}^2 are presented, respectively, and the agents dynamics are transformed into the common framework. In Section 3.3.8, asymptotic synchronization is established for the common framework vector field. In Section 3.3.9, illustrative simulations are presented.

3.3.2 Preliminaries

In what follows, let $n, N \in \mathbb{N}$. Consider a time dependent switching signal $\sigma : \mathbb{R}_{\geq 0} \mapsto \{1, \dots, p\} =: \mathcal{P}$, which is continuous from the right, and $\mathbf{x} = (\mathbf{x}_1, \dots, \mathbf{x}_N) : \mathbb{R}_{\geq 0} \ni t \mapsto \mathbf{x}(t) \in (\mathbb{R}^n)^N$ evolving according to the switched system

$$\dot{\mathbf{x}}(t) = \mathbf{f}(t, \mathbf{x}(t)) =: \mathbf{f}_{\sigma(t)}(\mathbf{x}(t)), \mathbf{x}(0) \in \mathbb{R}^{nN}, \quad (3.3.1)$$

where $\mathbf{f}_p(\cdot) := (\mathbf{f}_{1,p}(\cdot), \dots, \mathbf{f}_{N,p}(\cdot)) : (\mathbb{R}^n)^N \mapsto (\mathbb{R}^n)^N$ for every $p \in \mathcal{P}$. We consider a network of $N \geq 2$ agents, with $n \geq 1$ the dimension of the space which the agents belong to, and with $\mathbf{f}_{i,\sigma(\cdot)}(\cdot)$ the dynamics of agent $i \in \mathcal{N} = \{1, \dots, N\}$. We denote by $\mathcal{T} = \{t_1, t_2, \dots\}$ the increasing sequence of switching time instants, where, $\forall t_k, t_{k+1} \in \mathcal{T}$, it holds that $\sigma(t_k) \neq \sigma(t_{k+1})$, $\sigma|_{[t_k, t_{k+1}]} = q \in \mathcal{P}$ and either $\lim_{k \rightarrow \infty} t_k = \infty$ or $t_k = \infty$ for some $k \in \mathbb{N}$. Since \mathcal{T} is a countable set, the switching signal σ is constant almost everywhere. Additionally, $\{\mathbf{f}_p\}_{p \in \mathcal{P}}$ are assumed to be locally Lipschitz continuous,

and thus, since $|\mathcal{P}| < \infty$, $\mathbf{f}(t, \cdot) = \mathbf{f}_{\sigma(t)}(\cdot)$ is locally Lipschitz continuous. Thus the conditions of Theorem 54 in [110] are satisfied, which implies that the initial value problem,

$$\mathbf{x}(t) = \mathbf{x}(0) + \int_0^t \mathbf{f}_{\sigma(\tau)}(\mathbf{x}(\tau)) d\tau, \quad (3.3.2)$$

has a unique solution $\mathbf{x} : [0, T_{\max}) \mapsto \mathbb{R}^{nN}$, which is an absolutely continuous function defined on the maximal right interval $[0, T_{\max})$.

3.3.3 Assumptions on the dynamics $\mathbf{f}_{i,p}$

We now present conditions on the vector fields $\{\mathbf{f}_p\}_{p \in \mathcal{P}}$, which guarantee that the solution of (3.3.2) converges to the consensus set $\mathcal{C} = \{\mathbf{x} = (\mathbf{x}_1, \dots, \mathbf{x}_N) \in (\mathbb{R}^n)^N : \mathbf{x}_1 = \dots = \mathbf{x}_N\}$. In later sections, when studying synchronization in \mathcal{S}^2 and $\mathbb{SO}(3)$, given the proposed control laws, we verify that the dynamics of all agents satisfy these conditions, allowing us to refer to the results in this section. Moreover, for these systems, convergence to a constant vector is guaranteed after some further analysis.

Denote, for every $i \in \mathcal{N}$,

$$\mathbf{v}_i^{\max}(\mathbf{x}) = \max_{p \in \mathcal{P}} \mathbf{x}_i^T \mathbf{f}_{i,p}(\mathbf{x}), \quad (3.3.3)$$

which quantifies an upper bound on the time derivative of $\frac{1}{2}\|\mathbf{x}_i\|^2$ along a solution of (3.3.1), since $\frac{d}{dt} \frac{1}{2}\mathbf{x}_i^T(t)\mathbf{x}_i(t) = \mathbf{x}_i^T(t)\mathbf{f}_{i,\sigma(t)}(\mathbf{x}(t)) \leq \mathbf{v}_i^{\max}(\mathbf{x}(t))$, for all time instants t where the derivative is well defined.

Also, given $\mathbf{x} = (\mathbf{x}_1, \dots, \mathbf{x}_N) \in (\mathbb{R}^n)^N$, denote $\mathcal{H}(\mathbf{x}) = \{i \in \mathcal{N} : i = \arg \max_{j \in \mathcal{N}} (\|\mathbf{x}_j\|)\}$ as the set of indexes $i \in \mathcal{H}(\mathbf{x}) \subseteq \mathcal{N}$ for which $\|\mathbf{x}_i\|$ is larger than or equal to $\|\mathbf{x}_j\|$ for all $j \in \mathcal{N}$. Given $\mathbf{x} \notin \mathcal{C}$, assume that $\mathbf{v}_i^{\max}(\mathbf{x}) \leq 0$ for all $i \in \mathcal{H}(\mathbf{x})$ and that

$$\forall p \in \mathcal{P} \exists k \in \mathcal{H}(\mathbf{x}) : \mathbf{x}_k^T \mathbf{f}_{k,p}(\mathbf{x}) < 0. \quad (3.3.4)$$

Condition (3.3.4) implies that, for every switching signal $p \in \mathcal{P}$, and within the set $\{\frac{1}{2}\|\mathbf{x}_i\|^2\}_{i \in \mathcal{H}(\mathbf{x})}$, one can always find an element whose time derivative along a solution of (3.3.1), if well defined, is negative. Then, given any $\mathbf{x} \notin \mathcal{C}$ and $p \in \mathcal{P}$, denote $\mathcal{H}^*(\mathbf{x}, p) = \{i \in \mathcal{H}(\mathbf{x}) : \mathbf{x}_i^T \mathbf{f}_{i,p}(\mathbf{x}) < 0\}$, which due to (3.3.4) is a non-empty subset of $\mathcal{H}(\mathbf{x})$, i.e., $\emptyset \neq \mathcal{H}^*(\mathbf{x}, p) \subseteq \mathcal{H}(\mathbf{x})$. Finally, define $\mathbf{v}^{\max}(\mathbf{x}) := \max_{p \in \mathcal{P}} \max_{i \in \mathcal{H}^*(\mathbf{x}, p)} \mathbf{x}_i^T \mathbf{f}_{i,p}(\mathbf{x})$.

From the definition of $\mathcal{H}^*(\cdot, \cdot)$ it follows that $\mathbf{v}^{\max}(\mathbf{x}) < 0$ for all $\mathbf{x} \notin \mathcal{C}$. Additionally, for each $\mathbf{x} \notin \mathcal{C}$, $\mathbf{v}^{\max}(\mathbf{x})$ quantifies an upper bound on the time derivative of $\frac{1}{2}\|\mathbf{x}_i\|^2$ along the solution of (3.3.1), at a time instant $t \geq 0$ and for $i \in \mathcal{H}^*(\mathbf{x}, \sigma(t))$. Based on this consideration, it is shown in [111] that the time derivative of $V(\mathbf{x}) = \max_{i \in \mathcal{N}} \frac{1}{2}\mathbf{x}_i^T \mathbf{x}_i$ along the solution of (3.3.1) is bounded a.e. by $\mathbf{v}^{\max}(\mathbf{x}) < 0$, for all $\mathbf{x} = (\mathbf{x}_1, \dots, \mathbf{x}_N) \notin \mathcal{C}$. The latter property is central for the proof of the following theorem, which establishes asymptotic convergence of the solution to \mathcal{C} and constitutes the main result of this section.

Theorem 3.3.1. Consider the system (3.3.1) and assume that for certain $r > 0$ and all $\mathbf{x} = (\mathbf{x}_1, \dots, \mathbf{x}_N) \in \mathcal{B}(r)^N$ the following hold:

1. when $\mathbf{x} \notin \mathcal{C}$,

- a) $\mathbf{v}_i^{\max}(\mathbf{x}) \leq 0 \forall i \in \mathcal{H}(\mathbf{x})$,
- b) $\forall p \in \mathcal{P} \exists k \in \mathcal{H}(\mathbf{x}) : \mathbf{x}_k^T \mathbf{f}_{k,p}(\mathbf{x}) < 0$,

2. when $\mathbf{x} \in \mathcal{C}$, $\mathbf{x}_i^T \mathbf{f}_{i,p}(\mathbf{x}) = \mathbf{0} \forall i \in \mathcal{N}, p \in \mathcal{P}$,

Then for each initial condition $\mathbf{x}(0) \in \mathcal{B}(r)^N$, the set $\bar{\mathcal{B}}(r_0)^N$, with $r_0 = \max_{i \in \mathcal{N}} \|\mathbf{x}_i(0)\| < r$, is positively invariant and $\mathbf{x}(\cdot)$, as the solution (3.3.2), converges asymptotically to $\Omega = \{\mathbf{x} \in \bar{\mathcal{B}}(r_0)^N : \mathbf{x}_1 = \dots = \mathbf{x}_N\} = \bar{\mathcal{B}}(r_0)^N \cap \mathcal{C}$. Moreover, given $V : (\mathbb{R}^n)^N \mapsto \mathbb{R}_{\geq 0}$, defined as $V(\mathbf{x}) = \max_{i \in \mathcal{N}} \frac{1}{2} \mathbf{x}_i^T \mathbf{x}_i$, $\lim_{t \rightarrow \infty} V(\mathbf{x}(t)) = V^\infty \in [0, V(\mathbf{x}(0))]$.

The complete proof is found in [111]. Briefly, it is shown that $\dot{V}(\mathbf{x}(t))$ exists almost everywhere and is almost always upper bounded by $\mathbf{v}^{\max}(\mathbf{x}(t))$, i.e., $\dot{V}(\mathbf{x}(t)) \leq^{a.e.} \mathbf{v}^{\max}(\mathbf{x}(t))$, where $\mathbf{v}^{\max}(\mathbf{x}) < 0$ for $\mathbf{x} \notin \Omega = \Omega_0 \cap \mathcal{C}$. It then follows that Ω_0 is positively invariant, and thus, from compactness of Ω_0 , that the solution of (3.3.1) is defined for all positive times, namely $T_{\max} = \infty$ [110, Proposition C.3.6]. Asymptotic convergence of $\mathbf{x}(\cdot)$ to $\Omega = \Omega_0 \cap \mathcal{C}$ is then proved by contradiction.

Example 3.3.1. Consider $\sigma : \mathbb{R}_{\geq 0} \mapsto \{1, 2\}$, defined as $\sigma(t \in [k, k+1)) := 1$ for $k \in \mathbb{N}$ even and $\sigma(t \in [k, k+1)) := 2$ for $k \in \mathbb{N}$ odd; and $\mathbf{x} := (\mathbf{x}_1, \mathbf{x}_2, \mathbf{x}_3) : \mathbb{R}_{\geq 0} \mapsto (\mathbb{R}^2)^3$, evolving according to $\dot{\mathbf{x}}(t) = \mathbf{f}_{\sigma(t)}(\mathbf{x})$ where

$$\mathbf{f}_1(\mathbf{x}) = (\mathbf{x}_2 - \mathbf{x}_1 + \mathcal{S}(\mathbf{x}_1) \mathbf{k}, \mathbf{x}_3 - \mathbf{x}_2 + \mathcal{S}(\mathbf{x}_2) \mathbf{k}, \mathbf{x}_1 - \mathbf{x}_3 + \mathcal{S}(\mathbf{x}_3) \mathbf{k}). \quad (3.3.5)$$

$$\mathbf{f}_2(\mathbf{x}) = (\mathbf{x}_3 - \mathbf{x}_1 + \mathcal{S}(\mathbf{x}_1) \mathbf{k}, \mathbf{x}_1 - \mathbf{x}_2 + \mathcal{S}(\mathbf{x}_2) \mathbf{k}, \mathbf{x}_2 - \mathbf{x}_3 + \mathcal{S}(\mathbf{x}_3) \mathbf{k}). \quad (3.3.6)$$

Then, for $\mathbf{x} = (\mathbf{x}_1, \mathbf{x}_2, \mathbf{x}_3) \in (\mathbb{R}^2)^3 \setminus \mathcal{C}$ and for all $i \in \mathcal{H}(\mathbf{x})$,

$$\mathbf{v}_i^{\max}(\mathbf{x}) := \max_{p \in \{1, 2\}} \mathbf{x}_i^T \mathbf{f}_p(\mathbf{x}) = -\|\mathbf{x}_i\|^2 + \mathbf{x}_i^T \mathbf{x}_j < 0, j \in \{1, 2, 3\} \setminus \{i\}, \quad (3.3.7)$$

and for $\mathbf{x} = (\mathbf{x}_1, \mathbf{x}_2, \mathbf{x}_3) \in \mathcal{C}$ and for all $i \in \{1, 2, 3\}$,

$$\mathbf{x}_i^T \mathbf{f}_p(\mathbf{x}_1, \mathbf{x}_2, \mathbf{x}_3) = 0 \forall p \in \{1, 2\} \quad (3.3.8)$$

and thus all conditions of Theorem 3.3.1 are satisfied. Notice, however, that if $\mathbf{k} = \mathbf{e}_3 \in \mathbb{R}^3$, then $t \in \mathbb{R}_{\geq 0} \mapsto \mathbf{1}_3 \otimes (\cos(t), \sin(t), 0)$ is a non-constant solution of $\dot{\mathbf{x}}(t) = \mathbf{f}_{\sigma(t)}(\mathbf{x})$.

3.3.4 Synchronization

In the next subsections, we study synchronization in \mathbb{S}^2 and $\mathbb{SO}(3)$. We also present decentralized output feedback control laws for the angular velocities and the closed

loop dynamics that follow from the chosen control laws. Afterwards, by means of appropriate transformations, those dynamics are rewritten in a common form that allows us to study synchronization in \mathbb{S}^2 and $\mathbb{SO}(3)$ under a common framework. Additionally, we also show that consensus in \mathbb{R}^n can be casted as a synchronization problem in \mathbb{S}^n , for any $n \in \mathbb{N}$.

At this point, we recall Definition 1.3.3 of cone, and as illustrated in Fig. 1.3

Definition 3.3.2. Let $N, n \geq 1$. We say that $\boldsymbol{\nu} = (\boldsymbol{\nu}_1, \dots, \boldsymbol{\nu}_N) \in (\mathbb{S}^n)^N$ belongs to an open (closed) α -cone, for some $\alpha \in [0, \pi]$, if $\exists \bar{\boldsymbol{\nu}} \in \mathbb{S}^n : \boldsymbol{\nu} \in \mathcal{C}(\alpha, \bar{\boldsymbol{\nu}})^N (\bar{\mathcal{C}}(\alpha, \bar{\boldsymbol{\nu}})^N)$. We say that $\boldsymbol{\nu}$ is synchronized if $\boldsymbol{\nu}_1 = \dots = \boldsymbol{\nu}_N$.

In the previous definition $\boldsymbol{\nu} = (\boldsymbol{\nu}_1, \dots, \boldsymbol{\nu}_N) \in (\mathbb{S}^n)^N$ stands for a group of N unit vectors we wish to synchronize. We show later that, given the proposed control laws, synchronization of a group of unit vectors takes place asymptotically if the group of unit vectors is initially contained in an open α^* -cone, where $\alpha^* = \frac{\pi}{2}$ for synchronization in \mathbb{S}^2 and consensus in \mathbb{R}^n ; and where $\alpha^* = \frac{\pi}{4}$ for synchronization in $\mathbb{SO}(3)$.

In the next subsections, we always consider a group of N agents, indexed by the set $\mathcal{N} = \{1, \dots, N\}$, operating in either \mathbb{S}^2 , $\mathbb{SO}(3)$ or \mathbb{R}^n . The agents' network is modeled as a time varying digraph, $\mathcal{G}(\sigma(\cdot)) = \{\mathcal{N}, \mathcal{E}(\sigma(\cdot))\}$, with \mathcal{N} as the time invariant vertices' set containing the team members; with $\sigma : \mathbb{R}_{\geq 0} \mapsto \{1, \dots, p\} =: \mathcal{P}$ as the switching signal; and with $\mathcal{G}(q)$ and $\mathcal{E}(q)$ as the graph and edges' sets corresponding to the switching signal $q \in \mathcal{P}$ (and where $|\mathcal{P}| \leq 2^{N(N-1)}$ since $2^{N(N-1)}$ provides an upper bound on the number of possible digraphs). We also denote $\mathcal{N}_i(q) \subset \mathcal{N}$ as the neighbor set of agent $i \in \mathcal{N}$ for the switching signal $q \in \mathcal{P}$; and, for convenience, we also denote (with some abuse of notation) $\{j_1, \dots, j_{|\mathcal{N}_i(q)|}\} \equiv \mathcal{N}_i(q)$.

In order to perform analysis under a common framework, we transform all problems's dynamics into a standard form, namely that presented below. Given $n \geq 1$, we denote $\boldsymbol{\nu} = (\boldsymbol{\nu}_1, \dots, \boldsymbol{\nu}_N) : \mathbb{R}_{\geq 0} \ni t \mapsto \boldsymbol{\nu}(t) \in (\mathbb{S}^n)^N$ as the state of a group of unit vectors in \mathbb{S}^n , which evolves according to the dynamics

$$\dot{\boldsymbol{\nu}}(t) = \tilde{\mathbf{f}}_{\sigma(t)}(\boldsymbol{\nu}(t)) = (\tilde{\mathbf{f}}_{1,\sigma(t)}(\boldsymbol{\nu}(t)), \dots, \tilde{\mathbf{f}}_{N,\sigma(t)}(\boldsymbol{\nu}(t))), \boldsymbol{\nu}(0) \in (\mathbb{S}^n)^N \quad (3.3.9)$$

where, for some $\alpha \in [0, \pi]$ and $\bar{\boldsymbol{\nu}} \in \mathbb{S}^n$, $\tilde{\mathbf{f}}_{i,\sigma(t)} : (\mathbb{S}^n)^N \ni \boldsymbol{\nu} \mapsto \tilde{\mathbf{f}}_{i,\sigma(t)}(\boldsymbol{\nu}) \in T_{\boldsymbol{\nu}} \mathbb{S}^n \subset \mathbb{R}^{n+1}$ is defined as

$$\tilde{\mathbf{f}}_{i,\sigma(t)}(\boldsymbol{\nu}) = \sum_{j \in \mathcal{N}_i(\sigma(t))} \tilde{w}_{ij}(\boldsymbol{\nu}_i, \boldsymbol{\nu}_j) \Pi(\boldsymbol{\nu}_i) \boldsymbol{\nu}_j, \quad (3.3.10)$$

for each $i \in \mathcal{N}$; i.e., $\dot{\boldsymbol{\nu}}_i(t) = \tilde{\mathbf{f}}_{i,\sigma(t)}(\boldsymbol{\nu}(t))$. Notice that $\boldsymbol{\nu}_i^T \tilde{\mathbf{f}}_{i,p}(\boldsymbol{\nu}) = 0$ for all $i \in \mathcal{N}$, $p \in \mathcal{P}$ and $\boldsymbol{\nu} \in (\mathbb{S}^n)^N$, which implies that the set $(\mathbb{S}^n)^N$ is positively invariant with respect to (3.3.9).

The system (3.3.9)-(3.3.10) is the standard form all problems are transformed into: for synchronization in \mathbb{S}^2 , $\boldsymbol{\nu} : \mathbb{R}_{\geq 0} \mapsto (\mathbb{S}^2)^N$; for synchronization in $\mathbb{SO}(3)$, $\boldsymbol{\nu} : \mathbb{R}_{\geq 0} \mapsto (\mathbb{SO}(3))^N$; and for consensus in \mathbb{R}^n , $\boldsymbol{\nu} : \mathbb{R}_{\geq 0} \mapsto (\mathbb{R}^n)^N$.

The functions $\tilde{w}_{ij} : \mathcal{C}(\alpha, \bar{\boldsymbol{\nu}})^2 \mapsto \mathbb{R}_{\geq 0}$ in (3.3.10) are continuous weight functions, for some $\alpha \in [\frac{\pi}{2}, \pi]$ and $\bar{\boldsymbol{\nu}} \in \mathbb{S}^n$. Thus, given $(\boldsymbol{\nu}_i, \boldsymbol{\nu}_j) \in \mathcal{C}(\alpha, \bar{\boldsymbol{\nu}})^2$, $\tilde{w}_{ij}(\boldsymbol{\nu}_i, \boldsymbol{\nu}_j)$ is the

weight agent i assigns to the deviation between itself and its neighbor j , for all $i, j \in \mathcal{N}$ (and where we emphasize that the agents are within the same cone). All functions \tilde{w}_{ij} are assumed to satisfy the following condition,

$$\tilde{w}_{ij}(\boldsymbol{\nu}_i, \boldsymbol{\nu}_j) > 0 \forall (\boldsymbol{\nu}_i, \boldsymbol{\nu}_j) \in \mathcal{C}(\alpha, \bar{\nu})^2 \text{ with } \boldsymbol{\nu}_i^T \boldsymbol{\nu}_j \neq 1. \quad (3.3.11)$$

Thus, from continuity, it follows that the weight between two neighbors is zero if and only if they are synchronized, though the weight may be arbitrarily small when the neighbors are arbitrarily close to each other or when the neighbors are close to the boundaries of the domain of the weight functions.

The dependency of the dynamics (3.3.9)-(3.3.10) on time comes from the time varying network graph, and more specifically, the time varying neighbor set of each agent, as specified in (3.3.10).

Although the results in this section remain valid under arbitrary switching, in practical cases the switching instants of each agent's control law cannot accumulate to a certain time value. In order to formulate this observation as an assumption, we adopt Definition 2.3. in [106], and say that the switching signal $\sigma(\cdot)$ has an average dwell-time $\tau_D > 0$ and a chatter bound $N_0 \in \mathbb{N}$ if the number of switching times of $\sigma(\cdot)$ in any open finite interval $(t_1, t_2) \subset \mathbb{R}_{\geq 0}$ is upper bounded by $N_0 + \frac{t_2 - t_1}{\tau_D}$.

Assumption 3.3.3. *For each agent $i \in \mathcal{N}$, we assume its neighbor set $\mathcal{N}_i(\sigma) : \mathbb{R}_{\geq 0} \mapsto \mathcal{N}$ switches, independently from all other agents in the network, with an average dwell-time $\tau_D^i > 0$ and chatter bound $N_0^i \in \mathbb{N}$.*

As explained in more detail in the next sections, each agent $i \in \mathcal{N}$ is in charge of providing the input that follows from composing the proposed output feedback control laws with the measurements made at each time instant. Thus, requiring an agent's neighbor set to switch with an average dwell time guarantees that the agent's input does not experience infinite many discontinuities in any time interval of finite length. In fact, if Assumption 3.3.3 is satisfied, then σ has an average dwell time, and therefore it follows that the set of switching times of the network dynamics \mathcal{T} has zero measure in $\mathbb{R}_{\geq 0}$, a necessary condition in order to invoke the results from Section 3.3.3.

Proposition 3.3.4. *If each agent's $i \in \mathcal{N}$ neighbor set $\mathcal{N}_i(\sigma) : \mathbb{R}_{\geq 0} \mapsto \mathcal{N}$ switches with an average dwell-time τ_D^i and chatter bound N_0^i , then the network dynamics (3.3.9) has a switching signal with average dwell time $\tau_D = \frac{1}{N} \min_{i \in \mathcal{N}} \tau_D^i$ and chatter bound $N_0 = N \max_{i \in \mathcal{N}} N_0^i$.*

A proof is found in [111].

3.3.5 Complete synchronization in $\mathbb{SO}(3)$ casted as synchronization in \mathbb{S}^3

In this section, we consider a group of N rotations matrices, and we wish to accomplish complete synchronization, as explained and illustrated in Section 3.2.1, page 72.

For each $i \in \mathcal{N}$, $\omega_i : \mathbb{R}_{\geq 0} \mapsto \mathbb{R}^3$ denotes the body-framed angular velocity of agent i , which can be actuated. Each rotation matrix $\mathcal{R}_i : \mathbb{R}_{\geq 0} \ni t \mapsto \mathcal{R}_i(t) \in \mathbb{SO}(3)$ evolves according to

$$\dot{\mathcal{R}}_i(t) = \mathbf{f}_R(\mathcal{R}_i(t), \omega_i(t)), \mathcal{R}_i(0) \in \mathbb{SO}(3), \quad (3.3.12)$$

and with $\mathbf{f}_R : \mathbb{SO}(3) \times \mathbb{R}^3 \ni (\mathcal{R}_i, \omega_i) \mapsto \mathbf{f}_R(\mathcal{R}_i, \omega_i) \in T_{\mathcal{R}_i} \mathbb{SO}(3) \subset \mathbb{R}^{3 \times 3}$ given by

$$\mathbf{f}_R(\mathcal{R}_i, \omega_i) := \mathcal{R}_i \mathcal{S}(\omega_i). \quad (3.3.13)$$

It may be verified that $\mathbf{f}_R(\mathcal{R}_i, \cdot) \in T_{\mathcal{R}_i} \mathbb{SO}(3)$ for every $\mathcal{R}_i \in \mathbb{SO}(3)$, via the same steps as in Section 2.3 (see (2.3.7) and (2.3.8), in page 29). If, at a time instant $t \in \mathbb{R}_{\geq 0}$, agent $i \in \mathcal{N}$ is aware of the relative attitude between itself and another agent j , then $j \in \mathcal{N}_i(\sigma(t))$, where $\sigma(t)$ encodes the network graph at time t . In particular, for each time instant $t \in \mathbb{R}_{\geq 0}$, each agent $i \in \mathcal{N}$ is equipped with the output function $\mathbf{h}_i(t, \cdot) : \mathbb{SO}(3)^N \ni \mathcal{R} \mapsto \mathbf{h}_i(t, \mathcal{R}) \in \mathbb{SO}(3)^{|\mathcal{N}_i(\sigma(t))|}$ defined as

$$\mathbf{h}_i(t, \mathcal{R}) := (\mathbf{h}_{ij_1}(\mathcal{R}), \dots, \mathbf{h}_{ij_{|\mathcal{N}_i(\sigma(t))|}}(\mathcal{R})) \in \mathbb{SO}(3)^{|\mathcal{N}_i(\sigma(t))|}, \quad (3.3.14)$$

where $\{j_1, \dots, j_{|\mathcal{N}_i(\sigma(t))|}\} \equiv \mathcal{N}_i(\sigma(t))$ and where

$$\mathbf{h}_{ij} : \mathbb{SO}(3)^N \ni (\mathcal{R}_1, \dots, \mathcal{R}_N) = \mathcal{R} \mapsto \mathbf{h}_{ij}(\mathcal{R}) := \mathcal{R}_i^T \mathcal{R}_j \in \mathbb{SO}(3), \quad (3.3.15)$$

for each $j \in \mathcal{N}_i(\sigma(t))$. Thus, at each time instant $t \in \mathbb{R}_{\geq 0}$, agent $i \in \mathcal{N}$ measures the $|\mathcal{N}_i(\sigma(t))|$ rotation matrices of its neighbors in its own coordinate frame. We emphasize that the measurement as defined in (3.3.15) does not require an agent to be aware of its own rotation matrix or its neighbors rotation matrices (recall that these are specified in an unknown inertial orientation frame); rather it requires an agent to measure the projection of each of its neighbors three axes onto its own three axes.

At this point, we recall the notion of decentralized output feedback control law as defined in Section 3.2.2, which should made clear the previous definition of output function and the Problem statement presented next.

Problem 3.3.5. *For each $i \in \mathcal{N}$, design time-varying decentralized feedback laws ω_i^h , with $\omega_i^h(t, \cdot) : \mathbb{SO}(3)^{|\mathcal{N}_i(\sigma(t))|} \mapsto \mathbb{R}^3$ depending on the measurements $\mathbf{h}_i(t, \cdot)$ in (3.3.14) for each $t \geq 0$, such that asymptotic synchronization of $\mathcal{R} = (\mathcal{R}_1, \dots, \mathcal{R}_N) : \mathbb{R}_{\geq 0} \mapsto \mathbb{SO}(3)^N$ is accomplished, where $\dot{\mathcal{R}}_i(t) = \mathbf{f}_R(\mathcal{R}_i(t), \omega_i^h(t, \mathbf{h}_i(t, \mathcal{R}(t))))$ for every $i \in \mathcal{N}$.*

Problem 3.3.5 may be restated as finding a control law for each agent that depends exclusively on the measurement function as defined in (3.3.14), and which encodes the partial state information available to each agent at a given time instant.

Definition 3.3.6. *We define the angular displacement between two rotation matrices $\theta : \mathbb{SO}(3) \times \mathbb{SO}(3) \ni (\mathcal{R}_i, \mathcal{R}_j) \mapsto \theta(\mathcal{R}_i, \mathcal{R}_j) = \arccos\left(\frac{\text{tr}(\mathcal{R}_i^T \mathcal{R}_j) - 1}{2}\right) \in [0, \pi]$.*

For each agent $i \in \mathcal{N}$ and each $t \in \mathbb{R}_{\geq 0}$, we propose the control law $\omega_i^h(t, \cdot) : \mathbb{SO}(3)^{|\mathcal{N}_i(\sigma(t))|} \ni (\mathbf{h}_{ij_1}, \dots, \mathbf{h}_{ij_{|\mathcal{N}_i(\sigma(t))|}}) = \mathbf{h}_i \mapsto \omega_i^h(t, \mathbf{h}_i) \in \mathbb{R}^3$ defined as

$$\omega_i^h(t, \mathbf{h}_i) := \sum_{j \in \mathcal{N}_i(\sigma(t))} w_{ij}(\theta(\mathbf{I}, \mathbf{h}_{ij})) \mathcal{S}^{-1}\left(\frac{\mathbf{h}_{ij} - \mathbf{h}_{ij}^T}{2}\right), \quad (3.3.16)$$

where $w_{ij} : [0, \pi] \mapsto \mathbb{R}_{\geq 0}$ is continuous and satisfies

$$w_{ij}(\theta) > 0 \quad \forall \theta \in (0, \pi]. \quad (3.3.17)$$

Notice that w_{ij} corresponds to a weight agent i assigns to the displacement between itself and its neighbor j . In addition, by defining $\omega_i^{cl} : \mathbb{R}_{\geq 0} \times \mathbb{SO}(3)^N \ni (t, \mathcal{R}) \mapsto \omega_i^{cl}(t, \mathcal{R}) := \omega_i^h(t, \mathbf{h}_i(t, \mathcal{R})) \in \mathbb{R}^3$, and exploiting (3.3.14) and (3.3.15), it follows that

$$\begin{aligned} \omega_i^{cl}(t, \mathcal{R}) &= \sum_{j \in \mathcal{N}_i(\sigma(t))} w_{ij}(\theta(\mathbf{I}, \mathcal{R}_i^T \mathcal{R}_j)) \mathcal{S}^{-1}\left(\frac{\mathcal{R}_i^T \mathcal{R}_j - \mathcal{R}_j^T \mathcal{R}_i}{2}\right) \\ &= \sum_{j \in \mathcal{N}_i(\sigma(t))} w_{ij}(\theta(\mathcal{R}_i, \mathcal{R}_j)) \mathcal{S}^{-1}\left(\frac{\mathcal{R}_i^T \mathcal{R}_j - \mathcal{R}_j^T \mathcal{R}_i}{2}\right), \end{aligned} \quad (3.3.18)$$

where we have made use of the fact that $\theta(\mathcal{R}_i, \mathcal{R}_j) = \theta(\mathcal{R} \mathcal{R}_i, \mathcal{R} \mathcal{R}_j)$ for any $\mathcal{R}, \mathcal{R}_i, \mathcal{R}_j \in \mathbb{SO}(3)$. We emphasize that if Assumption 3.3.3 is satisfied, then (3.3.16) (and (3.3.18)) does not have infinite many discontinuities in any time interval of finite length, which in turn implies that it can be implemented in a practical scenario.

Recall that we wish to analyze different problems under a common framework where agents are unit vectors. Thus, in order to cast complete synchronization in $\mathbb{SO}(3)$ in the form (3.3.9), we perform a change of coordinates based on unit quaternions. This change of variables serves only the purpose of analysis, while the implemented control law is still that in (3.3.16). Consider then a unit quaternion $\mathbf{q} \in \mathbb{S}^3$ as a parametrization of a rotation matrix $\mathcal{R} \in \mathbb{SO}(3)$, i.e., consider the mapping $\bar{\mathcal{R}}_q : \mathbb{S}^3 \ni \mathbf{q} \mapsto \bar{\mathcal{R}}_q(\mathbf{q}) = \mathcal{R} \in \mathbb{SO}(3)$ (details on the next derivations are found in Subsection 3.3.11). Given that there exist N rotation matrices, it is convenient to define $\mathcal{R}_q : (\mathbb{S}^3)^N \ni (\mathbf{q}_1, \dots, \mathbf{q}_N) = \mathbf{q} \mapsto \mathcal{R}_q(\mathbf{q}) := (\bar{\mathcal{R}}_q(\mathbf{q}_1), \dots, \bar{\mathcal{R}}_q(\mathbf{q}_N)) \in \mathbb{SO}(3)^N$. For this parameterization, the control law (3.3.18) may be rewritten as

$$\omega_i^q : \mathbb{R}_{\geq 0} \times (\mathbb{S}^3)^N \ni (t, \mathbf{q}) \mapsto \omega_i^q(t, \mathbf{q}) := \omega_i^{cl}(t, \mathcal{R}_q(\mathbf{q})) \in \mathbb{R}^3, \quad (3.3.19)$$

$$\omega_i^q(t, \mathbf{q}) = \sum_{j \in \mathcal{N}_i(\sigma(t))} 2\mathbf{q}_i^T \mathbf{q}_j w_{ij}(\arccos(2(\mathbf{q}_i^T \mathbf{q}_j)^2 - 1)) [\mathbf{I}_3 \quad \mathbf{0}] Q(\mathbf{q}_i^*) \mathbf{q}_j, \quad (3.3.20)$$

where $\mathbf{q}_i^* \in \mathbb{S}^3$ denotes the conjugate quaternion of $\mathbf{q}_i \in \mathbb{S}^3$ and $Q(\cdot)$ is defined in (3.3.46) (in Subsection 3.3.11). Denote

$$\tilde{w}_{ij}(\mathbf{q}_i, \mathbf{q}_j) := \mathbf{q}_i^T \mathbf{q}_j w_{ij}(\arccos(2(\mathbf{q}_i^T \mathbf{q}_j)^2 - 1)), \quad (3.3.21)$$

and notice that this satisfies (3.3.11) for $\alpha = \frac{\pi}{4}$ and for any $\bar{\nu} \in \mathbb{S}^3$ (see (3.3.17) and Proposition 3.3.18 in Subsection 3.3.10). Then the dynamics of each agent,

parametrized by unit quaternions, when composed with the control law (3.3.19), are described by $\dot{\mathbf{q}}_i(t) = \tilde{\mathbf{f}}_{i,\sigma(t)}(\mathbf{q}(t))$, where $\tilde{\mathbf{f}}_{i,\sigma(t)} : (\mathbb{S}^3)^N \ni (\mathbf{q}_1, \dots, \mathbf{q}_N) = \mathbf{q} \mapsto \tilde{\mathbf{f}}_{i,\sigma(t)}(\mathbf{q}) \in T_{\mathbf{q}_i} \mathbb{S}^3$ is given by

$$\begin{aligned} \tilde{\mathbf{f}}_{i,\sigma(t)}(\mathbf{q}) &\stackrel{(3.3.52)}{=} \frac{1}{2} Q(\mathbf{q}_i) \begin{bmatrix} \mathbf{I}_3 & \mathbf{0} \end{bmatrix}^T \boldsymbol{\omega}_i^q(t, \mathbf{q}) \\ &\stackrel{(3.3.20)}{=} \sum_{j \in \mathcal{N}_i(\sigma(t))} \tilde{w}_{ij}(\mathbf{q}_i, \mathbf{q}_j) Q(\mathbf{q}_i) (\mathbf{I}_3 - \mathbf{e}_4 \mathbf{e}_4^T) Q(\mathbf{q}_i^*) \mathbf{q}_j \\ &\stackrel{(3.3.47)}{=} \sum_{j \in \mathcal{N}_i(\sigma(t))} \tilde{w}_{ij}(\mathbf{q}_i, \mathbf{q}_j) \Pi(\mathbf{q}_i) \mathbf{q}_j. \end{aligned} \quad (3.3.22)$$

We have then casted this problem in the form (3.3.9) with $\boldsymbol{\nu} = \mathbf{q} = (\mathbf{q}_1, \dots, \mathbf{q}_N) \in (\mathbb{S}^3)^N$.

Remark 3.3.7. Consider $\mathbf{q} = (\mathbf{q}_1, \dots, \mathbf{q}_N) \in (\mathbb{S}^3)^N$ and let $\mathcal{R}_i = \bar{\mathcal{R}}(\mathbf{q}_i) \in \mathbb{SO}(3)$ for every $i \in \mathcal{N}$. If there exists $\bar{\mathbf{q}} \in \mathbb{S}^3$ such that $\mathbf{q} \in \mathcal{C}(\frac{\pi}{4}, \bar{\mathbf{q}})^N$, then, by definition, $\bar{\mathbf{q}}^T \mathbf{q}_i > \cos(\frac{\pi}{4})$ for all $i \in \mathcal{N}$. Thus, it follows that $\theta(\bar{\mathcal{R}}(\bar{\mathbf{q}}), \mathcal{R}_i) = \arccos(2(\bar{\mathbf{q}}^T \mathbf{q}_i)^2 - 1) \leq \arccos(2\cos^2(\frac{\pi}{4}) - 1) = \frac{\pi}{2}$ for all $i \in \mathcal{N}$, i.e. all rotation matrices are $\frac{\pi}{2}$ close to some other rotation matrix, namely $\bar{\mathcal{R}}(\bar{\mathbf{q}})$. See also Proposition 3.3.21 in Subsection 3.3.11.

Remark 3.3.8. Notice that $\boldsymbol{\omega}_i^q(\cdot, \mathbf{q}) = \boldsymbol{\omega}_i^q(\cdot, \tilde{\mathbf{q}})$ for any $(\mathbf{q}, \tilde{\mathbf{q}}) \in \{(\mathbf{q}_1, \dots, \mathbf{q}_N, \tilde{\mathbf{q}}_1, \dots, \tilde{\mathbf{q}}_N) \in (\mathbb{S}^3)^N \times (\mathbb{S}^3)^N : \mathbf{q}_i = \pm \tilde{\mathbf{q}}_i, i \in \mathcal{N}\}$, owing to the fact that \mathbb{S}^3 is a double cover of $\mathbb{SO}(3)$ [112]. Indeed, if $\mathbf{q}_i \in \mathbb{S}^3$ parametrizes $\mathcal{R}_i \in \mathbb{SO}(3)$ then so does $-\mathbf{q}_i \in \mathbb{S}^3$, i.e., $\mathcal{R}_i = \bar{\mathcal{R}}_q(\mathbf{q}_i) = \bar{\mathcal{R}}_q(-\mathbf{q}_i)$.

3.3.6 Incomplete synchronization in $\mathbb{SO}(3)$ casted as synchronization in \mathbb{S}^2

In this section, we consider again a group of N agents operating in $\mathbb{SO}(3)$, but instead we wish to accomplish incomplete synchronized as explained and illustrated in Section 3.2.1. We note that, as explained in Section 3.2.1, incomplete synchronization is not necessarily accomplished if complete synchronization is accomplished.

Similarly to Section 3.3.5, for each $i \in \mathcal{N}$, $\boldsymbol{\omega}_i : \mathbb{R}_{\geq 0} \mapsto \mathbb{R}^3$ denotes the body-framed angular velocity of agent i , which can be actuated. Again, each rotation matrix $\mathcal{R}_i : \mathbb{R}_{\geq 0} \ni t \mapsto \mathcal{R}_i(t) \in \mathbb{SO}(3)$ evolves according to $\dot{\mathcal{R}}_i(t) = \mathbf{f}_{\mathcal{R}}(\mathcal{R}_i(t), \boldsymbol{\omega}_i(t))$ with $\mathbf{f}_{\mathcal{R}}$ as defined in (3.3.13). Consider that each agent $i \in \mathcal{N}$ has a body direction $\bar{\mathbf{n}}_i \in \mathbb{S}^2$ it wishes to synchronize with the other agents, and denote for convenience

$$\bar{\mathbf{n}} := (\bar{\mathbf{n}}_1, \dots, \bar{\mathbf{n}}_N) \in (\mathbb{S}^2)^N, \quad (3.3.23)$$

$$\mathcal{R} := (\mathcal{R}_1, \dots, \mathcal{R}_N) \in (\mathbb{SO}(3))^N, \quad (3.3.24)$$

$$\mathbf{n} := (\mathbf{n}_1, \dots, \mathbf{n}_N) := (\mathcal{R}_1 \bar{\mathbf{n}}_1, \dots, \mathcal{R}_N \bar{\mathbf{n}}_N) \in (\mathbb{S}^2)^N. \quad (3.3.25)$$

Thus, if we consider $\mathbf{n} = (\mathbf{n}_1, \dots, \mathbf{n}_N) : \mathbb{R}_{\geq 0} \ni t \mapsto \mathbf{n}(t) = (\mathbf{n}_1(t), \dots, \mathbf{n}_N(t)) = (\mathcal{R}_1(t) \bar{\mathbf{n}}_1, \dots, \mathcal{R}_N(t) \bar{\mathbf{n}}_N) \in (\mathbb{S}^2)^N$, it follows that, for each $i \in \{1, \dots, n\}$,

$$\dot{\mathbf{n}}_i(t) = \dot{\mathcal{R}}_i(t) \bar{\mathbf{n}}_i = \mathcal{S}(\mathcal{R}_i(t) \boldsymbol{\omega}_i(t)) \mathbf{n}_i(t) =: \mathbf{f}_n(\mathcal{R}(t), \boldsymbol{\omega}(t), \bar{\mathbf{n}}_i), \quad (3.3.26)$$

where $\mathbf{f}_n : \mathbb{SO}(3) \times \mathbb{R}^3 \times \mathbb{S}^2 \ni (\mathcal{R}_i, \boldsymbol{\omega}_i, \bar{\mathbf{n}}_i) \mapsto \mathbf{f}_n(\mathcal{R}_i, \boldsymbol{\omega}_i, \bar{\mathbf{n}}_i) \in T_{\mathcal{R}_i \bar{\mathbf{n}}_i} \mathbb{S}^2$ is given by

$$\mathbf{f}_n(\mathcal{R}_i, \boldsymbol{\omega}_i, \bar{\mathbf{n}}_i) := \mathbf{f}_R(\mathcal{R}_i, \boldsymbol{\omega}_i) \bar{\mathbf{n}}_i = \mathcal{S}(\mathcal{R}_i \boldsymbol{\omega}_i) \mathcal{R}_i \bar{\mathbf{n}}_i. \quad (3.3.27)$$

If, at a time instant $t \in \mathbb{R}_{\geq 0}$, agent $i \in \mathcal{N}$ is aware of the relative attitude between itself and another agent j , then $j \in \mathcal{N}_i(\sigma(t))$, where $\sigma(t)$ encodes the network graph at time instant t . Notice that agent $i \in \mathcal{N}$ is not aware of $\mathbf{n}_i(\cdot)$, since this is specified in an unknown inertial orientation frame; instead, it is aware of its direction $\bar{\mathbf{n}}_i$, fixed in its own orientation frame, and the attitude of its neighbors' own directions relative to its own orientation frame. Specifically, for each time instant $t \in \mathbb{R}_{\geq 0}$, each agent $i \in \mathcal{N}$ is equipped with the output function $\mathbf{h}_i(t, \cdot) : \mathbb{SO}(3)^N \ni \mathcal{R} \mapsto \mathbf{h}_i(t, \mathcal{R}) \in (\mathbb{S}^2)^{|\mathcal{N}_i(\sigma(t))|}$ defined as

$$\mathbf{h}_i(t, \mathcal{R}) := (\mathbf{h}_{ij_1}(\mathcal{R}), \dots, \mathbf{h}_{ij_{|\mathcal{N}_i(\sigma(t))|}}(\mathcal{R})) \in (\mathbb{S}^2)^{|\mathcal{N}_i(\sigma(t))|} \quad (3.3.28)$$

where

$$\mathbf{h}_{ij} : \mathbb{SO}(3)^N \ni (\mathcal{R}_1, \dots, \mathcal{R}_N) = \mathcal{R} \mapsto \mathbf{h}_{ij}(\mathcal{R}) := \mathcal{R}_i^T \mathcal{R}_j \bar{\mathbf{n}}_j = \mathcal{R}_i^T \mathbf{n}_j \in \mathbb{S}^2 \quad (3.3.29)$$

for each $j \in \mathcal{N}_i(\sigma(t))$ and where we have used the notation (3.3.25). Thus, at each time instant $t \in \mathbb{R}_{\geq 0}$, agent $i \in \mathcal{N}$ measures the $|\mathcal{N}_i(\sigma(t))|$ unit vectors corresponding to the projection of a neighbor's unit vector onto agent's i body frame.

At this point, we recall the notion of decentralized output feedback control law as defined in Section 3.2.2, which should made clear the previous definition of output function and the Problem statement presented next.

Problem 3.3.9. For each $i \in \mathcal{N}$, design time-varying decentralized feedback laws $\boldsymbol{\omega}_i^h$, with $\boldsymbol{\omega}_i^h(t, \cdot) : (\mathbb{S}^2)^{|\mathcal{N}_i(\sigma(t))|} \mapsto \mathbb{R}^3$ depending on the measurements $\mathbf{h}_i(t, \cdot)$ in (3.3.28) for each $t \geq 0$, such that asymptotic synchronization of $\mathbf{n} = (\mathcal{R}_1 \bar{\mathbf{n}}_1, \dots, \mathcal{R}_N \bar{\mathbf{n}}_N) : \mathbb{R}_{\geq 0} \mapsto (\mathbb{S}^2)^N$ is accomplished, where $\dot{\mathcal{R}}_i(t) = \mathbf{f}_R(\mathcal{R}_i(t), \boldsymbol{\omega}_i^h(t, \mathbf{h}_i(t, \mathcal{R}(t))))$ for every $i \in \mathcal{N}$.

Problem 3.3.9 may be restated as finding a control law for each agent that depends exclusively on the measurement function as defined in (3.3.28), and which encodes the partial state information available to each agent at a given time instant.

Definition 3.3.10. We define the angular displacement between two unit vectors $\theta : \mathbb{S}^2 \times \mathbb{S}^2 \ni (\mathbf{n}_i^T \mathbf{n}_j) \mapsto \theta(\mathbf{n}_i, \mathbf{n}_j) := \arccos(\mathbf{n}_i^T \mathbf{n}_j) \in [0, \pi]$.

For each $t \in \mathbb{R}_{\geq 0}$ and agent $i \in \mathcal{N}$, we propose the control law $\boldsymbol{\omega}_i^h(t, \cdot) : (\mathbb{S}^2)^{|\mathcal{N}_i(\sigma(t))|} \ni (\mathbf{h}_{ij_1}, \dots, \mathbf{h}_{ij_{|\mathcal{N}_i(\sigma(t))|}}) = \mathbf{h}_i \mapsto \boldsymbol{\omega}_i^{cl}(t, \mathbf{h}_i) \in T_{\bar{\mathbf{n}}_i} \mathbb{S}^2 \subset \mathbb{R}^3$ defined as

$$\boldsymbol{\omega}_i^{cl}(t, \mathbf{h}_i) := \sum_{j \in \mathcal{N}_i(\sigma(t))} w_{ij}(\theta(\bar{\mathbf{n}}_i, \mathbf{h}_{ij})) \mathcal{S}(\bar{\mathbf{n}}_i) \mathbf{h}_{ij}, \quad (3.3.30)$$

where $w_{ij} : [0, \pi] \mapsto \mathbb{R}_{\geq 0}$ is a continuous function satisfying

$$w_{ij}(\theta) > 0, \forall \theta \in (0, \pi], \quad (3.3.31)$$

and corresponding to a weight agent i assigns to the displacement between itself and its neighbor j . Denote $\omega_i^{cl} : \mathbb{R}_{\geq 0} \times \mathbb{SO}(3)^N \ni (t, \mathcal{R}) \mapsto \omega_i^{cl}(t, \mathcal{R}) := \omega_i^h(t, \mathbf{h}_i(t, \mathcal{R})) \in \mathbb{R}^3$ as the composition of the output feedback control law (3.3.30) with the output function (3.3.28). It follows that

$$\omega_i^{cl}(t, \mathcal{R}) = \sum_{j \in \mathcal{N}_i(\sigma(t))} w_{ij}(\theta(\bar{\mathbf{n}}_i, \mathcal{R}_i^T \mathcal{R}_j \bar{\mathbf{n}}_j)) \mathcal{S}(\bar{\mathbf{n}}_i) \mathcal{R}_i \mathcal{R}_j \bar{\mathbf{n}}_j \quad (3.3.32)$$

$$= \mathcal{R}_i^T \sum_{j \in \mathcal{N}_i(\sigma(t))} w_{ij}(\theta(\mathbf{n}_i, \mathbf{n}_j)) \mathcal{S}(\mathbf{n}_i) \mathbf{n}_j, \quad (3.3.33)$$

where we have used the notation in (3.3.24) and (3.3.25); and where we have made use of the fact that $\theta(\mathbf{n}_i, \mathbf{n}_j) = \theta(\mathcal{R}_i^T \mathbf{n}_i, \mathcal{R}_i^T \mathbf{n}_j)$ for any $\mathcal{R}_i \in \mathbb{SO}(3)$ and any $\mathbf{n}_i, \mathbf{n}_j \in \mathbb{S}^2$. We emphasize that the control law (3.3.33) is based on the output feedback control law, and thus depends only on the relative orientation measurements (see (3.3.28) and (3.3.29)); moreover, (3.3.33) is orthogonal to $\bar{\mathbf{n}}_i$, which implies that full angular velocity control is not necessary, i.e. we only need to control the angular velocity along the two directions orthogonal to $\bar{\mathbf{n}}_i$.

Denote $\tilde{w}_{ij}(\mathbf{n}_i, \mathbf{n}_j) = w_{ij}(\theta(\mathbf{n}_i, \mathbf{n}_j))$, which satisfies (3.3.11) for any $\alpha \in [0, \pi]$ and $\tilde{\nu} \in \mathbb{S}^2$, due to (3.3.31) and Definition 3.3.10. With the above in mind, the dynamics (3.3.27), when composed with the proposed law (3.3.33), are given by $\dot{\mathbf{n}}_i(t) = \tilde{\mathbf{f}}_{i,\sigma(t)}(\mathbf{n}(t))$, where $\tilde{\mathbf{f}}_{i,\sigma(t)} : (\mathbb{S}^2)^N \ni (\mathbf{n}_1, \dots, \mathbf{n}_N) = \mathbf{n} \mapsto \tilde{\mathbf{f}}_{i,\sigma(t)}(\mathbf{n}) \in T_{\mathbf{n}_i} \mathbb{S}^2$ is given by

$$\begin{aligned} \tilde{\mathbf{f}}_{i,\sigma(t)}(\mathbf{n}) &:= \mathbf{f}_n(\mathcal{R}_i, \omega_i^{cl}(t, \mathcal{R}), \bar{\mathbf{n}}_i) \\ &= \mathcal{S}(\mathcal{R}_i \omega_i^{cl}(t, \mathcal{R})) \mathcal{R}_i \bar{\mathbf{n}}_i \\ &= -\mathcal{S}(\mathbf{n}_i) \mathcal{R}_i \omega_i^{cl}(t, \mathcal{R}) \\ &= \sum_{j \in \mathcal{N}_i(\sigma(t))} \tilde{w}_{ij}(\mathbf{n}_i, \mathbf{n}_j) \Pi(\mathbf{n}_i) \mathbf{n}_j, \end{aligned} \quad (3.3.34)$$

where we have used the notation in (3.3.24) and (3.3.25). We have thus casted this problem in the form (3.3.9)-(3.3.10) with $\nu \equiv \mathbf{n} \in (\mathbb{S}^2)^N$.

3.3.7 Consensus in \mathbb{R}^n casted as synchronization in \mathbb{S}^n

As stated in Section 3.3.4, consensus in \mathbb{R}^n can also be casted as a synchronization problem in \mathbb{S}^n , for any $n \in \mathbb{N}$. Consider $\mathbf{x} = (\mathbf{x}_1, \dots, \mathbf{x}_N) : \mathbb{R}_{\geq 0} \ni t \mapsto \mathbf{x}(t) = (\mathbf{x}_1(t), \dots, \mathbf{x}_N(t)) \in (\mathbb{R}^n)^N$, evolving according to $\dot{\mathbf{x}}_i(t) = \mathbf{f}_x(\mathbf{x}(t))$ for every $i \in \mathcal{N}$, where $\mathbf{f}_x : (\mathbb{R}^n)^N \ni (\mathbf{x}_1, \dots, \mathbf{x}_N) = \mathbf{x} \mapsto \mathbf{f}_x(\mathbf{x}) \in \mathbb{R}^n$ is given by

$$\mathbf{f}_x(\mathbf{x}) := \sum_{j \in \mathcal{N}_i(\sigma(t))} w_{ij}(\|\mathbf{x}_j - \mathbf{x}_i\|)(\mathbf{x}_j - \mathbf{x}_i), \quad (3.3.35)$$

and which is the dynamics of one agent in consensus [98], and which is not in the form (3.3.10). In order to write the closed loop dynamics (3.3.35) as in (3.3.10), we perform a transformation which is discussed next.

In order to analyze consensus in \mathbb{R}^n under the same framework as synchronization in \mathbb{S}^2 and $\mathbb{SO}(3)$, we now perform a change of variables that serves only the purpose

of analysis. Consider the unit vector $\mathbf{e}_{n+1} = (\mathbf{0}_n, 1) \in \mathbb{S}^n \subset \mathbb{R}^{n+1}$ and the matrix $P = [\mathbf{I}_n \ \mathbf{0}_n]^T \in \mathbb{R}^{(n+1) \times n}$. Consider also the mapping

$$\mathbf{h} : \mathbb{R}^n \ni \mathbf{x}_i \mapsto \mathbf{h}(\mathbf{x}_i) = \frac{P\mathbf{x}_i + \mathbf{e}_{n+1}}{\|P\mathbf{x}_i + \mathbf{e}_{n+1}\|} \in \mathcal{C}\left(\frac{\pi}{2}, \mathbf{e}_{n+1}\right) \subset \mathbb{S}^n \subset \mathbb{R}^{n+1}, \quad (3.3.36)$$

where $\|P\mathbf{x}_i + \mathbf{e}_{n+1}\| = \sqrt{1 + \mathbf{x}_i^T \mathbf{x}_i} \geq 1 > 0$ for all $\mathbf{x}_i \in \mathbb{R}^n$. This transformation is illustrated in Fig. 3.7. Notice that \mathbf{h} is, in fact, a diffeomorphism between \mathbb{R}^n and $\mathcal{C}\left(\frac{\pi}{2}, \mathbf{e}_{n+1}\right)$, with $\mathbf{h}^{-1} : \mathcal{C}\left(\frac{\pi}{2}, \mathbf{e}_{n+1}\right) \ni \mathbf{z}_i \mapsto \mathbf{h}^{-1}(\mathbf{z}_i) = P^T \left(\frac{1}{\mathbf{z}_i^T \mathbf{e}_{n+1}} \mathbf{z}_i - \mathbf{e}_{n+1} \right) \in \mathbb{R}^n$. Denote then $\mathbf{H}(\mathbf{x}) = (\mathbf{h}(\mathbf{x}_1), \dots, \mathbf{h}(\mathbf{x}_N))$ for $\mathbf{x} = (\mathbf{x}_1, \dots, \mathbf{x}_N) \in (\mathbb{R}^n)^N$ and $\mathbf{H}^{-1}(\mathbf{z}) = (\mathbf{h}^{-1}(\mathbf{z}_1), \dots, \mathbf{h}^{-1}(\mathbf{z}_N))$ for $\mathbf{z} = (\mathbf{z}_1, \dots, \mathbf{z}_N) \in \mathcal{C}\left(\frac{\pi}{2}, \mathbf{e}_{n+1}\right)^N$.

Let $\mathbf{x} = (\mathbf{x}_1, \dots, \mathbf{x}_N) \in (\mathbb{R}^n)^N$ and $\mathbf{z} = (\mathbf{z}_1, \dots, \mathbf{z}_N) \in \mathcal{C}\left(\frac{\pi}{2}, \mathbf{e}_{n+1}\right)^N$ where $\mathbf{z} = \mathbf{H}(\mathbf{x}) \Leftrightarrow \mathbf{x} = \mathbf{H}^{-1}(\mathbf{z})$. It holds that

$$\begin{aligned} d\mathbf{h}(\mathbf{x}_i) \mathbf{f}_x(\mathbf{u}_i^{cl,x}(t, \mathbf{x}))|_{\mathbf{x}=\mathbf{H}^{-1}(\mathbf{z})} &= \\ &= \sum_{j \in \mathcal{N}_i(\sigma(t))} \frac{\mathbf{e}_{n+1}^T \mathbf{z}_i}{\mathbf{e}_{n+1}^T \mathbf{z}_j} w_{ij} \left(\left\| \frac{\mathbf{z}_j}{\mathbf{e}_{n+1}^T \mathbf{z}_j} - \frac{\mathbf{z}_i}{\mathbf{e}_{n+1}^T \mathbf{z}_i} \right\| \right) \Pi(\mathbf{z}_i) \mathbf{z}_j \end{aligned} \quad (3.3.37)$$

$$=: \sum_{j \in \mathcal{N}_i(\sigma(t))} \tilde{w}_{ij}(\mathbf{z}_i, \mathbf{z}_j) \Pi(\mathbf{z}_i) \mathbf{z}_j, \quad (3.3.38)$$

where, in the last step, we defined $\tilde{w}_{ij}(\mathbf{z}_i, \mathbf{z}_j) := \frac{\mathbf{z}_i^T \mathbf{e}_{n+1}}{\mathbf{z}_j^T \mathbf{e}_{n+1}} w_{ij} \left(\left\| \frac{\mathbf{z}_j}{\mathbf{z}_j^T \mathbf{e}_{n+1}} - \frac{\mathbf{z}_i}{\mathbf{z}_i^T \mathbf{e}_{n+1}} \right\| \right)$, which satisfies (3.3.11) for $\alpha = \frac{\pi}{2}$ and for $\bar{\nu} = \mathbf{e}_{n+1} \in \mathbb{S}^n$. Details of the previous derivations are found in [111].

Consider then $\mathbf{x} = (\mathbf{x}_1, \dots, \mathbf{x}_N) : \mathbb{R}_{\geq 0} \ni t \mapsto \mathbf{x}(t) \in (\mathbb{R}^n)^N$ where $\mathbf{x}_i(\cdot)$ evolves according to (3.3.35) for each $i \in \mathcal{N}$. Then, if we consider $\mathbf{z} = (\mathbf{z}_1, \dots, \mathbf{z}_N) : \mathbb{R}_{\geq 0} \ni t \mapsto \mathbf{z}(t) := \mathbf{H}(\mathbf{x}(t)) \in \mathcal{C}\left(\frac{\pi}{2}, \mathbf{e}_{n+1}\right)^N$, it follows from (3.3.38) that $\dot{\mathbf{z}}_i(t) = \tilde{\mathbf{f}}_{i,\sigma(t)}(\mathbf{z}(t))$, where $\tilde{\mathbf{f}}_{i,\sigma(t)} : (\mathbb{S}^n)^N \ni (\mathbf{z}_1, \dots, \mathbf{z}_N) = \mathbf{z} \mapsto \tilde{\mathbf{f}}_{i,\sigma(t)}(\mathbf{z}) \in T_{\mathbf{z}_i} \mathbb{S}^n$ is given by

$$\tilde{\mathbf{f}}_{i,\sigma(t)}(\mathbf{z}) = \sum_{j \in \mathcal{N}_i(\sigma(t))} \tilde{w}_{ij}(\mathbf{z}_i, \mathbf{z}_j) \Pi(\mathbf{z}_i) \mathbf{z}_j. \quad (3.3.39)$$

We have thus casted this problem in the form (3.3.9) with $\boldsymbol{\nu} \equiv \mathbf{z} \in (\mathbb{S}^n)^N$.

Remark 3.3.11. Unlike synchronization in \mathbb{S}^2 and $\mathbb{SO}(3)$, the unit vectors in this section are by construction contained in a $\frac{\pi}{2}$ -cone formed by the unit vector \mathbf{e}_{n+1} (see the co-domain of \mathbf{h} in (3.3.36)). Also, note that \mathbf{h} in (3.3.36) may be defined with other vectors other than \mathbf{e}_{n+1} , i.e., $\mathbf{h}(\mathbf{x}_i) = \frac{P\mathbf{x}_i + \tilde{\mathbf{e}}}{\|P\mathbf{x}_i + \tilde{\mathbf{e}}\|}$ with some $\tilde{\mathbf{e}} \in \mathbb{S}^n$ satisfying $\mathbf{e}_{n+1}^T \tilde{\mathbf{e}} \neq 0$ also works as an alternative transformation.

3.3.8 Analysis

In this section, we analyze the solutions of (3.3.9)-(3.3.10), and show that given a wide set of initial conditions, asymptotic synchronization is guaranteed. Specifically, asymptotic synchronization is guaranteed if all unit vectors are initially contained in an open α^* -cone, i.e. if $\exists \bar{\nu} \in \mathbb{S}^n : \boldsymbol{\nu}(0) \in \mathcal{C}(\alpha^*, \bar{\nu})^N$, where $\alpha^* = \frac{\pi}{2}$ for synchronization in \mathbb{S}^2 and consensus in \mathbb{R}^n , and $\alpha^* = \frac{\pi}{4}$ for synchronization in $\mathbb{SO}(3)$.

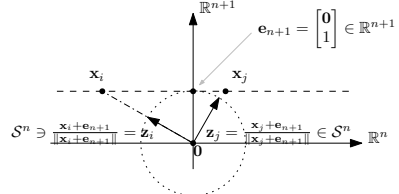


Figure 3.7: Casting consensus in \mathbb{R}^n as synchronization in \mathbb{S}^n .

Remark 3.3.12. If $\nu(0) \in \mathcal{C}(\alpha, \bar{\nu})^N$ for some $\alpha \in [0, \alpha^*)$ and some $\bar{\nu} \in \mathbb{S}^n$, then Proposition 3.3.20 in Subsection 3.3.10 guarantees that there exist $n+1$ linearly independent unit vectors $\{\bar{\nu}_k \in \mathbb{S}^n\}_{k \in \{1, \dots, n+1\}}$ such $\nu(0) \in \mathcal{C}(\alpha^*, \bar{\nu}_k)^N \forall k \in \{1, \dots, n+1\}$. Thus, if $\nu(0)$ is contained in an open α cone, then there exist other bigger cones that contain $\nu(0)$; as such, the choice of $\bar{\nu}$ is not unique.

Next, we introduce a coordinate transformation that we exploit in order to cast the dynamics (3.3.10) into a form that satisfies the conditions of Theorem 3.3.1. In particular, given some $\bar{\nu} \in \mathbb{S}^2$ we consider the projection of the cone $\mathcal{C}(\frac{\pi}{2}, \bar{\nu})$ to the plane in \mathbb{R}^{n+1} orthogonal to $\bar{\nu}$ and containing zero, and then map this plane isometrically to \mathbb{R}^n .

Definition 3.3.13. Let $\bar{\nu} \in \mathbb{S}^n$ and $Q_\nu \in \mathbb{R}^{(n+1) \times n}$ such that $\bar{\nu}$ and the columns of Q_ν form an orthonormal basis of \mathbb{R}^{n+1} , and consider the diffeomorphism $\mathbf{h}_\nu : \mathcal{C}(\frac{\pi}{2}, \bar{\nu}) \ni \nu_i \mapsto \mathbf{h}_\nu(\nu_i) \in \mathcal{B}(1)$ (see Notation for the definition of $\mathcal{B}(\cdot)$), defined as

$$\mathbf{h}_\nu(\nu_i) := Q_\nu^T \nu_i. \quad (3.3.40)$$

Its inverse is $\mathbf{h}_\nu^{-1} : \mathcal{B}(1) \ni \mathbf{x}_i \mapsto \mathbf{h}_\nu^{-1}(\mathbf{x}_i) = \sqrt{1 - \|\mathbf{x}_i\|^2} \bar{\nu} + Q_\nu \mathbf{x}_i \in \mathcal{C}(\frac{\pi}{2}, \bar{\nu})$. Denote also $\mathbf{H}_\nu : \mathcal{C}(\frac{\pi}{2}, \bar{\nu})^N \ni (\nu_1, \dots, \nu_N) = \nu \mapsto \mathbf{H}_\nu(\nu) \in \mathcal{B}(1)^N$, defined as $\mathbf{H}_\nu(\nu) := (\mathbf{h}_\nu(\nu_1), \dots, \mathbf{h}_\nu(\nu_N))$, with \mathbf{H}_ν^{-1} defined similarly.

Figure 3.8 illustrates the mapping \mathbf{h}_ν as introduced in Definition 3.3.13, for $n=2$ and $N=3$: in the figure, $\mathbf{x}_i = \mathbf{h}_\nu(\nu_i) \stackrel{(3.3.40)}{=} Q_\nu^T \nu_i$, and green lines are those spanned by the columns of Q_ν (which form a plane).

Proposition 3.3.14. Consider $\bar{\nu} \in \mathbb{S}^n$ and $\nu_i, \nu_j \in \mathcal{C}(\frac{\pi}{2}, \bar{\nu})$. Then, $\bar{\nu}^T \nu = \sqrt{1 - \|\mathbf{h}_\nu(\nu)\|^2} > 0$ and the following implications hold: $\|\mathbf{h}_\nu(\nu_i)\| > \|\mathbf{h}_\nu(\nu_j)\| \Leftrightarrow 0 < \bar{\nu}^T \nu_i < \bar{\nu}^T \nu_j$, and $\|\mathbf{h}_\nu(\nu_i)\| \geq \|\mathbf{h}_\nu(\nu_j)\| \Leftrightarrow 0 < \bar{\nu}^T \nu_i \leq \bar{\nu}^T \nu_j$.

Proof. Since $\mathbf{h}_\nu(\nu) = Q_\nu \nu$, then $\|\mathbf{h}_\nu(\nu)\|^2 = \nu^T Q_\nu Q_\nu^T \nu = \nu^T \Pi(\bar{\nu}) \nu = 1 - (\bar{\nu}^T \nu)^2$ (notice that $Q_\nu Q_\nu^T = \Pi(\bar{\nu})$). Since $\bar{\nu}^T \nu > 0$, for any $\nu \in \mathcal{C}(\frac{\pi}{2}, \bar{\nu})$, it follows that $\bar{\nu}^T \nu = \sqrt{1 - \|\mathbf{h}_\nu(\nu)\|^2}$. The implications in the Proposition follow since $\bar{\nu}^T \nu = \sqrt{1 - \|\mathbf{h}_\nu(\nu)\|^2}$ is decreasing with $\|\mathbf{h}_\nu(\nu)\|$, and since $\nu_i, \nu_j \in \mathcal{C}(\frac{\pi}{2}, \bar{\nu})$. \square

Consider now the solution $\nu : \mathbb{R}_{\geq 0} \mapsto (\mathbb{S}^n)^N$ of (3.3.9)-(3.3.10) with $\nu(0) \in \mathcal{C}(\frac{\pi}{2}, \bar{\nu})^N$ for some $\bar{\nu} \in \mathbb{S}^n$, which, as will be shown in Theorem 3.3.17, remains in

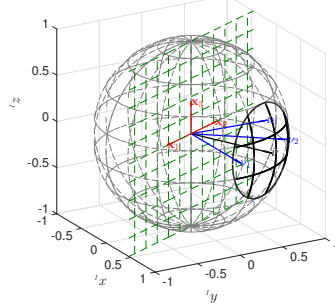


Figure 3.8: Illustration of diffeomorphism as in Definition (3.3.13)

$\mathcal{C}(\frac{\pi}{2}, \bar{\nu})^N$ for all $t \geq 0$; and define $\mathbf{x} : \mathbb{R}_{\geq 0} \mapsto (\mathbb{R}^n)^N$ as $\mathbf{x}(t) = \mathbf{H}_\nu(\boldsymbol{\nu}(t))$. Then, based on the transformation introduced in Definition 3.3.13, it follows that $\dot{\mathbf{x}}(t) = \mathbf{f}_{\sigma(t)}(\mathbf{x}(t))$, where

$$\mathbf{f}_{\sigma(t)}(\mathbf{x}) = d\mathbf{H}_\nu(\boldsymbol{\nu})\tilde{\mathbf{f}}_{\sigma(t)}(\boldsymbol{\nu})|_{\boldsymbol{\nu}=\mathbf{H}_\nu^{-1}(\mathbf{x})}, \quad (3.3.41)$$

and $\dot{\mathbf{x}}_i(t) = \mathbf{h}_\nu(\boldsymbol{\nu}_i(t))$ evolves according to $\dot{\mathbf{x}}_i(t) = \mathbf{f}_{i,\sigma(t)}(\mathbf{x}(t))$, where

$$\begin{aligned} \mathbf{f}_{i,\sigma(t)}(\mathbf{x}) &= d\mathbf{h}_\nu(\boldsymbol{\nu}_i)\tilde{\mathbf{f}}_{\sigma(t)}(\boldsymbol{\nu})|_{\boldsymbol{\nu}=\mathbf{H}_\nu^{-1}(\mathbf{x})} \\ &= Q_\nu^T \sum_{j \in \mathcal{N}_i(\sigma(t))} \tilde{w}_{ij}(\boldsymbol{\nu}_i, \boldsymbol{\nu}_j) \Pi(\boldsymbol{\nu}_i) \boldsymbol{\nu}_j |_{\boldsymbol{\nu}=\mathbf{H}_\nu^{-1}(\mathbf{x})}. \end{aligned} \quad (3.3.42)$$

It follows from (3.3.42) that, for $\boldsymbol{\nu} \in \mathcal{C}(\frac{\pi}{2}, \bar{\nu})^N$ with $\bar{\nu} \in \mathbb{S}^n$, $\mathbf{x} = \mathbf{H}_\nu(\boldsymbol{\nu}) \in \mathcal{B}(1)^N$ and any $p \in \mathcal{P}$,

$$\begin{aligned} \mathbf{x}_i^T \mathbf{f}_{i,p}(\mathbf{x}) &\stackrel{(3.3.42)}{=} \boldsymbol{\nu}_i^T Q_\nu Q_\nu^T \sum_{j \in \mathcal{N}_i(p)} \tilde{w}_{ij}(\boldsymbol{\nu}_i, \boldsymbol{\nu}_j) \Pi(\boldsymbol{\nu}_i) \boldsymbol{\nu}_j \\ &= \boldsymbol{\nu}_i^T \Pi(\bar{\nu}) \sum_{j \in \mathcal{N}_i(p)} \tilde{w}_{ij}(\boldsymbol{\nu}_i, \boldsymbol{\nu}_j) \Pi(\boldsymbol{\nu}_i) \boldsymbol{\nu}_j \\ &= (\boldsymbol{\nu}_i^T - (\boldsymbol{\nu}_i^T \bar{\nu}) \bar{\nu}^T) \sum_{j \in \mathcal{N}_i(p)} \tilde{w}_{ij}(\boldsymbol{\nu}_i, \boldsymbol{\nu}_j) \Pi(\boldsymbol{\nu}_i) \boldsymbol{\nu}_j \\ &= -\bar{\nu}^T \boldsymbol{\nu}_i \sum_{j \in \mathcal{N}_i(p)} \tilde{w}_{ij}(\boldsymbol{\nu}_i, \boldsymbol{\nu}_j) \bar{\nu}^T \Pi(\boldsymbol{\nu}_i) \boldsymbol{\nu}_j. \end{aligned} \quad (3.3.43)$$

The following result provides certain properties that are exploited in determining the sign of (3.3.43).

Proposition 3.3.15. Consider three unit vectors $\boldsymbol{\nu}_1, \boldsymbol{\nu}_2, \bar{\nu} \in \mathbb{S}^n$, satisfying $0 < \bar{\nu}^T \boldsymbol{\nu}_1 \leq \bar{\nu}^T \boldsymbol{\nu}_2$. Then (a) $\bar{\nu}^T \Pi(\boldsymbol{\nu}_1) \boldsymbol{\nu}_2 = 0$ iff $\boldsymbol{\nu}_1 = \boldsymbol{\nu}_2$, and (b) $\bar{\nu}^T \Pi(\boldsymbol{\nu}_1) \boldsymbol{\nu}_2 > 0$ iff $\boldsymbol{\nu}_2 \neq \boldsymbol{\nu}_1$.

Proof. Sufficiency: Regarding (a), if $\boldsymbol{\nu}_2 = \boldsymbol{\nu}_1$, then $\bar{\nu}^T \Pi(\boldsymbol{\nu}_1) \boldsymbol{\nu}_2 = \bar{\nu}^T \Pi(\boldsymbol{\nu}_1) \boldsymbol{\nu}_1 = 0$. Regarding (b), if $\boldsymbol{\nu}_1 \neq \boldsymbol{\nu}_2$ then $\boldsymbol{\nu}_1^T \boldsymbol{\nu}_2 < 1$. Consider then the following two cases: (1) $\bar{\nu}^T \boldsymbol{\nu}_1 = \bar{\nu}^T \boldsymbol{\nu}_2$ and (2) $\bar{\nu}^T \boldsymbol{\nu}_1 \neq \bar{\nu}^T \boldsymbol{\nu}_2$. For case (1), it follows that $\bar{\nu}^T \Pi(\boldsymbol{\nu}_1) \boldsymbol{\nu}_2 = \bar{\nu}^T \boldsymbol{\nu}_2 - \bar{\nu}^T \boldsymbol{\nu}_1 \boldsymbol{\nu}_1^T \boldsymbol{\nu}_2 = \bar{\nu}^T \boldsymbol{\nu}_1 (1 - \boldsymbol{\nu}_1^T \boldsymbol{\nu}_2) > 0$, where the inequality applies since $\boldsymbol{\nu}_1^T \boldsymbol{\nu}_2 < 1$ and

since, by assumption $0 < \bar{\nu}^T \boldsymbol{\nu}_1$. For case (2), the Proposition's assumption becomes $0 < \bar{\nu}^T \boldsymbol{\nu}_1 < \bar{\nu}^T \boldsymbol{\nu}_2$. Then, since $\boldsymbol{\nu}_1^T \boldsymbol{\nu}_2 < 1$, it follows that $0 < \bar{\nu}^T \boldsymbol{\nu}_1 < \bar{\nu}^T \boldsymbol{\nu}_1 \boldsymbol{\nu}_1^T \boldsymbol{\nu}_2 \Rightarrow \bar{\nu}^T \Pi(\boldsymbol{\nu}_1) \boldsymbol{\nu}_2 > 0$. *Necessity:* Regarding (a), if we assume on the contrary that $\boldsymbol{\nu}_1 \neq \boldsymbol{\nu}_2$, then it follows from before that $\bar{\nu}^T \Pi(\boldsymbol{\nu}_1) \boldsymbol{\nu}_2 = \bar{\nu}^T \boldsymbol{\nu}_2 - \bar{\nu}^T \boldsymbol{\nu}_1 \boldsymbol{\nu}_1^T \boldsymbol{\nu}_2 > 0$, which implies that $\boldsymbol{\nu}_1 = \boldsymbol{\nu}_2$. Similarly, regarding (b), if we assume on the contrary that $\boldsymbol{\nu}_1 = \boldsymbol{\nu}_2$, then it follows from before that $\bar{\nu}^T \Pi(\boldsymbol{\nu}_1) \boldsymbol{\nu}_2 = \bar{\nu}^T \Pi(\boldsymbol{\nu}_1) \boldsymbol{\nu}_1 = 0$, which implies that $\boldsymbol{\nu}_1 \neq \boldsymbol{\nu}_2$. \square

We show next, by combining Propositions 3.3.14 and 3.3.15 and exploiting (3.3.43), that the conditions of Theorem 3.3.1 are satisfied for the dynamics (3.3.41)-(3.3.42).

Proposition 3.3.16. *Consider the vector field as defined in (3.3.41)-(3.3.42) for certain $\bar{\nu} \in \mathbb{S}^n$ and assume that the switching signal $\sigma : \mathbb{R}_{\geq 0} \mapsto \{1, \dots, p\}$ encodes only connected network graphs. Then the vector field (3.3.41)-(3.3.42) satisfies the conditions of Theorem 3.3.1 for $r = 1$.*

Proof. In order to verify that the conditions of Theorem 3.3.1 are satisfied by the vector field in (3.3.41)-(3.3.42), we exploit (3.3.43) and the fact that for each $\mathbf{x} = (\mathbf{x}_1, \dots, \mathbf{x}_N) \in \mathcal{B}(1)^N$ there exists a (unique) $\boldsymbol{\nu} = (\boldsymbol{\nu}_1, \dots, \boldsymbol{\nu}_N) \in \mathcal{C}(\alpha^*, \bar{\nu})^N$ such that $\mathbf{x} = \mathbf{H}(\boldsymbol{\nu})$. We proceed with the verification of Condition 1) of Theorem 3.3.1 and pick $\mathbf{x} \in \mathcal{B}(1)^N$, where $\mathbf{x} = \mathbf{H}(\boldsymbol{\nu})$ for certain $\boldsymbol{\nu} \in \mathcal{C}(\alpha^*, \bar{\nu})^N$. Notice, that since $\boldsymbol{\nu} \in \mathcal{C}(\alpha^*, \bar{\nu})^N$, it holds by definition that $\bar{\nu}^T \boldsymbol{\nu}_i > \cos(\alpha^*) \geq 0 \forall i \in \mathcal{N}$. Therefore, since Condition 1)a) depends exclusively on the sign of (3.3.43), we can ignore the effect of the positive term $\bar{\nu}^T \boldsymbol{\nu}_i$.

In order to show Condition 1)a), pick any $p \in \mathcal{P}$ and notice, that due to (3.3.11) and continuity of $\tilde{w}_{ij}(\cdot, \cdot)$ it holds $\tilde{w}_{ij}(\boldsymbol{\nu}_i, \boldsymbol{\nu}_j) \geq 0$ for any $\boldsymbol{\nu}_i, \boldsymbol{\nu}_j \in \mathcal{C}(\alpha^*, \bar{\nu})$ and $i, j \in \mathcal{N}$. In addition, by recalling that $\mathcal{H}(\mathbf{x}) = \{i \in \mathcal{N} : i = \arg \max_{j \in \mathcal{N}} \|\mathbf{x}_j\|\}$ and thus, that $\|\mathbf{x}_i\| \geq \|\mathbf{x}_j\|$ for all $j \in \mathcal{N} \setminus \{i\}$, it follows from Proposition 3.3.14 that $\bar{\nu}^T \boldsymbol{\nu}_i \leq \bar{\nu}^T \boldsymbol{\nu}_j$ for all $j \in \mathcal{N} \setminus \{i\}$. From the latter and the result of Proposition 3.3.15, we get that $\bar{\nu}^T \Pi(\boldsymbol{\nu}_i) \boldsymbol{\nu}_j \geq 0$ for all $j \in \mathcal{N}(p)$. Thus, we conclude from (3.3.43) that for any $p \in \mathcal{P}$ and $\mathbf{x} \in \mathcal{B}(1)^N$ it holds $\mathbf{x}_i^T \mathbf{f}_{i,p}(\mathbf{x}) \leq 0$, which by virtue of (3.3.3) implies that Condition 1)a) is satisfied.

For the verification of Condition 1)b), we additionally assume that $\mathbf{x} \notin \mathcal{C}$, where $\mathcal{C} = \{\mathbf{x} \in (\mathbb{R}^n)^N : \mathbf{x}_1 = \dots = \mathbf{x}_N\}$. We will show that for each $p \in \mathcal{P}$ there exists $k \in \mathcal{H}(\mathbf{x})$ such that $\mathbf{x}_k^T \mathbf{f}_{k,p}(\mathbf{x}) < 0$. Indeed, suppose on the contrary that there exists $p \in \mathcal{P}$ such that

$$\mathbf{x}_i^T \mathbf{f}_{i,p}(\mathbf{x}) = 0 \quad \forall i \in \mathcal{H}(\mathbf{x}), \quad (3.3.44)$$

and recall that the agents' network is not synchronized, since $\mathbf{x} \notin \mathcal{C}$. Consider then an $l \in \mathcal{H}(\mathbf{x})$, for which $\mathbf{x}_l^T \mathbf{f}_{l,p}(\mathbf{x}) = 0$ according to assumption (3.3.44). Notice also, that due to (3.3.11), Propositions 3.3.14, 3.3.15 and (3.3.43), it can be shown (as in the proof of Condition 1)a) above) that $\mathbf{x}_l^T \mathbf{f}_{l,p}(\mathbf{x}) = 0$ is satisfied only if all neighbors of agent l are synchronized with agent l , i.e., only if $\boldsymbol{\nu}_j = \boldsymbol{\nu}_l \Leftrightarrow \mathbf{x}_j = \mathbf{x}_l$ for all $j \in \mathcal{N}_l(p)$. This implies that all $j \in \mathcal{N}_l(p)$ are contained in $\mathcal{H}(\mathbf{x})$, i.e., $\mathcal{N}_l(p) \cup \{l\} \subseteq \mathcal{H}(\mathbf{x})$. As

such, by assumption (3.3.44), $\mathbf{x}_j^T \mathbf{f}_{j,p}(\mathbf{x}) = 0$ for all $j \in \mathcal{N}_l(p)$, which means that the previous rationale is applicable for all $j \in \mathcal{N}_l(p)$, thus leading to the conclusion that all neighbors of all neighbors of agent l are necessarily synchronized with each other. Since the graph encoded by $p \in \mathcal{P}$ is connected, the previous rationale, applied $N - 1$ times, leads to the conclusion that all agents are synchronized. Since $\mathbf{x} \notin \mathcal{C}$, a contradiction has been reached, and therefore, for each $p \in \mathcal{P}$, there exists a $k \in \mathcal{H}(\mathbf{x})$ for which $\mathbf{x}_k^T \mathbf{f}_{k,p}(\mathbf{x}) < 0$, and therefore condition 1)b) of Theorem 3.3.1 is satisfied.

Finally, let $\mathbf{x} = (\mathbf{x}_1, \dots, \mathbf{x}_N) \in \mathcal{C}$. Since $\mathbf{x}_1 = \dots = \mathbf{x}_N \Leftrightarrow \boldsymbol{\nu}_1 = \dots = \boldsymbol{\nu}_N$, it follows from Proposition 3.3.15 that $\mathbf{x}_i^T \mathbf{f}_p(\mathbf{x}) = \mathbf{0}$ for all $p \in \mathcal{P}$. Thus, the second condition of Theorem 3.3.1 is also satisfied. \square

Theorem 3.3.17. *Consider the solution $\boldsymbol{\nu} : \mathbb{R}_{\geq 0} \mapsto (\mathbb{S}^n)^N$ of (3.3.9) with $\boldsymbol{\nu}(0) \in \mathcal{C}(\alpha^*, \bar{\boldsymbol{\nu}})^N$ for some $\bar{\boldsymbol{\nu}} \in \mathbb{S}^n$. Then, for a network graph connected at all times, i) $\boldsymbol{\nu}(t) \in \bar{\mathcal{C}}(\alpha, \bar{\boldsymbol{\nu}})^N$ for all $t \geq 0$, where $\alpha = \arccos(\max_{i \in \mathcal{N}} \bar{\boldsymbol{\nu}}^T \boldsymbol{\nu}_i(0)) \in [0, \alpha^*]$; ii) $\boldsymbol{\nu}(\cdot)$ synchronizes asymptotically and $\lim_{t \rightarrow \infty} \bar{\boldsymbol{\nu}} \boldsymbol{\nu}_i(t)$ exists for all $i \in \mathcal{N}$; and iii) all unit vectors converge to a constant unit vector, i.e. $\exists \boldsymbol{\nu}^* \in \mathbb{S}^n : \lim_{t \rightarrow \infty} \boldsymbol{\nu}(t) \in \mathcal{C}(0, \boldsymbol{\nu}^*)^N$.*

Proof. Consider a solution $\boldsymbol{\nu}(\cdot)$ of (3.3.9), and $\mathbf{x}(\cdot) = \mathbf{H}_{\bar{\boldsymbol{\nu}}}(\boldsymbol{\nu}(\cdot))$. Since α^* is either $\frac{\pi}{2}$ or $\frac{\pi}{4}$, then $\boldsymbol{\nu}(0)$ is within the domain of $\mathbf{H}_{\bar{\boldsymbol{\nu}}}(\cdot)$ and moreover $\bar{\mathcal{B}}(r_0)^N \subset \mathcal{B}(1)^N$ where $r_0 \stackrel{(3.3.40)}{=} \max_{i \in \mathcal{N}} \|Q_{\bar{\boldsymbol{\nu}}}^T \boldsymbol{\nu}_i(0)\| \stackrel{\text{Prop 3.3.14}}{=} \sqrt{1 - \max_{i \in \mathcal{N}} (\bar{\boldsymbol{\nu}}^T \boldsymbol{\nu}_i(0))^2} < 1$ (where the latter inequality follows from the fact that $\boldsymbol{\nu}(0) \in \mathcal{C}(\alpha^*, \bar{\boldsymbol{\nu}})^N$). From Proposition 3.3.16, the dynamics (3.3.41) satisfy Theorem's 3.3.1 conditions and therefore the set $\bar{\mathcal{B}}(r_0)^N$ is positively invariant for trajectories of $\dot{\mathbf{x}}(t) = \mathbf{f}_{\sigma(t)}(\mathbf{x}(t))$. This in turn implies that the set $\mathbf{H}_{\bar{\boldsymbol{\nu}}}^{-1}(\bar{\mathcal{B}}(r_0)^N) = \bar{\mathcal{C}}(\alpha, \bar{\boldsymbol{\nu}})^N$, where $\alpha = \arccos(\max_{i \in \mathcal{N}} \bar{\boldsymbol{\nu}}^T \boldsymbol{\nu}_i(0)) \in [0, \alpha^*]$, is positively invariant for trajectories of $\dot{\boldsymbol{\nu}}(t) = \tilde{\mathbf{f}}_{\sigma(t)}(\boldsymbol{\nu}(t))$; i.e., all unit vectors are forever contained in the closed α -cone they start on. This suffices to conclude i) in the Theorem.

Let us now focus on part ii) of the Theorem. From Proposition 3.3.16, the dynamics (3.3.41) satisfy Theorem's 3.3.1 conditions. It follows from Theorem 3.3.1 that $\lim_{t \rightarrow \infty} \mathbf{x}_i(t) - \mathbf{x}_j(t) = 0$ for all $i, j \in \mathcal{N}$, which implies that $\lim_{t \rightarrow \infty} \boldsymbol{\nu}_i(t) - \boldsymbol{\nu}_j(t) = 0$, for all $i, j \in \mathcal{N}$ (see Proposition 3.3.14). Moreover, it follows that the Lyapunov function in Theorem 3.3.1 converges to a constant, i.e., $\lim_{t \rightarrow \infty} V(t) = \lim_{t \rightarrow \infty} \max_{i \in \mathcal{N}} \frac{1}{2} \|\mathbf{x}_i(t)\|^2 = \lim_{t \rightarrow \infty} \frac{1}{2} \|\mathbf{x}_1(t)\|^2 = V^\infty$, for some constant $0 \leq V^\infty \leq V(0) < \frac{1}{2}$. From Proposition 3.3.14, it follows that $\lim_{t \rightarrow \infty} \bar{\boldsymbol{\nu}} \boldsymbol{\nu}_i(t) = \lim_{t \rightarrow \infty} \sqrt{1 - \|\mathbf{x}_i(t)\|^2} = \sqrt{1 - 2V^\infty}$.

We now prove part iii) of the Theorem. Since $\boldsymbol{\nu}(0) \in \mathcal{C}(\alpha^*, \bar{\boldsymbol{\nu}})^N$ for some $\bar{\boldsymbol{\nu}} \in \mathbb{S}^n$, Proposition 3.3.20 guarantees that there exist $n + 1$ linearly independent unit vectors $\{\bar{\boldsymbol{\nu}}_1, \dots, \bar{\boldsymbol{\nu}}_{n+1}\}$ such that $\boldsymbol{\nu}(\cdot) \in \mathcal{C}(\alpha^*, \bar{\boldsymbol{\nu}}_k)^N$ for all $k \in \{1, \dots, n + 1\}$. From part ii) of this Theorem, it follows that, for each $k \in \{1, \dots, n + 1\}$, there exists a constant $V_k^\infty < \frac{1}{2}$ such that $\lim_{t \rightarrow \infty} \bar{\boldsymbol{\nu}}_k^T \boldsymbol{\nu}_1(t) = \sqrt{1 - 2V_k^\infty}$. Thus, it follows that $\lim_{t \rightarrow \infty} A \boldsymbol{\nu}_1(t) = b \Leftrightarrow \lim_{t \rightarrow \infty} \boldsymbol{\nu}_1(t) = A^{-1}b$, where $A^T = [\bar{\boldsymbol{\nu}}_1 \dots \bar{\boldsymbol{\nu}}_{n+1}]$ is non-singular, since $\bar{\boldsymbol{\nu}}_1, \dots, \bar{\boldsymbol{\nu}}_{n+1}$ are linearly independent, and $b^T = [\sqrt{1 - 2V_1^\infty} \dots \sqrt{1 - 2V_{n+1}^\infty}]$. Since synchronization is asymptotically reached, $\lim_{t \rightarrow \infty} \boldsymbol{\nu}_i(t) = A^{-1}b$ for all $i \in \mathcal{N}$. \square

3.3.9 Simulations

In this section, we present simulations that illustrate some of the results in the previous sections.

All simulations are provided for a network of six agents, i.e., $\mathcal{N} = \{1, \dots, 6\}$, whose network topology is presented in Fig. 3.10. The neighbor sets for all agents change in time: for agent 1, $\mathcal{N}_1(\cdot)$ alternates between $\{2\}$ and $\{2, 4\}$; for agent 2, $\mathcal{N}_2(\cdot)$ alternates between $\{3\}$ and $\mathcal{N}_2(\cdot) = \{3, 6\}$; for agent 3, $\mathcal{N}_3(\cdot)$ alternates between $\{4\}$ and $\{4, 5\}$; for agent 4, $\mathcal{N}_4(\cdot)$ alternates between $\{5\}$ and $\{5, 1\}$; for agent 5, $\mathcal{N}_5(\cdot)$ alternates between $\{6\}$ and $\{6, 3\}$; for agent 6, $\mathcal{N}_6(\cdot)$ alternates between $\{1\}$ and $\{1, 2\}$. For these time-varying neighbor sets, the network graph is connected at all times.

The switching time instants for the neighbor set of each agent $i \in \mathcal{N}$ are those from the sequences $\mathcal{T}^i = \{\frac{1}{i} + ki\}_{k \in \mathbb{N}}$, which are shown in the time axes in Fig 3.9. For the same initial conditions, we perform two simulations, each one with different weight functions: for agents whose $i \in \mathcal{N}$ is even, $g_{ij}(\theta) = j$ for both simulations; for agents whose $i \in \mathcal{N}$ is odd, we consider $g_{ij}(\theta) = j(2 - \cos(\theta))$ for simulation 1 and $g_{ij}(\theta) = j(1 - \cos(\theta))$ for simulation 2. Notice that $g_{ij}(0) = j > 0$ for the former case, and $g_{ij}(0) = 0$ for the latter case, which means odd agents penalize small errors differently between the two simulations.

In Figs. 3.9a-3.9f, six unit vectors are randomly initialized in an open $\frac{\pi}{2}$ -cone around $[100]^T$. In Figs. 3.9a and 3.9d, the trajectories of the unit vectors on the unit sphere is shown, and a visual inspection indicates convergence to a synchronized network. In Figs. 3.9b and 3.9e, the function $V(\mathbf{x}) = \max_{i \in \mathcal{N}} \frac{1}{2} \|\mathbf{x}_i\|^2$ – used in Theorem 3.3.17 – is provided, and we can verify that despite being non-smooth, it is almost always decreasing; notice that $V(\mathbf{x}(\cdot))$ converges to a constant which quantifies the asymptotic angular distance between all unit vectors and $[100]^T$. In Figs. 3.9c and 3.9f, the angular distance, i.e., $\theta(\cdot, \cdot)$ as in Definition 3.3.10, between some agents is presented, and it indicates convergence to a synchronized network. Notice that in simulation 1 convergence is quicker when compared to simulation 2. This is a consequence of choosing, for simulation 2, weight functions that are zero when two unit vectors are synchronized, i.e., $g_{ij}(0) = 0$ for i odd. This means that odd agents do not penalize the error between themselves and their neighbors *as much* when they are *close*, and thus leading to a slow convergence to a synchronized network. In turn, even agents $i \in \mathcal{N}$ tend to converge to some odd agent, when $|\mathcal{N}_i(\cdot)| = 1$ (if $|\mathcal{N}_i(\cdot)| = 1$ then $\mathcal{N}_i(\cdot)$ is a set composed of one odd number); and tend to converge to somewhere in between their two neighbors when $|\mathcal{N}_i(\cdot)| = 2$. This explains the oscillatory behavior for simulation 2 in Figs. 3.9e and 3.9f.

In Figs. 3.9g-3.9l, six rotation matrices were randomly initialized such that $\theta(\mathbf{I}, \mathcal{R}_i) \leq \frac{\pi}{2}$ for all $i \in \mathcal{N}$. In Figs. 3.9g and 3.9j, the trajectories of the rotation matrices are shown on a sphere of π radius¹, and a visual inspection indicates convergence to a synchronized network. In Figs. 3.9h and 3.9k, the function $V(\mathbf{x}) =$

¹For each rotation matrix \mathcal{R}_i , we plot $\mathbf{v}(\mathcal{R}_i)$ with \mathbf{v} as defined in (3.2.2).

$\max_{i \in \mathcal{N}} \frac{1}{2} \|\mathbf{x}_i\|^2$ – used in Theorem 3.3.17 – is provided, and we can verify that despite being non-smooth, it is almost always decreasing; notice that $V(\mathbf{x}(\cdot))$ converges to a constant which quantifies the asymptotic angular distance between all rotation matrices and \mathbf{I} (the rotation matrix that all rotation matrices start *close to*). In Figs. 3.9i and 3.9l, the angular distance, i.e., $\theta(\cdot, \cdot)$ as in Definition 3.3.6, between some agents is presented, and indicating convergence to a synchronized network. Notice that in simulation 1 convergence is quicker when compared to simulation 2. The explanation for this behavior is the same as that provided before, and it is a consequence of choosing, for simulation 2, weight functions that are zero when the two rotation matrices are synchronized, i.e., $g_{ij}(0) = 0$ for i odd. The oscillatory behavior for simulation 2 in Figs. 3.9k and 3.9l is also explained by the same reasoning described before.

3.3.10 Auxiliary results

The following Proposition is a direct consequence of Proposition 1.3.4.

Proposition 3.3.18. *If $(\boldsymbol{\nu}_1, \boldsymbol{\nu}_2) \in \mathcal{C}(\alpha, \bar{\boldsymbol{\nu}})^2$ for some $\bar{\boldsymbol{\nu}} \in \mathbb{S}^n$ and some $\alpha \in [0, \frac{\pi}{2}]$, then $\boldsymbol{\nu}_1^T \boldsymbol{\nu}_2 > \cos(2\alpha)$. If $\boldsymbol{\nu} = (\boldsymbol{\nu}_1, \dots, \boldsymbol{\nu}_N) \in \mathcal{C}(\alpha, \boldsymbol{\nu})^N$ for some $\bar{\boldsymbol{\nu}} \in \mathbb{S}^n$ and some $\alpha \in [0, \frac{\pi}{2}]$, then $\boldsymbol{\nu}_i^T \boldsymbol{\nu}_j > \cos(2\alpha)$ for all $i, j \in \mathcal{N}$.*

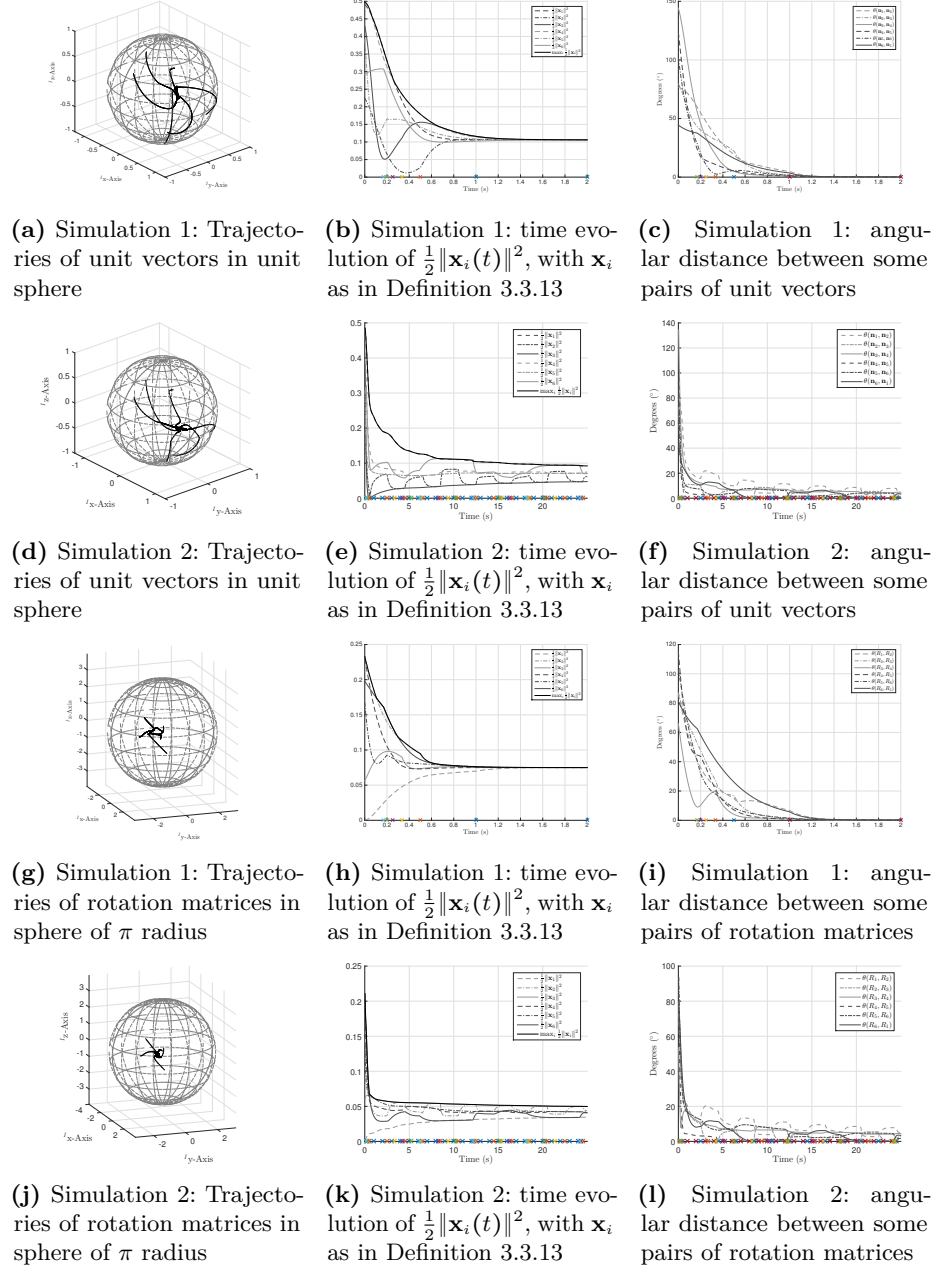
Proposition 3.3.19. *Consider $n + 1$ linearly independent unit vectors $\boldsymbol{\nu}_1, \dots, \boldsymbol{\nu}_{n+1} \in \mathcal{S}^n \subset \mathbb{R}^{n+1}$, and $n + 1$ constants $v_1, \dots, v_{n+1} \in (-1, 1)$. There exists no more than one $\boldsymbol{\nu}^* \in \mathcal{S}^n$ that satisfies $v_i = \boldsymbol{\nu}_i^T \boldsymbol{\nu}^*$, for all $i = \{1, \dots, n + 1\}$.*

Proof. Denote $\mathbf{N} = [\boldsymbol{\nu}_1 \cdots \boldsymbol{\nu}_n]^T \in \mathbb{R}^{(n+1) \times (n+1)}$ and $\mathbf{V} = [v_1 \cdots v_n]^T \in \mathbb{R}^{n+1}$. The system of equations $v_i = \boldsymbol{\nu}_i^T \boldsymbol{\nu}^*$, for $i = \{1, \dots, n + 1\}$, can be rewritten as $\mathbf{N} \boldsymbol{\nu}^* = \mathbf{V}$. Since $\boldsymbol{\nu}_1, \dots, \boldsymbol{\nu}_{n+1}$ are linearly independent, \mathbf{N} is non-singular, and a unique solution exists and is given by $\boldsymbol{\nu}^* = \mathbf{N}^{-1} \mathbf{V}$. The unique solution $\boldsymbol{\nu}^*$ is a unit vector if $\|\mathbf{N}^{-1} \mathbf{V}\| = 1$. \square

Figure 3.12 illustrates the result in Proposition 3.3.19, which essentially implies that in a sphere in \mathbb{R}^n , the intersection of the boundaries of n cones yields a unit vector (each circle in the figure represents the vectors $\boldsymbol{\nu} \in \mathcal{S}^2$ for which $\boldsymbol{\nu}^T \boldsymbol{\nu}_i = v_i$, for $i \in \{1, 2, 3\}$).

Proposition 3.3.20. *Let $\boldsymbol{\nu} \in \mathcal{S}^n$ and $\alpha \in [0, \frac{\pi}{2}]$. There exist $n + 1$ linearly independent unit vectors $\boldsymbol{\nu}_1, \dots, \boldsymbol{\nu}_{n+1} \in \mathcal{S}^n$ such that $\mathcal{C}(\alpha, \boldsymbol{\nu}) \subset \mathcal{C}(\alpha + \delta, \boldsymbol{\nu}_i) \subset \mathcal{C}(\frac{\pi}{2}, \boldsymbol{\nu}_i)$ for all $i \in \{1, \dots, n + 1\}$ and for some $\delta \in (0, \frac{\pi}{2} - \alpha)$.*

Proof. It is trivial to verify that $\mathcal{C}(\alpha, \boldsymbol{\nu}) \subset \mathcal{C}(\alpha + \delta, \boldsymbol{\nu}_i)$ for any $\delta \in (0, \frac{\pi}{2} - \alpha)$. Now, recall that, by definition, $\boldsymbol{\nu}^T \mathbf{n} > \cos(\alpha) > 0$ for all $\mathbf{n} \in \mathcal{C}(\alpha, \boldsymbol{\nu})$. Consider then the unit vector $\boldsymbol{\eta}_i = \cos(\delta)\boldsymbol{\nu} + \sin(\delta)\boldsymbol{\nu}_i^\perp \in \mathbb{S}^n$, for some $\delta \in (0, \frac{\pi}{2} - \alpha)$ and where $\boldsymbol{\nu}_i^\perp \in \mathcal{S}^n$ is an unit vector orthogonal to $\boldsymbol{\nu}$. Since $\delta \in (0, \frac{\pi}{2} - \alpha)$, it follows that $\cos(\delta) > 0$. Then $\mathbf{n}^T \boldsymbol{\eta}_i = \cos(\delta)\mathbf{n}^T \boldsymbol{\nu} + \sin(\delta)\mathbf{n}^T \boldsymbol{\nu}_i^\perp > \cos(\delta)\cos(\alpha) - \sin(\delta)\sin(\alpha) = \cos(\alpha + \delta) > \cos(\alpha)$, for all $\mathbf{n} \in \mathcal{C}(\alpha, \boldsymbol{\nu})$. Since there are n unit vectors $\boldsymbol{\nu}_1^\perp, \dots, \boldsymbol{\nu}_n^\perp$ orthogonal to $\boldsymbol{\nu}$, it follows that we can find n linearly independent unit vectors $\boldsymbol{\eta}_1, \dots, \boldsymbol{\eta}_n$ such that

**Figure 3.9:** Simulations 1 and 2.

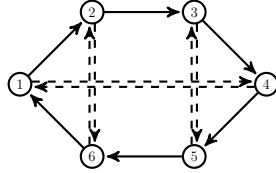


Figure 3.10: Time-varying digraph with 6 agents.

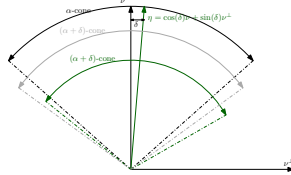


Figure 3.11: Illustration of result in Proposition 3.3.20 for $n = 2$: closed $(\alpha + \delta)$ -cones formed by ν and η contain closed α -cone formed by ν ; also, ν and η are linearly independent.

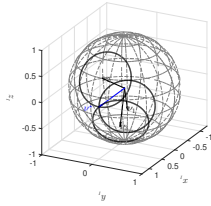


Figure 3.12: Illustration of result in Proposition 3.3.19 for $n = 3$.

$\mathcal{C}(\alpha, \nu) \subset \mathcal{C}(\alpha + \delta, \eta_i)$ for all $i \in \{1, \dots, n\}$. Moreover, $\{\nu, \eta_1, \dots, \eta_n\}$ are $n + 1$ linearly independent unit vectors. \square

Figure 3.11 illustrates the result in Proposition 3.3.20 for $n = 2$. From Proposition 3.3.20 it follows that if a group of unit vectors (in \mathbb{R}^{n+1}) is contained in a closed α -cone for some $\alpha \in [0, \frac{\pi}{2}]$, then we can find $n + 1$ larger (by δ) closed cones that contain the same group of unit vectors; i.e., given $\nu = (\nu_1, \dots, \nu_N) \in \bar{\mathcal{C}}(\alpha, \bar{\nu})^N$ for some $\bar{\nu} \in \mathbb{S}^n$, there exist $n + 1$ linearly independent unit vectors, $\{\bar{\nu}_1, \dots, \bar{\nu}_{n+1}\}$, such that $\nu \in \bar{\mathcal{C}}(\alpha + \delta, \bar{\nu}_i)^N$ for all $i \in \{1, \dots, n + 1\}$ and for some $\delta \in (0, \frac{\pi}{2} - \alpha)$.

3.3.11 Auxiliary results: Quaternions

For details on unit quaternions, we refer to [108]. We denote by $\mathbf{q} = (\hat{\mathbf{q}}, \bar{q}) \in \mathcal{S}^3$ a unit quaternion, where $\hat{\mathbf{q}}$ is the quaternion's vector component and \bar{q} is the quaternion's scalar component, and $\mathbf{q}^* = (-\hat{\mathbf{q}}, \bar{q})$ denotes the quaternion's conjugate. A rotation matrix $\mathcal{R} \in \mathbb{SO}(3)$ can be parametrized by a unit quaternion $\mathbf{q} \in \mathcal{S}^3$, i.e., $\bar{\mathcal{R}}_q : \mathcal{S}^3 \mapsto \mathbb{SO}(3)$, defined as

$$\bar{\mathcal{R}}_q(\mathbf{q}) = \mathbf{q}^T \mathbf{q}^* \mathbf{I}_3 + 2\bar{q}\mathcal{S}(\hat{\mathbf{q}}) + 2\hat{\mathbf{q}}\hat{\mathbf{q}}^T, \quad (3.3.45)$$

provides a mapping from \mathbb{S}^3 to $\mathbb{SO}(3)$. Notice that $\bar{\mathcal{R}}_q(\mathbf{q}) = \bar{\mathcal{R}}_q(-\mathbf{q})$, and, in fact, \mathbb{S}^3 provides a double covering of $\mathbb{SO}(3)$, where only two diametrically opposed unit quaternions correspond to the same rotation matrix [112]. For convenience denote $Q : \mathbb{S}^3 \mapsto \mathbb{R}^{4 \times 4}$ defined as

$$Q(\mathbf{q}) = \bar{q}\mathbf{I}_4 + \begin{bmatrix} \mathcal{S}(\hat{\mathbf{q}}) & \hat{\mathbf{q}} \\ -\hat{\mathbf{q}}^T & 0 \end{bmatrix}, \quad (3.3.46)$$

which satisfies $Q^T(\mathbf{q}) = Q(\mathbf{q}^*)$, $Q(\mathbf{q}^*)Q(\mathbf{q}) = Q(\mathbf{q})Q(\mathbf{q}^*) = \mathbf{I}_4$ and $Q(\mathbf{q})\mathbf{e}_4 = \bar{q}\mathbf{e}_4 + (\hat{\mathbf{q}}, 0) = \mathbf{q}$. As such,

$$Q(\mathbf{q})(\mathbf{I}_4 - \mathbf{e}_4\mathbf{e}_4^T)Q(\mathbf{q}^*) = Q(\mathbf{q})Q(\mathbf{q}^*) - Q(\mathbf{q})\mathbf{e}_4\mathbf{e}_4^TQ(\mathbf{q}^*) = \mathbf{I} - \mathbf{q}\mathbf{q}^T = \Pi(\mathbf{q}). \quad (3.3.47)$$

Thus, given two unit quaternions $\mathbf{q}_1, \mathbf{q}_2 \in \mathbb{S}^3$, it holds that $\bar{\mathcal{R}}_q(\mathbf{q}_1)^T = \bar{\mathcal{R}}_q(\mathbf{q}_1^*)$, and that $\bar{\mathcal{R}}_q(\mathbf{q}_1)\bar{\mathcal{R}}_q(\mathbf{q}_2) = \bar{\mathcal{R}}_q(Q(\mathbf{q}_1)\mathbf{q}_2)$, where $Q(\mathbf{q}_1)\mathbf{q}_2 \in \mathbb{S}^3$ is also a unit quaternion.

Given $\mathbf{q} \in \mathbb{S}^3$, it is easy to verify that

$$\mathcal{S}^{-1}(\bar{\mathcal{R}}_q(\mathbf{q}) - \mathcal{R}^T(\mathbf{q})) = \mathcal{S}^{-1}(4\bar{q}\mathcal{S}(\hat{\mathbf{q}})) = 4\bar{q}\hat{\mathbf{q}} = 4\bar{q}[\mathbf{I}_3 \mathbf{0}] \mathbf{q}. \quad (3.3.48)$$

As such, since $\bar{\mathcal{R}}_q^T(\mathbf{q}_1)\bar{\mathcal{R}}_q(\mathbf{q}_2) = \bar{\mathcal{R}}_q(Q(\mathbf{q}_1^*)\mathbf{q}_2)$ and $Q(\mathbf{q}_1^*)\mathbf{q}_2 = \mathbf{q}_1^T\mathbf{q}_2$ for any $\mathbf{q}_1, \mathbf{q}_2 \in \mathbb{S}^3$, it follows that

$$\mathcal{S}^{-1}(\mathcal{R}^T(\mathbf{q}_1)\bar{\mathcal{R}}_q(\mathbf{q}_2) - \mathcal{R}^T(\mathbf{q}_2)\bar{\mathcal{R}}_q(\mathbf{q}_1)) \stackrel{(3.3.48)}{=} 4\mathbf{q}_1^T\mathbf{q}_2 \begin{bmatrix} \mathbf{I}_3 & \mathbf{0} \end{bmatrix} Q(\mathbf{q}_1^*)\mathbf{q}_2. \quad (3.3.49)$$

Finally, notice that

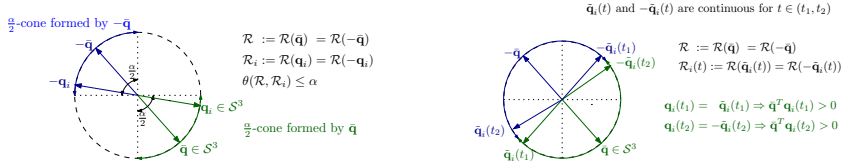
$$\begin{aligned} \frac{\text{tr}(\bar{\mathcal{R}}_q(\mathbf{q})) - 1}{2} &= \frac{\text{tr}(\mathbf{q}^T\mathbf{q}^*\mathbf{I}_3 + 2\bar{q}\mathcal{S}(\hat{\mathbf{q}}) + 2\hat{\mathbf{q}}\hat{\mathbf{q}}^T) - 1}{2} \\ &= \frac{3\mathbf{q}^T\mathbf{q}^* + 2\hat{\mathbf{q}}^T\hat{\mathbf{q}} - \mathbf{q}^T\mathbf{q}}{2} = \frac{3(\bar{q}^2 - \hat{\mathbf{q}}^T\hat{\mathbf{q}}) + 2\hat{\mathbf{q}}^T\hat{\mathbf{q}} - \mathbf{q}^T\mathbf{q}}{2} \\ &= \bar{q}^2 - \hat{\mathbf{q}}^T\hat{\mathbf{q}} = \mathbf{q}^T\mathbf{q}^*, \end{aligned} \quad (3.3.50)$$

and therefore

$$\begin{aligned} \frac{\text{tr}(\mathcal{R}^T(\mathbf{q}_1)\bar{\mathcal{R}}_q(\mathbf{q}_2)) - 1}{2} &= \frac{\text{tr}(\bar{\mathcal{R}}_q(Q(\mathbf{q}_1^*)\mathbf{q}_2)) - 1}{2} = \mathbf{q}^T\mathbf{q}^*|_{\mathbf{q}=Q(\mathbf{q}_1^*)\mathbf{q}_2} \\ &= (Q(\mathbf{q}_1^*)\mathbf{q}_2)^T(Q(\mathbf{q}_1^*)\mathbf{q}_2)^* = \mathbf{q}_2^TQ(\mathbf{q}_1)(Q(\mathbf{q}_1^*)\mathbf{q}_2)^* \\ &= \mathbf{q}_2^TQ(\mathbf{q}_1)\begin{bmatrix} -\mathbf{I} & \mathbf{0} \\ \mathbf{0} & 1 \end{bmatrix}Q(\mathbf{q}_1^*)\mathbf{q}_2 = -\mathbf{q}_2^TQ(\mathbf{q}_1)Q(\mathbf{q}_1^*)\mathbf{q}_2 + 2\mathbf{q}_2^TQ(\mathbf{q}_1)\mathbf{e}_4\mathbf{e}_4^TQ(\mathbf{q}_1^*)\mathbf{q}_2 \\ &= -\mathbf{q}_2^T\mathbf{q}_2 + 2\mathbf{q}_2^T\mathbf{q}_1\mathbf{q}_1^T\mathbf{q}_2 = 2(\mathbf{q}_1^T\mathbf{q}_2)^2 - 1. \end{aligned} \quad (3.3.51)$$

Given an angular velocity $\boldsymbol{\omega} : \mathbb{R}_{\geq 0} \mapsto \mathbb{R}^3$, and given $\mathcal{R} : \mathbb{R}_{\geq 0} \mapsto \mathbb{SO}(3)$ evolving according to $\dot{\mathcal{R}}(t) = \mathcal{R}(t)\mathcal{S}(\boldsymbol{\omega}(t))$, a parameterizing quaternion $\mathbf{q} : \mathbb{R}_{\geq 0} \ni t \mapsto \mathbf{q}(t) \in \mathbb{S}^3$ evolves according to [108]

$$\dot{\mathbf{q}}(t) = \frac{1}{2}Q(\mathbf{q}(t)) \begin{bmatrix} \mathbf{I} \\ \mathbf{0} \end{bmatrix} \boldsymbol{\omega}(t). \quad (3.3.52)$$



- (a) If $\theta(\bar{\mathcal{R}}_q(\bar{\mathbf{q}}), \mathcal{R}_i) \leq \alpha$, then there exists (b) Given a continuous $\mathcal{R}_i : \mathbb{R} \mapsto \mathcal{SO}(3)$, a unit quaternion \mathbf{q}_i in the $\frac{\alpha}{2}$ -cone formed by the unit quaternion $\bar{\mathbf{q}}$ that parametrizes $\bar{\mathcal{R}}_q(\mathbf{q}_i(\cdot))$ and satisfying $\bar{\mathbf{q}}^T \mathbf{q}_i(\cdot) > 0$, may not be found.

Figure 3.13: Illustration for the result in Proposition 3.3.21

Proposition 3.3.21. Consider $\mathcal{R} = (\mathcal{R}_1, \dots, \mathcal{R}_N) \in \mathbb{SO}(3)^N$ such that $\theta(\bar{\mathcal{R}}, \mathcal{R}_i) \leq \alpha$, for some $\alpha \in [0, \pi]$ and $\bar{\mathcal{R}} \in \mathbb{SO}(3)$, and for all $i \in \mathcal{N}$. If $\mathcal{R} = \bar{\mathcal{R}}_q(\bar{\mathbf{q}})$ for some $\bar{\mathbf{q}} \in \mathcal{S}^3$, then there exists $\mathbf{q} = (\mathbf{q}_1, \dots, \mathbf{q}_N) \in (\mathcal{S}^3)^N$ such that $\mathcal{R}_i = \bar{\mathcal{R}}_q(\mathbf{q}_i)$ for each $i \in \mathcal{N}$ and such that $\mathbf{q} \in \bar{\mathcal{C}}\left(\frac{\alpha}{2}, \bar{\mathbf{q}}\right)^N$.

Proof. Recall that (3.3.45) provides a double cover of $\mathbb{SO}(3)$. Therefore there exists $\bar{\mathbf{q}} \in \mathcal{S}^3$ such that $\bar{\mathcal{R}} = \bar{\mathcal{R}}_q(\bar{\mathbf{q}}) = \bar{\mathcal{R}}_q(-\bar{\mathbf{q}}) \in \mathbb{SO}(3)$. Similarly, for every $i \in \{1, \dots, N\}$, there exists a pair $\{\mathbf{q}_i \in \mathcal{S}^3, -\mathbf{q}_i \in \mathcal{S}^3\}$ such that $\mathcal{R}_i = \bar{\mathcal{R}}_q(\mathbf{q}_i) = \bar{\mathcal{R}}_q(-\mathbf{q}_i) \in \mathbb{SO}(3)$. Denote $\tilde{\mathbf{q}}_i \in \{\mathbf{q}_i, -\mathbf{q}_i\}$. From (3.3.50)-(3.3.51), it follows that

$$\cos(\theta(\mathcal{R}, \mathcal{R}_i)) = 2(\bar{\mathbf{q}}^T \tilde{\mathbf{q}}_i)^2 - 1 \Leftrightarrow \quad (3.3.53)$$

$$\Leftrightarrow |\bar{\mathbf{q}}^T \tilde{\mathbf{q}}_i| = \sqrt{\frac{\cos(\theta(\mathcal{R}, \mathcal{R}_i)) + 1}{2}} = \left| \cos\left(\frac{\theta(\mathcal{R}, \mathcal{R}_i)}{2}\right) \right| = \cos\left(\frac{\theta(\mathcal{R}, \mathcal{R}_i)}{2}\right), \quad (3.3.54)$$

where the latter equality follows since $\theta(\mathcal{R}, \mathcal{R}_i) \in [0, \pi]$. Thus, there always exists a unit quaternion $\tilde{\mathbf{q}}_i \in \{\mathbf{q}_i, -\mathbf{q}_i\}$ that parametrizes \mathcal{R}_i and that satisfies $\bar{\mathbf{q}}^T \tilde{\mathbf{q}}_i = \cos\left(\frac{\theta(\mathcal{R}, \mathcal{R}_i)}{2}\right) \geq \cos\left(\frac{\alpha}{2}\right)$. As such, it follows that $\mathbf{q} = (\mathbf{q}_1, \dots, \mathbf{q}_N) \in \bar{\mathcal{C}}\left(\frac{\alpha}{2}, \bar{\mathbf{q}}\right)^N$. \square

Remark 3.3.22. In the proof of Proposition 3.3.21, we note that, had we chosen $-\bar{\mathbf{q}} \in \mathcal{S}^3$ as the other possible parameterization of $\bar{\mathcal{R}} \in \mathbb{SO}(3)$, then we would find that $-\tilde{\mathbf{q}}_i$ parametrizes \mathcal{R}_i , for every $i \in \mathcal{N}$, and that $(-\tilde{\mathbf{q}}_1, \dots, -\tilde{\mathbf{q}}_N) \in \mathcal{C}\left(\frac{\alpha}{2}, -\bar{\mathbf{q}}\right)^N$.

Figure 3.13 illustrates the results of Proposition 3.3.21.

3.4 Controllers for attitude synchronization on the sphere

3.4.1 Introduction

In this Section, we focus on *incomplete* attitude synchronization, as described in Section 3.2.1. In this problem, there exists a group of rigid bodies, each one with a main direction, and the global objective is to guarantee alignment of all rigid bodies' main directions. The space orthogonal to each main direction can be left free of actuation or controlled to accomplish some other goals. Complete, attitude

synchronization, as opposed to incomplete, requires more measurements and it might be the case that a rigid body is not fully actuated but rather only actuated in the space orthogonal to a specific direction, in which case incomplete attitude synchronization is still feasible. *Incomplete* attitude synchronization is also denoted synchronization on the sphere in [80–84, 86], where the focus has been on kinematic or point mass dynamic agents, i.e., dynamical agents without moment of inertia.

In [80, 81], incomplete synchronization of kinematic agents on the sphere is studied, with a constant edge weight function for all edges. In particular, in [81], incomplete synchronization is used for accomplishing a flocking behavior, where a group of agents moves in a common direction. In [82], dynamic agents, which move at constant speed on a sphere, are controlled by a state feedback control law that steers their velocity vector so as to force the agents to attain a collective circular motion; since the agents are mass points, the effect of the moment of inertia is not studied. In [83], dynamic point mass agents, constrained to move on a sphere, are controlled to form patterns on the sphere, by constructing attractive and repelling forces; in the absence of repelling forces, synchronization is achieved. Also, the closed-loop dynamics of these agents are invariant to rotations, or symmetry preserving, as those in [80, 81], in the sense that two trajectories, whose initial condition – composed of position and velocity – differs only on a rotation, are the same at each time instant apart from the previous rotation. In the framework of this section, this property does not hold, since our dynamic agents have a moment of inertia, unlike the agents in [80, 81, 83], and constitutes therefore a novel result.

In this Section, we propose a distributed control strategy for synchronization of elements in the unit sphere domain. The controllers for accomplishing synchronization are constructed as functions of distance functions (or *reshaping functions* as denoted in [75]), and, in order to exploit results from graph theory, we impose a condition on those distance functions that will restrict them to be invariant to rotations of their arguments. As a consequence, the proposed controllers can be implemented by each agent without the need of a common orientation frame. We restrict the proposed controllers to be continuous, which means that a synchronized network of agents cannot be a global equilibrium configuration, since \mathbb{S}^2 is a non-contractible set [113]. Our main contributions lie in proposing for the first time a controller that does not require full torque when performing synchronization along a principal axis, but rather torque orthogonal to that axis; in finding conditions on the distance functions that guarantee that a synchronized network is locally asymptotically stable for arbitrary connected network graphs, and that guarantee that a synchronized network is achieved for almost all initial conditions in a tree graph; in providing explicit domains of attraction for the network to converge to a synchronized network; and in characterizing the equilibria configurations for some general, yet specific, types of network graphs. The results here presented are based on those in [114] and [115].

The remainder of this section is structured as follows: in Subsection 3.4.3, the problem statement is described; in Subsection 3.4.4, the proposed solution is presented; in Subsections 3.4.5 and 3.4.6, convergence to a synchronized network

is discussed for tree and arbitrary graphs, respectively; and, in Subsection 3.4.7, simulations are presented that illustrate the theoretical results.

3.4.2 Notation

We refer the reader to the notation presented in Section 1.3, in page 5. In addition, we say $\mathbf{a} \neq \mathbf{0}$ and $\mathbf{b} \neq \mathbf{0}$ have the same direction if $\mathbf{b} = \lambda \mathbf{a}$ for some $\lambda \in \mathbb{R}$. Given $\mathbf{a}, \mathbf{b} \in \mathbb{R}^n$, $\mathbf{a} = \pm \mathbf{b} \Leftrightarrow \mathbf{a} = \mathbf{b} \vee \mathbf{a} = -\mathbf{b}$. In the list below, let $N \in \mathbb{N}$, $i \in \{1, \dots, N\}$, RB stands for rigid body, BOF stands for body orientation frame, and, lastly, IOR stands for an (unknown and common for all $i \in \{1, \dots, N\}$) inertial orientation frame.

$J_i \in M_{3,3}$	Moment of inertia of RB i ($J_i = J_i^T \in \mathbb{R}^{3 \times 3}$)
$\mathcal{R}_i \in \mathbb{SO}(3)$	BOF of RB i
$\bar{\mathbf{n}}_i \in \mathbb{S}^2$	Direction of RB i to be synchronized, expressed in BOF of RB i
$\mathbf{n}_i \in \mathbb{S}^2$	Direction of RB i to be synchronized, expressed in IOR
$\boldsymbol{\omega}_i \in \mathbb{R}^3$	Angular velocity of RB i , expressed in BOF of RB i
$\mathbf{T}_i \in \mathbb{R}^3$	Torque input of RB i , expressed in BOF of RB i

3.4.3 Problem Statement

We consider a group of N agents, indexed by the set $\mathcal{N} = \{1, \dots, N\}$, operating in the unit sphere domain, i.e., in $\mathbb{S}^2 = \{\mathbf{x} \in \mathbb{R}^3 : \mathbf{x}^T \mathbf{x} = 1\}$. The agents' network is modeled as an undirected static graph, $\mathcal{G} = \{\mathcal{N}, \mathcal{E}\}$, with \mathcal{N} as the vertices' set indexed by the team members, and \mathcal{E} as the edges' set. For every pair of agents $(i, j) \in \mathcal{N} \times (\mathcal{N} \setminus \{i\})$, that are *aware of* and can measure each other's relative attitude, we say that agent j is a neighbor of agent i , and vice-versa; also, we denote $\mathcal{N}_i \subset \mathcal{N}$ as the neighbor set of agent i . We consider a group of N rotations matrices, whose goal is to synchronize one of their directions, in a problem that we call incomplete synchronization, which has been described and illustrated in Section 3.2.1, page 72. Notice that an agent $i \in \mathcal{N}$ is not aware of \mathbf{n}_i , since this is specified w.r.t. an unknown inertial orientation frame; instead, agent i is aware of its own direction $\bar{\mathbf{n}}_i$ – fixed in its own orientation frame – and the projection of its neighbors directions onto its own orientation frame.

Consider the variables introduced in the Notation section, and denote

$$\bar{\mathbf{n}} = (\bar{\mathbf{n}}_1, \dots, \bar{\mathbf{n}}_N) \in (\mathbb{S}^2)^N \quad (3.4.1)$$

$$\mathcal{R} = (\mathcal{R}_1, \dots, \mathcal{R}_N) \in \mathbb{SO}(3)^N \quad (3.4.2)$$

$$\mathbf{n} = (\mathcal{R}_1 \bar{\mathbf{n}}_1, \dots, \mathcal{R}_N \bar{\mathbf{n}}_N) \in (\mathbb{S}^2)^N \quad (3.4.3)$$

$$\boldsymbol{\omega} = (\boldsymbol{\omega}_1, \dots, \boldsymbol{\omega}_N) \in (\mathbb{R}^3)^N \quad (3.4.4)$$

$$\mathbf{x} = (\mathcal{R}, \boldsymbol{\omega}) \in \mathbb{SO}(3)^N \times (\mathbb{R}^3)^N =: \Omega_x \quad (3.4.5)$$

$$\mathbf{T} = (\mathbf{T}_1, \dots, \mathbf{T}_N) \in (\mathbb{R}^3)^N. \quad (3.4.6)$$

where \mathbf{x} is the state of the system, and where \mathbf{T} is the input to the system. Consider then any agent $i \in \mathcal{N}$, a rotation matrix $\mathcal{R}_i : \mathbb{R}_{\geq 0} \mapsto \mathbb{SO}(3)$, a unit vector

$\mathbf{n}_i : \mathbb{R}_{\geq 0} \ni t \mapsto \mathbf{n}_i(t) = \mathcal{R}_i(t)\bar{\mathbf{n}}_i \in \mathbb{S}^2$, a body-framed angular velocity $\boldsymbol{\omega}_i : \mathbb{R}_{\geq 0} \mapsto \mathbb{R}^3$ and body frame torque $\mathbf{T}_i : \mathbb{R}_{\geq 0} \mapsto \mathbb{R}^3$. The rotation matrix $\mathcal{R}_i : \mathbb{R}_{\geq 0} \ni t \mapsto \mathcal{R}_i(t) \in \mathbb{SO}(3)$ evolves according to

$$\dot{\mathcal{R}}_i(t) = \mathbf{f}_R(\mathcal{R}_i(t), \boldsymbol{\omega}_i(t)), \mathcal{R}_i(0) \in \mathbb{SO}(3), \quad (3.4.7)$$

where $\mathbf{f}_R : \mathbb{SO}(3) \times \mathbb{R}^3 \ni (\mathcal{R}, \boldsymbol{\omega}) \mapsto \mathbf{f}_R(\mathcal{R}, \boldsymbol{\omega}) \in T_{\mathcal{R}}\mathbb{SO}(3)$ is defined as

$$\mathbf{f}_R(\mathcal{R}, \boldsymbol{\omega}) := \mathcal{R}\mathcal{S}(\boldsymbol{\omega}), \quad (3.4.8)$$

while each unit vector $\mathbf{n}_i : \mathbb{R}_{\geq 0} \ni t \mapsto \mathbf{n}_i(t) \in \mathbb{S}^2$ evolves according to $\dot{\mathbf{n}}_i(t) = \mathbf{f}_n(\mathcal{R}_i(t), \boldsymbol{\omega}_i(t), \bar{\mathbf{n}}_i)$, where $\mathbf{f}_n : \mathbb{SO}(3) \times \mathbb{R}^3 \times \mathbb{S}^2 \ni (\mathcal{R}_i, \boldsymbol{\omega}, \bar{\mathbf{n}}_i) \mapsto \mathbf{f}_n(\mathcal{R}_i, \boldsymbol{\omega}, \bar{\mathbf{n}}_i) \in T_{\bar{\mathbf{n}}_i}\mathbb{S}^2$ is defined as

$$\mathbf{f}_n(\mathcal{R}_i, \boldsymbol{\omega}, \bar{\mathbf{n}}_i) := \mathbf{f}_R(\mathcal{R}_i, \boldsymbol{\omega})\bar{\mathbf{n}}_i = \mathcal{R}_i\mathcal{S}(\boldsymbol{\omega})\bar{\mathbf{n}}_i = \mathcal{S}(\mathcal{R}_i\boldsymbol{\omega})\mathcal{R}_i\bar{\mathbf{n}}_i. \quad (3.4.9)$$

Finally, the body-framed angular velocity $\boldsymbol{\omega}_i : \mathbb{R}_{\geq 0} \ni t \mapsto \boldsymbol{\omega}_i(t) \in \mathbb{R}^3$ evolves according to the dynamics

$$\frac{d}{dt}(\mathcal{R}_i(t)J_i\boldsymbol{\omega}_i(t)) = \mathcal{R}_i(t)\mathbf{T}_i(t) \Leftrightarrow \quad (3.4.10)$$

$$\Leftrightarrow \dot{\boldsymbol{\omega}}_i(t) = J_i^{-1}(-\mathcal{S}(\boldsymbol{\omega}_i(t))J_i\boldsymbol{\omega}_i(t) + \mathbf{T}_i(t)) \quad (3.4.11)$$

$$\Leftrightarrow \dot{\boldsymbol{\omega}}_i(t) = \mathbf{f}_{\boldsymbol{\omega}_i}(\boldsymbol{\omega}_i(t), \mathbf{T}_i(t)), \quad (3.4.12)$$

where $\mathbf{f}_{\boldsymbol{\omega}_i} : \mathbb{R}^3 \times \mathbb{R}^3 \ni (\boldsymbol{\omega}, \mathbf{T}) \mapsto \mathbf{f}_{\boldsymbol{\omega}_i}(\boldsymbol{\omega}, \mathbf{T}) \in \mathbb{R}^3$ is given by

$$\mathbf{f}_{\boldsymbol{\omega}_i}(\boldsymbol{\omega}, \mathbf{T}) := J_i^{-1}(-\mathcal{S}(\boldsymbol{\omega})J_i\boldsymbol{\omega} + \mathbf{T}). \quad (3.4.13)$$

Definition 3.4.1. Two unit vectors $(\mathbf{n}_1, \mathbf{n}_2) \in (\mathbb{S}^2)^2$ are diametrically opposed if $\mathbf{n}_1^T \mathbf{n}_2 = -1$, and synchronized if $\mathbf{n}_1^T \mathbf{n}_2 = 1$. A group of unit vectors $(\mathbf{n}_1, \dots, \mathbf{n}_N) \in (\mathbb{S}^2)^N$ is synchronized if $\mathbf{n}_i^T \mathbf{n}_j = 1$ for all $i, j \in \{1, \dots, N\}$.

Problem 3.4.2. Given a group of rotation matrices $(\mathcal{R}_1, \dots, \mathcal{R}_N) : \mathbb{R}_{\geq 0} \mapsto \mathbb{SO}(3)^N$, with angular velocities $(\boldsymbol{\omega}_1, \dots, \boldsymbol{\omega}_N) : \mathbb{R}_{\geq 0} \mapsto \mathbb{R}^3$ and moments of inertia J_1, \dots, J_N satisfying (3.4.7) and (3.4.11), design distributed control laws for the torques $\{\mathbf{T}_i : \mathbb{R}_{\geq 0} \mapsto \mathbb{R}^3\}_{i \in \mathcal{N}}$, in the absence of a common inertial orientation frame, that guarantee that the group of unit vectors $(\mathbf{n}_1, \dots, \mathbf{n}_N) := (\mathcal{R}_1\bar{\mathbf{n}}_1, \dots, \mathcal{R}_N\bar{\mathbf{n}}_N) : \mathbb{R}_{\geq 0} \mapsto (\mathbb{S}^2)^N$ is asymptotically synchronized.

For the purposes of analysis, we consider the state \mathbf{x} and the control input \mathbf{T} , as introduced in (3.4.5) and (3.4.6), respectively. Then, a trajectory of system $\mathbf{x} : \mathbb{R}_{\geq 0} \mapsto \Omega_x$ evolves according to $\dot{\mathbf{x}}(t) = \mathbf{f}_x(\mathbf{x}(t), \mathbf{T}(t))$ where

$$\mathbf{f}_x(\mathbf{x}, \mathbf{T}) := (\mathbf{F}_R(\mathcal{R}, \boldsymbol{\omega}), \mathbf{F}_{\boldsymbol{\omega}}(\boldsymbol{\omega}, \mathbf{T})) \in (\mathbb{R}^{3 \times 3})^3 \times \mathbb{R}^{3N}, \quad (3.4.14)$$

with

$$\mathbf{F}_R(\mathcal{R}, \boldsymbol{\omega}) := (\mathbf{f}_R(\mathcal{R}_1, \boldsymbol{\omega}_1), \dots, \mathbf{f}_R(\mathcal{R}_N, \boldsymbol{\omega}_N)) \in (\mathbb{R}^{3 \times 3})^N, \quad (3.4.15)$$

$$\mathbf{F}_{\boldsymbol{\omega}}(\boldsymbol{\omega}, \mathbf{T}) := (\mathbf{f}_{\boldsymbol{\omega}_1}(\boldsymbol{\omega}_1, \mathbf{T}_1), \dots, \mathbf{f}_{\boldsymbol{\omega}_N}(\boldsymbol{\omega}_N, \mathbf{T}_N)) \in (\mathbb{R}^3)^N, \quad (3.4.16)$$

where we have made of use of the notation (3.4.1)–(3.4.4). We also denote, for convenience,

$$\mathbf{F}_n(\mathcal{R}, \boldsymbol{\omega}, \bar{\mathbf{n}}) := (\mathbf{f}_n(\mathcal{R}_1, \boldsymbol{\omega}_1, \bar{\mathbf{n}}_1), \dots, \mathbf{f}_n(\mathcal{R}_N, \boldsymbol{\omega}_N, \bar{\mathbf{n}}_N)) \in (\mathbb{R}^3)^N. \quad (3.4.17)$$

3.4.4 Proposed Solution

Preliminaries

Refer the reader to the subsection on graph theory on Section 3.2.

Denote by $C \subseteq \{1, \dots, M\}$ the set of indices corresponding the edges that form a cycle. Consider a network with $n \in \mathbb{N}$ cycles, $\{C_i\}_{i=\{1, \dots, n\}}$. A cycle C_i is said to be independent if $C_i \cap C_j = \emptyset$ for all $j \in \{1, \dots, n\} \setminus \{i\}$. In Fig. 3.14a, a graph with two independent cycles is presented. Additionally, we say two cycles C_1 and C_2 share only one edge when $|C_1 \cap C_2| = 1$ and $C_1 \cup C_2$ contains edges from only the following three cycles (in $\{C_i\}_{i=\{1, \dots, n\}}$): C_1 , C_2 and $C_3 = C_1 \cup C_2 \setminus \{C_1 \cap C_2\}$, with $|C_3| = |C_1| + |C_2| - 2$. Figures 3.14b and 3.18c present graphs with two cycles that share only one edge.

Proposition 3.4.3. Consider a graph \mathcal{G} with m independent cycles, $\{C_i\}_{i=\{1, \dots, m\}}$. Then the null space of B is given by $\mathcal{N}(B) = \{\mathbf{e} = (e_1, \dots, e_M) \in \mathbb{R}^M : e_k = \pm e_l, \forall k, l \in C_i, i = \{1, \dots, m\}\}$; and the null space of $B \otimes \mathbf{I}_n$ is given by $\mathcal{N}(B \otimes \mathbf{I}_n) = \{\mathbf{e} = (\mathbf{e}_1, \dots, \mathbf{e}_M) \in (\mathbb{R}^n)^M : \mathbf{e}_k = \pm \mathbf{e}_l, \forall k, l \in C_i, i = \{1, \dots, m\}\}$.

Notice that, for an incidence matrix $B \in \mathbb{R}^{N \times M}$, there are M edges and these *belong* to \mathbb{R} . On the other hand, for the incidence matrix $B \otimes \mathbf{I}_n$ (with $B \in \mathbb{R}^{N \times M}$), there are M edges, but, since the agents operate in an n -dimensional space, those edges *belong* to \mathbb{R}^n . With that in mind, under the conditions of Proposition 3.4.3, $\mathcal{N}(B) = \{\mathbf{e} = (e_1, \dots, e_M) \in \mathbb{R}^M : e_k = \pm e_l, \forall k, l \in C_i, i = \{1, \dots, m\}\}$ means that $\mathcal{N}(B)$ is the space where all edges of an independent cycle have the same absolute value. On the other hand, $\mathcal{N}(B \otimes \mathbf{I}_n) = \{\mathbf{e} = (\mathbf{e}_1, \dots, \mathbf{e}_M) \in (\mathbb{R}^n)^M : \mathbf{e}_k = \pm \mathbf{e}_l, \forall k, l \in C_i, i = \{1, \dots, m\}\}$ means that $\mathcal{N}(B \otimes \mathbf{I}_n)$ is the space where all edges of an independent cycle have the same direction and norm (or are all zero).

Proposition 3.4.4. Consider a graph \mathcal{G} with n_1 independent cycles, $\{C_i\}_{i=\{1, \dots, n_1\}}$, and n_2 pairs of cycles that share only one edge, $\{(C_i^1, C_i^2)\}_{i=\{1, \dots, n_2\}}$. Then the null space of B is given by $\mathcal{N}(B) = \{\mathbf{e} = (e_1, \dots, e_M) \in \mathbb{R}^M : e_k = \pm e_l, \forall k, l \in C_i, i = \{1, \dots, n_1\}\} \cup \{\mathbf{e} = (e_1, \dots, e_M) \in \mathbb{R}^M : e_k = \pm e_l, \forall k, l \in C_i^1 \setminus \{C_i^1 \cap C_i^2\}, e_p = \pm e_q, \forall p, q \in C_i^2 \setminus \{C_i^1 \cap C_i^2\}, i = \{1, \dots, n_2\}\}$; and the null space of $B \otimes \mathbf{I}_n$ is given by $\mathcal{N}(B \otimes \mathbf{I}_n) = \{\mathbf{e} = (\mathbf{e}_1, \dots, \mathbf{e}_M) \in (\mathbb{R}^n)^M : \mathbf{e}_k = \pm \mathbf{e}_l, \forall k, l \in C_i, i = \{1, \dots, n_1\}\} \cup \{\mathbf{e} = (\mathbf{e}_1, \dots, \mathbf{e}_M) \in (\mathbb{R}^n)^M : \mathbf{e}_k = \pm \mathbf{e}_l, \forall k, l \in C_i^1 \setminus \{C_i^1 \cap C_i^2\}, \mathbf{e}_p = \pm \mathbf{e}_q, \forall p, q \in C_i^2 \setminus \{C_i^1 \cap C_i^2\}, i = \{1, \dots, n_2\}\}$.

The results of Proposition 3.4.4 can be interpreted as follows: $\mathcal{N}(B)$ is the space where, for each cycle, all its edges ($\in \mathbb{R}$), except the one that is shared, have the

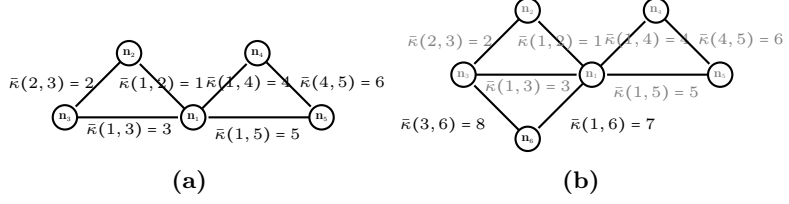


Figure 3.14: Two graphs: (a) graph with two independent cycles; (b) graph with one independent cycle and two cycles that share only one edge.

same absolute value; while $\mathcal{N}(B \otimes \mathbf{I}_n)$ is the space where, for each cycle, all its edges ($\in \mathbb{R}^n$), except the one that is shared, have the same direction and norm (or are all zero). Examples 3.4.1 and 3.4.2 illustrate Propositions 3.4.3 and 3.4.4. Proofs of Propositions 3.4.3 and 3.4.4 are found in Appendix [115]. These Propositions are useful in a later section, where we prove that for network graphs that satisfy the conditions of either Proposition, the agents converge to a configuration where all unit vectors belong to a common plane.

Example 3.4.1. Figure 3.14a displays a graph with two independent cycles, with incidence matrix and its null space in (3.4.18).

$$B_1 = \begin{bmatrix} 1 & 0 & 1 & 1 & 1 & 0 \\ -1 & 1 & 0 & 0 & 0 & 0 \\ 0 & -1 & -1 & 0 & 0 & 0 \\ 0 & 0 & 0 & -1 & 0 & 1 \\ 0 & 0 & 0 & 0 & -1 & -1 \end{bmatrix}, \mathcal{N}(B_1) = \text{span} \left\{ \begin{bmatrix} 1 \\ 1 \\ -1 \\ 0 \\ 0 \\ 0 \end{bmatrix}, \begin{bmatrix} 0 \\ 0 \\ 0 \\ 1 \\ 1 \\ -1 \end{bmatrix} \right\}. \quad (3.4.18)$$

Example 3.4.2. Figure 3.14b displays a graph with one independent cycle and two cycles that share only one edge, with incidence matrix and its null space in (3.4.19) (B_1 defined in (3.4.18)).

$$B = \begin{bmatrix} B_1 & \begin{bmatrix} 1 & 0 \\ 0 & 0 \end{bmatrix} \\ 0 & \begin{bmatrix} 1 & 0 \\ 0 & 0 \end{bmatrix} \\ 0 & \begin{bmatrix} 0 & 0 \\ 0 & 0 \end{bmatrix} \\ 0 & \begin{bmatrix} 0 & 0 \\ 0 & 0 \end{bmatrix} \\ \mathbf{0} & \begin{bmatrix} 0 & -1 & -1 \end{bmatrix} \end{bmatrix}, \mathcal{N}(B) = \text{span} \left\{ \begin{bmatrix} 1 \\ 1 \\ -1 \\ 0 \\ 0 \\ 0 \end{bmatrix}, \begin{bmatrix} 0 \\ 0 \\ 0 \\ 1 \\ 1 \\ -1 \end{bmatrix}, \begin{bmatrix} 0 \\ 0 \\ 0 \\ 0 \\ 0 \\ 1 \end{bmatrix} \right\}. \quad (3.4.19)$$

Once again, we refer the reader to the definition of cone, namely Definition 1.3.3, and Proposition 1.3.4.

Definition 3.4.5. Let $\alpha \in [0, \pi]$ and $\mathbf{n} = (\mathbf{n}_1, \dots, \mathbf{n}_N) \in (\mathbb{S}^2)^N$. We say that $\mathbf{n} \in \mathcal{C}(\alpha)[\bar{\mathcal{C}}(\alpha)]$, if $\mathbf{n} \in (\mathcal{C}(\alpha, \boldsymbol{\nu}))^N[(\bar{\mathcal{C}}(\alpha, \boldsymbol{\nu}))^N]$, for some $\boldsymbol{\nu} \in \mathbb{S}^2$.

Proposition 3.4.6. If $\mathbf{n} \in \mathcal{C}(\alpha)$, for some $\alpha \in [0, \frac{\pi}{2}]$, then $\max_{(i,j) \in \mathcal{N}^2} (1 - \mathbf{n}_i^T \mathbf{n}_j) < 1 - \cos(2\alpha)$.

This proposition follows immediately after Proposition 1.3.4.

Proposition 3.4.7. If, given $\mathbf{n} = (\mathbf{n}_1, \dots, \mathbf{n}_N) \in (\mathbb{S}^2)^N$, $\max_{(i,j) \in \mathcal{N}^2} (1 - \mathbf{n}_i^T \mathbf{n}_j) \leq 1 - \cos(\frac{2}{3}\alpha)$ holds for some $\alpha \in [0, \pi]$, then $\mathbf{n} \in \bar{\mathcal{C}}(\alpha)$.

A proof of Proposition 3.4.7 is found in [116].

Distance in \mathcal{S}^2

Consider an arbitrary distance function between unit vectors $d : \mathcal{S}^2 \times \mathcal{S}^2 \rightarrow \mathbb{R}_0^+$, satisfying $d(\mathbf{n}_1, \mathbf{n}_2) = 0 \Leftrightarrow \mathbf{n}_1 = \mathbf{n}_2$. We say that $d \in \mathcal{D}$, if, for all $(\mathbf{n}_1, \mathbf{n}_2) \in \mathcal{S}^2 \times \mathcal{S}^2$, it satisfies the partial differential equation

$$\mathcal{S}(\mathbf{n}_1) \partial_{\mathbf{n}} d(\mathbf{n}, \mathbf{n}_2)|_{\mathbf{n}=\mathbf{n}_1} + \mathcal{S}(\mathbf{n}_2) \partial_{\mathbf{n}} d(\mathbf{n}_1, \mathbf{n})|_{\mathbf{n}=\mathbf{n}_2} = \mathbf{0}. \quad (3.4.20)$$

Let us motivate the introduction of (3.4.20). Given $d \in \mathcal{D}$, it follows that (3.4.14),

$$\partial_{\mathbf{n}} d(\mathbf{n}, \mathbf{n}_2)|_{\mathbf{n}=\mathbf{n}_1} \mathbf{f}_n(\mathcal{R}_1, \boldsymbol{\omega}_1, \bar{\mathbf{n}}_2) + \partial_{\mathbf{n}} d(\mathbf{n}_1, \mathbf{n})|_{\mathbf{n}=\mathbf{n}_2} \mathbf{f}_n(\mathcal{R}_2, \boldsymbol{\omega}_2, \bar{\mathbf{n}}_2) = \quad (3.4.21)$$

$$\stackrel{(3.4.9)}{=} \boldsymbol{\omega}_1^T \mathcal{R}_1^T \mathcal{S}(\mathbf{n}_1) \partial_{\mathbf{n}} d(\mathbf{n}, \mathbf{n}_2)|_{\mathbf{n}=\mathbf{n}_1} + \boldsymbol{\omega}_2^T \mathcal{R}_2^T \mathcal{S}(\mathbf{n}_2) \partial_{\mathbf{n}} d(\mathbf{n}_1, \mathbf{n})|_{\mathbf{n}=\mathbf{n}_2} \quad (3.4.22)$$

$$\stackrel{(3.4.20)}{=} \begin{bmatrix} \boldsymbol{\omega}_1 \\ \boldsymbol{\omega}_2 \end{bmatrix}^T \begin{bmatrix} \mathcal{R}_1^T & \mathbf{0} \\ \mathbf{0} & \mathcal{R}_2^T \end{bmatrix} \begin{pmatrix} 1 \\ -1 \end{pmatrix} \otimes \mathbf{I} \mathcal{S}(\mathbf{n}_1) \partial_{\mathbf{n}} d(\mathbf{n}, \mathbf{n}_2)|_{\mathbf{n}=\mathbf{n}_1}. \quad (3.4.23)$$

where we identify an incidence matrix $[1 - 1]^T$ corresponding to an edge between unit vectors $\mathbf{n}_1 := \mathcal{R}_1 \bar{\mathbf{n}}_1$ and $\mathbf{n}_2 := \mathcal{R}_2 \bar{\mathbf{n}}_2$. For reasons that will become apparent later, we restrict the previous functions $f_k(\cdot)$ to satisfy some more properties.

Definition 3.4.8. Consider a function $f \in C^2((0, 2), \mathbb{R}_{>0})$, satisfying *i)* $f'(s) > 0 \forall s \in (0, 2)$, *ii)* $\lim_{s \rightarrow 0^+} f(s) = 0$, and *iii)* $\limsup_{s \rightarrow 0^+} f'(s), f''(s) < \infty$. Denote $f_2 := \lim_{s \rightarrow 2^-} f(s)$ and $f'_0 := \lim_{s \rightarrow 0^+} f'(s)$. We say

- $f \in \mathcal{P}_0$ if $f'_0 = 0$ and $f \in \bar{\mathcal{P}}_0$ if $f'_0 \neq 0$,
- $f \in \mathcal{P}^\infty$ if $f_2 = \infty$, and $f \in \bar{\mathcal{P}}^\infty$ if $f_2 < \infty$,
- $f \in \mathcal{P}^0$ if $f \in \mathcal{P}^\infty \wedge \lim_{s \rightarrow 2^-} f'(s)\sqrt{2-s} = 0$,
- $f \in \bar{\mathcal{P}}^0$ if $f \in \bar{\mathcal{P}}^\infty \wedge \lim_{s \rightarrow 2^-} f'(s)\sqrt{2-s} \neq 0$,
- $f \in \bar{\mathcal{P}}$ if $f(\cdot)$ is of any of the previous classes.

Figure 3.16 illustrates the different classes introduced in Definition 3.4.8 while Fig. 3.15 illustrates how the properties that $f(\cdot)$ satisfies affects the classes it belongs to. In [75], the notion of *reshaping function* is introduced, whose definition is within the same spirit as that of Definition 3.4.8.

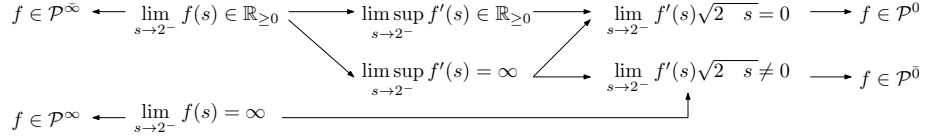


Figure 3.15: Relation between properties of function f and the classes it belongs to.

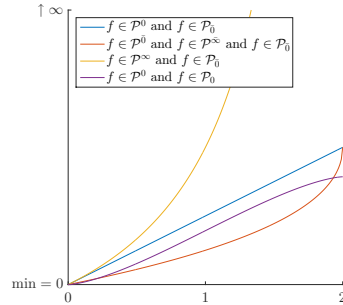


Figure 3.16: Four functions belonging to different classes as introduced in Definition 3.4.8: (from top to bottom in legend) $f(s) = s$, $f(s) = \pi^{-2} \arccos^2(1-s)$, $f(s) = \tan^2(0.5 \arccos(1-s))$ and $f(s) = 0.25(\sqrt{s(2-s)}(s-1) + \arccos(1-s))$.

It can be verified that distance functions of the type

$$d(\mathbf{n}_1, \mathbf{n}_2) = f(1 - \mathbf{n}_1^T \mathbf{n}_2), f \in C^1((0, 2), \mathbb{R}_{\geq 0}) \quad (3.4.24)$$

are the only type of functions for which $d \in \mathcal{D}$. In [115], f is further restricted to be of class $\bar{\mathcal{P}}$ (note that $f \in \bar{\mathcal{P}} \Rightarrow f \in C^1((0, 2), \mathbb{R}_{\geq 0})$). Here, however, and for simplicity, we make a further restriction and assume that $f(s) = \gamma s$ for some $\gamma > 0$, and we refer the interested reader to [114, 115], where for each edge may have a different distance function (i.e., to each edge $k \in \mathcal{M}$ on the network, we associate a distance function $d_k(\mathbf{n}_1, \mathbf{n}_2) = f_k(1 - \mathbf{n}_1^T \mathbf{n}_2)$, where $f_k \in \bar{\mathcal{P}}$).

Motivated by (3.4.23), let us define two functions. Define then $\mathbf{e} : \mathcal{S}^2 \times \mathcal{S}^2 \mapsto \mathbb{R}^3$ as

$$\mathbf{e}(\mathbf{n}_1, \mathbf{n}_2) = \mathcal{S}(\mathbf{n}_1) \frac{\partial d(\mathbf{n}_1, \mathbf{n}_2)}{\partial \mathbf{n}_1} = k \mathcal{S}(\mathbf{n}_1) \mathbf{n}_2, \quad (3.4.25)$$

to be the error of edge k , and for each $k \in \mathcal{M}$, Define also $\mathbf{E} : (\mathcal{S}^2)^N \ni \mathbf{n} \mapsto \mathbf{E}(\mathbf{n}) \in \mathbb{R}^{3N}$ as

$$\mathbf{E}(\mathbf{n}) = (\mathbf{e}({}_1 \mathbf{n}, {}_1 \mathbf{n}), \dots, \mathbf{e}({}_M \mathbf{n}, {}_M \mathbf{n})), \quad (3.4.26)$$

(notation used described in Section 3.2.3, page 75). Define, also, $D : (\mathcal{S}^2)^N \ni \mathbf{n} \mapsto D(\mathbf{n}) \in \mathbb{R}_{\geq 0}$ as

$$D(\mathbf{n}) = \sum_{k=1}^{k=M} d_k({}_k \mathbf{n}, {}_k \mathbf{n}) = \gamma \sum_{k=1}^{k=M} (1 - {}_k \mathbf{n}^T {}_k \mathbf{n}), \quad (3.4.27)$$

named, hereafter, total distance function in the network of unit vectors. Note that $D(\mathbf{n}) = 0 \Leftrightarrow \exists \mathbf{n}^* \in \mathbb{S}^2 : \mathbf{n} = (\mathbf{1}_N \otimes \mathbf{n}^*)$, which means Problem 3.4.2 is solved, if along a trajectory $\mathbf{x}(\cdot)$ of (3.4.14), $\lim_{t \rightarrow \infty} D(\mathbf{n}(t)) = 0$. It follows from (3.4.23) that, if $d_k \in \mathcal{D}$ for all $k \in \mathcal{M}$, then (consider notation (3.4.1)-(3.4.4))

$$dD(\mathbf{n})\mathbf{F}_n(\mathcal{R}, \boldsymbol{\omega}, \bar{\mathbf{n}}) \stackrel{(3.4.17),(3.4.23)}{=} \boldsymbol{\omega}^T(\mathcal{R}_1 \oplus \dots \mathcal{R}_N)(B \otimes \mathbf{I})\mathbf{e}(\mathbf{n}). \quad (3.4.28)$$

Notice that (3.4.28) follows from (3.4.20), which is the reason for imposing such condition. For convenience, denote

$$d^{\min} := \max_{\mathbf{n}_1, \mathbf{n}_2 \in \mathbb{S}^2} d(1 - \mathbf{n}_1^T \mathbf{n}_2) = \max_{s \in [0, 2]} f(s) = 2\gamma, \quad (3.4.29)$$

which plays an important role in this and the following sections.

Proposition 3.4.9. *Given (3.4.25) and (3.4.27), it holds that (let $\mathbf{n} = (\mathbf{n}_1, \dots, \mathbf{n}_N) \in (\mathbb{S}^2)^N$)*

$$D(\mathbf{n}) < d^{\min} \Leftrightarrow \max_{(i,j) \in \mathcal{E}} \mathbf{n}_i^T \mathbf{n}_j > -1, \quad (3.4.30)$$

$$\max_{\mathbf{n} \in (\mathbb{S}^2)^N} \|\mathbf{E}(\mathbf{n})\| < \infty. \quad (3.4.31)$$

Proof. The fist inequality follows from the definition of D in (3.4.27) (and from (3.4.29)). The latter inequality holds, since the set $(\mathbb{S}^2)^N$ is compact and the function \mathbf{e} is continuous in $(\mathbb{S}^2)^N$. \square

Solution to Problem 3.4.2

In this section, we present the controllers for the torques of each agent. For each agent $i \in \mathcal{N}$, we design a controller that is a function of $|\mathcal{N}_i| + 1$ measurements: $|\mathcal{N}_i|$ measurements corresponding to the *distance measurements* between agent i and its $|\mathcal{N}_i|$ neighbors, and 1 measurement corresponding to the body frame angular velocity. More specifically, at the state $\mathbf{x} \in \Omega_x$, we assume each agent i measures $\mathbf{h}_i(\mathbf{x})$, where $\mathbf{h}_i : \Omega_x \ni \mathbf{x} \mapsto \mathbf{h}_i(\mathbf{x}) \in (\mathbb{S}^2)^{|\mathcal{N}_i|} \times \mathbb{R}^3$ is given by

$$\mathbf{h}_i(\mathbf{x}) := (\mathcal{R}_i^T \mathcal{R}_{j_1} \bar{\mathbf{n}}_j, \dots, \mathcal{R}_i^T \mathcal{R}_{j_{|\mathcal{N}_i|}} \bar{\mathbf{n}}_j, \boldsymbol{\omega}_i), \quad (3.4.32)$$

where we used the notation $\mathcal{N}_i = \{i_1, \dots, i_{|\mathcal{N}_i|}\}$. Physically, this means that agent i knows $\bar{\mathbf{n}}_j$ (the *constant* unit vector that it is required to synchronize with), and that it can measure the projection of this unit vector on its orientation frame; each agent i must also measure $\boldsymbol{\omega}_i \in \mathbb{R}^3$, which does not require an inertial reference frame. We then propose, for each agent $i \in \mathcal{N}$, the following decentralized output feedback control law $\mathbf{T}_i^h : (\mathbb{S}^2)^{|\mathcal{N}_i|} \times \mathbb{R}^3 \ni (\mathbf{h}_{i,1}, \dots, \mathbf{h}_{i,|\mathcal{N}_i|}, \mathbf{h}_{i,|\mathcal{N}_i|+1}) = \mathbf{h}_i \mapsto \mathbf{T}_i^{cl}(\mathbf{h}_i) \in \mathbb{R}^3$ defined as

$$\mathbf{T}_i^{cl}(\mathbf{h}_i) := -\boldsymbol{\sigma}(\mathbf{h}_{i,|\mathcal{N}_i|+1}) - \sum_{l=1}^{l=|\mathcal{N}_i|} \mathbf{e}(\bar{\mathbf{n}}_i, \mathbf{h}_{i,l}), \quad (3.4.33)$$

with $\sigma(\mathbf{x}) = k \frac{\sigma \mathbf{x}}{\sqrt{\sigma^2 + \mathbf{x}^T \mathbf{x}}}$ (for some $k, \sigma > 0$). We can then also write the control law $\mathbf{T}_i^{cl} : \Omega_x \ni \mathbf{x} \mapsto \mathbf{T}_i^{cl}(\mathbf{x}) \in \mathbb{R}^3$ as the composition of (3.4.33) with the output function (3.4.32), i.e.,

$$\mathbf{T}_i^{cl}(\mathbf{x}) := \mathbf{T}_i^h(\mathbf{h}_i(\mathbf{x})) = -\sigma(\boldsymbol{\omega}_i) - \sum_{l=1}^{l=|\mathcal{N}_i|} \mathbf{e}_{\kappa(i, i_l)} (\bar{\mathbf{n}}_i, \mathcal{R}_i^T \mathbf{n}_{i_l}). \quad (3.4.34)$$

The controller function in (3.4.34) is decentralized since it depends on the output function (3.4.32) which is not surjective, and thus the complete state (at a particular time instant) of the system cannot be reconstructed from one single measurement. Also, (3.4.34) can be implemented without the knowledge of an inertial reference: in (3.4.32) measuring $\mathcal{R}_i^T \mathcal{R}_{i_l} \bar{\mathbf{n}}_{i_l}$ for all $l \in \{1, \dots, |\mathcal{N}_i|\}$ only requires the measurement of the projection of $\bar{\mathbf{n}}_{i_l}$ in agent's i body orientation frame; while $\boldsymbol{\omega}_i$ is also measured in agent's i body orientation frame. Moreover the proposed control law in (3.4.34) may also be implemented with limited actuation, since

$$\|\mathbf{T}_i^{cl}(\cdot)\| \leq k\sigma + |\mathcal{N}_i|\gamma, \text{ for each } i \in \mathcal{N}. \quad (3.4.35)$$

We can now present the complete control law $\mathbf{T}^{cl} : \Omega_x \ni \mathbf{x} \mapsto \mathbf{T}^{cl}(\mathbf{x}) \in \mathbb{R}^{3N}$, (see Notation in Section 1.3, 8, for \oplus)

$$\mathbf{T}^{cl}(\mathbf{x}) := (\mathbf{T}_1^{cl}(\mathbf{x}), \dots, \mathbf{T}_N^{cl}(\mathbf{x})) \quad (3.4.36)$$

$$= -(\sigma(\boldsymbol{\omega}_1), \dots, \sigma(\boldsymbol{\omega}_N)) - (\mathcal{R}_1 \oplus \dots \oplus \mathcal{R}_N)^T (B \otimes \mathbf{I}) \mathbf{e}(\mathbf{n}). \quad (3.4.37)$$

Constrained Torque

A natural constraint in a physical system is to require the torque provided by agent $i \in \mathcal{N}$ to be orthogonal to $\bar{\mathbf{n}}_i$. In satellites, thrusters that provide torque along $\bar{\mathbf{n}}_i$ might be unavailable; also, controlling the space orthogonal to $\bar{\mathbf{n}}_i$ can be left as an additional degree of freedom, in order to accomplish some other control objectives. However, the control laws proposed in (3.4.34) require full torque actuation, in particular, (3.4.34) requires each agent to provide torque on the plane orthogonal to $\bar{\mathbf{n}}_i$. Indeed, since $\mathbf{n}_1^T \mathbf{e}(\mathbf{n}_1, \cdot) = 0, \forall \mathbf{n}_1 \in \mathbb{S}^2$ (see (3.4.25)), it follows that, for all $i \in \mathcal{N}$,

$$\bar{\mathbf{n}}_i^T \mathbf{T}_i^{cl}(\mathbf{x}) = \bar{\mathbf{n}}_i^T \sigma(\boldsymbol{\omega}_i), \quad (3.4.38)$$

which is not necessarily 0 (with \mathbf{x} as in (3.4.5)). In short, previously, we provided control laws $\mathbf{T}_i^{cl} : \Omega_x \mapsto \mathbb{R}^3$ which require full torque by each agent $i \in \mathcal{N}$, and in this section we provide constrained control laws $\bar{\mathbf{T}}_i^{cl} : \Omega_x \mapsto \{\mathbf{z} \in \mathbb{R}^3 : \mathbf{z}^T \bar{\mathbf{n}}_i = 0\}$, i.e., control laws which do not require torque along $\bar{\mathbf{n}}_i$. Let us anticipate a future result by announcing that the constrained control law can only be used by agent $i \in \mathcal{N}$ when the unit vector to be synchronized by agent $i \in \mathcal{N}$, namely $\bar{\mathbf{n}}_i$, is a principal axis of that agent (i.e., when $\bar{\mathbf{n}}_i$ is an eigenvector of J_i). Consider then $\bar{\mathbf{T}}_i^{cl} : \Omega_x \ni \mathbf{x} \mapsto \bar{\mathbf{T}}_i^{cl}(\mathbf{x}) \in \{\mathbf{z} \in \mathbb{R}^3 : \mathbf{z}^T \bar{\mathbf{n}}_i = 0\}$ defined as (\mathbf{x} as in (3.4.5))

$$\bar{\mathbf{T}}_i^{cl}(\mathbf{x}) = \Pi(\bar{\mathbf{n}}_i) \mathbf{T}_i^{cl}(\mathbf{x}) \stackrel{(3.4.34)}{=} -\sigma(\Pi(\bar{\mathbf{n}}_i) \boldsymbol{\omega}_i) - \sum_{l=1}^{l=|\mathcal{N}_i|} \mathbf{e}(\bar{\mathbf{n}}_i, \mathcal{R}_i^T \mathbf{n}_{i_l}). \quad (3.4.39)$$

Additionally, consider a partition of \mathcal{N} , i.e., $\bar{\mathcal{L}} \cup \mathcal{L} = \mathcal{N}$ with $\bar{\mathcal{L}} \cap \mathcal{L} = \emptyset$; where $\bar{\mathcal{L}}$ is a subset (possibly empty) of the agents whose unit vector to synchronize is an eigenvector of their moment of inertia, i.e.,

$$\bar{\mathcal{L}} \subseteq \{i \in \mathcal{N} : \exists \lambda_i \text{ s.t. } J_i \bar{\mathbf{n}}_i = \lambda_i \bar{\mathbf{n}}_i\}. \quad (3.4.40)$$

Then we propose the complete control law $\bar{\mathbf{T}}^{cl} : \Omega_x \mapsto \mathbb{R}^{3N}$ defined as

$$\begin{cases} (\mathbf{e}_i \otimes \mathbf{1}_3)^T \bar{\mathbf{T}}^{cl}(\mathbf{x}) := \bar{\mathbf{T}}_i^{cl}(\mathbf{x}) & \forall i \in \bar{\mathcal{L}}, \\ (\mathbf{e}_i \otimes \mathbf{1}_3)^T \bar{\mathbf{T}}^{cl}(\mathbf{x}) := \mathbf{T}_i^{cl}(\mathbf{x}) & \forall i \in \mathcal{L}, \end{cases} \quad (3.4.41)$$

i.e., for agents whose unit vector to synchronize is a principal axis, either control law (3.4.34) or (3.4.39) is chosen, and, for all other agents, control law (3.4.34) is chosen. As such, agents whose unit vector to synchronize is a principal axis have an option between using full torque control or constrained torque control. The disadvantage with the control law in (3.4.39) is that, along a trajectory of the closed-loop system, and for all $i \in \bar{\mathcal{L}}$, $\lim_{t \rightarrow \infty} \bar{\mathbf{n}}_i^T \boldsymbol{\omega}_i(t)$ is not guaranteed to exist and be 0; i.e., an agent that opts for (3.4.39) can asymptotically spin, with non-zero angular velocity, around $\bar{\mathbf{n}}_i$ (nonetheless, we can guarantee that $\sup_{t \geq 0} \|\boldsymbol{\omega}_i(t)\| < \infty \Rightarrow \sup_{t \geq 0} |\bar{\mathbf{n}}_i^T \boldsymbol{\omega}_i(t)| < \infty$, i.e., if an agent applies (3.4.39) it never spins infinitely fast around its principal axis $\bar{\mathbf{n}}_i$).

For the remainder of this paper, we dedicate efforts in studying the equilibria configurations induced by this control law (for different types of graphs), their stability, and what is the effect of the chosen distance functions.

Lyapunov Function

In addition to the total distance function of the network (3.4.27), let us also define the total rotational kinetic energy of the network

$$H : \mathbb{R}^{3N} \ni (\boldsymbol{\omega}_1, \dots, \boldsymbol{\omega}_N) = \boldsymbol{\omega} \mapsto H(\boldsymbol{\omega}) = \frac{1}{2} \sum_{i=1}^{i=N} \boldsymbol{\omega}_i^T J_i \boldsymbol{\omega}_i \in \mathbb{R}_{\geq 0} \quad (3.4.42)$$

which satisfies

$$dH(\boldsymbol{\omega}) \mathbf{F}_\omega(\boldsymbol{\omega}, \mathbf{T}) \stackrel{(3.4.16)}{=} \sum_{i=1}^{i=N} \boldsymbol{\omega}_i^T J_i \mathbf{f}_{\boldsymbol{\omega}_i}(\boldsymbol{\omega}_i, \mathbf{T}_i) \stackrel{(3.4.13)}{=} \sum_{i=1}^{i=N} \boldsymbol{\omega}_i^T \mathbf{T}_i = \boldsymbol{\omega}^T \mathbf{T} \quad (3.4.43)$$

where we used the notation (3.4.1)–(3.4.6). Combining (3.4.27) and (3.4.42), consider then the Lyapunov function (next, we use the notation in (3.4.1)–(3.4.4))

$$V : \Omega_x \ni \mathbf{x} \mapsto V(\mathbf{x}) = D(\mathbf{n}) + H(\boldsymbol{\omega}) \in \mathbb{R}_{\geq 0}, \quad (3.4.44)$$

and the function $W : \mathbb{R}^{3N} \in \boldsymbol{\omega} \mapsto W(\boldsymbol{\omega}) \in \mathbb{R}_{\geq 0}$ defined as

$$\begin{aligned} W(\boldsymbol{\omega}) &:= -dV(\mathbf{x}) \mathbf{f}_x(\mathbf{x}, \bar{\mathbf{T}}^{cl}(\mathbf{x})) (\forall \mathbf{n} \in (\mathbb{S}^2)^N) \\ &\stackrel{(3.4.28)}{=} -\boldsymbol{\omega}^T (\mathcal{R}_1 \oplus \dots \oplus \mathcal{R}_N)^T (B \otimes \mathbf{I}) \mathbf{e}(\mathbf{n}) - \boldsymbol{\omega}^T \bar{\mathbf{T}}^{cl}(\mathbf{x}) \\ &\stackrel{(3.4.37)}{=} \sum_{i \in \mathcal{L}} \boldsymbol{\omega}_i^T \boldsymbol{\sigma}(\boldsymbol{\omega}_i) + \sum_{j \in \bar{\mathcal{L}}} \boldsymbol{\omega}_j^T \Pi(\bar{\mathbf{n}}_j) \boldsymbol{\sigma}(\boldsymbol{\omega}_j). \end{aligned} \quad (3.4.45)$$

Finally, denote (\mathbf{x} as in (3.4.5))

$$\begin{aligned}\Gamma := & \{\mathbf{x} \in \Omega_x : W(\boldsymbol{\omega}) = \mathbf{0}\} \\ (3.4.45) = & \{\mathbf{x} \in \Omega_x : \boldsymbol{\omega}_i = \mathbf{0}, i \in \mathcal{L}, \Pi(\bar{\mathbf{n}}_j)\boldsymbol{\omega}_j = \mathbf{0}, j \in \bar{\mathcal{L}}\} \\ = & \{\mathbf{x} \in \Omega_x : \boldsymbol{\omega}_i = \mathbf{0}, i \in \mathcal{L}, \boldsymbol{\omega}_j = \bar{\mathbf{n}}_j(\bar{\mathbf{n}}_j^T \boldsymbol{\omega}_j), j \in \bar{\mathcal{L}}\}\end{aligned}\quad (3.4.46)$$

In what follows, let $\mathbf{x} \in \Gamma$. It then follows that for $i \in \mathcal{L}$

$$\mathbf{f}_n(\mathcal{R}_i, \boldsymbol{\omega}_i, \bar{\mathbf{n}}_i) \stackrel{(3.4.46)}{=} \mathbf{f}_n(\mathcal{R}_i, \mathbf{0}, \bar{\mathbf{n}}_i) \stackrel{(3.4.9)}{=} \mathbf{0}, \quad (3.4.47)$$

and for $i \in \bar{\mathcal{L}}$

$$\mathbf{f}_n(\mathcal{R}_i, \boldsymbol{\omega}_i, \bar{\mathbf{n}}_i) \stackrel{(3.4.46)}{=} \mathbf{f}_n(\mathcal{R}_i, \bar{\mathbf{n}}_i(\bar{\mathbf{n}}_i^T \boldsymbol{\omega}_i), \bar{\mathbf{n}}_i) \stackrel{(3.4.9)}{=} (\bar{\mathbf{n}}_i^T \boldsymbol{\omega}_i) \mathcal{S}(\mathcal{R}_i \bar{\mathbf{n}}_i) \mathcal{R}_i \bar{\mathbf{n}}_i = \mathbf{0}. \quad (3.4.48)$$

Moreover, for $\mathbf{x} \in \Gamma$, it also follows that $\bar{\mathbf{T}}_i^{cl}(\mathbf{x}) = \sum_{l=1}^{l=|\mathcal{N}_i|} \mathbf{e}(\bar{\mathbf{n}}_i, \mathcal{R}_i^T \mathbf{n}_{i_l})$, for every $i \in \mathbb{N}$, and that

$$\begin{aligned}\mathbf{0} = \mathbf{F}_\omega(\mathbf{x}, \bar{\mathbf{T}}^{cl}(\mathbf{x})) := & (\mathbf{f}_{\omega_1}(\boldsymbol{\omega}_1, \bar{\mathbf{T}}_1^{cl}(\mathbf{x})), \dots, \mathbf{f}_{\omega_N}(\boldsymbol{\omega}_N, \bar{\mathbf{T}}_N^{cl}(\mathbf{x}))) \\ (3.4.13) \Leftrightarrow & \mathbf{0} = -\mathcal{S}(\boldsymbol{\omega}_i) J_i \boldsymbol{\omega}_i + \sum_{l=1}^{l=|\mathcal{N}_i|} \mathbf{e}(\bar{\mathbf{n}}_i, \mathcal{R}_i^T \mathbf{n}_{i_l}) \\ (3.4.46) \Leftrightarrow & \mathbf{0} = \sum_{l=1}^{l=|\mathcal{N}_i|} \mathbf{e}(\bar{\mathbf{n}}_i, \mathcal{R}_i^T \mathbf{n}_{i_l}), \forall i \in \mathcal{L} \quad \wedge \\ & \mathbf{0} = \sum_{l=1}^{l=|\mathcal{N}_i|} \mathbf{e}(\bar{\mathbf{n}}_i, \mathcal{R}_i^T \mathbf{n}_{i_l}) - (\bar{\mathbf{n}}_j^T \boldsymbol{\omega}_j)^2 \mathcal{S}(\bar{\mathbf{n}}_j) J_i \bar{\mathbf{n}}_j, \forall i \in \bar{\mathcal{L}} \\ (3.4.40) \Leftrightarrow & \mathbf{0} = \sum_{l=1}^{l=|\mathcal{N}_i|} \mathbf{e}(\bar{\mathbf{n}}_i, \mathcal{R}_i^T \mathbf{n}_{i_l}), \forall i \in \mathcal{N} \\ \Leftrightarrow & \mathbf{0} = (B \otimes \mathbf{I})\mathbf{E}(\mathbf{x}).\end{aligned}\quad (3.4.49)$$

As such, it follows that the largest invariant set contained in (3.4.46) is a subset of $\{\mathbf{x} \in \Omega_x : (B \otimes \mathbf{I})\mathbf{E}(\mathbf{x}) = \mathbf{0}\}$. We see later that, for specific types of graphs, only *planar* equilibria are contained in the previous set.

Proposition 3.4.10. Consider the vector field (3.4.14), the control law (3.4.41), and a trajectory $\mathbf{x}(\cdot)$ of $\dot{\mathbf{x}}(t) = \mathbf{f}_x(t, \mathbf{x}(t), \bar{\mathbf{T}}^{cl}(t, \mathbf{x}(t)))$. Then $\lim_{t \rightarrow \infty} (B \otimes \mathbf{I})\mathbf{E}(\mathbf{x}(t)) = \mathbf{0}$, $\lim_{t \rightarrow \infty} \boldsymbol{\omega}_i(t) = \mathbf{0}$ for $i \in \mathcal{L}$ and $\lim_{t \rightarrow \infty} \Pi(\bar{\mathbf{n}}_j)\boldsymbol{\omega}_j(t) = \mathbf{0}$ for $j \in \bar{\mathcal{L}}$. Moreover, $\sup_{t \geq 0} |\bar{\mathbf{n}}_j^T \boldsymbol{\omega}_j(t)| < \infty$ for $j \in \bar{\mathcal{L}}$.

For the first part of the proof it suffices to apply the LaSalle's invariance principle. For the final part, since $H(\boldsymbol{\omega}(t)) \leq V(\mathbf{x}(t)) \leq V(\mathbf{x}(0))$, for all $t \geq 0$, it follows that $\sup_{t \geq 0} |\bar{\mathbf{n}}_j^T \boldsymbol{\omega}_j(t)| < \infty$.

Denote $\mathbf{f}_x^{cl}(t, \mathbf{x}) := \mathbf{f}_x(t, \mathbf{x}, \bar{\mathbf{T}}^{cl}(t, \mathbf{x}))$ as the closed-loop vector field. Note then that $\Omega_x^{\text{eq}} = \{\mathbf{x} \in \Omega_x : \forall t \geq 0, \mathbf{f}_x^{cl}(t, \mathbf{x}) = \mathbf{0}\}$ provides the set of all equilibrium points, and moreover $\{\mathbf{x} \in \Omega_x : (B \otimes \mathbf{I})\mathbf{E}(\mathbf{x}) = \mathbf{0}, \boldsymbol{\omega}_i = \mathbf{0} \text{ for } i \in \mathcal{L}, \Pi(\bar{\mathbf{n}}_j)\boldsymbol{\omega}_j = \mathbf{0} \text{ for } j \in \bar{\mathcal{L}}\} \subseteq \Omega_x^{\text{eq}}$. As such, Propositions 3.4.10 imply that, under the Proposition's conditions, a trajectory $\mathbf{x}(\cdot)$ converges to the set of equilibrium points (not all points in that set are stable though). Note also then that all configurations where all agents are synchronized are equilibrium configurations (agents are synchronized and not moving

for $i \in \mathcal{L}$, and agents are synchronized and spinning around their principal axis for $i \in \bar{\mathcal{L}}$). Finally, notice that since $\mathbf{e}(\mathbf{S}\mathbf{n}) = \mathbf{e}(\mathbf{n})$ for all $\mathbf{S} \in \{\mathbf{I}_N \otimes \mathcal{R} \in \mathbb{R}^{3N \times 3N} : \mathcal{R} \in \mathbb{SO}(3)\}$ and for all $\mathbf{n} \in (\mathbb{S}^2)^N$, it follows that Ω_x^{eq} has *geometric isomerism* [83]; this means that for every equilibrium configuration, there exists infinite other equilibria configurations which are the same up to a rotation. In Subsection 3.4.5, for tree graphs, we show that Ω_x^{eq} is composed of configurations where agents are either synchronized or diametrically opposed; while in Section 3.4.6, for graphs discussed in Propositions 3.4.3 and 3.4.4, we show that Ω_x^{eq} is composed of configurations where agents belong to a common plane.

Remark 3.4.11. Consider the closed-loop vector field $\mathbf{f}_x^{\text{cl}}(\mathbf{x}) = \mathbf{f}_x(\mathbf{x}, \bar{\mathbf{T}}^{\text{cl}}(\mathbf{x}))$. Additionally, consider the alternative state (denote, for convenience $\mathcal{R}(t) = \mathcal{R}_1(t) \oplus \dots \oplus \mathcal{R}_N \in \mathbb{SO}(3) \oplus \dots \oplus \mathbb{SO}(3)$)

$$\tilde{\mathbf{x}}(t) = (\mathbf{I}_{3N} \oplus \mathcal{R}(t))\mathbf{x}(t) \Leftrightarrow \mathbf{x}(t) = (\mathbf{I}_{3N} \oplus \mathcal{R}^T(t))\tilde{\mathbf{x}}(t) \quad (3.4.50)$$

which evolves according to

$$\dot{\tilde{\mathbf{x}}}(t) = (\mathbf{0} \oplus \dot{\mathcal{R}}(t))\mathbf{x}(t) + (\mathbf{I}_{3N} \oplus \mathcal{R}(t))\mathbf{f}_x^{\text{cl}}(\mathbf{x}(t))|_{\mathbf{x}(t)=(\mathbf{I}_{3N} \oplus \mathcal{R}^T(t))\tilde{\mathbf{x}}(t)} \quad (3.4.51)$$

$$= (\mathbf{I}_{3N} \oplus \mathcal{R}(t))\mathbf{f}_x^{\text{cl}}((\mathbf{I}_{3N} \oplus \mathcal{R}^T(t))\tilde{\mathbf{x}}(t)) =: \mathbf{f}_{\tilde{x}}^{\text{cl}}(\tilde{\mathbf{x}}(t)) \quad (3.4.52)$$

The difference between $\tilde{\mathbf{x}}(\cdot)$ and $\mathbf{x}(\cdot)$ is that all quantities in $\tilde{\mathbf{x}}(\cdot)$ are expressed in the inertial reference frame, while in $\mathbf{x}(\cdot)$ the angular velocities are expressed in the body reference frame of each agent. If $J_i = j_i \mathbf{I}$ for all $i \in \mathcal{N}$, then for any $\mathbf{S} \in \{\mathcal{R} \otimes \mathbf{I}_{2N} \in \mathbb{R}^{6N \times 6N} : \mathcal{R} \in \mathbb{SO}(3)\}$, it can be verified that $\mathbf{f}_{\tilde{x}}^{\text{cl}}(\mathbf{S}\tilde{\mathbf{x}}) = \mathbf{S}\mathbf{f}_{\tilde{x}}^{\text{cl}}(\tilde{\mathbf{x}})$, which implies that the closed-loop dynamics of the agents are invariant to rotations; i.e., given two initial conditions $\tilde{\mathbf{x}}^1(0)$ and $\tilde{\mathbf{x}}^2(0)$ satisfying $\tilde{\mathbf{x}}^1(0) = \mathbf{S}\tilde{\mathbf{x}}^2(0)$, it follows that $\tilde{\mathbf{x}}^1(t) = \mathbf{S}\tilde{\mathbf{x}}^2(t)$ for all $t \geq 0$. This is the case, because when $J_i = j_i \mathbf{I}$, then (3.4.13) reduces to a second order integrator. A similar result has been reported in [83], where the agents are mass points (i.e., agents without moment of inertia). However, in our framework, where in general $J_i \neq j_i \mathbf{I}$ for some $i \in \mathcal{N}$, invariance of the closed-loop dynamics to rotations does not hold due to the term $\mathcal{S}(\boldsymbol{\omega}_i) J_i \boldsymbol{\omega}_i$ in (3.4.13).

3.4.5 Tree Graphs

Let us focus first on static tree graphs. For these graphs, Proposition 3.2.1 states that $\mathcal{N}(B \otimes \mathbf{I}) = \{\mathbf{0}\}$. In this section, we quantify the domain of attraction for synchronization to be asymptotically reached, i.e., we construct a domain Ω_x^0 such that if $\mathbf{x}(0) \in \Omega_x^0$, then all trajectories of (3.4.14) under control law (3.4.41) asymptotically converge to a configuration where all unit vectors are synchronized. Later, we construct another Ω_x^0 , for graphs other than tree graphs, which is smaller in size, and we quantify how much smaller it is.

Theorem 3.4.12. Consider a static tree graph, the vector field (3.4.14), the control law (3.4.41), and a trajectory $\mathbf{x}(\cdot)$ of $\dot{\mathbf{x}}(t) = \mathbf{f}_x(\mathbf{x}(t), \bar{\mathbf{T}}^{\text{cl}}(\mathbf{x}(t)))$. If $\mathbf{x}(0) \in \Omega_x^0 :=$

$\{\mathbf{x} \in \Omega_x : V(\mathbf{x}) < d^{\min} := 2\gamma\}$ then synchronization is asymptotically reached, i.e., $\lim_{t \rightarrow \infty} (\mathbf{n}_i(t) - \mathbf{n}_j(t)) = \mathbf{0}$, for all $(i, j) \in \mathcal{N}^2$.

Proof. Under the Theorem's conditions, we can invoke Proposition 3.4.10 to conclude that $\lim_{t \rightarrow \infty} (B \otimes \mathbf{I})\mathbf{E}(\mathbf{n}(t)) = \mathbf{0}$ and Proposition 3.4.9 to conclude that two neighbors are never arbitrarily close to a configuration where they are diametrically opposed. Since $\mathcal{N}(B \otimes \mathbf{I}) = \{\mathbf{0}\}$, it follows that $\lim_{t \rightarrow \infty} (B \otimes \mathbf{I})\mathbf{E}(\mathbf{n}(t)) \Rightarrow \lim_{t \rightarrow \infty} \mathbf{E}(\mathbf{n}(t)) = \mathbf{0}$. As such, and since two neighbors are never arbitrarily close to a configuration where they are diametrically opposed, it follows that all unit vectors converge to one another. \square

Corollary 3.4.13. Proposition 3.4.10 holds if $r := \frac{H(\omega(0))}{d^{\min}} < 1$ and if

$$\mathbf{n}(0) := (\mathcal{R}_1(0)\bar{\mathbf{n}}_1, \dots, \mathcal{R}_N(0)\bar{\mathbf{n}}_N) \in \mathcal{C}\left(\frac{1}{2} \arccos\left(1 - 2\frac{1-r}{M}\right)\right). \quad (3.4.53)$$

Proof. From Proposition 3.4.6, it follows that, under the Corollary conditions, $D(\mathbf{n}(0)) \leq d^{\min}(1-r)$. Thus, $V(\mathbf{x}(0)) = D(\mathbf{n}(0)) + H(\omega(0)) \leq 1-r + H(\omega(0)) < d^{\min}$, and the Theorem's 3.4.12 conditions are satisfied. \square

Corollary 3.4.13 states that if the total kinetic energy is *small*, and if all neighbors are initially contained in a *small* cone, then synchronization is guaranteed.

If the Theorem's 3.4.12 conditions are not satisfied (namely if $\mathbf{x}(0) \notin \Omega_x^0$), the group of agents can converge to configurations where one or more pairs of neighbors are diametrically opposed. However, it does not provide any insight on whether these equilibrium configurations are stable or unstable. For tree graphs, a configuration where p pairs of neighbors are diametrically opposed can be shown to be unstable. For proving this statement, it suffices to find initial conditions which are arbitrarily close to an equilibrium where p pairs of neighbors are diametrically opposed, but for which convergence to a configuration where at most $p-1$ pairs of neighbors are diametrically opposed is guaranteed; this reasoning implies that all configurations where neighbors are diametrically opposed are unstable, and therefore, only synchronized configurations are stable. A similar result on synchronization in $\mathbb{SO}(3)$ is found in [75], and of synchronization on the sphere is found in [80]. Also, Theorem 3.4.12 does not provide any insight on whether the limits $\lim_{t \rightarrow \infty} \mathbf{n}_i(t)$ (for all $i \in \mathcal{N}$) exist; i.e., even if the unit vectors synchronize, it is not known whether those unit vectors converge to a constant unit vector or a time-varying unit vector. Some preliminaries results are found in cite [116].

3.4.6 Non-Tree Graphs

In this section, we study the equilibria configuration induced by some more general, yet specific, network graphs. Also, we study the local stability properties of the synchronized configuration for arbitrary graphs. We first give the following definition.

Definition 3.4.14. Given n vectors $\mathbf{x}_1, \dots, \mathbf{x}_n \in \mathbb{R}^3$, for $i \in \{1, \dots, n\}$, we say that $\mathbf{x}_1, \dots, \mathbf{x}_n$ belong to a common plane if there exists a unit vector $\boldsymbol{\nu} \in \mathcal{S}^2$ such that $\Pi(\boldsymbol{\nu})\mathbf{x}_i = \mathbf{x}_i$ for all $i \in \{1, \dots, n\}$. We say that $\mathbf{x}_1, \dots, \mathbf{x}_n$ belong to a common unique plane if there exists a single pair of unit vectors $(+\boldsymbol{\nu}, -\boldsymbol{\nu})$, with $\boldsymbol{\nu} \in \mathcal{S}^2$ such that $\Pi(\boldsymbol{\nu})\mathbf{x}_i = \mathbf{x}_i$ for all $i \in \{1, \dots, n\}$.

Let us first discuss a property that is exploited later in this section.

Proposition 3.4.15. Consider $\mathbf{n}_1, \mathbf{n}_2 \in \mathbb{S}^2$. If $\mathcal{S}(\mathbf{n}_1)\mathbf{n}_2 \neq \mathbf{0}$, then \mathbf{n}_1 and \mathbf{n}_2 belong to a common plane.

Proof. Consider $\boldsymbol{\nu} = \frac{\mathcal{S}(\mathbf{n}_1)\mathbf{n}_2}{\|\mathcal{S}(\mathbf{n}_1)\mathbf{n}_2\|} \in \mathcal{S}^2$, which is well defined since $\mathcal{S}(\mathbf{n}_1)\mathbf{n}_2 \neq \mathbf{0}$. It follows that $\Pi(\boldsymbol{\nu})\mathbf{n}_1 = \mathbf{n}_1$ and that $\Pi(\boldsymbol{\nu})\mathbf{n}_2 = \mathbf{n}_2$, which implies that \mathbf{n}_1 and \mathbf{n}_2 belong to a common plane. Moreover, \mathbf{n}_1 and \mathbf{n}_2 belong to a common unique plane, since \mathbf{n}_1 and \mathbf{n}_2 span a two dimensional space. \square

Proposition 3.4.16. Consider $\mathbf{n}_1, \dots, \mathbf{n}_n \in \mathbb{S}^2$, with $|\mathbf{n}_i^T \mathbf{n}_{i+1}| \neq 1$ for all $i = \{1, \dots, n-1\}$. If

$$\pm \frac{\mathcal{S}(\mathbf{n}_1)\mathbf{n}_2}{\|\mathcal{S}(\mathbf{n}_1)\mathbf{n}_2\|} = \dots = \pm \frac{\mathcal{S}(\mathbf{n}_{n-1})\mathbf{n}_n}{\|\mathcal{S}(\mathbf{n}_{n-1})\mathbf{n}_n\|}, \quad (3.4.54)$$

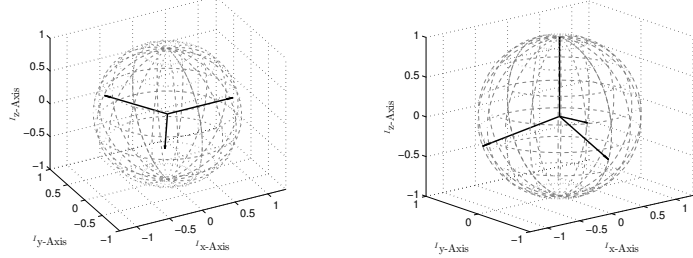
then all unit vectors belong to a common unique plane.

Proof. Consider $n = 3$. Since $|\mathbf{n}_1^T \mathbf{n}_2| \neq 1$ and $|\mathbf{n}_2^T \mathbf{n}_3| \neq 1$, it follows that $\|\mathcal{S}(\mathbf{n}_1)\mathbf{n}_2\| \neq 0$ and $\|\mathcal{S}(\mathbf{n}_2)\mathbf{n}_3\| \neq 0$. Additionally, by assumption, $\pm \frac{\mathcal{S}(\mathbf{n}_1)\mathbf{n}_2}{\|\mathcal{S}(\mathbf{n}_1)\mathbf{n}_2\|} = \pm \frac{\mathcal{S}(\mathbf{n}_2)\mathbf{n}_3}{\|\mathcal{S}(\mathbf{n}_2)\mathbf{n}_3\|}$, is satisfied. Consider then $\boldsymbol{\nu} = \frac{\mathcal{S}(\mathbf{n}_1)\mathbf{n}_2}{\|\mathcal{S}(\mathbf{n}_1)\mathbf{n}_2\|} \in \mathcal{S}^2$. It follows immediately that $\Pi(\boldsymbol{\nu})\mathbf{n}_1 = \mathbf{n}_1$ and that $\Pi(\boldsymbol{\nu})\mathbf{n}_2 = \mathbf{n}_2$. It also follows that $\Pi(\boldsymbol{\nu})\mathbf{n}_3 = (\mathbf{I} - \boldsymbol{\nu}\boldsymbol{\nu}^T)\mathbf{n}_3 = \mathbf{n}_3 - \boldsymbol{\nu}(\boldsymbol{\nu}^T\mathbf{n}_3) = \mathbf{n}_3$, where $\boldsymbol{\nu}^T\mathbf{n}_3 = 0$ follows from taking the inner product of (3.4.54) with \mathbf{n}_3 . Altogether, it follows that $\mathbf{n}_1, \mathbf{n}_2$ and \mathbf{n}_3 belong to a common unique plane (see Proposition 3.4.15). For $n > 3$, it suffices to apply the previous argument $n - 2$ times. \square

Proposition 3.4.17. Consider $\mathbf{n}_1, \dots, \mathbf{n}_n \in \mathbb{S}^2$. If $\pm \mathbf{e}(\mathbf{n}_1, \mathbf{n}_2) = \dots = \pm \mathbf{e}_{n-1}(\mathbf{n}_{n-1}, \mathbf{n}_n)$ then all unit vectors belong to a common plane, which is unique if $\pm \mathbf{e}(\mathbf{n}_1, \mathbf{n}_2) = \dots = \pm \mathbf{e}_{n-1}(\mathbf{n}_{n-1}, \mathbf{n}_n) \neq \mathbf{0}$.

Proof. If $\pm \mathbf{e}(\mathbf{n}_1, \mathbf{n}_2) = \dots = \pm \mathbf{e}_{n-1}(\mathbf{n}_{n-1}, \mathbf{n}_n) \neq \mathbf{0}$, it suffices to invoke Proposition 3.4.16. If $\pm \mathbf{e}(\mathbf{n}_1, \mathbf{n}_2) = \dots = \pm \mathbf{e}_{n-1}(\mathbf{n}_{n-1}, \mathbf{n}_n) = \mathbf{0}$, it follows that $\pm \mathbf{n}_1 = \dots = \pm \mathbf{n}_n$, and therefore, all unit vectors belong to a common plane. \square

Theorem 3.4.18. Consider the vector field (3.4.14), the control law (3.4.41), and a trajectory $\mathbf{x}(\cdot)$ of $\dot{\mathbf{x}}(t) = \mathbf{f}_x(\mathbf{x}(t), \bar{\mathbf{T}}^{cl}(\mathbf{x}(t)))$. If the network graph contains only independent cycles, then for each cycle, all its unit vectors converge to a common plane.



(a) Triangular configuration. (b) Tetrahedron configuration.

Figure 3.17: Equilibrium configurations in a complete graph (\mathcal{K}_3 in Fig. 3.17a and \mathcal{K}_4 in Fig. 3.17b).

Proof. By invoking Proposition 3.4.10, it follows that $\lim_{t \rightarrow \infty} (B \otimes \mathbf{I})\mathbf{E}(\mathbf{n}(t)) = \mathbf{0}$, i.e., $\mathbf{E}(\mathbf{n}(\cdot))$ converges to the null space of $B \otimes \mathbf{I}$. Now, consider a graph with only independent cycles and recall Proposition 3.4.3. Without loss of generality, consider that there is only one independent cycle and that the first $n \geq 3$ edges form that cycle. From Proposition 3.4.3, it follows that $\mathbf{E}(\mathbf{n}) \in \mathcal{N}(B \otimes \mathbf{I}) \Rightarrow \pm \mathbf{e}(_1\mathbf{n}, _1\mathbf{n}) = \dots = \pm \mathbf{e}(_n\mathbf{n}, _n\mathbf{n})$. In turn, from Proposition 3.4.17, it follows that all unit vectors that form the cycle belong to a common plane when $(B \otimes \mathbf{I})\mathbf{E}(\cdot) = \mathbf{0}$. \square

Figure 3.17a exemplifies the statement in Theorem 3.4.18, where three agents form a complete graph, and thus there is one independent cycle, and where the distance function is the same for all edges. In this scenario, and because the distance function is the same for all edges, the unit vectors form an equilateral triangle. In Fig. 3.17b, four agents form a complete graph, which does not fit the conditions of Theorem 3.4.18 (a complete graph with four agents has three cycles, but they all share edges with each other, i.e., they are not independent); for this scenario, we can find equilibria configurations where the unit vectors do not belong to a common plane, and, in Fig. 3.17b, an equilibrium configuration is shown where the four agents form a tetrahedron.

Theorem 3.4.19. Consider the vector field (3.4.14), the control law (3.4.41), and a trajectory $\mathbf{x}(\cdot)$ of $\dot{\mathbf{x}}(t) = \mathbf{f}_x(\mathbf{x}(t), \bar{\mathbf{T}}^{cl}(\mathbf{x}(t)))$. If the network graph contains only independent cycles or cycles that share only one edge, then all unit vectors belonging to each independent cycle converge to a common plane, and all unit vectors belonging to each pair of cycles that share only one edge also converge to a common plane.

Proof. For network graphs with only independent cycles, the proof follows the same steps as those in the proof of Theorem 3.4.18. Thus, and w.l.o.g, consider graphs with only two cycles that share only one edge, and recall Proposition 3.4.4 (adding other cycles does not affect the following conclusions, as long as those cycles are formed by other edges other than those that form the two previously mentioned cycles). W.l.o.g, assume that the first $n = q + s - 1 \geq 5$ edges are part of the two cycles that share only

one edge, where the edges $\{1, \dots, q-1, q\}$ form the first cycle ($|\{1, \dots, q-1, q\}| = q$), while the edges $\{q, q+1, \dots, n\}$ form the second cycle ($|\{q, q+1, \dots, n\}| = s$), and with the q^{th} edge as the shared edge between cycles (for brevity, denote $p = q-1$ and $r = q+1$). Under the Theorem's conditions, and by invoking Proposition 3.4.10, it follows that $\lim_{t \rightarrow \infty} (B \otimes \mathbf{I}) \mathbf{E}(\mathbf{n}(t)) = \mathbf{0}$, i.e., $\mathbf{E}(\mathbf{n}(\cdot))$ converges to the null space of $B \otimes \mathbf{I}$. From Proposition 3.4.4, $\mathcal{N}(B \otimes \mathbf{I})$ is spanned by the vector

$$\left[(\bar{\mathbf{1}}_{q-1} \otimes \boldsymbol{\alpha})^T \quad (\boldsymbol{\alpha} + \boldsymbol{\beta})^T \quad (\bar{\mathbf{1}}_{s-1} \otimes \boldsymbol{\beta})^T \quad \mathbf{0}^T \right]^T, \quad (3.4.55)$$

for any $\boldsymbol{\alpha}, \boldsymbol{\beta} \in \mathbb{R}^3$ (see Proposition 3.4.4).

Suppose ${}_q\mathbf{n} \neq \pm {}_{\bar{q}}\mathbf{n}$, where ${}_q\mathbf{n}$ and ${}_{\bar{q}}\mathbf{n}$ are the unit vectors that form edge q ; then $\mathbf{e}({}_q\mathbf{n}, {}_{\bar{q}}\mathbf{n}) \neq \mathbf{0}$ and therefore $\boldsymbol{\alpha} + \boldsymbol{\beta} \neq \mathbf{0} \Rightarrow \boldsymbol{\alpha} \neq \mathbf{0} \vee \boldsymbol{\beta} \neq \mathbf{0}$; moreover, ${}_q\mathbf{n}$ and ${}_{\bar{q}}\mathbf{n}$ form a common unique plane (see Proposition 3.4.15).

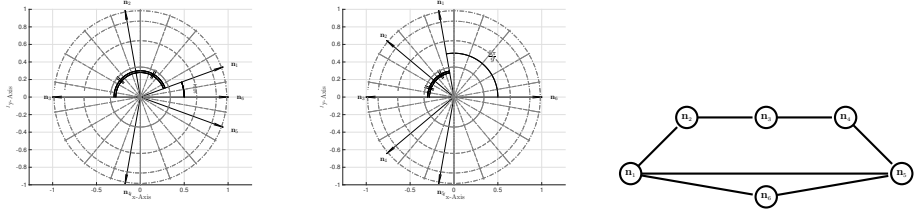
If $\boldsymbol{\alpha} = \mathbf{0}$ (or $\boldsymbol{\beta} = \mathbf{0}$), it follows that $\pm \mathbf{e}({}_1\mathbf{n}, {}_1\mathbf{n}) = \dots = \pm \mathbf{e}({}_p\mathbf{n}, {}_{\bar{p}}\mathbf{n}) = \mathbf{0}$, and therefore the unit vectors in the first (or second) cycle belong to a common plane (Proposition 3.4.17). Also, if $\boldsymbol{\alpha} = \mathbf{0}$ (or $\boldsymbol{\beta} = \mathbf{0}$), it follows that $\boldsymbol{\beta} \neq \mathbf{0}$ (or $\boldsymbol{\alpha} \neq \mathbf{0}$), and therefore $\pm \mathbf{e}({}_r\mathbf{n}, {}_{\bar{r}}\mathbf{n}) = \dots = \pm \mathbf{e}({}_n\mathbf{n}, {}_{\bar{n}}\mathbf{n}) \neq \mathbf{0}$, and therefore all unit vectors in the second (or first) cycle belong to a common unique plane (Proposition 3.4.17). However, since the unit vectors of the first (or second) cycle are either all synchronized or some are diametrically opposed to others, it follows that all unit vectors in both cycles belong to a common unique plane.

Consider now the case where $\boldsymbol{\alpha} \neq \mathbf{0}$ and $\boldsymbol{\beta} \neq \mathbf{0}$, which implies that $\pm \mathbf{e}({}_1\mathbf{n}, {}_1\mathbf{n}) = \dots = \pm \mathbf{e}({}_p\mathbf{n}, {}_{\bar{p}}\mathbf{n}) \neq \mathbf{0}$ as well as $\pm \mathbf{e}({}_r\mathbf{n}, {}_{\bar{r}}\mathbf{n}) = \dots = \pm \mathbf{e}({}_n\mathbf{n}, {}_{\bar{n}}\mathbf{n}) \neq \mathbf{0}$. Thus, by Proposition 3.4.17, it follows that all unit vectors in each cycle belong to a common plane. Since ${}_q\mathbf{n}$ and ${}_{\bar{q}}\mathbf{n}$ form a common unique plane, and since ${}_q\mathbf{n}$ and ${}_{\bar{q}}\mathbf{n}$ belong simultaneously to both cycles, it follows that all unit vectors in both cycles belong to a common unique plane.

Suppose now that ${}_q\mathbf{n} = \pm {}_{\bar{q}}\mathbf{n}$. Then $\mathbf{e}({}_q\mathbf{n}, {}_{\bar{q}}\mathbf{n}) = \mathbf{0}$, and it follows that $\boldsymbol{\alpha} + \boldsymbol{\beta} = \mathbf{0} \Rightarrow \boldsymbol{\alpha} = -\boldsymbol{\beta} \neq \mathbf{0} \vee \boldsymbol{\alpha} = \boldsymbol{\beta} = \mathbf{0}$. If $\boldsymbol{\alpha} = \boldsymbol{\beta} = \mathbf{0}$, then $\mathbf{E}(\mathbf{n}) = \mathbf{0} \Leftrightarrow \pm \mathbf{n}_1 = \dots = \pm \mathbf{n}_N$ and the Theorem's conclusions follow. If $\boldsymbol{\alpha} = -\boldsymbol{\beta} \neq \mathbf{0}$, then $\pm \mathbf{e}({}_1\mathbf{n}, {}_1\mathbf{n}) = \dots = \pm \mathbf{e}({}_p\mathbf{n}, {}_{\bar{p}}\mathbf{n}) = \pm \mathbf{e}({}_r\mathbf{n}, {}_{\bar{r}}\mathbf{n}) = \dots = \pm \mathbf{e}({}_n\mathbf{n}, {}_{\bar{n}}\mathbf{n}) \neq \mathbf{0}$, which implies that all unit vectors in both cycles belong to a common unique plane (Proposition 3.4.17). \square

Figure 3.18 exemplifies the statement in Theorem 3.4.19, with a network of six agents, with the network graph in Fig. 3.18c. In this scenario, there are two cycles that share only one edge, one cycle composed of unit vectors $\{\mathbf{n}_1, \mathbf{n}_2, \mathbf{n}_3, \mathbf{n}_4, \mathbf{n}_5\}$, a second cycle composed of unit vectors $\{\mathbf{n}_1, \mathbf{n}_5, \mathbf{n}_6\}$, and where the shared edge is formed by $\{\mathbf{n}_1, \mathbf{n}_5\}$. There are at least two equilibria configurations (apart from configurations where $\mathbf{n}_i = \pm \mathbf{n}_j$ for some i and j), which are given in Fig. 3.18a and Fig. 3.18b, where in both cases all unit vectors belong to a common plane.

Propositions 3.4.18 and 3.4.19 focus on equilibria for some general, yet specific, network graphs. For arbitrary graphs, we can find equilibria configurations as exemplified in Fig. 3.17b, where four agents in a complete graph are at equilibrium when forming a tetrahedron.



(a) Equilibrium configuration with network graph shown in Fig. 3.18c. (b) Equilibrium configuration with network graph shown in Fig. 3.18c. (c) Graph with two cycles that share only one edge.

Figure 3.18: Two equilibrium configurations for group with network graph shown in Fig. 3.18c.

We now present a proposition, which will be useful in guaranteeing local asymptotic stability of incomplete attitude synchronization for arbitrary graphs.

Proposition 3.4.20. Consider $\mathbf{n} \in \bar{\mathcal{C}}(\alpha)$, for some $\alpha \in [0, \frac{\pi}{2})$, and assume that *i*) the network graph is connected; *ii*) $\mathbf{E}(\mathbf{n}) \in \mathcal{N}(B \otimes \mathbf{I})$, with $\mathbf{E}(\cdot)$ as defined in (3.4.26). This takes place if and only if $\exists \boldsymbol{\nu} \in \mathbb{S}^2 : \mathbf{n} = (\mathbf{1}_N \otimes \boldsymbol{\nu}) \Leftrightarrow \mathbf{n} \in \bar{\mathcal{C}}(0) \Leftrightarrow \alpha = 0$.

Proof. For the sufficiency statement, it follows that, if $\exists \boldsymbol{\nu} \in \mathbb{S}^2 : \mathbf{n} = (\mathbf{1}_N \otimes \boldsymbol{\nu})$, then all unit vectors are contained in a $\frac{\pi}{2}$ -cone, i.e., $\mathbf{n} \in \mathcal{C}(\frac{\pi}{2})$; and, moreover, $\mathbf{E}(\mathbf{1}_N \otimes \boldsymbol{\nu}) = \mathbf{0} \subseteq \mathcal{N}(B \otimes \mathbf{I})$.

For the necessity statement, the proof is as follows. For a tree graph, $(B \otimes \mathbf{I})\mathbf{E}(\mathbf{n}) = \mathbf{0} \Leftrightarrow \mathbf{E}(\mathbf{n}) = \mathbf{0}$ follows. This implies that $\mathbf{n}_i = \pm \mathbf{n}_j$ for all $(i, j) \in \mathcal{N} \times \mathcal{N}_i$, but since $\mathbf{n} \in \mathcal{C}(\frac{\pi}{2})$, it follows that $\mathbf{n}_i = \mathbf{n}_j$ for all $(i, j) \in \mathcal{N} \times \mathcal{N}_i$. In a connected graph, this implies that $\mathbf{n}_i = \mathbf{n}_j$ for all $(i, j) \in \mathcal{N} \times \mathcal{N}$, and therefore $\exists \boldsymbol{\nu} \in \mathbb{S}^2 : \mathbf{n} = (\mathbf{1}_N \otimes \boldsymbol{\nu})$.

For an arbitrary graph, the null space of $(B \otimes \mathbf{I})$ may be more than $\mathbf{0}$, i.e., $(B \otimes \mathbf{I})\mathbf{E}(\cdot) = \mathbf{0} \neq \mathbf{E}(\cdot) = \mathbf{0}$. We anticipate the final result by stating that if $\mathbf{n} \in \mathcal{C}(\frac{\pi}{2})$, then $(B \otimes \mathbf{I})\mathbf{E}(\mathbf{n}) = \mathbf{0} \Rightarrow \mathbf{E}(\mathbf{n}) = \mathbf{0}$, in which case we conclude again that $\exists \boldsymbol{\nu} \in \mathbb{S}^2 : \mathbf{n} = (\mathbf{1}_N \otimes \boldsymbol{\nu})$. Consider then an $\mathbf{n} \in (\mathcal{S}^2)^N$, such that $(B \otimes \mathbf{I})\mathbf{E}(\mathbf{n}) = \mathbf{0}$. This means that, for every $i \in \mathcal{N}$ (B_{ii} stands for the i^{th} row of B),

$$\mathbf{0} = (B_{ii} \otimes \mathbf{I})\mathbf{E}(\mathbf{n}) \stackrel{(3.4.26)}{=} \mathcal{S}(\mathbf{n}_i) \sum_{j \in \mathcal{N}_i} (1 - \mathbf{n}_i^T \mathbf{n}_j) \mathbf{n}_j. \quad (3.4.56)$$

Since $\mathbf{n} \in \bar{\mathcal{C}}(\alpha)$, it follows that there exists a unit vector $\boldsymbol{\mu} \in \mathbb{S}^2$, such that $\boldsymbol{\mu}^T \mathbf{n}_i \geq \cos(\alpha) > 0$ for all $i \in \mathcal{N}$. Taking the inner product of (3.4.56) with $\mathcal{S}(\mathbf{n}_i) \boldsymbol{\mu}$, it follows that $\boldsymbol{\mu}^T \Pi(\mathbf{n}_i) \sum_{j \in \mathcal{N}_i} \mathbf{n}_j = \mathbf{0}$, which can be expanded into

$$\sum_{j \in \mathcal{N}_i} (\boldsymbol{\mu}^T \mathbf{n}_j - (\boldsymbol{\mu}^T \mathbf{n}_i) \mathbf{n}_i^T \mathbf{n}_j) = 0. \quad (3.4.57)$$

Now, consider the set $\mathcal{T} = \{i \in \mathcal{N} : i = \arg \max_{i \in \mathcal{N}} (1 - \boldsymbol{\mu}^T \mathbf{n}_i)\}$, and choose $k \in \mathcal{T}$ (in the end, we show that, in fact, $\mathcal{T} = \mathcal{N}$). Notice that $0 < \cos(\alpha) \leq \boldsymbol{\mu}^T \mathbf{n}_k \leq \boldsymbol{\mu}^T \mathbf{n}_j$ for all $k \in \mathcal{T}$ and all $j \in \mathcal{N}$. As such, it follows from (3.4.57) with $i = k$ that

$$0 \leq \cos(\alpha) \gamma \sum_{j \in \mathcal{N}_k} (1 - \mathbf{n}_k^T \mathbf{n}_j) \leq \gamma \sum_{j \in \mathcal{N}_k} (\boldsymbol{\mu}^T \mathbf{n}_j - (\boldsymbol{\mu}^T \mathbf{n}_k) \mathbf{n}_k^T \mathbf{n}_j) = 0. \quad (3.4.58)$$

Notice that the lower bound (on the left side of (3.4.58)) is non-negative and zero if and only if all neighbors of agent k are synchronized with itself. As such, it follows from (3.4.58) that all neighbors of agent k are contained in \mathcal{T} , i.e., $\mathcal{N}_k \subset \mathcal{T}$. As such, the same procedure as before can be followed for the neighbors of agent k , to conclude that the neighbors of the neighbors of agent k are all synchronized. In a connected graph, by applying the previous reasoning at most $N - 1$ times, it follows that all unit vectors are synchronized, or, equivalently, that $\exists \boldsymbol{\nu} \in \mathbb{S}^2 : \mathbf{n} = (\mathbf{1}_N \otimes \boldsymbol{\nu})$. \square

Proposition 3.4.20 has the following interpretation. Recall that $\{\mathbf{x} \in \Omega_x : (B \otimes \mathbf{I})\mathbf{E}(\mathbf{n}) = \mathbf{0}, \boldsymbol{\omega}_i = \mathbf{0} \text{ for } i \in \mathcal{L}, \Pi(\bar{\mathbf{n}}_j)\boldsymbol{\omega}_j = \mathbf{0} \text{ for } j \in \bar{\mathcal{L}}\} \subseteq \Omega_x^{\text{eq}}$, where Ω_x^{eq} is the set of equilibrium points. For example, we have seen that, for specific graphs, all equilibrium configurations are such that all unit vectors belong to a common plane (see Theorems 3.4.18 and 3.4.19), as illustrated in Fig. 3.18. However, if we can guarantee that along a trajectory $\mathbf{x}(\cdot)$ of $\dot{\mathbf{x}}(t) = \mathbf{f}_x(\mathbf{x}(t), \bar{\mathbf{T}}^{cl}(\mathbf{x}(t)))$, $\exists \alpha \in [0, \frac{\pi}{2}] : \mathbf{n}(t) \in \bar{\mathcal{C}}(\alpha)$, $\forall t \geq 0$, i.e., if we can guarantee that all unit vectors remain in a closed α -cone smaller than an open $\frac{\pi}{2}$ -cone, then we can invoke Proposition 3.4.20 to conclude that $\lim_{t \rightarrow \infty} (B \otimes \mathbf{I})\mathbf{E}(\mathbf{n}(t)) = \mathbf{0} \Rightarrow \lim_{t \rightarrow \infty} (\mathbf{n}_i(t) - \mathbf{n}_j(t)) = \mathbf{0}$; i.e., that convergence of $\mathbf{E}(\mathbf{n}(\cdot))$ to the null space of $B \otimes \mathbf{I}$ implies synchronization of the agents.

This motivates us to introduce a distance $d^* > 0$, which will be useful in guaranteeing that, along a trajectory $\mathbf{x}(\cdot)$, $\exists \alpha \in [0, \frac{\pi}{2}] : \mathbf{n}(t) \in \bar{\mathcal{C}}(\alpha)$, $\forall t \geq 0$. Define

$$d^* = \gamma \left(1 - \cos \left(\frac{\pi}{3} \frac{1}{N-1} \right) \right) < d^{\min} := 2\gamma. \quad (3.4.59)$$

Notice that $d^* < d^{\min}$ (since $N \geq 2$). As shown next, if $D(\mathbf{n}(0)) < \frac{d^*}{M}$ (and $H(\boldsymbol{\omega}(0)) = 0$), then the network of unit vectors is forever contained in a closed α -cone, for some $\alpha \in [0, \frac{\pi}{2}]$.

Theorem 3.4.21. *Consider an arbitrary network graph, the vector field (3.4.14), the control law (3.4.41), and a trajectory $\mathbf{x}(\cdot)$ of $\dot{\mathbf{x}}(t) = \mathbf{f}_x(\mathbf{x}(t), \bar{\mathbf{T}}^{cl}(\mathbf{x}(t)))$. If $\mathbf{x}(0) \in \Omega_x^0 = \{\mathbf{x} \in \Omega_x : V(\mathbf{x}) < d^*\}$ then synchronization is asymptotically reached, i.e., $\lim_{t \rightarrow \infty} (\mathbf{n}_i(t) - \mathbf{n}_j(t)) = \mathbf{0}$, for all $(i, j) \in \mathcal{N}^2$. Moreover, all implications of Proposition 3.4.10 also follow.*

Proof. Since $d^* < d^{\min}$, we can invoke Proposition 3.4.10, and infer that $\lim_{t \rightarrow \infty} (B \otimes \mathbf{I})\mathbf{E}(t) = \mathbf{0}$ (as well as all other implications stated in the Proposition). Since $\dot{V}(\mathbf{x}(t)) \leq 0$ for all $t \geq 0$, it follows that $\gamma(1 - {}_k \mathbf{n}^T(\cdot) {}_{\bar{k}} \mathbf{n}(\cdot)) \leq D(\mathbf{n}(\cdot)) \leq V(\mathbf{x}(\cdot)) \leq V(0) < d^*$, for all $k \in \mathcal{M}$. In turn, this implies that $\theta({}_k \mathbf{n}(\cdot), {}_{\bar{k}} \mathbf{n}(\cdot)) \leq \arccos(1 - f_k^{-1}(d^*)) < \frac{\pi}{3} \frac{1}{N-1}$, for all $k \in \mathcal{M}$. Since the angular displacement between any two unit vectors \mathbf{n}_i and \mathbf{n}_j in a connected graph satisfies $\theta(\mathbf{n}_i(\cdot), \mathbf{n}_j(\cdot)) \leq (N-1) \max_{k \in \mathcal{M}} \theta({}_k \mathbf{n}(\cdot), {}_{\bar{k}} \mathbf{n}(\cdot))$ (see Proposition 1.3.4), it follows that $\sup_{t \geq 0} \theta(\mathbf{n}_i(t), \mathbf{n}_j(t)) < \frac{\pi}{3}$ between any two unit vectors \mathbf{n}_i and \mathbf{n}_j . As such, it follows from Proposition 3.4.7 that $\mathbf{n}(\cdot) \in \bar{\mathcal{C}}(\frac{3}{2} \sup_{t \geq 0} \theta(\mathbf{n}_i(t), \mathbf{n}_j(t)))$, where $\frac{3}{2} \sup_{t \geq 0} \theta(\mathbf{n}_i(t), \mathbf{n}_j(t)) < \frac{\pi}{2}$. Finally, we invoke Proposition 3.4.20, which implies that $\lim_{t \rightarrow \infty} (B \otimes \mathbf{I})\mathbf{E}(\mathbf{n}(t)) = \mathbf{0} \Rightarrow \lim_{t \rightarrow \infty} (\mathbf{n}_i(t) - \mathbf{n}_j(t)) = \mathbf{0}$. \square

Let us provide a corollary to Theorem 3.4.21, with an easier to visualize region of attraction.

Corollary 3.4.22. *Theorem 3.4.21 holds if $r := \frac{H(\omega(0))}{d^{\min}} < 1$ and if*

$$\mathbf{n}(0) \in \mathcal{C} \left(\frac{1}{2} \arccos \left(1 - \left(1 - \cos \left(\frac{\pi}{3} \frac{1}{N-1} \right) \right) \frac{1-r}{M} \right) \right). \quad (3.4.60)$$

For proving Corollary 3.4.22 it suffices to check that if its conditions are satisfied, then $V(\mathbf{x}(0)) < d^*$.

Remark 3.4.23. *Comparing Theorems 3.4.12 and 3.4.21, it follows that the region of attraction in Theorem 3.4.12 is larger than that in Theorem 3.4.21. Loosely speaking, the region of attraction in Theorem 3.4.12 is $\frac{d^{\min}}{d^*} = \frac{2}{1-\cos(\frac{\pi}{3} \frac{1}{N-1})} = \sin^{-2}(\frac{\pi}{6} \frac{1}{N-1}) > 1$ times larger than the region of attraction in Theorem 3.4.21. This difference comes from the network graph topology, and in fact, a tree network graph provides stronger results.*

3.4.7 Simulations

We now present simulations that illustrate some of the results presented previously. For the simulations, we have a group of ten agents, whose network graph is that presented in Fig. 3.19. The moments of inertia were generated by adding a random symmetric matrix (between $-\mathbf{I}$ and \mathbf{I} , entry-wise) to the identity matrix. For the initial conditions, we have chosen $\omega(0) = \mathbf{0}$ and we have randomly generated one set of 10 rotation matrices. In Fig. 3.20, $\bar{\mathbf{n}}_i = (1, 0, 0)$ for $i = \{1, 2, 3, 4, 5\}$ and $\bar{\mathbf{n}}_i = (1, 0, 0)$ for $i = \{6, 7, 8, 9, 10\}$, and since these are not necessarily principal axes, we apply the control law (3.4.41), with $\bar{\mathcal{L}} = \emptyset$ and $\mathcal{L} = \mathcal{N}$. In Fig. 3.21, $\bar{\mathbf{n}}_i$ is the principal axis of J_i , with largest eigenvalue, for $i = \{1, 2, 3, 4, 5\}$, and $\bar{\mathbf{n}}_i = (1, 0, 0)$ for $i = \{6, 7, 8, 9, 10\}$. Therefore, we apply the control law (3.4.41), with $\bar{\mathcal{L}} = \{1, 2, 3, 4, 5\}$ and $\mathcal{L} = \{6, 7, 8, 9, 10\}$. For the edge 1, we have chosen $f_1(s) = 10 \tan^2(0.5 \arccos(1-s))$. For the other edges, we have chosen $f_k(s) = 5s$, for $k = \mathcal{M} \setminus \{1\}$. Notice that we have chosen a distance function (for edge 1) that grows unbounded when two unit vectors are diametrically opposed. As such, it follows that agents 1 and 6 will never be diametrically opposed, under the condition that they are not initially diametrically opposed. We have also chosen $\sigma(\mathbf{x}) = k \frac{\sigma_x \mathbf{x}}{\sqrt{\sigma_x^2 + \mathbf{x}^T \mathbf{x}}}$ with $k = 10$ and $\sigma_x = 1$. As such, for all agents, except 1 and 6, an upper bound on the norm of their torque is given by $\sigma^{\max} + 2 \cdot 5 = 20$. Given these choices, it follows from Corollary 3.4.22 that if $\mathbf{n}(0) \in \mathcal{C}(\approx 1^\circ)$ then synchronization is guaranteed. We emphasize, nonetheless, that Corollary 3.4.22 provides conservative conditions for synchronization to be achieved, and the domain of attraction is in fact larger. We also emphasize that, for tree graphs, the domain of attraction is considerably larger: for example, if we removed the edges between agents 1 and 2, and between agents 6 and 7, we would obtain a tree graph, and Corollary 3.4.13 would read as $\mathbf{n}(0) \in \mathcal{C}(\approx 18^\circ)$.

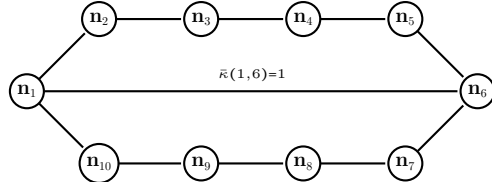


Figure 3.19: Graph with 10 agents, where edge 1 is formed by agents 1 and 6

For each simulation, one in Fig. 3.20 the other in Fig. 3.21, we provide one simulation where the control law is that in (3.4.41) and another where the control law in (3.4.41) is corrupted by noise; in fact, for each agent $i \in \mathcal{N}$, $\mathbf{T}_i(t) = \bar{\mathbf{T}}_i^{cl}(\mathbf{x}(t)) + 0.1\lambda_i(0, 0, 1)$, where λ_i corresponds to the largest eigenvalue of J_i .

The trajectories of the unit vectors for described conditions are presented in Figs. 3.20a–3.20b and 3.21a–3.21b. Notice that despite not satisfying conditions of Theorem 3.4.21 (the unit vectors are not always in a $\frac{\pi}{2}$ cone), incomplete attitude synchronization is still achieved. This can be verified in Figs. 3.20c–3.20d and 3.21c–3.21d, which present the angular error between neighboring agents. In Figs. 3.21a and 3.21b, the control laws are different between agents 1–5 and 6–10. The former perform synchronization of principal axes, by applying the constrained control law (3.4.39); while the latter perform synchronization of their first axes, i.e., $\bar{\mathbf{n}}_i = (1, 0, 0)$, by applying the control law (3.4.34). In Figs. 3.20d and 3.21d, for which the control laws were corrupted by noise, perfect synchronization is not asymptotically achieved. Instead, the unit vectors converge to a configuration where they remain close to each other (error of $\approx 5^\circ$ between neighbors).

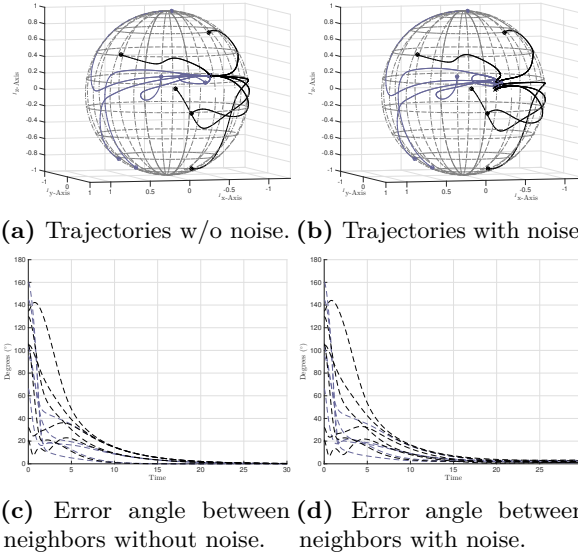


Figure 3.20: Synchronization in network of 10 unit vectors with and without noise, where blue agents perform synchronization of their first axes ($\bar{\mathbf{n}}_i = (1, 0, 0)$) and black agents synchronization of their second axes ($\bar{\mathbf{n}}_i = (1, 0, 0)$).

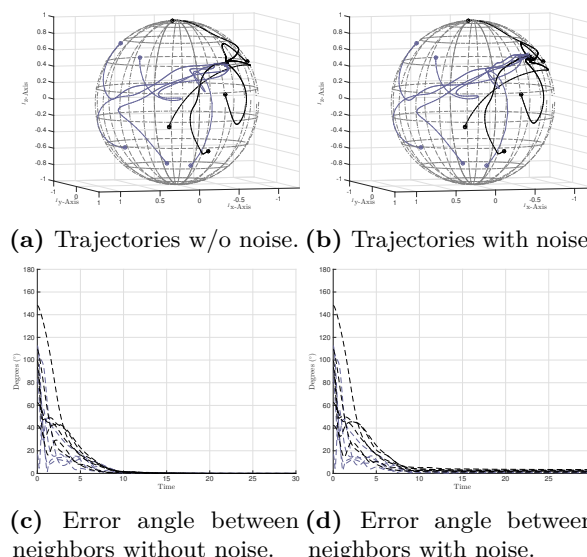


Figure 3.21: Synchronization in network of 10 unit vectors with and without noise, where blue agents perform synchronization of principal axes and black agents synchronization of their first axes (i.e., $\bar{\mathbf{n}}_i = (1, 0, 0)$).

Chapter 4

Summary and future research directions

This thesis was divided in two main parts, corresponding to Chapters 2 and 3. In the first, we developed controllers for thrust-propelled systems, while in the second, we studied synchronization of unit vectors and of rotation matrices. The main concept of each chapter is illustrated in Fig. 1.2, in page 3.

In Chapter 2 we explored the idea of using a common controller to accomplish different trajectory tracking goals in different physical systems, a concept illustrated in Fig. 2.1, in page 13.

In Section 2.2, we described the abstract concept of a thrust propelled system and proposed a controller that steers the system's position to the origin, while in Section 2.3 we exemplified the previous concepts for the quadrotor system.

In Section 2.4, we modeled the slung load system and transformed it into the thrust propelled form, allowing us to reuse the controller from Section 2.2. For this system, we also designed a disturbance estimator for a constant unknown thrust input disturbance. There are interesting research directions left unexplored, such as the design of disturbance removal techniques for other types of disturbances, like an unknown load mass or an unknown cable length. Another intriguing research direction involves the study of the dynamic effects introduced when the cable is not exactly attached to the quadrotor's center-of-mass. This introduces an extra layer of complexity, since the attitude dynamics of the quadrotor need to be considered and since the cable tension produces a torque on the quadrotor (while such a torque is nonexistent when the cable is attached to the vehicle's center-of-mass).

In Section 2.5, we proposed a control law for stabilization of a quadrotor-load system, and provided conditions on the control law's gains that guarantee exponential stability of the equilibrium corresponding to a hover condition. The system was modeled assuming that the quadrotor provides the requested control input with a delay, and an upper bound on that delay, for which exponential stability of the equilibrium is preserved, was provided. Experiments for different scenarios demonstrated and validated the robustness of the proposed control law. A subject under current investigation, and in the same vein of the previous problem, includes determining how far a cable can be attached away from the vehicle's center-of-mass

before exponential stability of the equilibrium (corresponding to a hover condition) is lost. This is of importance in practical applications, since the cable is never exactly attached to the vehicle's center-of-mass and one must provide a margin of error for which stability is guaranteed.

In Section 2.6, we modeled the system composed of a quadrotor and a rigid manipulator, and transformed it into two thrust propelled systems, allowing us once again to reuse the controller from Section 2.2. For this system, and similarly to as in Section 2.4, we also designed a disturbance estimator for a constant unknown thrust input disturbance. Interesting research directions include extending the work for a manipulator with multiple degrees of freedom (rather than just one), and to design disturbance removal techniques for other types of disturbances. One may think that the previous control strategy may be extended to the case where the manipulator interacts with the environment (say, the manipulator is used to drill a hole in a wall), but such a case exhibits different dynamics when compared to those of a manipulator that does not interact with the environment, and therefore the previous control strategy is not immediately applicable.

Finally, in Section 2.7, we modeled a point mass load and two fully actuated aerial vehicles connected by cables, and proposed controllers that guarantee that the load tracks a desired position trajectory. By appropriately choosing the control law, the quadrotors-load system was decomposed into three decoupled systems. One subsystem, concerning the position of the load, has the dynamics of a thrust propelled system, allowing us to leverage the control strategy from Section 2.2. One of the other subsystems is related to the angle between the cables, with which we can guarantee that the transporting aerial vehicles do not collide. Future work includes the design of an attitude control layer when considering the case of vehicles that are not fully actuated, and to experimentally validate the proposed strategy.

In summary, in Chapter 2 we explored the idea of using a common controller to accomplish different trajectory tracking goals in different physical systems, and we exemplified this concept with four different systems described from Section 2.3 to Section 2.7.

The main concept explored in Chapter 3 was that of synchronization of unit vectors and rotations matrices.

In Section 3.3, we studied attitude synchronization in \mathbb{S}^2 and in $\mathbb{SO}(3)$, for a group of agents under connected switching network graphs. We proposed switching decentralized output feedback control laws for each agent's angular velocity, which do not require a common orientation frame among agents. Our main contribution lied in transforming those two problems into a common framework, where all agents dynamics are transformed into unit vectors' dynamics on a sphere of appropriate dimension. Convergence to a synchronized network was guaranteed for a wide range of initial conditions. Directions for future work include extending all results to agents controlled at the torque level, rather than the angular velocity level.

In Section 3.4, we proposed a distributed control strategy that guarantees attitude synchronization of unit vectors, representing a specific body direction of a rigid body. The proposed control torque laws depend on distance functions in \mathbb{S}^2 , and we

provided conditions on these distance functions that guarantee that a synchronized network is locally asymptotically stable in an arbitrary connected undirected network graph. We imposed conditions on the distance functions that guaranteed that these are invariant to rotation of their arguments, which means that the proposed control laws can be implemented by each individual rigid body in the absence of a global common orientation frame, i.e., by using only local information. Additionally, if the direction to be synchronized is a principal axis of the rigid body, we proposed a control law that does not require full torque actuation, and, more specifically, it only requires torque in the plane orthogonal to the principal axis. We also studied the equilibria configurations that come with certain types of network graphs. Directions for future work include studying the stability of all equilibria configurations, apart from the synchronized configuration; to determine whether a synchronized network converges to a constant unit vector in a fixed, though unknown, orientation frame; and to extend the results to complete attitude synchronization. For complete attitude synchronization, though, it is not possible to construct a constrained control law, since it requires full torque actuation.

Bibliography

- [1] Aeroworks aim. <http://www.aeroworks2020.eu/>. Accessed: September, 2016.
- [2] Senstry metane leak detection. <http://www.psicorp.com/content/psi-s-rmld%284%A2-sentry-methane-leak-detection-0>. Accessed: October, 2016.
- [3] Cyberhawk boiler inspection. <http://www.thecyberhawk.com/2016/04/cyberhawk-completes-internal-power-station-boiler-inspection-eastern-europe-using-uav/>. Accessed: October, 2016.
- [4] Gri managing of forest. https://www.gri.msstate.edu/news_events/news_item.php?d=586. Accessed: October, 2016.
- [5] Flirtey drone delivery. <http://fortune.com/2016/06/25/flirtey-ships-shore-drone-delivery/>. Accessed: October, 2016.
- [6] W. Lohmiller and J.J. Slotine. On contraction analysis for non-linear systems. *Automatica*, 34(6):683–696, 1998.
- [7] R. Mahony, V. Kumar, and P. Corke. Multirotor aerial vehicles: Modeling, estimation, and control of quadrotor. *Robotics Automation Magazine, IEEE*, 19(3):20–32, Sept 2012.
- [8] F. Kendoul. Survey of advances in guidance, navigation, and control of unmanned rotorcraft systems. *Journal of Field Robotics*, 29(2):315–378, 2012.
- [9] F. Augugliaro, A. Mirjan, F. Gramazio, M. Kohler, and R. D’Andrea. Building tensile structures with flying machines. In *2013 IEEE/RSJ International Conference on Intelligent Robots and Systems*, pages 3487–3492. IEEE, 2013.
- [10] N. Michael, J. Fink, and V. Kumar. Cooperative manipulation and transportation with aerial robots. *Autonomous Robots*, 30(1):73–86, 2011.
- [11] M. Orsag, C.M. Korpela, S. Bogdan, and P. Oh. Hybrid adaptive control for aerial manipulation. *Journal of intelligent & robotic systems*, 73(1-4):693–707, 2014.

- [12] J. Scholten, M. Fumagalli, S. Stramigioli, and R. Carloni. Interaction control of an UAV endowed with a manipulator. In *IEEE International Conference on Robotics and Automation (ICRA)*, pages 4910–4915, May 2013.
- [13] H. Lee, H. Kim, and H.J. Kim. Path planning and control of multiple aerial manipulators for a cooperative transportation. In *IEEE/RSJ International Conference on Intelligent Robots and Systems (IROS)*, pages 2386–2391, Sept 2015.
- [14] T. Lee. Geometric control of multiple quadrotor UAVs transporting a cable-suspended rigid body. In *Conference on Decision and Control*, pages 6155–6160. IEEE, 2014.
- [15] P. Pereira, R. Zanella, and D.V. Dimarogonas. Decoupled design of controllers for aerial manipulation with quadrotors. In *IEEE/RSJ International Conference on Intelligent Robots and Systems*, pages 4849–4855, 2016.
- [16] L. D. Minh and C. Ha. Modeling and control of quadrotor MAV using vision-based measurement. In *International Forum on Strategic Technology (IFOST)*, pages 70–75, Oct 2010.
- [17] D. Scaramuzza and et al. Vision-controlled micro flying robots: From system design to autonomous navigation and mapping in GPS-denied environments. *Robotics Automation Magazine, IEEE*, 21(3):26–40, Sept 2014.
- [18] M. Bisgaard, A. la Cour-Harbo, and J. Bendtsen. Full state estimation for helicopter slung load system. In *AIAA Guidance, Navigation and Control Conference and Exhibit*, pages 6762–6774, 2007.
- [19] P. Pounds, D.R. Bersak, and A.M. Dollar. Grasping from the air: Hovering capture and load stability. In *IEEE International Conference on Robotics and Automation*, pages 2491–2498, May 2011.
- [20] M. Hua, T. Hamel, P. Morin, and C. Samson. Introduction to feedback control of underactuated VTOL vehicles: A review of basic control design ideas and principles. *Control Systems*, 33(1):61–75, 2013.
- [21] E. Frazzoli, M. Dahleh, E. Feron, et al. Trajectory tracking control design for autonomous helicopters using a backstepping algorithm. In *American Control Conference*, pages 4102–4107. IEEE, 2000.
- [22] P. Cheng, J. Keller, and V. Kumar. Time-optimal UAV trajectory planning for 3D urban structure coverage. In *IROS 2008 IEEE/RSJ International Conference on Intelligent Robots and Systems*, pages 2750–2757, Sept 2008.
- [23] M. B. Srikanth, A. Soto, A. Annaswamy, E. Lavretsky, and J.J. Slotine. Controlled manipulation with multiple quadrotors. In *AIAA Guidance, Navigation, and Control Conference*, Aug 2011.

- [24] F. Ruggiero et al. A multilayer control for multirotor UAVs equipped with a servo robot arm. In *International Conference on Robotics and Automation*, pages 4014–4020. IEEE, 2015.
- [25] M. Tognon and A. Franchi. Nonlinear observer-based tracking control of link stress and elevation for a tethered aerial robot using inertial-only measurements. In *IEEE International Conference on Robotics and Automation*, pages 3994–3999, 2015.
- [26] M. Bernard and K. Kondak. Generic slung load transportation system using small size helicopters. In *International Conference on Robotics and Automation*, pages 3258–3264. IEEE, 2009.
- [27] M. Bisgaard, J. D. Bendtsen, and A. L. Cour-Harbo. Modeling of generic slung load system. *Journal of guidance, control, and dynamics*, 32(2):573–585, 2009.
- [28] M. Bisgaard, A. Cour-Harbo, E. N. Johnson, and J. D. Bendtsen. Vision aided state estimator for helicopter slung load system. *17th IFAC Symposium on Automatic Control in Aerospace*, 2007.
- [29] I. Palunko, P. Cruz, and R. Fierro. Agile load transportation: Safe and efficient load manipulation with aerial robots. *IEEE robotics & automation magazine*, 19(3):69–79, 2012.
- [30] K. Sreenath, N. Michael, and V. Kumar. Trajectory generation and control of a quadrotor with a cable-suspended load - A differentially-flat hybrid system. In *International Conference on Robotics and Automation*, pages 4888–4895. IEEE, 2013.
- [31] É. Servais, H. Mounier, and B. d’Andréa Novel. Trajectory tracking of trirotor UAV with pendulum load. In *20th International Conference on Methods and Models in Automation and Robotics (MMAR)*, pages 517–522, Aug 2015.
- [32] T. Lee, K. Sreenath, and V. Kumar. Geometric control of cooperating multiple quadrotor UAVs with a suspended payload. In *Conference on Decision and Control*, pages 5510–5515. IEEE, 2013.
- [33] P. Pereira, M. Herzog, and D.V. Dimarogonas. Slung load transportation with single aerial vehicle and disturbance removal. In *Mediterranean Conference on Control and Automation*, pages 671–676, 2016.
- [34] S. Dai, T. Lee, and D. S. Bernstein. Adaptive control of a quadrotor UAV transporting a cable-suspended load with unknown mass. In *Conference on Decision and Control*, pages 6149–6154. IEEE, 2014.

- [35] I. Maza, K. Kondak, M. Bernard, and A. Ollero. Multi-UAV cooperation and control for load transportation and deployment. *Journal of Intelligent and Robotic Systems*, 57(1-4):417–449, 2010.
- [36] D. Mellinger, Q. Lindsey, M. Shomin, and V. Kumar. Design, modeling, estimation and control for aerial grasping and manipulation. In *International Conference on Intelligent Robots and Systems*, pages 2668–2673. IEEE, 2011.
- [37] P. Pounds, D. Bersak, and A. Dollar. Grasping from the air: Hovering capture and load stability. In *International Conference on Robotics and Automation*, pages 2491–2498. IEEE, 2011.
- [38] J. Thomas, J. Polin, K. Sreenath, and V. Kumar. Avian-inspired grasping for quadrotor micro UAV’s. In *ASME 2013 International Design Engineering Technical Conferences and Computers and Information in Engineering Conference*. American Society of Mechanical Engineers, 2013.
- [39] D. Mellinger, M. Shomin, N. Michael, and V. Kumar. Cooperative grasping and transport using multiple quadrotors. In *Distributed autonomous robotic systems*, pages 545–558. Springer, 2013.
- [40] F. Huber et al. First analysis and experiments in aerial manipulation using fully actuated redundant robot arm. In *International Conference on Intelligent Robots and Systems*, pages 3452–3457. IEEE, 2013.
- [41] A. Jimenez-Cano, J. Martin, G. Heredia, Aníbal Ollero, and R. Cano. Control of an aerial robot with multi-link arm for assembly tasks. In *International Conference on Robotics and Automation*, pages 4916–4921. IEEE, 2013.
- [42] C. Korpela, M. Orsag, M. Pekala, and P. Oh. Dynamic stability of a mobile manipulating unmanned aerial vehicle. In *International Conference on Robotics and Automation*, pages 4922–4927, 2013.
- [43] J. Escareno, G. Flores, M. Rakotondrabe, H. Romero, R. Lozano, and E. Rubio. Task-based control of a multirotor miniature aerial vehicle having an onboard manipulator. In *International Conference on Unmanned Aircraft Systems*, pages 857–863. IEEE, 2014.
- [44] S. Kannan, M. Alma, M. Olivares-Mendez, and H. Voos. Adaptive control of aerial manipulation vehicle. In *International Conference on Control System, Computing and Engineering*, pages 273–278. IEEE, 2014.
- [45] G. Antonelli and E. Cataldi. Adaptive control of arm-equipped quadrotors. Theory and simulations. In *Mediterranean Conference of Control and Automation*, pages 1446–1451. IEEE, 2014.

- [46] Pedro Pereira and Dimos V. Dimarogonas. Lyapunov-based generic controller design for thrust-propelled underactuated systems. In *IEEE European Control Conference*, pages 594–599, Jun 2016.
- [47] G. Hoffmann, S. Waslander, and C. Tomlin. Quadrotor helicopter trajectory tracking control. In *AIAA Guidance, Navigation and Control Conference and Exhibit*, pages 1–14, 2008.
- [48] J. Koo and S. Sastry. Output tracking control design of a helicopter model based on approximate linearization. In *Conference on Decision and Control*, volume 4, pages 3635–3640. IEEE, 1998.
- [49] N. Michael, D. Mellinger, Q. Lindsey, and V. Kumar. The GRASP multiple micro-UAV testbed. *Robotics & Automation Magazine, IEEE*, 17(3):56–65, 2010.
- [50] P. Casau, R. Sanfelice, R. Cunha, D. Cabecinhas, and C. Silvestre. Global trajectory tracking for a class of underactuated vehicles. In *American Control Conference*, pages 419–424. IEEE, 2013.
- [51] A. Roberts and A. Tayebi. Adaptive position tracking of VTOL UAVs. *IEEE Transactions on Robotics*, 27(1):129–142, 2011.
- [52] F. Mazenc and A. Iggidr. Backstepping with bounded feedbacks. *Systems & control letters*, 51(3):235–245, 2004.
- [53] I. Palunko, R. Fierro, and P. Cruz. Trajectory generation for swing-free maneuvers of a quadrotor with suspended payload: A dynamic programming approach. In *IEEE International Conference on Robotics and Automation*, pages 2691–2697, 2012.
- [54] P. Pereira, M. Herzog, and D.V. Dimarogonas. Slung load transportation with single aerial vehicle and disturbance removal. In *IEEE Mediterranean Conference on Control and Automation*, pages 671–676, 2016.
- [55] Z. Cai, M.S. de Queiroz, and D.M. Dawson. A sufficiently smooth projection operator. *IEEE Transactions on Automatic Control*, 51(1):135–139, Jan 2006.
- [56] Video of load lifting experiment. https://d1.dropboxusercontent.com/u/39547631/LoadQuadrotor_v2.mp4. 2016-02-22.
- [57] R. C. Nelson. *Flight stability and automatic control*, volume 2. WCB/McGraw Hill, 1998.
- [58] P. Pereira and D.V. Dimarogonas. Stability of load lifting by a quadrotor under attitude control delay. In *IEEE International Conference on Robotics and Automation*, 2017 (submitted).

- [59] V. Lippiello and F. Ruggiero. Exploiting redundancy in cartesian impedance control of UAVs equipped with a robotic arm. In *International Conference on Intelligent Robots and Systems*, pages 3768–3773. IEEE, 2012.
- [60] J. Acosta, M.I. Sanchez, and A. Ollero. Robust control of underactuated aerial manipulators via IDA-PBC. In *Conference on Decision and Control*, pages 673–678. IEEE, 2014.
- [61] J. Escareno, M. Rakotondrabe, G. Flores, and R. Lozano. Rotorcraft MAV having an onboard manipulator: Longitudinal modeling and robust control. In *European Control Conference*, pages 3258–3263, 2013.
- [62] S. Kim, S. Choi, and H. Kim. Aerial manipulation using a quadrotor with a two DOF robotic arm. In *International Conference on Intelligent Robots and Systems*, pages 4990–4995. IEEE, 2013.
- [63] Z. Cai, M.S. de Queiroz, and D.M. Dawson. A sufficiently smooth projection operator. *Transactions on Automatic Control*, 51(1):135–139, Jan 2006.
- [64] P. Pereira and D.V. Dimarogonas. Control framework for slung load transportation with two aerial vehicles. In *American Control Conference*, 2017 (submitted).
- [65] V. Rao and D. Bernstein. Naive control of the double integrator. *Control Systems Magazine*, 21(5):86–97, 2001.
- [66] P.O. Pereira and D.V. Dimarogonas. Lyapunov-based generic controller design for thrust-propelled underactuated systems. In *European Control Conference*, pages 594–599, 2016.
- [67] J.R. Lawton and R.W. Beard. Synchronized multiple spacecraft rotations. *Automatica*, 38(8):1359–1364, 2002.
- [68] A. Abdessameud and A. Tayebi. Attitude synchronization of a group of spacecraft without velocity measurements. *IEEE Transactions on Automatic Control*, 54(11):2642–2648, 2009.
- [69] N.E. Leonard, D.A. Paley, F. Lekien, R. Sepulchre, D.M. Fratantoni, and R.E. Davis. Collective motion, sensor networks, and ocean sampling. *Proceedings of the IEEE*, 95(1):48–74, Jan 2007.
- [70] T. Hatanaka, Y. Igarashi, M. Fujita, and M.W. Spong. Passivity-based pose synchronization in three dimensions. *IEEE Transactions on Automatic Control*, 57(2):360–375, 2012.
- [71] W. Ren. Distributed attitude consensus among multiple networked spacecraft. In *American Control Conference*, pages 1760–1765. IEEE, June 2006.

- [72] A. Sarlette, R. Sepulchre, and N.E. Leonard. Autonomous rigid body attitude synchronization. *Automatica*, 45(2):572–577, 2009.
- [73] D.V. Dimarogonas, P. Tsiotras, and K. Kyriakopoulos. Leader–follower cooperative attitude control of multiple rigid bodies. *Systems & Control Letters*, 58(6):429–435, 2009.
- [74] H. Bai, M. Arcak, and J.T. Wen. Rigid body attitude coordination without inertial frame information. *Automatica*, 44(12):3170–3175, 2008.
- [75] R. Tron, B. Afsari, and R. Vidal. Intrinsic consensus on $\mathbb{SO}(3)$ with almost-global convergence. In *IEEE Conference on Decision and Control*, pages 2052–2058, 2012.
- [76] S. Chung, S. Bandyopadhyay, I. Chang, and F. Hadaegh. Phase synchronization control of complex networks of lagrangian systems on adaptive digraphs. *Automatica*, 49(5):1148–1161, 2013.
- [77] A.K. Bondhus, K.Y. Pettersen, and J.T. Gravdahl. Leader/follower synchronization of satellite attitude without angular velocity measurements. In *IEEE Conference on Decision and Control and European Control Conference*, pages 7270–7277, 2005.
- [78] T.R. Krogstad and J.T. Gravdahl. Coordinated attitude control of satellites in formation. In *Group Coordination and Cooperative Control*, pages 153–170. Springer, 2006.
- [79] K.K. Oh and H.S. Ahn. Formation control and network localization via orientation alignment. *IEEE Transactions on Automatic Control*, 59(2):540–545, 2014.
- [80] R. Olfati-Saber. Swarms on sphere: A programmable swarm with synchronous behaviors like oscillator networks. In *IEEE Conference on Decision and Control*, pages 5060–5066, 2006.
- [81] N. Moshtagh and A. Jadbabaie. Distributed geodesic control laws for flocking of nonholonomic agents. *Transactions on Automatic Control*, 52(4):681–686, 2007.
- [82] D. Paley. Stabilization of collective motion on a sphere. *Automatica*, 45(1):212–216, 2009.
- [83] W. Li and M.W. Spong. Unified cooperative control of multiple agents on a sphere for different spherical patterns. *IEEE Transactions on Automatic Control*, 59(5):1283–1289, 2014.
- [84] A. Sarlette, S. Emre Tuna, V. Blondel, and R. Sepulchre. Global synchronization on the circle. In *Proceedings of the 17th IFAC world congress*, pages 9045–9050, 2008.

- [85] A. Sarlette and R. Sepulchre. Synchronization on the circle. *arXiv preprint arXiv:0901.2408*, 2009.
- [86] F. Dörfler and F. Bullo. Synchronization in complex networks of phase oscillators: A survey. *Automatica*, 50(6):1539–1564, 2014.
- [87] L. Moreau. Stability of continuous-time distributed consensus algorithms. In *Conference on Decision and Control*, volume 4, pages 3998–4003. IEEE, 2004.
- [88] L. Moreau. Stability of multiagent systems with time-dependent communication links. *Transactions on Automatic Control*, 50(2):169–182, 2005.
- [89] H.T. Zhang, C. Zhai, and Z. Chen. A general alignment repulsion algorithm for flocking of multi-agent systems. *IEEE Transactions on Automatic Control*, 56(2):430–435, 2011.
- [90] P.O. Pereira and D.V. Dimarogonas. Family of controllers for attitude synchronization on the sphere. In *Automatica*, 2016, to appear.
- [91] H. Cai and J. Huang. The leader-following attitude control of multiple rigid spacecraft systems. *Automatica*, 50(4):1109–1115, 2014.
- [92] S. Nair and N. Leonard. Stable synchronization of rigid body networks. *Networks and Heterogeneous Media*, 2(4):597, 2007.
- [93] J. Thunberg, W. Song, E. Montijano, Y. Hong, and X. Hu. Distributed attitude synchronization control of multi-agent systems with switching topologies. *Automatica*, 50(3):832–840, 2014.
- [94] W. Song, J. Thunberg, X. Hu, and Y. Hong. Distributed high-gain attitude synchronization using rotation vectors. *Journal of Systems Science and Complexity*, 28(2):289–304, 2015.
- [95] S. Chung, U. Ahsun, and J.E. Slotine. Application of synchronization to formation flying spacecraft: Lagrangian approach. *Journal of Guidance, Control, and Dynamics*, 32(2):512–526, 2009.
- [96] C.G. Mayhew, R.G. Sanfelice, J. Sheng, M. Arcak, and A.R. Teel. Quaternion-based hybrid feedback for robust global attitude synchronization. *IEEE Transactions on Automatic Control*, 57(8):2122–2127, Aug 2012.
- [97] C.D. Godsil, G. Royle, and C.D. Godsil. *Algebraic graph theory*, volume 207. Springer New York, 2001.
- [98] D.V. Dimarogonas and K.H. Johansson. Further results on the stability of distance-based multi-robot formations. In *IEEE American Control Conference*, pages 2972–2977, 2009.

- [99] S. Guattery and G.L. Miller. Graph embeddings and Laplacian eigenvalues. *SIAM Journal on Matrix Analysis and Applications*, 21(3):703–723, 2000.
- [100] Y. Igarashi, T. Hatanaka, M. Fujita, and M.W. Spong. Passivity-based attitude synchronization in $\mathbb{SE}(3)$. *IEEE Transactions on Control Systems Technology*, 17(5):1119–1134, 2009.
- [101] R. Sepulchre. Consensus on nonlinear spaces. *Annual reviews in control*, 35(1):56–64, 2011.
- [102] A. Sarlette and R. Sepulchre. Consensus optimization on manifolds. *SIAM Journal on Control and Optimization*, 48(1):56–76, 2009.
- [103] Z. Lin, B. Francis, and M. Maggiore. State agreement for continuous-time coupled nonlinear systems. *SIAM Journal on Control and Optimization*, 46(1):288–307, 2007.
- [104] J.P. Hespanha. Uniform stability of switched linear systems: extensions of LaSalle’s invariance principle. *IEEE Transactions on Automatic Control*, 49(4):470–482, 2004.
- [105] A. Bacciotti and L. Mazzi. An invariance principle for nonlinear switched systems. *Systems & Control Letters*, 54(11):1109–1119, 2005.
- [106] J.L. Mancilla-Aguilar and R.A. García. An extension of LaSalle’s invariance principle for switched systems. *Systems & Control Letters*, 55(5):376–384, 2006.
- [107] N. Fischer, R. Kamalapurkar, and W.E. Dixon. LaSalle-Yoshizawa corollaries for nonsmooth systems. *IEEE Transactions on Automatic Control*, 9(58):2333–2338, 2013.
- [108] D. Pence. *Spacecraft Attitude, Rotations and Quaternions*, volume 5. Birkhäuser, 1984.
- [109] P. Pereira, D. Boskos, and D.V. Dimarogonas. A common framework for attitude synchronization of unit vectors in networks with switching topology. In *55th IEEE Conference on Decision and Control*, 2016 (to appear).
- [110] E.D. Sontag. *Mathematical Control Theory*. Springer, 1998.
- [111] P. Pereira, D. Boskos, and D.V. Dimarogonas. A common framework for attitude synchronization of unit vectors in networks with switching topology. *arXiv*, 2015.
- [112] C.G. Mayhew, R.G. Sanfelice, and A.R. Teel. On quaternion-based attitude control and the unwinding phenomenon. In *American Control Conference*, pages 299–304. IEEE, 2011.

- [113] D. Liberzon. *Switching in systems and control*. Springer, 2003.
- [114] P. Pereira and D.V. Dimarogonas. Family of controllers for attitude synchronization in \mathbb{S}^2 . In *54th IEEE Conference on Decision and Control*, pages 6761–6766, Dec 2015.
- [115] P. Pereira and D.V. Dimarogonas. Family of controllers for attitude synchronization on the sphere. In *Automatica*, 2016 (to appear).
- [116] P. Pereira and D.V. Dimarogonas. Family of controllers for attitude synchronization on the sphere. *arXiv*, 2016.